LIBRARY
Michigan State
University

This is to certify that the

dissertation entitled

HYDROGEN BONDING INTERACTIONS IN
CYTOCHROME A OF CYTOCHROME OXIDASE:
A RESONANCE RAMAN STUDY.

presented by

Jose A. Centeno-Ortiz

has been accepted towards fulfillment
of the requirements for

Ph.D. degree in Chemistry

Gerald T. Babcock
Major professor

Date Sept 18, 1987

MSU is an Affirmative Action/Equal Opportunity Institution

O-12771

MSU
LIBRARIES

RETURNING MATERIALS:
Place in book drop to remove this checkout from your record. FINES will be charged if book is returned after the date stamped below.

HYDROGEN BONDING INTERACTIONS IN CYTOCHROME A OF CYTOCHROME OXIDASE: A RESONANCE RAMAN STUDY

By

Jose Antonio Centeno Ortiz

A DISSERTATION

Submitted to

Michigan State University
in partial fulfillment of the requirements
for the degree

DOCTOR OF PHILOSOPHY

Department of Chemistry

1987

ABSTRACT

HYDROGEN BONDING INTERACTIONS IN CYTOCHROME A OF CYTOCHROME OXIDASE: A RESONANCE RAMAN STUDY.

By

Jose Antonio Centeno Ortiz

Hydrogen bonding interactions at the formyl (-CHO) group of cytochrome a in cytochrome oxidase have been investigated by using spectroscopic and chemical methods. Heme a model compounds that mimic the spectroscopic properties of cytochrome a have been isotopically synthesized with formyl (-CDO) and ($-CH^{18}O$) groups. With the aid of these isotopic substitutions we have identified essentially all the internal formyl vibrations, and compared them with similar isotopic and H-bonding effects in benzaldehyde. To identify resonance Raman enhancement of cytochrome a^{2+} formyl related modes, we have obtained the resonance Raman spectra in the range from 150 - 1700 cm^{-1}, under four different experimental conditions: visible excitation in resonance with the $Q_{(0-0)}$ ----> * transition; acidic denaturing conditions; H/D exchange; and ligand deconvolution. From these spectra the hydrogen bond sensitive vibrations of cytochrome a^{2+} can be identified and a comparison of these vibrations with those previously

obs

con

Bec

the

C=C

sy

in

re

a

ex

Th

r

t

p

i

observed for heme a and benzaldehyde under H-bonding conditions provide the assignment of -CHO internal modes. Because of the lower symmetry of the heme a macrocycle and the strong electron withdrawing character of the H-bonded C=O, we observed RR activity (and intensity changes) for symmetry forbidden Eu modes.

The importance of the cytochrome a^{2+} H-bonded structure in the oxidase proton pumping activity was examined. Our results reveal significant perturbations at the cytochrome a^{2+} H-bond interaction as the adjacent protein protons are exchanged by deuterons during enzyme turnover conditions. The suggested involvement of the Cu_A^{2+} atom in the oxidase redox-linked mechanism was also investigated by ENDOR spectroscopy. Our results reveal the occurrence of exchangeable protons at sites near the Cu_A site; however, their involvement in the H^+-pump remains unclear.

To

Maria

Joselito

and

Waldemar

I

many b

encour

I

readin

educa

membe

durin

paren

Mervi

Babco

and

than

rese

assi

the

comp

prog

use

than

Marc

hel

is

ACKNOWLEDGMENTS:

I would like to thank Prof. Gerald T. Babcock for his many helpul suggestions to this project and for the encouragement he offered me when I most needed it.

I am deeply grateful to Dr. George Leroi for critical reading and unconditional support during my graduate education.

I would like to express my gratitude to all my family members and friends who, in their own way, motivated me during my graduate career at Michigan State. So to my parents, Amelia and Domingo; my brothers, Luis, Alex, and Mervin; my uncles Papo and Adelina; and my friends, Jerry Babcock, Roberto Lopez, Ismael Scott, Luis Garcia, Benito, and Juan Lopez; I extend my heartfelt appreciation. My thanks are also extended to members of Prof. Babcock's research group for their contribution and general technical assistance, in particular, Dr. Robert Kean, who helped me in the design of the Raman difference cuvette and the necessary computer programming; Mr. Dwight Lillie for computer programming; and Tony Oertling for his instruction in the use of the lasers (and for his occasional delicatessen). My thanks are also extended to Drs. Patricia Callahan, Patricia Maroney, and Juan Lopez, for their encouragement, many helpful discussions, and constant cooperation. My gratitude is also extended Mr. Hak-Hyum Nam and Mr. Dean Petersen for

their
would
not f

Manfr
of th
possi
you g

Ingle
maize
progr

Cent
appr

the
Affa
Casa
this

the
from
care

their assistance on the recording of the FTIR spectra. I would still be doing the work in Chapters 3 and 5 if it were not for the valuable assistance I received from them.

I would like to thank Mr. Ron Hass, Marti Rabb, and Manfred Langer for their technical assistance. The design of the Raman difference apparatus would not have been possible without the assistance of Marti and Manfred. Thank you guys !!!

I would like to acknowledge research efforts with Bob Ingle and Prof. Sheilagh Ferguson-Miller on the study of maize cytochrome oxidase developed while this project was in progress.

The efforts of Mrs. Dianne Kazmierski and Maria Centeno, in the preparation of this manuscript are greatly appreciated.

I also wish to acknowledge the Department of Chemistry, the National Institutes of Health, and the Office of Urban Affairs at Michigan State University and its Director Dr. Casandra Simmons, for financial support during the course of this project.

Finally, I don't have words that can compensate for all the love, understanding, and endurance that I have received from Maria and my kids during the course of my graduate career. I couldn't have done it without you!

TABLE OF CONTENTS

List of Tables xi

List of Figures xiii

Chapter I 1

I. Cytochrome c Oxidase: Structure and Functions 1

A. Introduction and Overview of Thesis . . . 1

B. Brief History 5

II. Cytochrome Oxidase: Structure and Metal Active Sites. 8

A. Subunit Composition and Protein Structure 8

B. Metal Centers: Structure and Protein Environment 14

C. Chromophore Geometry and Ligand-Coordination 22

III. Proton Pumping 26

IV. Concluding Remarks 30

V. Aims and Strategy of this Thesis 32

Chapter II Materials and Methods 34

I. Introduction 34

II. Materials 35

A. Isolation of Cytochrome c Oxidase 35

B. Preparation of Cytochrome c Oxidase Derivatives 36

C. Alkaline and acidic pH-modification of Purizied Cytochrome Oxidase 37

D. Redox-cycled Cytochrome Oxidase 38

E. Preparation of Heme a Derivatives 39

III. Methods 44

A. Electronic Optical Absorption Spectroscopy 47

B. Resonance Raman Spectroscopy 52

1) Resonance Raman Difference Spectroscopy 56

C. Electron Nuclear Double Resonance Spectroscopy (ENDOR) 67

D. Infrared (IR) Spectroscopy 68

Chapter III Formyl Isotopic Substitution and Hydrogen Bond Sensitive Modes in Heme a Model Compounds: Models for Cytochrome a 69

Summary 69

I. Introduction 70

II. Results and Discussion 74

A. Effects of Hydrogen Bonding on the Absorption Spectra of Heme a Complexes. . 74

B. Effects of H-bonding and isotopic substitution on the Raman spectra of benzaldehyde 82

C. Formyl modes in the RR and IR spectra of heme a and its Cu^{2+} Porphyrin Analog 86

D. H-bonding effects in Heme a Models. . . . 110

III. Conclusions 119

Chapter IV Visible Excitation Resonance Raman Spectra of Cytochrome a in Cytochrome Oxidase 121

I. Introduction 121

II. Materials and Methods 123

A. Materials 123

B. Instrumentation 125

III. Results 125

A. Visible Excitation Resonance Raman Spectra

IV.

V.

Chapt

I.

II.

III.

IV.

V.

Chap

I.

II.

of Cytochrome a^{2+} in H_2O/D_2O Buffers . . 125

B. Effects of deuterium substitution for cyt a^{2+} modes above 1000 cm^{-1} 130

C. Low-frequency cytochrome a^{2+} vibration below 1000 cm^{-1} 136

IV. Discussion 143

A. High-frequency vibrational assignments of cyt a^{2+} 143

B. Low-frequency vibrations of cyt a^{2+} . . . 147

V. Conclusions 150

Chapter V Hydrogen Bond Sensitive Vibrations of Cytochrome a in Cytochrome Oxidase . . . 152

I. Introduction 152

II. Materials and Methods 153

III. Results 153

A. Low pH Effects on the RR spectra of Radical Cytochrome Oxidase 153

B. Low pH Effects on the RR spectra of Cyanide inhibited Cytochrome Oxidase. . . 162

IV. Discussion. 174

A. Assignments of H-Bonding Sensitive Vibrations of Cyt a^{2+} 181

B. Low frequency Vibrational Assignments . . 184

V. Concluding Remarks 187

Chapter VI Evidence for cyt a Involvement on the cyt c oxidase Proton Pump Mechanism: A Resonance Raman and ENDOR study 188

I. Introduction 188

II. Results 191

A. Resonance Raman Spectra of Resting Cytochrome Oxidase 191

B. Resonance Raman Spectra of Redox-Cycled Oxidase. 197

C. EPR and ENDOR Studies and Redox-Activated Oxidase 216

III. Discussion 227

A. Enhancement of Cytochrome a Formyl H-bonding Sensitive Modes: Slow H/D Exchange Process 227

B. Low Frequency Region 234

C. ENDOR Results 236

IV. Conclusions 236

Chapter VII Summary and Future Work 239

I. Summary 239

II. Future Work 241

A. Spectroscopy of Cyt Oxidase and Heme a Models 241

B. Hydrogen Bonding 245

References Cited 247

LIST OF TABLES

Page

Chapter III.

Table 3.1 Spectroscopic Characteristics of Hydrogen Bonded Complexes of Heme a, Cu^{2+} a, and Cu^{2+} Porphyrin 77

Table 3.2 Summary of Raman Frequencies (cm^{-1}) for Hydrogen-Bond Modes in Benzaldehyde 84

Table 3.3 Formyl-Sensitive Modes in Heme a (N-MeIm)$_2$ (-CHO/-CDO) and Cu^{2+} Porphyrin a (-CHO/-CDO). . . 92

Table 3.4 Resonance Raman (RR) and Infrared (IR) Frequencies (cm^{-1}) Sensitive to -CH^{16}O ----> -CH^{18}O Substitution at the Formyl Group of (4-Vinyl-8-Formyl) Porphyrin. 102

Chapter IV.

Table 4.1 Tentative Assignments for the Observed High-Frequency Modes in the Resonance Raman Spectrum of Cyt a^{2+}. 131

Table 4.2 Tentative Assignments for the Observed Low-Frequency Modes in the Visible Excitation Resonance Raman Spectrum of Cyt a^{2+}. 139

Table 4.3 Correlation Table for Species with D_{4h}, D_{2h}, and C_{2h} Point Group Symmetry. 149

Chapter V.

Table 5.1 High Frequency Vibrational Assignments of Cytochromes a and a$_3$ 172

Table 5.2 High Frequency Aldehyde Group Vibration Assignments and Shifts Observed for Benzaldehyde in the Presence of Hydrogen Donors and Cytochrome a^{2+} at Neutral and Acid pH. 173

Table 5.3 pH Senstive Vibrations (cm^{-1}) at Cytochrome a^{2+} Observed with 441.6 nm excitation 175

Chapter VI. Table 6.1 Tentative Raman Frequency Assignments for Cytochrome a Formyl Modes in Cytochrome c Oxidase 230

Table 6.2 Summary of Raman Frequency Assignments for Cytochrome a Vinyl Modes in Cytochrome c Oxidase 231

LIST OF FIGURES

Page

Chapter I.

Fig. 1.1 The geometrical arrangement of the polypeptides (subunits) in cytochrome c oxidase in the mitochondrial membrane 9
Fig. 1.2 The molecular structure of heme a and protoporphyrin IX 15
Fig. 1.3 Electronic optical absorption spectra of oxidized (——) and reduced (----) cytochrome c oxidase in the Soret, visible, and near-IR regions 17
Fig. 1.4 Geometry and coordination properties for cytochrome a, cytochrome a_3, Cu_A, and Cu_B in cytochrome c oxidase 24
Fig. 1.5 A simplified scheme of the redox-linked proton pumping activity on cytochrome c oxidase. ... 28

Chapter II.

Fig. 2.1 Structures of free base porphyrin a and its porphyrin analog 43
Fig. 2.2 Absorption spectra of formyl-substituted derivatives of 2,6-dipentyl-4-vinyl-8-formyl Cu^{2+} porphyrin 46
Fig. 2.3 Absorption Spectra of Free Base Porphyrin a and Cu^{2+}-substituted Porphyrin a 49
Fig. 2.4 Energy diagram for metalloporphyrin absorption spectra....... 51
Fig. 2.5 Diagram illustrating Raman and Rayleigh scattering and the resonance Raman effect 53
Fig. 2.6 Block diagram of the resonance Raman difference apparatus 57

Fig. 2.7 Schematic of the resonance Raman difference hardware and split spinning cuvette 58

Fig. 2.8 Schematic of the digital and timing logic for the resonance Raman difference apparatus. 61

Fig. 2.9 Resonance Raman spectra of cytochrome c^{2+} in protonated and deuterated buffers (pH=pD=7.4), and the associated Raman difference spectrum 65

Chapter III. Fig. 3.1 Proposed H-bonded structure of cyt a in cytochrome c oxidase 72

Fig. 3.2 Absorption spectra of heme a (N-MeIm)$_2$ under various hydrogen bonding conditions 76

Fig. 3.3 Plot of observed redshift in the Soret and α-band transition of Cu^{2+} porphyrin a as a function of the acidity (pka) of phenol H-donor derivative 81

Fig. 3.4 Raman spectra of benzaldehyde-CHO and its H-bonded derivatives with phenol-OH and phenol-OD as H-donors 83

Fig. 3.5 Resonance Raman (RR) spectra of oxidized and reduced detergent monomerized heme a (N-MeIm)$_2$ in dry CH_2Cl_2, after treatment with KCN/H_2O and KCN/D_2O 89

Fig. 3.6 Resonance Raman (RR) spectra of Cu^{2+} porphyrin a with normal (-CHO) and deuterated (-CDO) formyl group substituent, in dry CH_2Cl_2 91

Fig. 3.7 Resonance Raman (RR) spectra of 4-vinyl-8-formyl Cu^{2+} porphyrin with normal (-CH^{16}O) and ^{18}O-labelled (-CH^{18}O) formyl group substituent in dry CH_2Cl_2 96

Fig. 3.8 FTIR spectra of heme a^{3+}-Cl$^-$, Cu^{2+} (-CH^{16}O), and Cu^{2+}

(-$CH^{18}O$) porphyrin derivatives in KBR pellets in the region from 1000 to 1800 cm^{-1}........................ 98

Fig. 3.9 FTIR spectra of heme $\underline{a}^{3+}$-Cl^-, Cu^{2+} (-$CH^{16}O$) porphyrin, and the dimethylester derivative of protoporphyrin Fe^{3+}-Cl^- in carbon tetrachloride (CCl_4) 101

Fig. 3.10 Resonance Raman (RR) spectra of ferric nonhydrogen bonded heme $\underline{a}^{3+}$ $(N\text{-}MeIm)_2$ (in CH_2Cl_2) and ferric heme $\underline{a}^{3+}$ $(N\text{-}MeIm)_2$ (in CCl_4) hydrogen bonded to phenol-OH and phenol-OD................................ 112

Fig. 3.11 Resonance Raman spectra of ferrous heme a$(N\text{-}MeIm)_2$ H-bonded to phenol-OD_6 in dry CH_2Cl_2 113

Fig. 3.12 Resonance Raman (RR) spectra of Cu^{2+} (-$CH^{16}O$) porphyrin in CH_2Cl_2 and under H-bonding to phenol-OH and phenol-OD.......... 115

Fig. 3.13 Low-frequency resonance Raman (RR) spectra of ferrous heme $\underline{a}^{2+}$ $(N\text{-}MeIm)_2$ in CH_2Cl_2, in H_2O/detergent, and D_2O/detergent.... 116

Chapter IV. Fig. 4.1 Visible excitation (605 nm) resonance Raman spectra of reduced cytochrome oxidase from 1000 to 1300 cm^{-1}............. 127

Fig. 4.2 Visible excitation (605 nm) resonance Raman spectra of reduced cytochrome oxidase from 1250 to 1700 cm^{-1}............. 129

Fig. 4.3 Low frequency visible excitation (605 nm) resonance Raman spectra of fully reduced cytochrome oxidase 137

Fig. 4.4 Low frequency visible excitation (605 nm) resonance Raman spectra of fully reduced cytochrome oxidase. 138

Chapter V. Fig. 5.1 Optical absorption

spectra of reduced cytochrome oxidase at neutral and acidic pH.... 154

Fig. 5.2 High frequency resonance Raman spectra of reduced cytochrome oxidase at the indicated acidic pH level 157

Fig. 5.3 Low frequency resonance Raman spectra of reduced cytochrome oxidase at the indicated pH levles... 160

Fig. 5.4 Low frequency resonance Raman spectra of fully reduced and partially reduced cyanide inhibited cytochrome oxidase obtained with 441.6 nm excitation at the indicated pH levels 165

Fig. 5.5 Optical absorption spectra of partially reduced, cyanide-inhibited cytochrome oxidase at several pH levels 168

Fig. 5.6 Low frequency resonance Raman spectra of partially reduced cyanide inhibited cytochrome oxidase at several pH levels obtained with 441.6 nm excitation. 169

Fig. 5.7 High frequency resonance Raman spectra of mixed-valence cytochrome oxidase at the indicated pH levels. 170

Fig. 5.8 Schematic of proposed structural changes of reduced and partially reduced plus cyanide heme a chromophores of cytochrome oxidase at acid pH levels 180

Chapter VI. Fig. 6.1 Optical absorption spectra of resting cytochrome oxidase in protonated and deuterated buffers. 192

Fig. 6.2 Resonance Raman spectra and the associated Raman difference spectrum (RDS) of resting cytochrome oxidase in protonated and deuterated buffers from 1000 to 1440 cm^{-1} and from 1300 to 1700 cm^{-1} 194

Fig. 6.3 Resonance Raman spectra and cytochrome oxidase under various turnover conditions as monitored with 406.7 nm excitation............ 199

Fig. 6.4 Resonance Raman spectra of fully reduced cytochrome oxidase observed in the carbonyl stretching region of cytochrome $\underline{a}^{2+}$ 202

Fig. 6.5 Plot of frequency of the cytochrome $\underline{a}^{2+}$ carbonyl stretching frequency as a function of incubation time in D_2O. 205

Fig. 6.6 Resonance Raman spectra of redox-cycled oxidase as a function of enzyme turnover cycles induced by increasing the concentration of ascorbate in the solution 207

Fig. 6.7 Resonance Raman spectra and the associated difference spectrum of redox-cycled mixed-valence cytochrome oxidase obtained with 441.6 nm (7A) and 406.7 nm (7B) excitation frequencies.............. 210

Fig. 6.8 Low frequency resonance Raman spectra of reduced ($\underline{a}^{2+}\underline{a}_3{}^{2+}$) and redox-cycled ($\underline{a}^{2+}\underline{a}_3{}^{3+}\cdot CN^-$) cytochrome oxidase in protonated and deuterated buffers 214

Fig. 6.9 EPR spectra of cytochrome oxidase 219

Fig. 6.10 ENDOR spectra of cytochrome $\underline{a}^{3+}$ at the electronic g value of g=3.03 221

Fig. 6.11 Matrix ENDOR spectra of $Cu_A{}^{2+}$ in cytochrome oxidase at the electronic $g_{\perp}$ value of g=2.02 (perpendicular region)........ 224

Fig. 6.13 Matrix ENDOR spectra of $Cu_A{}^{2+}$ in cytochrome oxidase at the electronic g value of $g_{\parallel}$=2.1717 (parallel region)......... 226

Chapter VII. Fig. 7.1 Comparison of the resonance Raman spectra of cytochrome c oxidase isolated from maize (corn seedlings) and bovine beef heart mitochondria. 244

CHAPTER I

I. Cytochrome c Oxidase: Structure and Function

A. Introduction and Overview of the Thesis:

In the mitochondrial respiratory chain of eukaryotic cells the production of energy is based upon a sequence of electron transfer reactions through a set of redox proteins which culminates with the reduction of molecular oxygen to produce water (Wikstrom et al., 1982). The last enzyme in this mechanism is called cytochrome c oxidase. It catalyzes the reduction of dioxygen to water by transferring electrons from reduced cytochrome $\underline{c}^{2+}$ to oxygen. The overall reaction is described as follows:

$$4\ \text{cyt.}\underline{c}^{2+} + O_2 + nH^+(\text{in}) \dashrightarrow 4\ \text{cyt.}\underline{c}^{3+} + 2H_2O + (n-4)H^+(\text{out})$$

The transfer of electrons in this reaction is believed to be coupled to the generation of an electrochemical proton potential gradient ($\Delta\mu_{H^+}$) across the mitochondrial membrane (Wikstrom and Krab, 1979; Casey et al., 1979; Proteau et al., 1983; Wikstrom, 1984; Thelen et al., 1985; Malmstrom, 1985; Blair et al., 1986). This electrochemical proton potential is composed of a membrane potential ($\Delta\Psi$), which arises from vectorial electron transfer from the outside of the membrane, and of the consumption of H^+ in the inside giving rise to a ΔpH. The formation of ($\Delta\mu_{H^+}$) is linked to the production of adenosine triphosphate (ATP), an energy source which is used in biochemical reactions which require energy. In addition to the consumption of H^+ ions in the inner side of the membrane during reduction of O_2, the transfer of electrons through the oxidase is also known to be coupled to the translocation of at least one H^+/per electron to the cytosol side (or outside) of the membrane (Wikstrom, 1977; Wikstrom et al., 1982). This coupling between electron transfer and proton translocation is essential for energy transduction during respiration.

In this introduction I review recent research on the structural, functional, and physiological aspects of cytochrome c oxidase. In the following six Chapters, experiments will be presented which show the application of spectroscopic methods (Uv-vis, resonance Raman (RR), infrared (IR) electron paramagnetic resonance (EPR) and electron nuclear double resonance(ENDOR)) to study structural features of the enzyme and to provide insights into the *in vivo* structural/functional aspects of this important metalloprotein.

The spectroscopic techniques and experimental procedures used during the course of this work to study cytochrome oxidase, its ligand-bound derivatives, and its isolated heme a model compounds are described on Chapter II. A brief introduction to Uv-vis electronic optical absorption and resonance Raman spectroscopy (RRS) will be presented. The design of a home-made Raman difference apparatus, which features the use of a double-compartment spinning cuvette and digital gating logic, will be described.

Chapter III demonstrates the use of isolated heme a model compounds and the application of available spectroscopic techniques (UV-vis, infrared, and RR) to study the molecular structure and the sensitivity of Raman frequencies to porphyrin peripheral substituents. Results are presented from infrared (FTIR) and resonance Raman experiments on heme a model compounds with the aim of obtaining insights into the involvement of the π-conjugated peripheral substituents in the electronic states of heme a. I concentrate my efforts on elucidating Raman frequencies sensitive to formyl vibrations and on describing the sensitivity of these bands to formyl-proton and oxygen isotopic substitution in addition to hydrogen-bonding effects.

In Chapter IV, visible excitation resonance Raman studies of reduced and mixed-valence cytochrome oxidase in protonated and deuterated buffers are presented. Since cytochrome a^{2+} is the dominant contributor to the 605 nm absorption band of reduced cytochrome oxidase (Vanneste, 1967), laser excitation in this $Q_{(0-0)}$ π ----> π^* transition is expected to be dominated by cytochrome a^{2+} vibrational modes. The strong enhancement of cytochrome a modes with visible excitation, and their sensitivity upon protein H/D-exchange and pH-denaturation, is sugested to arise from interactions of the cytochrome a heme moiety with the surrounded protein residues. A detailed study of the

de
al

of
un
of
as
or
H-
re
vi
ox
id

ac
we
in
(-
re
re
Ch
ir
(-
Sc
oc
pr

depolarization ratios of cytochrome a vibrational modes is also presented.

Chapter V summarizes our results on the identification of the cytochrome a H-bonding vibrational modes as studied under Soret ($B_{(0-0)}$-transition) excitation. The sensitivity of these cytochrome a modes to protein perturbations, such as acidic pH effects, was also studied. Since, upon raising or lowering the pH of the oxidase solution, the cytochrome a H-bonding structure is expected to be disrupted,a systematic resonance Raman study on the pH-induced effects in the vibrational spectra of reduced and mixed-valence cytochrome oxidase, is expected to provide additional evidence on the identity of the cytochrome a H-bonding modes.

Soret excitation resonance Raman studies on the accessibility of labile protons, at the cytochrome a site, were also conducted, with the specific aim of gaining insight into the rate of H/D-exchange at the cytochrome a (-HC=O...H/D-protein) site and its relevance to enzymatic redox changes (as studied by repeated enzymatic cycles of reduction and reoxidation). This data is presented in Chapter VI. The results from these experiments are discussed in terms of the involvement of the cytochrome a formyl group (-HC=O) in the cytochrome oxidase proton pump mechanism. Soret excitation on the resting oxidase indicates the occurrence of exchangeable protons at the cytochrome a/ protein site, as well as spin-state transformations associated with the cytochrome a_3 site. This chapter also deals with the application of electron paramagnetic resonance (EPR) and electron nuclear double resonance (ENDOR) spectroscopies to study the metal active centers of cytochrome oxidase. In this work, EPR spectroscopy was used to monitor enzyme integrity and thus quality of the preparation, as judged by the cytochrome a and Cu_A EPR-signals. To study H_2O/D_2O exchange at the Cu_A^{2+} site (Gelles et al., 1986) ENDOR spectroscopy was used.

Finally, future experiments and new approaches are suggested in Chapter VII.

B. Brief History:

The initial investigations on the active role of cytochrome oxidase in the cellular respiratory chain were reported in 1939 by Keilin and Hartree. In their original work Keilin and Hartree (1939) showed that cytochrome oxidase was composed of two functionally distinct components, which they called cytochrome a and cytochrome a_3. They proposed that cytochrome a was involved in the electron uptake from cytochrome c while cytochrome a_3 was involved in the binding and reduction of dioxygen. Though Keilin and Hartree (1939) initially commented on the possibility of the participation of the copper atoms in the cytochrome oxidase oxygen reaction, their involvement was not considered seriously until 1962 when Beinert et al.

(19

res

the

196

com

tem

oxi

abs

(19

ele

cyt

int

wer

al.

197

stu

oxi

med

(19

al.

int

rep

fla

tro

by

the

(1962). first introduced the use of electron paramagnetic resonance (EPR) to study the electronic environment of the metal sites in the oxidase.

The pioneering work by Greenwood and Gibson (1963, 1965, & 1967) on the photolability of the cytochrome $\underline{a}_3^{2+}$-CO complex and its subsequent reaction with dioxygen at low temperatures, made it possible to start studies on the oxidation of the reduced enzyme by oxygen. Using optical absorption spectroscopy techniques, Greenwood and Gibson (1963,1965, & 1967) were able to follow the route of electron transfer from cytochrome $\underline{a}$ via Cu_A to the binuclear cytochrome $\underline{a}_3$ /Cu_B center by detecting short-lived enzyme intermediates. These short-lived transient intermediates were further characterized by using Uv-vis optical (Clore et al., 1980) and EPR (Karlson et al., 1981; Chance et al., 1975) spectroscopic techniques. The results from these studies indicated that the reaction of reduced cytochrome oxidase with dioxygen proceeds via at least three intermediates (termed compounds A, B, and C in the Chance et al., (1975) terminology; or compounds I, II, III in the Clore et al., (1980) terminology). Recent attempts to study these intermediates by resonance Raman sepectroscopy have been reported by Babcock et al. (1984 & 1985). By using flow-flash CO-photolysis and time-resolved resonance Raman spectroscopy during the oxidation of reduced cytochrome oxidase by oxygen, Babcock et al. (1984 & 1985) were able to detect the initial occurrence of a photolabile oxy-intermediate as the precursor to oxygen reduction, with the subsequent formation of a more stable oxygen-intermediate at the cytochrome $\underline{a}_3$ /Cu_B site. Another important finding with respect to the existence of these enzyme intermediates has been the recent resolution of this "oxy" intermediate at room temperature by using CO-flash-photolysis accompanied by rapid-scanning spectrophotometry (Orii, 1984). Therefore, the available data accumulated on the oxidation products of reduced cytochrome oxidase by oxygen support the formation of an "oxy" intermediate during the first stages of the reaction, which is subsequently followed by fast intermolecular electron transfer to dioxygen.

Research on the proton pumping mechanism of cytochrome oxidase was initiated by Wikstrom (1977) and later by Sigel and Carafoli (1978). The proton pumping action of cytochrome oxidase has been investigated in whole mitochondria as well as in isolated cytochrome oxidase reconstituted into phospholipid vesicles (Wikstrom and Saari, 1977). Recently, it was suggested that cytochrome oxidase depleted of subunit III did not show significant proton pumping activity even though the electron transfer capabilities were not significantly altered (Penttila, 1983). In addition, in order to maintain the obligatory coupling between electron transfer and proton translocation in cytochrome oxidase, two redox-linked proton pumping models have been suggested at the molecular level for cytochrome $\underline{a}$ (Babcock and Callahan, 1983) and Cu_A (Blair et al., 1986; Gelles et al., in press), res

and

in

II.

of

198

600

Da.

thr

by

sma

se

sim

oxi

Osh

thr

198

fro

al.

oxi

Exa

198

(So

(So

respectively. The mechanistic implications of both models and their relevance to the present study will be presented in Section III of this Chapter.

II. Cytochrome Oxidase: Structure and Metal Active Sites.

A. Subunit Composition and Protein Structure

Cytochrome oxidase from bovine heart muscle is composed of more than 12 polypeptide subunits (Capaldi, 1982; Azzi, 1980; Buse et al., 1985) with molecular weights ranging from 6000 to 40,000 Da. It has a total molecular mass of ~200,000 Da. The subunit arrangement is shown in Figure I-1. The three largest subunits (subunits I, II, III) are coded for by mitochondrial DNA (Tzagoloff et al., 1979), while the smaller subunits are coded by nuclear DNA. Cytochrome oxidase has been purified also from prokaryote sources with much simpler subunit composition. These range from an $\underline{aa}_3$-type oxidase with two subunits (Yamanaka et al., 1979; Honami and Oshima, 1984; and Fukumori et al., 1985), to oxidase with three subunits (Sone and Yanagita, 1982; De Vrij et al., 1983), to the recent characterization of cytochrome oxidase from Thermus thermophilus with just one subunit (Yoshida et al., 1984). As with bovine oxidase, these bacterial type oxidases have been reported to show proton pumping activity. Examples of these are Thermus thermophilus (Sone et al., 1984; Yoshiba and Fee, 1984), the Thermophilus bacterium PS3 (Sone and Hinckle, 1982), and Paracoccus denitrificcans (Solioz et al., 1982). Subunits I and II are known to

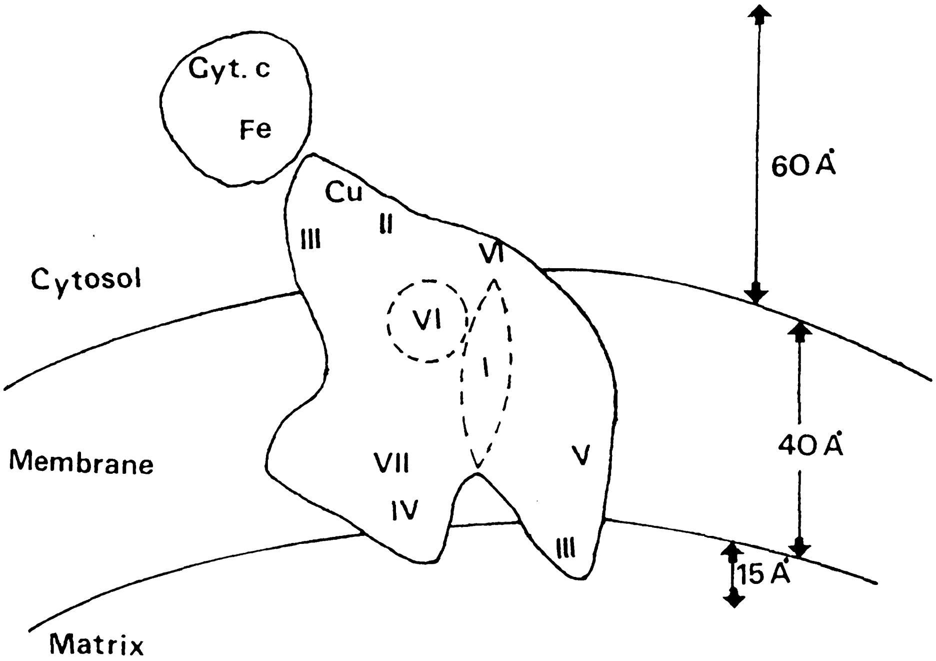
Cyt. c
Fe
Cu
II
III
VI
Cytosol
VI
I
Membrane
VII
IV
V
III
Matrix
60 Å
40 Å
15 Å

Figure 1.1: The geometrical arrangement of the polypeptides (subunits) in cytochrome c̲ oxidase in the mitochondrial membrane. Subunits I and II contain the two prosthetic heme groups and the two copper atoms. The binding site for ferrocytochrome c̲ is located on the outside of the membrane in close contact with the electron acceptor site, cytochrome a̲/Cu_A. Adapted from Azzi (1980).

con

cyt

Cu_A

exp

II

and

dep

loc

ret

Pen

oxi

et

sub

The

pro

a r

int

ele

dim

197

dom

the

pro

mem

inn

(Te

contain the four prosthetic groups, with cytochrome a, cytochrome a_3, and Cu_B most likely located in subunit I and Cu_A in subunit II (Winter et al., 1980). From labelling experiments with $^{51}Cr^{2+}$, it has been suggested that subunit II contains the electron entry site from cytochrome c (Jones and Wilson, 1984). It has been recently suggested that the depleted subunit III oxidase does not exhibit proton translocation even when 50% of the electron transfer activity is retained (Thelen et al., 1985; Nalecz et al., 1985; and Penttila, 1983). However, experiments with bacterial oxidase, with two subunits (I,II), from Paraccocus (Soliocz et al., 1982), have made this interpretation of the role of subunit III on the oxidase proton pump somewhat uncertain. The general consensus about the role of subunit III in the proton pumping activity of cytochrome oxidase is that it has a regulatory function for the pump rather than being an integral part of the mechanism (Thompson et al., 1985).

The structure of cytochrome oxidase has been studied by electron microscopy and image reconstitution of a two-dimensional crystalline array of the protein (Fuller et al., 1979 & 1982). Results from these studies revealed a three domain structure in the form of a Y shaped molecule, where the arms of the Y each span the membrane bilayer and protrude approximately 15-25 A° on the matrix side of the membrane; the stalk of the Y extends from the mitochondrial inner membrane into the intermembrane space (see Figure 1.1) (Terrence et al., 1985; and references therein). The aggre-

ga
ha
re
mu
19
cy
19
ma
en
hi
ap
(G
al
mo
fo
re
st
to
pr
19
st
pu
ac
ot
cy
mo
un

gation state of the oxidase has been controversial, but it has been recently proposed from experiments with vesicle reconstituted oxidase that the enzyme from bovine heart muscle is a dimer of cytochrome $\underline{aa}_3$ molecules (Capaldi, 1982; and references therein). The monomeric form of cytochrome oxidase from rat liver (Thompson and Ferguson, 1983) and bovine (Nalecz et al., 1983; Suarez et al., 1984) materials have been also described. Monomers of bovine enzyme could be prepared by treatment of the oxidase with high detergent concentrations and alkaline pH, which appears to be correlated with the loss of protein subunits (Georgevich et al., 1983). Kinetics studies (Reinhard et al., 1985) of cytochrome oxidase activity in its dimeric and monomeric forms indicate biphasic kinetics for the dimeric form and monophasic behavior towards the oxidation of reduced cytochrome $\underline{c}^{2+}$ in the momeric form. Changes in ionic strength, enzyme concentration, and type of detergent used to suspend the oxidase appear to influence the association properties of the oxidase (Thompson and Ferguson-Miller, 1983; Suarez et al., 1984; Thompson et al., 1985). The dimer structure appears to be necessary for the enzyme proton pumping activity, whereas the monomer structure may only be active in electron transfer (Wikstrom et al., 1981). On the other hand, recent kinetics experiments on the monomeric cytochrome oxidase from shark have suggested that the monomer containing the four metals is the basic functioning unit for dioxygen reduction (Bickar et al., 1985;

Ge

di
ar
te
ab
ad
ef
of
be
al
Oh
es
an
al

gi
st
El
of
19
cy
an
un

ri
hi

Georgevich et al., 1983).

The determination of the heme a-copper (or heme-heme) distances within the isolated oxidase has been an active area of research for the last few years. Two physical techniques, electron paramagnetic resonance (EPR) and X-ray absorption spectroscopy (EXAFS), have been widely applied to address these questions. For instance, by studying the effect of cytochrome a on the EPR-spin relaxation properties of NO-bound ferrocytochrome a_3, a distance of 15-20 A° between the irons of the two hemes was estimated (Boelens et al., 1984; Scholes et al., 1984; Brudvig et al., 1984; Ohnishi et al., 1981). Similarly, a distance of 8-12 A° was estimated between Cu_A and cytochrome a, while between Cu_B and cytochrome a_3 this appears to be ~3-4 A° (Stevens et al., 1982; Naqui et al., 1986).

The interaction of cytochrome oxidase and its physiological electron donor, reduced cytochrome c, have been studied by fluorescence measurements (Dockter et al., 1978). Electron transfer is believed to occur through the heme edge of cytochrome c (Timkovich,1980; Britain and Mattews, 1986) to the electron acceptor pole of cytochrome oxidase, cytochrome a/Cu_A. The precise distance between the heme c and the oxidase electron accepting center is still uncertain.

In addition to the mammalian mitochondrial and bacterial oxidases, cytochrome oxidase has been also studied in higher plant mitochondria (Denis, 1981; Dutch et al., 1986).

Initial results reported by Denis and Clore (1981) and Denis and Richaud (1982) suggested the possibility of differences in the heme $\underline{a}_3$-Cu_B environment in the plant system. Their results on the CO recombination studies in fully reduced cytochrome oxidase after low-temperature flash photolysis revealed a multiphasic rebinding of different conformers in the heme $\underline{a}_3$/Cu_B site (Denis and Richaud, 1982). Near infrared studies on the components of plant mitochondria (Richaud and Denis, 1984) reveal a reduced minus oxidized difference spectrum assigned to Cu_B, whereas in the mammalian material no Cu_B signal is observed. Interestingly, recent EPR studies on this plant material (Denis et al., 1984) suggested that the antiferromagnetic coupling responsible for heme $\underline{a}_3$ and Cu_B being EPR silent in the resting state of bovine oxidase (Tweedle et al., 1978) was not apparently present in resting whole plant mitochondria.

Recently, another plant oxidase, that from etiolated corn seedlings, was successfully isolated with high activity in the laboratory of Prof. Sheilagh Ferguson-Miller (Ingle, R. and Ferguson-Miller S., Michigan State University, unpublished results). The resonance Raman vibrational analysis of maize mitochondria and isolated corn protein was conducted in our laboratory yielding surprising results on the cytochrome $\underline{a}$ heme structure (Dutch et al., 1986). The optical absorption spectra of this enzyme, as well as our RR analysis, indicate that the heme $\underline{a}$ environment of maize

cy
en
fo

to
co
ce
nit
lig
equ
ce
by
for
sit
CN-
tha
mag
Cau

sho
mor
spe
as
por

cytochrome a is altered as compared to the bovine heart enzyme, suggesting that this change is associated with the formyl substituent of the heme a porphyrin ring.

B. Metal Centres: Structure and Protein Environment

Cytochrome oxidase catalyzes the reduction of dioxygen to water by using two different metals, heme iron and copper, which are organized in three different redox centers: cytochrome a is low-spin and six-coordinate with nitrogen from histidine residues as its fifth and sixth ligands (Martin et al., 1985) and is in rapid redox equilibrium with the EPR visible Cu_A(S=1/2). The third redox center, thecytochrome a_3/Cu_B binuclear site, is reduced by cytochrome a /Cu_A. This binuclear center is responsible for the binding and reduction of dioxygen and is the binding site for a number a small respiratory inhibitors such as CO, CN^- , NO, HN_3^-, and $HCOO^-$. Recently, it has been suggested that cytochrome oxidase preparations may contain zinc and magnesium in addition to Cu and Fe (Einarsdottir and Caughey, 1984 & 1985).

The structure of the heme a porphyrin macrocycle is shown in Figure 1.2A, where it is compared with that of the more commonly occurring protoheme species. The protoheme species contains vinyl groups at positions 2 and 4, as well as propionic groups at positions 6 and 7, with the remaining porphyrin positions occupied by methyl groups. In contrast,

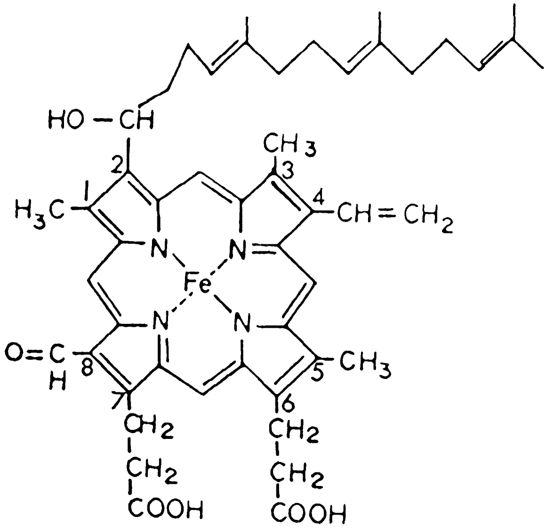
HO – CH
H$_3$C
CH$_3$
CH=CH$_2$
O=C
H
CH$_3$
CH$_2$
CH$_2$
COOH
CH$_2$
CH$_2$
COOH
1
2
3
4
5
6
7
8
N
N
N
N
Fe

heme a

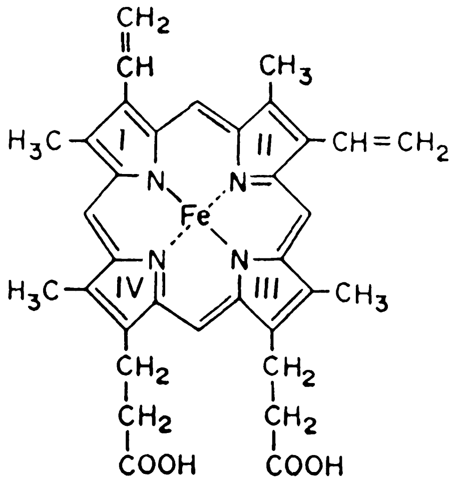
CH$_2$
CH
CH$_3$
H$_3$C
CH=CH$_2$
H$_3$C
CH$_3$
CH$_2$
CH$_2$
COOH
CH$_2$
CH$_2$
COOH
I
II
III
IV
N
N
N
N
Fe

protoheme

Figure 1.2: The molecular structure of heme a and protoporphyrin IX. The conventional heme substituent position numbering is indicated for heme a. Porphyrin pyrrole ring numbering is indicated for protoheme.

for heme a two major structural differences are present: the vinyl group at position-2 in protoheme has been replaced in heme a by a hydroxy-farnesyl group, and the methyl group at position 8 in protoheme has been oxidized to a formyl group in the heme a macrocycle. Owing to the more delocalized electronic distribution of the formyl and vinyl groups, and to the well known electron withdrawing capabilities of the C=O group (Vinogradov and Linell, 1972), it is expected that the optical absorption spectra of cytochrome oxidase will be significantly altered as compared to hemoglobin and myoglobin hemeproteins. Indeed, protoheme derivatives show α-band maxima in the range from 545-565 nm while cytochrome oxidase heme a derivatives display α-bands which range from 588 nm to 598 nm.

The electronic optical absorption spectra of oxidized and reduced cytochrome oxidase are presented in Figure 1.3 (Vanneste, 1967; Halaka, 1981). The uv- and visible regions of the spectrum are dominated by the heme chromophores of cytochrome a and cytochrome a_3, and are dependent on changes on the redox and spin state of the heme iron. By assuming no optical interactions between cytochromes a and a_3 and by using difference spectroscopy on ligated oxidized and reduced cytochrome a_3, Vanneste (1967) was able to separate the individual contributions of cytochrome a and cytochrome a_3 to the optical absorption spectrum of cytochrome oxidase. However, it was recognized by magnetic circular dichroism (MCD) (Palmer et al., 1976; Babcock et al., 1976) and

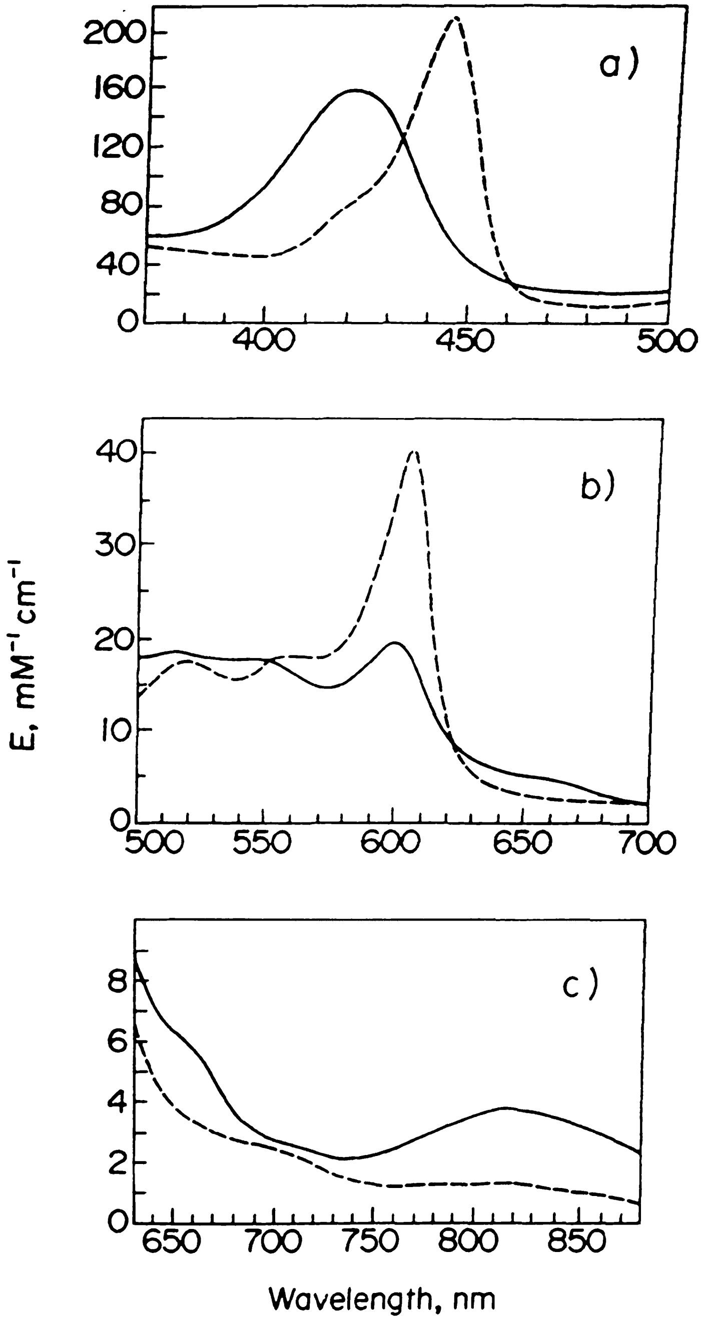

Figure 1.3: Electronic optical absorption spectra of oxidized (——) and reduced (----) cytochrome c oxidase in the Soret, visible, and near-IR regions. Extinction coefficients are expressed per enzyme functional unit containing two hemes and two copper atoms. The broad band at 830 nm is attributed to Cu_A. Similarly, the stronger shoulder at ~ 662 nm is attributed to the Fe_{a3}-L-Cu_B binuclear center. Reproduced from Halaka (1981).

resonance Raman (Babcock et al., 1981) experiments that strong redox interactions between cytochrome a and cytochrome a_3 were present. These results came from anaerobic redox titrations followed by MCD measurements (Palmer et al., 1976; Babcock et al., 1976). Similarly, resonance Raman spectroscopy (Babcock et al., 1981) experiments showed that cytochrome a and cytochrome a_3 are indeed spectrally distinct in both the absence or presence of ligands, and confirmed Vanneste's original work.

In addition to the heme a groups, the copper ions (mainly Cu_A) also contribute to the optical absorption spectrum of resting cytochrome oxidase. The near infrared region of beef heart cytochrome oxidase displays a broad and weak band centered at 830 nm ($\Delta\varepsilon = 2$ mM^{-1} cm^{-1}) (see Figure 1.3), assigned to oxidized Cu_A (Wharton and Tzagoloff, 1964; Yong and King, 1972), which vanishes upon copper ion reduction. The contribution of Cu_B to the 830 nm band has been estimated to be ~15% (Powers et al., 1979); however this falls within the range of experimental uncertainty (Beinert et al., 1980).

The spectral properties of the four metal ions have been most widely studied by electron paramagnetic resonance (EPR) spectroscopy owing to the fact that both the heme groups and the copper atoms may be identified in the EPR spectra. In the case of oxidized resting cytochrome oxidase, the low-spin, six-coordinated cytochrome a contributions are observed with g-values at 3.03, 2.213, and 1.5. The Cu_A

contribution is seen as an intense signal with a g-value of ~2.0 (Hartzell and Beinert, 1976; Aasa et al., 1976). The EPR signal from Cu_A was found to be unique for cytochrome oxidase (Aasa et al., 1976; and references therein) in that it displays low g-values (g=2.18, 2.03, 1.99), no resolvable copper hyperfine structure, and unusual EPR-signal saturation properties (its EPR signal is easily saturated at 10K in contrast to other Cu^{II} complexes). The unusual Cu_A EPR properties were suggested to originate from a unique ligand coordination (Chan et al, 1979). To account for these Cu_A spectral properties, Stevens et al. (1982) conducted electron nuclear double resonance (ENDOR) experiments on ^{15}N-isotopically substituted yeast cytochrome oxidase. Their findings reveal the presence of methylene protons of one or two cysteines and the presence of at least one nitrogeneous ligand from a histidine residue. Accordingly, Cu_A ligation with two cysteine-sulfur ligands and two histidine-nitrogen ligands was proposed (Stevens et al., 1982). A recent comparison of the amino acid sequence of subunit II of cytochrome oxidase with subunit II of a series of blue copper proteins appears to indicate that Cu_A is structurally related to type I copper while Cu_B is related to type 3 oxidases (Malmstrom, 1986). In the case of Cu_B, the ENDOR data reveal strong similarities with type-3 Cu^{II} as in the case of laccase, and a ligand coordination of three nitrogens was proposed (Cline et al., 1983).

The binuclear center heme $\underline{a}_3/Cu_B$ is EPR silent in

t
b
f
(
s
b
B
r
c
s
r
t
b
n
h
i
(

a
co
ti
he
th
e
ar

a

the resting oxidized oxidase. This was initially interpreted by Van Gelder and Beinert (1969) as due to a strong antiferromagnetic coupling between the high spin heme $\underline{a}_3$ iron (S=5/2) and the Cu_B ion (S=1/2) resulting in a total S=2 system. The magnetic interaction of this binuclear center is believed to be mediated by a bridging ligand (Van Gelder and Beinert, 1969). In the optical absorption spectrum of resting oxidized cytochrome oxidase, a relatively weak band, centered at 662 nm, has been attributed to the heme $\underline{a}_3$-L-Cu_B structure interaction (Beinert et al., 1976). For fully reduced cytochrome oxidase this band disappears, indicating the decoupling of the Fe_{a3}-Cu_B interaction. Upon ligand binding to the cytochrome $\underline{a}_3$ site, the occurrence of the 662 nm band is observed for ligands that maintain the Fe_{a3} in a high-spin configuration (i.e, $HCOO^-$), whereas for ligands inducing a low-spin transition, the 662 nm band vanishes (i.e., CN^-).

Partial reduction of cytochrome oxidase removes the antiferromagnetic coupling within the binuclear Fe_{a3}-Cu_B center rendering this site EPR detectable. This allows for the formation of the g=6 high-spin signal ascribed to ferric heme $\underline{a}_3$ (probably with Cu_B in the reduced state). However, this signal is not observed during enzyme turnover (Wilson et al., 1982), which suggested that Cu_B might be optically and EPR silent in all redox states of cytochrome oxidase.

To explain the EPR spectral properties of cytochrome $\underline{a}_3$/Cu_B in the resting enzyme, Seiter and Angelos (1980) and latter Hagan (1982) suggested the possibility of a cytochrome $\underline{a}_3$/Cu$_B$ pair in which the iron is in a high-spin ferryl (Fe^{IV}) state and Cu$_B^+$ is in the reduced cuprous state. However, the accumulated data on magnetic susceptibility, MCD, RR and Mossbauer spectroscopies (Kent et al., 1982 & 1983; Babcock et al., 1979) strongly argue against this suggestion. All these data are consistent with the original proposal that cytochrome $\underline{a}_3$ is spin-coupled to the cupric copper ion as Fe$_{a3}$-L-Cu$_B$.

Recently, X-ray absorption spectroscopy (Powers, 1982) was used to study metal atoms and their immediate environment in biological membranes. The application of this technique to oxidized cytochrome oxidase was pioneered by Powers et al. (1981) and their results suggest that the iron of cytochrome $\underline{a}_3$ is coordinated at the proximal site by a histidine and at the distal site by a sulfur atom, this latter ligand being responsible for the antiferromagnetic interaction by bridging to Cu$_B$. The interpretation offered by Powers et al. (1981) relies heavily on comparison with known model compounds and on assumptions that the Cu$_B$ was comparable to the type-I "blue copper" (as in stellacyanin), and that Cu$_B$ was responsible for the absorbance at 830 nm. Type-I blue-coppers are known for their strong optical electronic transitions on the 600 nm region, which upon reduction of Cu^{II} to Cu^{I} are abolished (Siiman et al., 1976). In reduced cytochrome oxidase, the largest contribution (80-100%) to the visible absorption α-band at 605 nm arises from cytochrome a^{2+} (Lemberg, 1969; Nicholls and Chanady, 1981). In addition, type-I coppers, such as in plastocyanin (Colman et al., 1978) and azurin (Adman et al., 1978), are known to be ligand coordinated by two histidine nitrogens, at least one cysteine, and one methionine sulfur atom, arranged in a near tetrahedral geometry. Resonance Raman studies in these blue-type-I copper compounds indicate that copper-ligand stretches, ligand deformations, and metal-ligand deformations are strongly enhanced in the low-frequency (<550 cm^{-1}) region of the spectrum (Woodruff et al., 1984; Musci et al., 1985; Bovil et al., 1986). However, resonance Raman spectra in the visible region of resting, oxidized plus cyanide, mixed-valence, and reduced cytochrome c oxidase (Bocian et al., 1979; Centeno and Babcock, unpublished results; see Chapter IV) fail to show any copper-ligand related modes in the low-frequency region. Furthermore, several authors have convincingly established that Cu$_A^{2+}$ is the responsible metal for the 830 nm band (Greenwood et al., 1983).

C. Chromophore Geometry and Ligand-Coordination

The main geometrical disposition, proposed coordination, and ligand binding parameters of cytochrome a /Cu$_A$ and cytochrome a$_3$/Cu$_B$ are displayed in Figure 1.4 (Brunori and Wilson, 1982; Callahan, 1983). Cytochrome a, as previously mentioned, is always in its low-spin, six-coordinated configuration independent of the iron redox

Figure 1.4: Geometry and coordination properties for cytochrome a, cytochrome a_3, Cu_A, and Cu_B in cytochrome c oxidase. Metal distances and Cu-ligand coordination geometries as suggested by Powers et al. (1981). Heme a chromophore and Cu_A contributions to the optical absorption spectra of resting and reduced cytochrome c oxidase as estimated by Vanneste (1967) and Beinert et al. (1972), respectively. Electron paramagnetic resonance (EPR) and carbonyl vibrational parameters as investigated by Babcock and coworkers (1978, 1981, and 1983). The identity of the bridging ligand (L) within the Fe_{a3}-Cu_B binuclear center is unknown; however, a sulfur ligand has been proposed based on EXAFS studies (Powers et al., 1981).

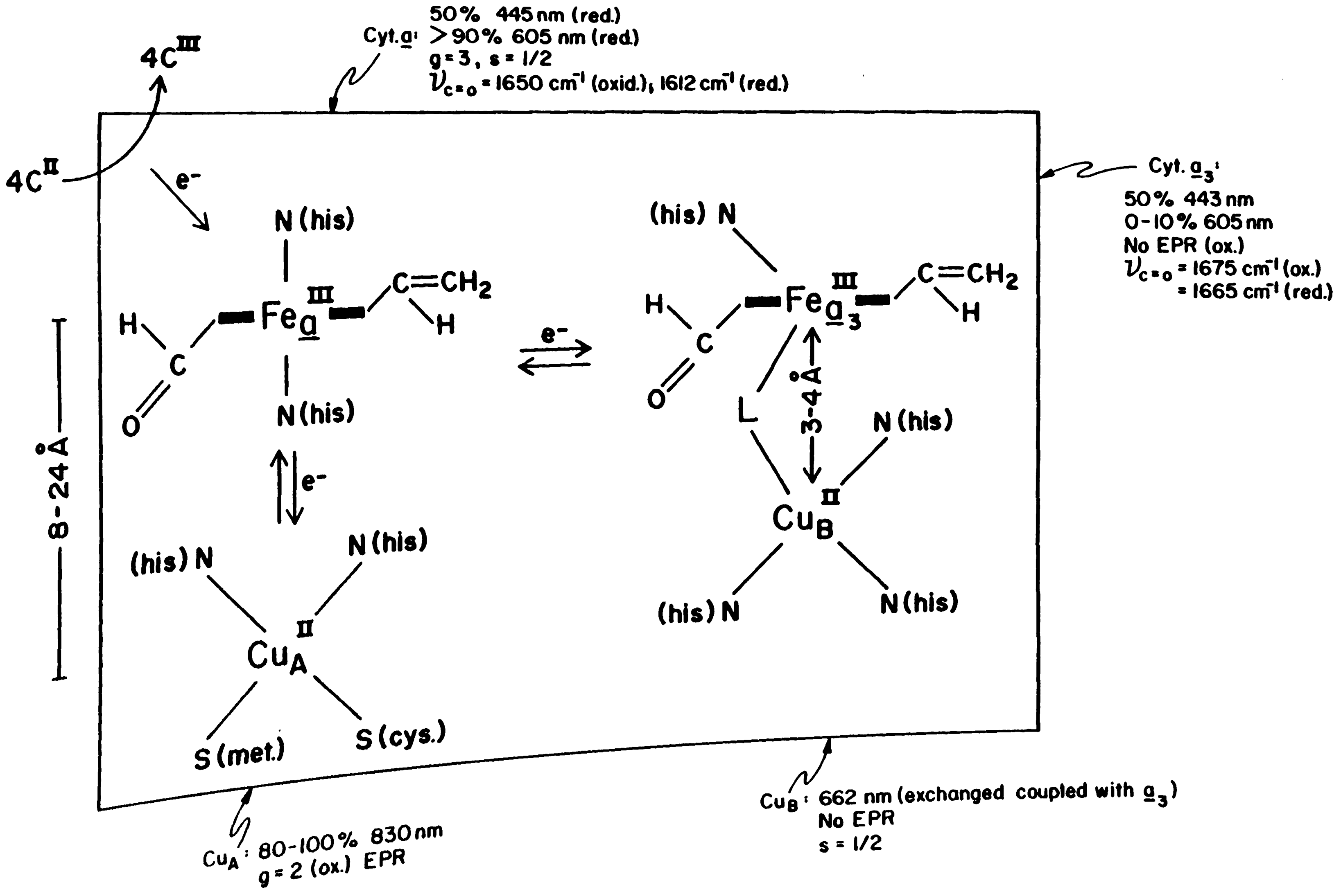

Cyt. a: 50% 445 nm (red.) >90% 605 nm (red.) g = 3, s = 1/2 $\nu_{c=o}$ = 1650 cm^{-1} (oxid.); 1612 cm^{-1} (red.)

Cyt. a$_3$: 50% 443 nm 0-10% 605 nm No EPR (ox.) $\nu_{c=o}$ = 1675 cm^{-1} (ox.) = 1665 cm^{-1} (red.)

Cu$_B$: 662 nm (exchanged coupled with a$_3$) No EPR s = 1/2

Cu$_A$: 80-100% 830 nm g = 2 (ox.) EPR

4C^{III}
4C^{II}
e$^-$
N (his)
Fe$^{III}_{a}$
C=CH$_2$
H
H
C
O
N (his)
e$^-$
(his) N
N (his)
Cu$^{II}_{A}$
S (met.)
S (cys.)
e$^-$
(his) N
Fe$^{III}_{a_3}$
L
3-4 Å
N (his)
Cu$^{II}_{B}$
(his) N
N (his)
8-24 Å

st

at

an

al

ge

co

19

wa

ac

EP

pr

st

co

li

un

oc

re

cy

hi

si

co

op

cy

fr

th

en

state (i.e., ferric or ferrous Fe a). Its associated Cu_A atom appears to be ligated by two cysteine sulfurs ligands and two histidines nitrogens in the Cu^{2+} state (Stevens et al., 1982). However, the redox state and ligand-coordination geometry around the Cu_A in resting oxidase are matters of controversy since, on the basis of EXAFS (Powers et al., 1981) and MCD (Greenwood et al., 1983) studies, a Cu^{2+} state was preferred. On the other hand, results from the amino acid sequencing of subunit II and studies on the unusual Cu_A EPR properties (Steffens and Buse, 1983; Chan et al., 1979), propose a Cu_A^+ state. Cytochrome a_3 in its resting oxidized state is six-coordinate, high-spin (S=5/2) and exchange coupled with its associated Cu_B partner through a bridging ligand. The identity of this bridging ligand is still unknown, although Powers et al. (1981) have suggested the ocurrence of a sulfur ligand based upon EXAFS studies on resting cytochrome c oxidase. In its reduced form cytochrome a_3 is five-coordinate, high-spin (S=2) with histidine nitrogen as the proximal ligand and with the sixth-ligand distal position available for further coordination.

The carbonyl group at position-8 contributes to the optical absorption properties and vibrational spectrum of cytochrome a and cytochrome a_3. Resonance Raman evidence from heme a model compounds has convincingly established that the formyl group of cytochrome a lies in a hydrophobic environment buried inside the protein surroundings

(VanS

cytoc

hydro

resid

commu

the p

(C=0.

stron

ion,

H-bon

Calla

III.

oxida

and M

the a

as an

in th

mecha

indic

imide

(Proc

the c

Moron

with

(VanSteelandt-Frentrup et al., 1981). However, for cytochrome a the carbonyl group appears to be involved in a hydrogen-bonding interaction with a protein polypeptide residue which serves as a structural intermediary in communicating redox events originating at the heme iron to the protein surroundings. The strength of this formyl (C=O...protein) hydrogen-bond interaction was observed to strongly depends on the redox state of the cytochrome a iron ion, and accordingly, a proton pump model that relies on a H-bond geometrical change was proposed (Babcock and Callahan, 1983).

III. Proton Pumping

Despite some arguments about the function of the oxidase as a redox-linked proton pumping system (Mitchell and Moyle, 1983; Lorusso et al., 1979; Papa et al., 1983), the available data strongly support proton pumping activity as an integral part of this mitochondrial terminal enzyme.

Subunit III has been reported to play an important role in the electron-transfer activity and proton pumping mechanism of oxidase from eukaryotic (mammalian) cells, as indicated by inhibitory experiments with dicyclohexylcarbo-imide (DCCD), whose binding site was located in subunit III (Prochaska et al., 1981). DCCD is a well known inhibitor of the cytochrome oxidase proton pumping activity (McGovern-Moroney et al., 1984; Casey et al., 1979). In experiments with oxidase from eukaryotic cells depleted of subunit III it

tr

ac

al

gr

su

Th

ox

ba

su

ac

Yo

cy

tr

cy

of

me

pr

cy

re

ad

in

as

wh

(W

Ra

it was observed that the oxidase retains its electron transfer activity but was totally deprived of proton pumping activity (Penttila, 1983; Thelen et al., 1985; Suarez et al., 1984; Prochaska and Reynolds, 1986). However, other groups had reported a partial proton pumping activity from subunit III depleted bovine oxidase (Puttner et al., 1985). The suggestion of subunit III being an integral part of the oxidase proton pump is also contradicted by experiments with bacterial cytochrome oxidase, which apparently does not have subunit III but nevertheless displays full proton pumping activity (Solioz et al., 1982; Sone and Hinkle, 1982; Yoshiba and Fee, 1984).

A simplified scheme of the proton pumping mechanism of cytochrome oxidase is depicted in Figure 1.5. Overall, the transfer of electrons from reduced cytochrome c to the cytochrome a/Cu_A metal active site is linked to the uptake of mitochondrial protons from the matrix side of the membrane and their subsequent release to the cytosol side, presumably triggered by conformational changes at the cytochrome a/Cu_A metal active sites. To complete the reduction of oxygen at the cytochrome a_3/Cu_B binuclear site, additional protons from the interior of the protein are used in the subsequent formation of H_2O. Cytochrome a and its associated Cu_A have both been suggested to serve as the site where the oxidase redox link to the proton pump occurs (Wikstrom et al., 1981). This is supported by resonance Raman studies, EPR, and other spectroscopic approaches used

CYTOSOL + Cyt. c^{2+}

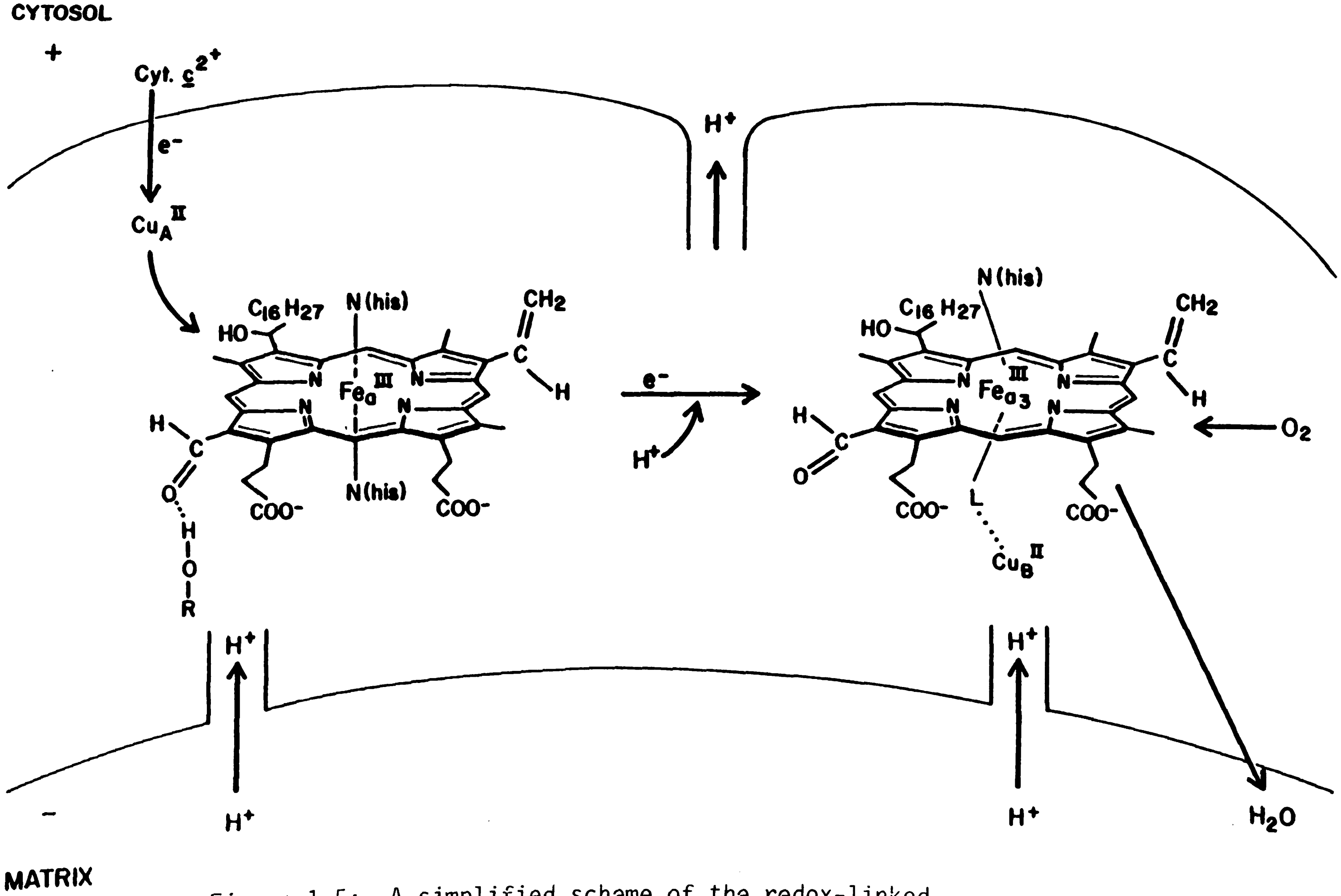
CYTOSOL
+
Cyt. c 2+
e-
Cu A II
C16 H27
HO
N(his)
Fe a III
N
N(his)
CH2
C
H
O
H
O
R
COO-
COO-
H+
e-
H+
N(his)
Fe a3 III
L
Cu B II
O2
H2O
H+
H+
H+
H+
–
MATRIX

Figure 1.5: A simplified scheme of the redox-linked proton pumping activity in cytochrome c oxidase. R denotes a protein H-donor group.

to
Cu
(C
Bl
ha
an
pr
Ra
di
he
pr
mo
cy
st
he
ad
ca
su
di
th
qu
et
th
su
cy
of
an

to study the molecular protein environment of the heme a and Cu_A sites in cytochrome oxidase and its derivatives (Callahan and Babcock, 1983; Babcock and Callahan, 1983; Blair et al., 1986; Gelles et al., in press). Two models have been proposed, one involving the heme a of cytochrome a and the other Cu_A, as individual molecular sites for the proton pumping mechanism. On the basis of resonance Raman spectroscopy, Babcock and coworkers had proposed a direct mechanism in which the peripheral formyl group of heme a is involved in a hydrogen bond interaction with a protein residue acting as the H-donor. In this molecular model, the hydrogen-bonded proton is pumped during the redox cycle, with the strength of the C=O...H(protein) H-bond strongly dependent upon the redox level of the Fe_a atom of heme a. Recently Copeland and Spiro (1986) presented additional evidence for the involvement of the cytochrome a carbonyl group in a H-bond interaction as initially suggested by Babcock and Callahan (1983). However, the direct participation of the cytochrome a carbonyl group in the oxidase redox-linked proton pumping mechanism was questioned by the above authors and recently by Argade et al. (1986). On the other hand, the molecular basis of the cytochrome oxidase proton pump had been recently suggested to occur at the Cu_A site rather that at the cytochrome a carbonyl site. This was proposed on the basis of extended x-ray absorption fine structure (EXAFS) studies and EPR data on the coordination and ligation properties of

Cu_A

al.

Cha

eve

pro

the

vic

pro

met

use

cyt

dou

Our

inv

int

dat

Cu_A

inv

IV.

ble

for

pro

oxi

Cu_A in cytochrome oxidase (Chan et al., 1979; Stevens et al., 1982; Blair et al., 1986; Gelles et al., in press). Chan and coworkers had suggested a model in which redox events at the Cu_A metal site could be coupled to the oxidase proton pump through a redox-linked ligand displacement at the Cu_A metal site with a protein H-donor in the immediate vicinity of the Cu_A ligation sphere.

Both proton pumping models predict the occurrence of protein exchangeable protons in the near vicinity of the metal center active sites. To test these two models I have used resonance Raman spectroscopy and H/D exchange at the cytochrome a...protein interaction site and electron nuclear double resonance (ENDOR) spectroscopy at the Cu_A metal site. Our results with resonance Raman spectroscopy support the involvement of the cytochrome a formyl group in an H-bonding interaction with an exchangeable protein H-donor; the ENDOR data reveal the existence of exchangeable protons in the Cu_A^{2+} protein vicinity, nevertheless, their identity and involvement in the oxidase H^+-pump remains unclear.

IV. Concluding Remarks:

Cytochrome c oxidase is a multi-metal enzyme responsible for the terminal reduction of molecular oxygen in the formation of H_2O during respiration in eukaryotic and prokaryotic cells. The marked difference and complexity of oxidase from mammalian, bacteria, and plant materials is

re
co
po
be
(I
al
ap
en
ir
th
re
it
ox

ap
ar
av
Cu
an
pr
cy
tw
en
po
a
on

recognized by their differences in protein subunit composition. Thus bovine cytochrome oxidase contains 12 polypeptide subunits while bacteria cytochrome oxidase has been reported to contain one (Yoshida et al., 1983), two (Ludvig and Schatz, 1986), and three subunits (De Vrij et al., 1983). However, common features among these oxidases appear to be conserved, such as the following: (1) the enzymatic minimum functional unit contains two heme a iron-containing chromophores and two copper atoms; (2) all these oxidases catalyze the electron transfer reaction from reduced cytochrome c to molecular oxygen to produce H_2O; (3) it is widely accepted that electron transfer in cytochrome oxidase is linked to proton pumping activity.

The magnetic properties of the heme a metal sites appear to be fairly well established. Cytochrome a and Cu_A are magnetically isolated and presumably separated by an average distance of >12 A°. Cytochrome a_3 and its associated Cu_B atom are close to one another (<3-4 A°) and there is an antiferromagnetic interaction between the two. Considerable progress has been made in understanding the cytochrome a and cytochrome a_3 ligand geometries. Cytochrome a is ligated by two histidines, and these remain bound throughout the enzymatic redox cycle, while cytochrome a_3 is known to possess one histidine ligand on the proximal side but lacks a ligand on the distal side in the reduced state. Research on the ligand and coordination geometry around the metal

ce
re
at

pr
cy
ch
ox
co
a/
ab
sp
ch
cy
me

V.

sy
sp
vi
se
id
th
gr
cy
th

centers is still a matter of controversy, especially with respect to the ligand coordination around the Cu_A and Cu_B atoms.

The molecular basis of the oxidase redox-link to the proton pump is suggested to occur at the level of the cytochrome a /Cu_A metal active sites. In the following chapters, research on the spectroscopy of cytochrome oxidase, its ligand bound derivatives, and heme a model compounds is described. The H_2O/D_2O exchangeabilities of the a/Cu_A sites has also been studied. I have used optical absorption, resonance Raman spectroscopy, EPR and ENDOR spectroscopies in order to investigate the molecular characteristics and hence functional involvement of cytochrome a as well as Cu_A in the oxidase proton pumping mechanism.

V. Aims and Strategy of This Thesis:

The aims of this thesis are two-fold: (1) to develop systematic vibrational analysis of the heme a $(N\text{-}MeIm)_2$ spectra with the goal of elucidating formyl related vibrational and deformation modes, and to establish their sensitivity to in vitro H-bonding effects; (2) identification of cytochrome a H-bonding sensitive modes and the structural relationship between the cytochrome a formyl group and the redox-linked proton pumping activity of cytochrome oxidase. To obtain the neccessary information on the heme a model compounds, results on the isotopic

re
fo
gr
cy
mi
cy
Th
in

re
be
tr
re
sp

replacement at the -HC=O group (i.e., deuteration of the formyl proton and substitution of ^{18}O for ^{16}O at the formyl group of heme a) will be discussed. Identification of cytochrome a H-bonding sensitive modes will be studied by mild denaturation of cytochrome oxidase (disruption of the cytochrome a hydrogen bond) and by H/D-exchange experiments. The redox dependent incorporation of D-atoms at the protein interacting site will be studied under turnover conditions.

The ligand-structure around the copper atom and its relationship with the oxidase proton pumping activity will be studied by using electron nuclear double resonance spectroscopy with the specific aims of investigating pathways of redox-linked proton pumping through the Cu_A-coordination sphere.

I.

cy

ha

dr

li

th

to

id

mo

th

wa

ne

ti

mo

th

pr

in

at

at

in

as

my

CHAPTER II

MATERIALS AND METHODS

I. Introduction:

In order to obtain information on the structure of the cytochrome a *in vivo* active site in cytochrome c oxidase, we have conducted resonance Raman experiments on submitochondria particles, detergent-solubilized cytochrome oxidase, ligated cytochrome oxidase, and isolated, as well as synthetic, heme a model compounds. Experiments with intact mitochondria membranes were conducted with the specific aim of identifying structural effects from the cytochrome aa_3 moiety in the mitochondria surrounded protein and comparing these to the spectra obtained for purified oxidase; in this way possible contributions from other mitochondrial components that might arise from heterogeneities in the preparation can be eliminated. Our studies with isolated heme a model compounds are expected to improve our understanding of the structure of the *in vivo* active site of cytochrome a, to predict molecular influences that might affect heme-protein interactions, and to determine structural changes occurring at the heme a periphery that might be linked to redox events at the heme metal ion. To achieve our goal, we were involved in the preparation of a series of H-bonded heme a compounds as well as the preparation of isotopically substituted formyl compounds. This Chapter describes in detail these prepa

us

II.

pr

(1

pr

(p

su

(p

ho

wi

ex

of

Mc

st

ex

de

ce

:

Mi

We

10

de

parative procedures and the experimental physical techniques used in the study.

II. Materials:

A. Isolation of Cytochrome c Oxidase

Cytochrome c oxidase from beef heart mitochondria was prepared according to the procedure of Hartzell and Beinert (1974), as modified by Babcock et al. (1976). The final precipitate was dissolved in a minimum volume of 50 mM HEPES (pH 7.4) buffer containing 0.5 % lauryl maltoside. The resuspended oxidase was dialyzed against buffer of 50 mM HEPES (pH 7.4), 0.5 % lauryl maltoside and 0.1 mM EDTA for three hours, and for two more hours against the same buffer but without EDTA. This dialysis results on the removal of excess $(NH_2)_2SO_4$ and cholate. Enzyme prepared by the method of Yonetani (1960) was a generous gift from Dr. Patricia McGovern-Moroney. Both oxidase preparations were frozen and stored in liquid N_2 until use. The enzyme concentration, expressed in terms of two molecules of heme a/enzyme, was determined from the optical absorption spectrum as the reduced minus oxidized difference spectrum ($\Delta\varepsilon = \varepsilon_{605} - \varepsilon_{598} = 27\ mM^{-1}\ cm^{-1}$) (Van Gelder, 1966; Babcock et al., 1976). Mitochondria membranes used for resonance Raman experiments were resuspended in a buffer containing 0.25 mM sucrose, 10 mM phosphate (pH 7.4), and the concentration was determined at 605 nm using the reduced minus oxidized di

mM

is

ox

Th

th

ma

fr

(1

42

ca

de

19

ox

(B

he

me

sp

ab

va

az

cy

lo

co

ne

difference spectrum with an extinction coefficient of 11.5 $mM^{-1}cm^{-1}$ (Baker et al., 1987).

B. Preparation of Cytochrome c Oxidase Derivatives

Resting or native cytochrome oxidase is the enzyme as isolated. All of its redox metal centers exist in their oxidized, high-valence state (i.e.; a^{3+}/Cu_A^{2+} a_3^{3+}/Cu_B^{2+}). The Soret maximum of resting oxidase is usually observed in the range from 420 to 424 nm (the position of the Soret maximum varies from preparation to preparation); however, from the photoinduced deconvoluted spectra of Vanneste (1967), it has been shown that cytochrome a^{3+} absorbs at 427 nm while cytochrome a_3^{3+} absorbs at 415 nm. The overall catalytic activity of isolated cytochrome oxidase appears to depend upon protein purification procedures (Suarez et al., 1984) and it has been shown that, for oxidized cytochrome oxidase, three different conformations can be detected (Brudvig et al., 1981). To simplify this apparent oxidase heterogeneity, we have made use of ligand-binding experiments with the specific aims of deconvoluting the different spectral contributions of each chromophore to the optical absorption (and resonance Raman spectra) of oxidized, mixed-valence, and reduced cytochrome oxidase. We used cyanide, azide, and formate as ligands to cytochrome oxidase. While cyanide and azide convert the heme of cytochrome a_3 into a low-spin iron, formate maintains the a_3 in a high-spin configuration. To form the cyanide and azide complexes, a near neutralized solution of NaCN (pH 8.0) and NaN_3 (pH 6.2)

wa
wa
sp
lo
in
sh
co
ca
sh
an
sh
an
di
$\underline{a}^3$
ox
nm

mi
wi
cy
ac
$\underline{a}$
ox
int
of
aci

was added to the resting oxidized protein and the binding was followed by the characteristic optical absorption spectral changes. The formation of the $\underline{a}^{3+}\underline{a}_3{}^{3+}$-CN was followed by increased intensity of the 428 nm Soret band, increased intensity of the 545 nm visible band, slight blue-shift of the α-band from 599 nm to 597.5 nm, and the concomitant disappearance of the 662 nm near-IR band. In the case of the $\underline{a}^{3+}\underline{a}_3{}^{3+}$-$HN_3{}^-$ complex, while the Soret band is shifted to 428 nm, the α-band is now red-shifted to 601 nm and the 662 nm absorption retains its intensity and red-shifts to 672 nm. In the fully oxidized enzyme plus formate and the mixed-valence with formate, cytochrome $\underline{a}_3{}^{3+}$-$HCOO^-$ display absorptions at 415 nm and 662 nm. The cytochrome $\underline{a}^{3+}$ and $\underline{a}^{2+}$ transitions in these two formate-inhibited oxidase forms are observed at 427 nm and 600 nm and at 441 nm and 603 nm, respectively.

C. Alkaline and Acidic pH-Modification of Purified Cytochrome c Oxidase

pH Modification studies on oxidized (non-inhibited), mixed-valence, and reduced cytochrome oxidase were conducted with the goal of analyzing the vibrational spectrum of cytochrome a under conditions in which the H-bonding interaction has been disrupted. Modes sensitive to the cytochrome a formyl H-bonded to the protein H-donor in intact native oxidase (Callahan and Babcock, 1983) are expected to display intensity and/or vibrational frequency changes upon removal of the protein H-bonded proton. To study the enzyme under acidic conditions we used a buffer containing 50 mM MES

(

pl

pr

va

th

qu

In

va

es

of

fo

no

pl

cu

sa

th

be

fo

so

ox

15

/T

wi

ne

co

(2-N-morpholinoethanesulfonic acid). To achieve the desired pH level we used 0.1 N NaOH and 0.1 N HCl. The formation of precipitates (due to protein denaturation) at the extreme pH values (pH 4.0 and 11.5) was somewhat more problematic in the acidic treated sample. The precipitate formed was quickly removed by gentle filtration using 0.45 μM(Millipore Inc.) filters. The pH induced effects in oxidized, mixed-valence, and reduced protein derivatives were immediately established; no incubation time was required. The progress of the pH-modification effects in cytochrome oxidase was followed by the resonance Raman difference technique. The non-pH treated and the pH-modified protein samples were placed in separated compartments of a divided Raman spinning cuvette. The resonance Raman spectra of these two oxidase samples were simultaneously recorded and directly compared; the relative uncertainty in peak positions was calculated to be no greater than 0.4 cm^{-1}.

D. Redox-Cycled Cytochrome Oxidase

Redox-activated cytochrome oxidase was prepared by the following method: concentrated cytochrome oxidase was redissolved in 3-5 mls of deuterated or protonated buffer (final oxidase concentration ~80 μM), the solution was aerated for 15-20 minutes, and then reductant ascorbate (4.8 to 10 mM) /TMPD (20 μM) was added in the presence of excess dioxygen with constant stirring. After 45-60 mins of reaction, neutralized cyanide (pH(pD) 8.0) was added to a final concentration of 10 mM, and the resonance Raman spectrum of the $\underline{a}^{2+}\underline{a}_3^{3+}$-$CN^-$ complex was immediately obtained. Redox-cycled oxidase used for the ENDOR experiments was similarly treated, with the following exceptions: the oxidase concentration was 0.6 to 0.8 mM; after the reduction and reoxidation cycles the reoxidized protein was reprecipitated by increasing the $(NH_4)_2SO_4$ concentration from 0 to 43% and no cyanide was added to the redox-activated protein.

We also studied the addition of cyanide to a resting (non-redox) activated protein. For this sample, cytochrome oxidase (80 μM) was added to a D_2O/ or H_2O buffer already containing cyanide (10 mM), and the resulting sample was incubated for 45 to 60 mins.

E. Preparation of Heme a Derivatives

The chloride complex of ferric heme a (high-spin, pentacoordinated) was isolated by acid/acetone extraction from purified cytochrome oxidase (Babcock et al., 1979). Low-spin, six-coordinate and high-spin, six- and five-coordinate heme a model compounds were prepared according to Van Steelandt-Frentrup et al. (1981) and Callahan and Babcock (1983). The high-spin, six-coordinate ferric heme a $(DMSO)_2$ complex was produced by small additions of DMSO-d_6 to heme $\underline{a}^{3+}$ Cl^- and monitored by the optical absorption spectrum. To produce the low-spin, hexacoordinate derivative, 0.6 M N-methylimidazole was added to the freshly prepared heme $\underline{a}^{3+}$ Cl^- solution.

Incorporation of deuterium at the heme a formyl proton

(
e
4
1
0
(
h
°
wa
s
th
pe
sy
wa
pl
cm
cm
he
ac
ex

ca
to
cr
in
Tr
gl

(i.e., -CHO --> CDO) was conducted as reported by Chancellor et al. (1978). The purified heme a^{3+} Cl$^-$ was dissolved in 4.0 to 6.0 mls of a buffer consisting of 10 mM phosphate (pD 11.4), 0.07 M cetryltetramethyl ammonium bromide (CTAB), 0.001 M EDTA, and 0.6N N-methylimidazole in D_2O. Solid KCN (in a molar ratio of 3:1 KCN/heme a) was added to the above heme solution and incubated (under constant stirring) at 4 °C. To avoid precipitation in the presence of cyanide, CTAB was used instead of other surfactants such as Brij-35 or sodium dodecyl sulfate (SDS). To monitor the progrees of the exchange reaction, small aliquots (~25 µlts) were periodically taken, dissolved in the same buffer/detergent system, reduced with minimum amount of $Na_2S_2O_4$ and the RR was obtained. For a fully exchanged sample, the RR displayed a slight shift in the high-frequency region from 1633 cm^{-1} to 1629 cm^{-1} and the appearance of a new band at 1083 cm^{-1}. After the exchange was completed, the bis-imidazole heme a^{3+}(-CDO) was washed several times with a slightly acidic solution of 10 mM succinate (pD 5.8-6.0) in D_2O and extrated in CH_2Cl_2.

Reduction of heme a^{3+}(N-MeIm)$_2$ in aprotic solvents was carried out by using the "Freeze-Pump-Thaw" (FPT) technique to remove oxygen, and a methanolic solution of 2,2,2-cryptand solubilized sodium dithionite as the reducing agent in a molar ratio of 2:1 (cryptand/dithionite) (Mincey and Traylor, 1978; Van Steelandt-Frentrup et al., 1981). The glassware used for these experiments consisted of a two-side

ar
cu
di
53
sh
re
le
19
by
56
so

Ni
st
re
Cu
od
ba
ro
fo
ut
ne
st
su
ch

arm apparatus with an attached optical (1 cm pathlentgh) cuvette. Reduced heme a^{2+}(N-MeIm)$_2$ in aprotic solvents displays optical transitions at 435 nm (Soret), 510 nm, 532 nm, and 588 nm. Special care in the reduction of heme a should be exercised, since it is known that excess reductant results in the saturation of the peripheral aldehyde group, leaving a monovinyl heme macrocycle (Vanderkoii and Stotz, 1965). Chemical saturation of the formyl group was detected by a new emerging band in the optical absorption spectrum at 565 nm independent of the presence of aprotic or protic solvents.

Metal removal (i.e., iron) and insertion (i.e., Cu^{2+}, Ni^{2+}) at the free base of porphyrin a was conducted by standard procedures (Fuhrop and Smith, 1975). The iron was removed by HCl/acetic acid treatment of heme a^{3+} Cl$^-$ and the Cu^{2+} and Ni^{2+} metal ions were inserted by the acetate method. The purity and separation of the metalated and free-base porphyrin of all the compounds used in this work was routinaly carried out by thin layer chromatography (TLC), followed by Sephadex G-10 column chromatography. The utilization of Cu^{2+} and Ni^{2+}-substituted porphyrin a was neccessary in order to study the formyl C=O H-bonded structure under strong H-bonding conditions. These metal substituted derivatives of heme a are known to mimic the charateristic vibrational properties of ferric heme a^{3+}

(l
he
po

tr
gr
vi
Ch
st
is
we
19
th
pr
pr
fo
mi
ex
po
mi
H_2
am
mi
eq
so
pl
as

$(N\text{-MeIm})_2$ (Callahan and Babcock, 1983), and in contrast to heme a, they appear to be unaffected by the oxidizing potential of phenol-OH compounds.

Synthetic porphyrin model compounds that mimic the trans- structural disposition of the heme a vinyl-formyl groups were also studied. The free base of 2,6-dipentyl-4-vinyl-8-formyl porphyrin was a generous gift from Prof. C.K. Chang's research group (Michigan State University). The structure of this porphyrin is shown in Figure 2.1, where it is compared with the porphyrin a structure. Cu^{2+} and Ni^{2+} were inserted by standard procedures (Fuhrop and Smith, 1975). Replacement of ^{16}O for ^{18}O at the formyl group of this model compound was conducted by hydrolysis of the protonated Schiff's base porphyrin derivative in the presence of ^{18}O-labelled water ($H_2{}^{18}O$, 98% ^{18}O) by the following procedure. The Schiff's base was prepared by mixing ~20-30 mg of Cu^{2+} ($-CH^{16}O$) porphyrin with a four-fold excess of N-butylamine (Ward et al., 1983). The Cu^{2+} porphyrin/amine solution was allowed to react for ~45-60 mins under an inert (Ar) atmosphere. Since any presence of H_2O is expected to establish an equilibrium between the amount of C=O available and the -C=N formed, an azeotropic mixture of benzene/CH_2Cl_2 was used, thus shifting the equilibrium towards the formation of the Schiff base. The solution was refluxed for 6-10 hours resulting in the complete formation of the Cu^{2+} (-C=N) Schiff's base porphyrin, as evidenced by the absorption spectrum shown in Figure 2.2,

Figure 2.1: Structures of free *base porphyrin a (1) and its porphyrin analog (2).*

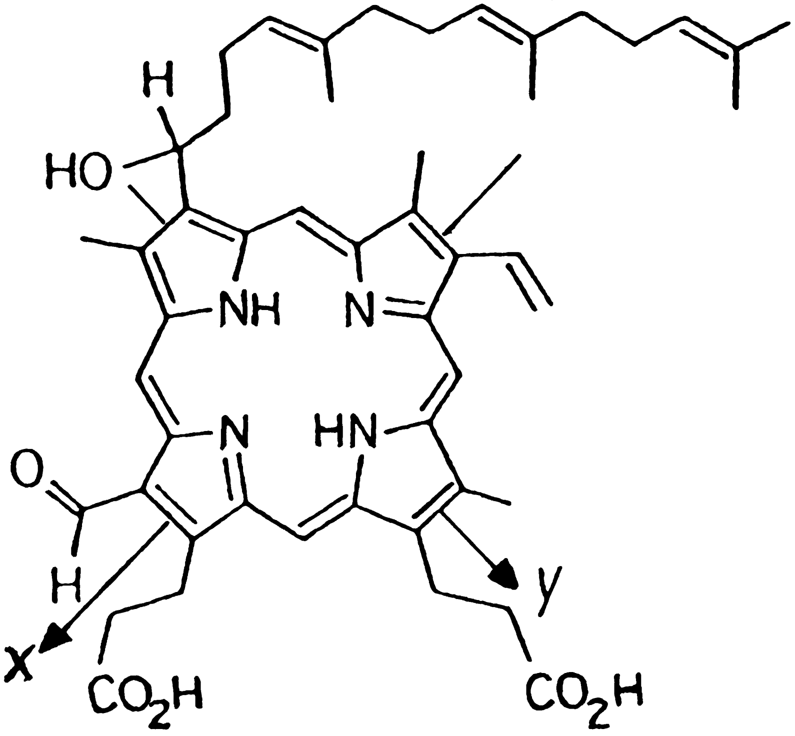
HO
H
NH
N
N
HN
O
H
x
y
CO₂H
CO₂H

1

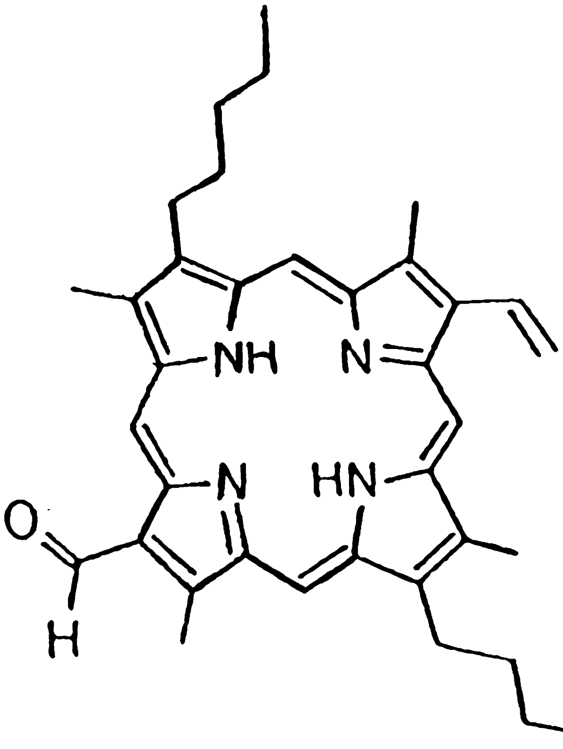

2

Figure 2.1: Structures of free base porphyrin a (1) and its porphyrin analog (2).

wi

al

on

nc

re

fo

in

st

ph

le

Th

in

op

po

III

de

na

el

lo

me

wi

mo

to

with Soret maximum at 408 nm and α-band at 586 nm (Ward et al., 1983). Addition of HCl vapors to this solution resulted on the spectrum of the protonated Schiff base ($-C=N^+H$) as noted by the split Soret (379 nm and 435 nm) and the large red-shift on the α-band to 632 nm. To reconstitute the formyl group with labelled-^{18}O, the Schiff base (dissolved in highly dry CH_2Cl_2) was placed in $H_2{}^{18}O$ under an Ar stream for 12-14 hours. After this, the aqueous and organic phases were removed by vacuum pumping at reduced pressure, leaving behind the reconstituted $Cu^{2+}(-CH^{18}O)$-porphyrin. This material was redissolved in dry CH_2Cl_2, distributed into small vials, and stored under Ar until use. The optical absorption of the Cu^{2+} ($-CH^{16}O$) and Cu^{2+} ($-CH^{18}O$)-porphyrins were identical (see Figure 2.2).

III. **Methods:**

To study cytochrome oxidase and its heme a porphyrin derivatives I have used electronic optical absorption, resonance Raman (RR), infrared (IR), and, to a lesser extent, electron nuclear double resonance spectroscopy. In the following sections a brief description of the basic theory of metalloporphyrin absorption and resonance Raman spectroscopy will be presented, with the aim of reviewing some of the most important and relevant concepts used in both techniques to interpret hemeprotein spectra.

Figure 2.2: Absorption spectra of formyl-substituted derivatives of 2,6-dipentyl-4-vinyl-8-formyl Cu^{2+} porphyrin. Solvent is dry CH_2Cl_2, except in protonated Schiff's base spectrum which contains HCl vapors. The samples are: A) Cu^{2+} porphyrin with $-CH^{16}O$; B) Cu^{2+} Schiff base (———) and protonated Schiff's base (----); and C) Cu^{2+} porphyrin reconstituted with ^{18}O at the formyl group.

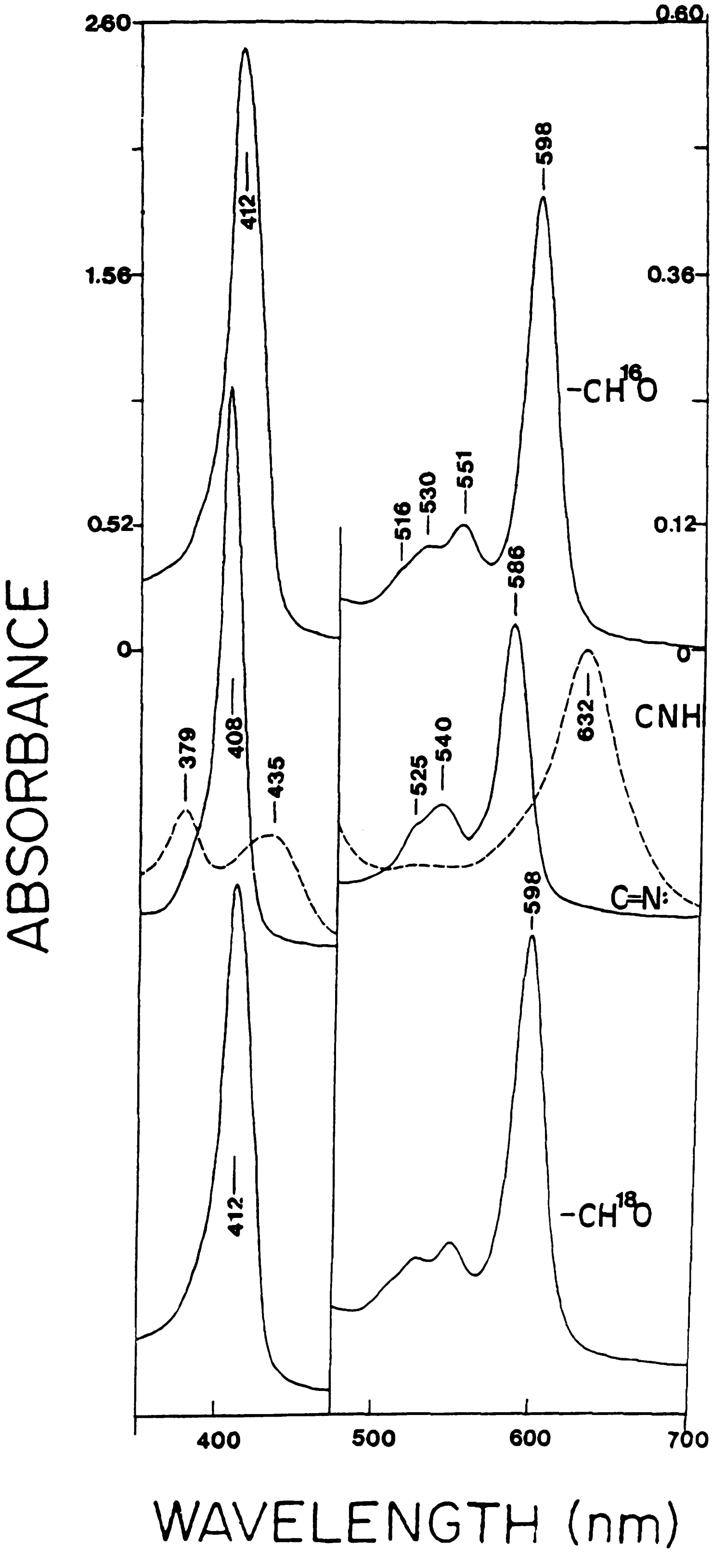
2.60
1.56
0.52
0
0.60
0.36
0.12
0
412
598
516
530
551
-CH^{16}O
586
632
CNH
379
408
435
525
540
C=N:
598
412
-CH^{18}O
400
500
600
700
ABSORBANCE
WAVELENGTH (nm)

s

t

m

t

m

(

l

Sc

of

ti

tr

el

tr

th

la

un

Eu

in

Th

fo

ta

th

vo

cu

to

A. Electronic Optical Absorption Spectroscopy

Typical optical absorption spectra of a metal-substituted heme and its metal-free (or free base) derivatives are shown in Figure 2.3. For the metal-substituted model, the absorption spectrum consists of a strong near UV-transition (~400-450 nm) called the Soret (or B) band (ε~100 mM^{-1} cm^{-1}) and weaker transitions in the visible region (~500-610 nm) called the Q-bands (ε~10-20 mM^{-1} cm^{-1}). The lowest energy Q-band is called the α-band, and like the Soret transition, is a fundamental electronic transition often referred to as the $Q_{y(0-0)}$. It arises from a transition from the zeroth vibrational level of the ground electronic state to the zeroth vibrational level of the first electronic excited state and occurs through a y-polarized transition dipole. The higher energy band to the blue of this α-band (~520 - 565 nm) constitutes a vibronic overtone labelled $Q_{y(0-1)}$. For totally symmetric hemes, i.e., those under D_{4h} point group symmetry, these two transitions are of Eu-symmetry, and hence doubly degenerate and x,y-polarized in the plane of the porphyrin plane (Gouterman, 1959). These symmetry properties have given rise to Gouterman's four-orbital model, which is widely applied in the interpretation of hemeprotein absorption spectra. The model predicts that the Soret (B-) and Q-bands arise from transitions involving electrons from the highest occupied porphyrin molecular orbitals (HOMO) of a_{1u} (π) and a_{2u} (π) symmetry, to the lowest unocupied molecular orbitals (LUMO) of e_g

Figure 2.3: Absorption spectra of free base porphyrin a (——) and Cu^{2+}-substituted porphyrin a (----). Solvent is CH_2Cl_2. The components of the the split Q-bands on the spectrum of the protonated free base porphyrin a are indicated.

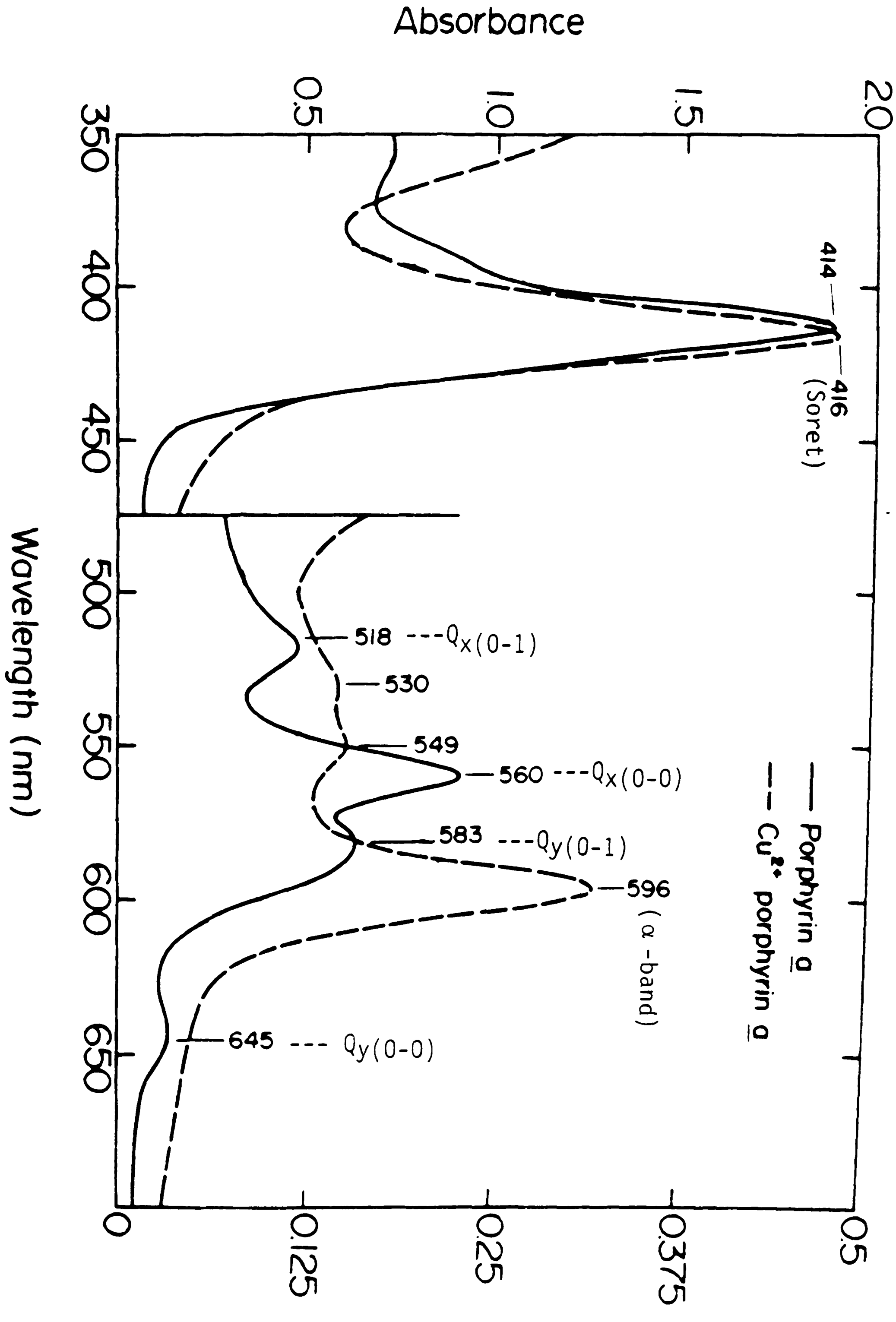
Absorbance
2.0
1.5
1.0
0.5
0.5
0.375
0.25
0.125
0
Wavelength (nm)
350
400
450
500
550
600
650
— Porphyrin a
-- Cu²⁺ porphyrin a
414
416 (Soret)
518 ---Qx(0-1)
530
549
560 ---Qx(0-0)
583 ---Qy(0-1)
596 (α-band)
645 --- Qy(0-0)

(m

of

in

th

X-

wi

il

ph

Qr

re

fo

sy

ad

19

co

ch

to

af

ti

by

fr

or

Fi

of

(π^*) symmetry (see Figure 2.4). If the molecular symmetry of the porphyrin macrocycle is perturbed by the placement of inequivalent peripheral substituents or by protonation of the opposite pyrrole nitrogens, then the degeneracy of the X- and Y-axes is usually lifted and results in split Q-bands with additional X- and Y- components. This is clearly illustrated in Figure 2.3 by the spectrum of free base porphyrin, with new energy transitions at $Q_{y(0-0)}$, $Q_{y(0-1)}$, $Q_{x(0-0)}$, and $Q_{x(0-1)}$, in order of increasing energy, respectively.

In the case of isolated heme a, with its vinyl and formyl groups trans to each other, it is expected that the symmetry of the porphyrin will be lower than D_{4h}, and hence additional optical features should be observed (Babcock, 1986). The situation is even more complicated when we consider the absorption spectrum of the in vivo cytochrome a chromophore in which heme-protein interactions are expected to influence the chromophore transitions as well.

The optical absorption spectra of heme proteins is also affected by other electronic factors such as, metal oxidation state, spin state, and axial-coordination, as well as by charge-transfer transitions. Charge-transfer bands arise from a sharing of energy between the porphyrin a_{1u} and a_{2u} orbitals and the metal d_π -orbitals (dxy and dyz) (see Figure 2.4), and are usually observed in the near-IR region of the spectra of high-spin hemes (Spiro, 1983).

Soret (B)
After C.I
b1g

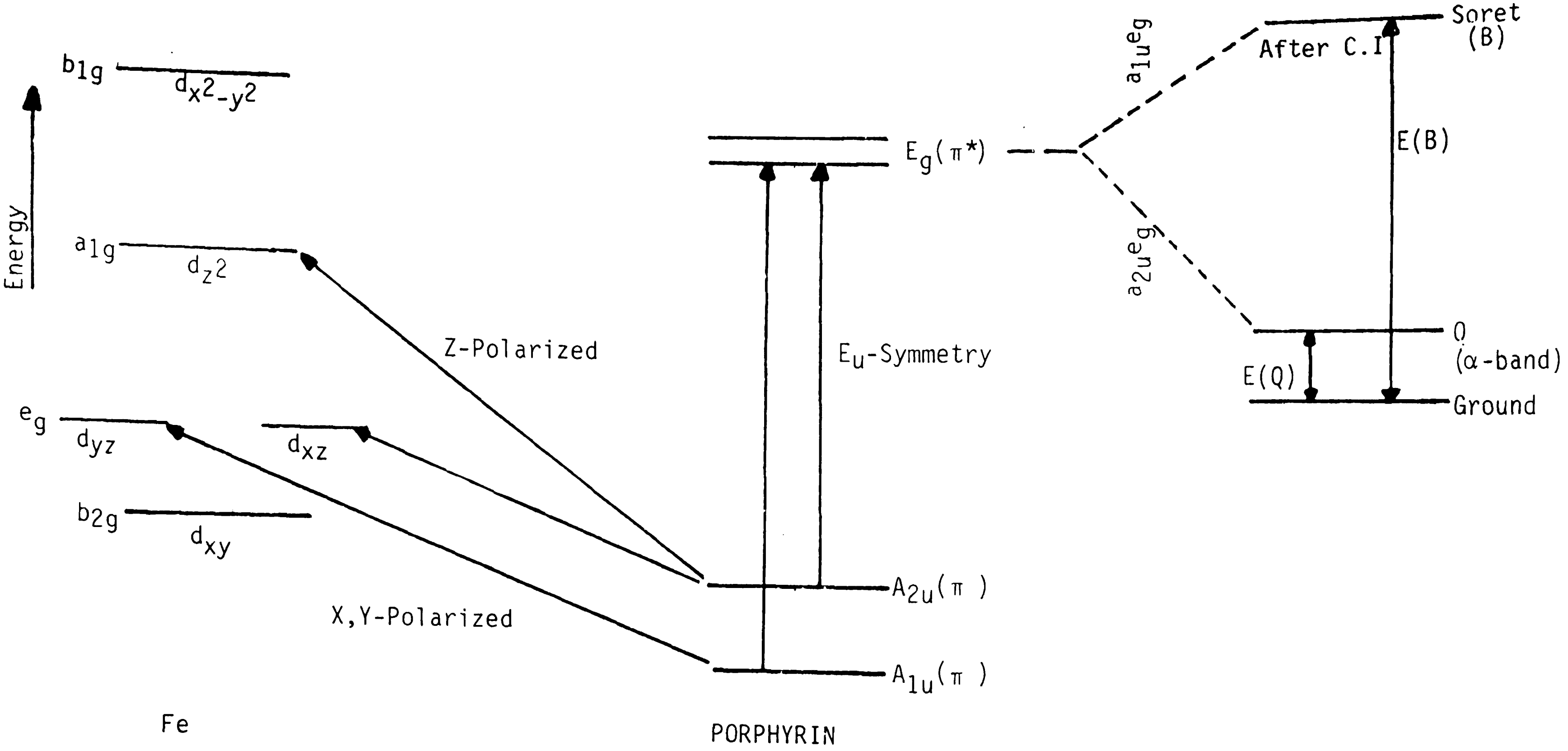
Energy
b_{1g}
$d_{x^2-y^2}$
a_{1g}
d_{z^2}
e_g
d_{yz}
d_{xz}
b_{2g}
d_{xy}
Z-Polarized
X,Y-Polarized
Fe
$E_g(\pi^*)$
E_u-Symmetry
$A_{2u}(\pi)$
$A_{1u}(\pi)$
PORPHYRIN
$a_{1u}e_g$
$a_{2u}e_g$
After C.I
Soret (B)
E(B)
Q (α-band)
E(Q)
Ground

Figure 2.4: Energy diagram for metalloporphyrin absorption spectra. The porphyrin orbitals are indicated at the center of the figure. The mixed-excited states ($a_{1u}{}^1e_g{}^1$) and ($a_{2u}{}^1e_g{}^1$) interact via configuration interaction (C.I.) to give the α-band and Soret, respectively. This is shown on the right hand side of the figure. Interaction of porphyrin orbitals (a_{1u},a_{2u}) with the metal orbitals of the appropiate symmetry (d_{xz} and d_{yz}) is shown on the left hand side of the figure.

chrom
all t
cance
absor
Perki
cuvet

tural
teris
the R
1928;
descr
that
loss
diagr
depic
spont
trans
ν_0 -
of hi
When
scatt
In Fi
as a s
radia

To interpret the optical absorption spectra of cytochrome oxidase and its heme a model compounds, we have taken all the above factors into consideration and their significance will be presented in the pertinent chapters. The absorption spectra reported here were obtained by using a Perkin-Elmer Lambda 5 UV/visible spectrophotometer. Optical cuvettes of 1 cm pathlength were routinally used.

B. Resonance Raman Spectroscopy

Raman spectroscopy is a powerful tool to study structural perturbations of molecules by following their characteristic molecular vibrations. The fundamental principle of the Raman process relies on the *Raman effect* (Raman, C.V., 1928; Krishnan and Shankar, 1981), which is a phenomenon describing the inelastic scattering of light by molecules; that is, the scattering process will result in a gain or loss of energy by the scattered molecules. A simplified diagram describing the energy of the Raman process is depicted in Figure 2.5. Notice that the normal (or spontaneous) Raman process can occur with two types of transitions; one at lower energy than the incident energy at $\nu_o - \Delta\nu$(called Stokes transitions), or a transition to state of higher energy, $\nu_o + \Delta\nu$(called anti-Stokes transitions). When the incident and scattered frequencies are equal, the scattering process is known as Rayleigh scattering ($\Delta\nu = 0$). In Figure 2.5 the resonance Raman effect is also illustrated as a scattering phenomenon in which the incident laser radiation is of sufficient energy to bridge the gap between

Figu
the
anti
impl
to t
labe

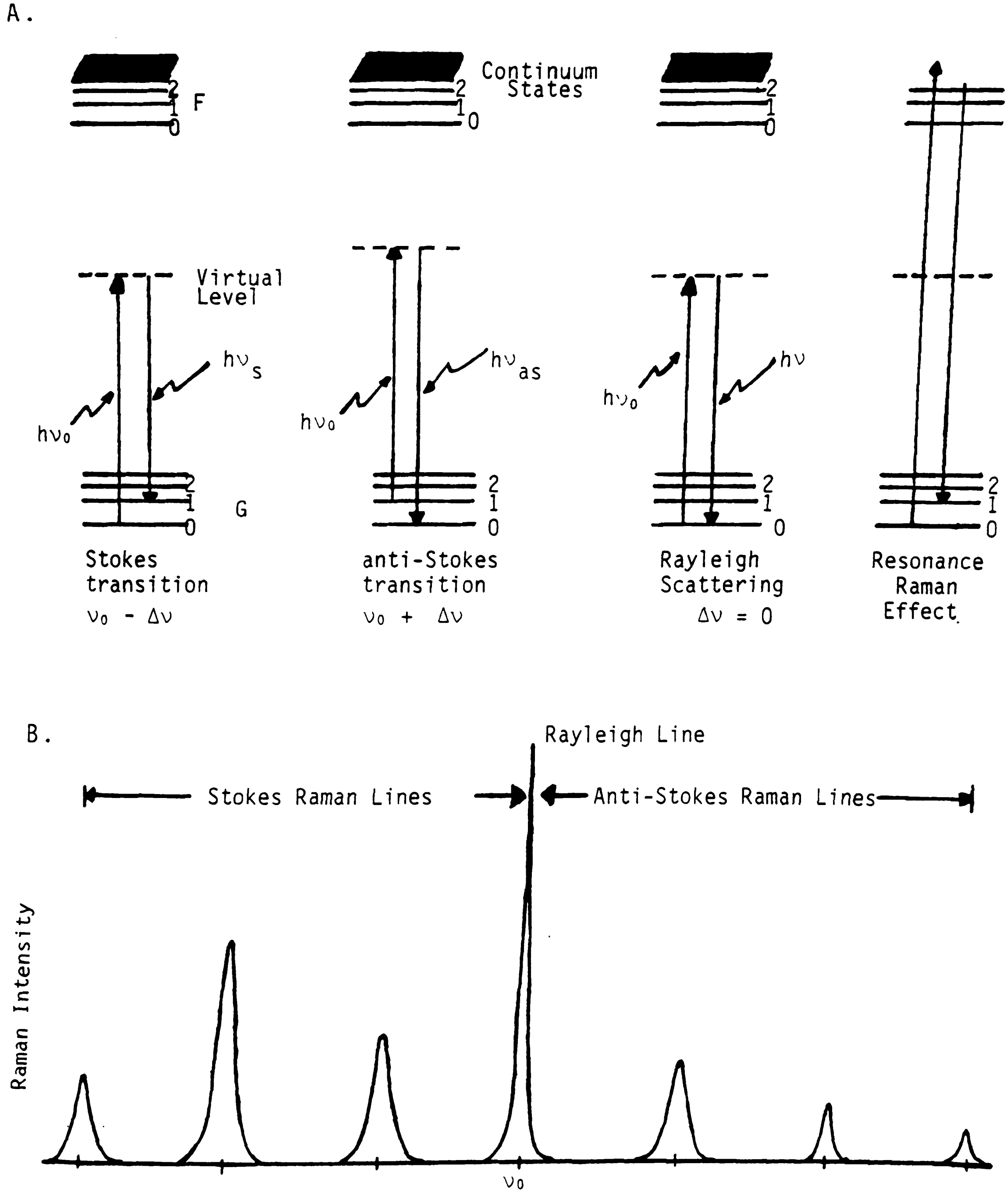
A.
Continuum States
F
2
1
0
Virtual Level
$h\nu_s$
$h\nu_0$
$h\nu_{as}$
$h\nu$
G
Stokes transition
$\nu_0 - \Delta\nu$
anti-Stokes transition
$\nu_0 + \Delta\nu$
Rayleigh Scattering
$\Delta\nu = 0$
Resonance Raman Effect
B.
Rayleigh Line
Stokes Raman Lines
Anti-Stokes Raman Lines
Raman Intensity
ν_0

Figure 2.5: Diagram illustrating Raman and Rayleigh scattering, and the resonance Raman effect (Fig. 5.A). An schematic of the Stokes and anti-Stokes Raman intensity is shown in 5.B. The dashed line in 5.A implies virtual (or intermediate) levels. The darker zone corresponds to the continuum state. The ground and excited electronic states are labelled G and F, respectively.

th
st
br
de

tr
ti
Ra
ea
of
th
Bo
Cl
tr

on
sq
fo

wh
sc
fo
st
an
po
19

the virtual (or intermediate) states and the continuum states denoted by the darker zone. The electronic and vibrational nature of the resonance Raman scattering will be described later in this section.

Returning to the definition of Stokes and anti-Stokes transitions in spontaneous Raman, even when these transitions are equally separated from the Rayleigh line, their Raman intensities may not be equal owing to the fact that each observed transition is proportional to the population of the energy level from which the transition originates; the population at each energy level is given by the Boltzmann distribution function (Rousseau et al., 1981; Clark and Stewart, 1979). This is diagramatically illustrated in Figure 2.5B.

The intensity of the Raman scattering also depends on the fourth power of the scattering frequency and on the square of the polarizability tensor, as given by the following expression:

$$I_s = \frac{8\pi \omega_s^4 I_L}{9c^4} \sum_{\rho\sigma} \left| (\alpha_{\rho\sigma})_{GF} \right|^2 \qquad (2.1)$$

where I_L is the intensity of the incident laser, ω_s is the scattering frequency, and α is the polarizability tensor for a transition from the ground $|G\rangle$ to the final excited state $|F\rangle$. The ρ and σ describe the direction (in x,y, and z Cartesian coordinates) of the incident and scattered polarizations (Rousseau et al., 1981; Clark and Stewart, 1979). In Raman spectroscopy we are primarily interested on

the

as:

whe

and

men

twe

ene

ele

a m

198

2.2

den

dif

(E

due

The

pli

the

dir

Ram

to

the

sec

str

spe

the form of the polarizability tensor, which is described as:

$$(\alpha_{\rho\sigma}) = \frac{1}{h} \sum_{i,f} \frac{\langle gn \mid R_{\sigma} \mid if\rangle\langle if \mid R_{\rho} \mid gn\rangle}{(E^{if} - E^{gn} - E_{L} - i\Gamma_{if})} \qquad (2.2)$$

where $|gn\rangle$ and $|if\rangle$ are the wavefunctions for the ground and excited state transitions, R is the electric dipole moment operator, $(E^{iv} - E^{gn})$ is the difference in energy between the ground state and excited state, E_L is the laser's energy, and Γ_{if} is the halfwidth at half-maximum of the electronic excited state transition and hence it represents a measure of the excited state ($|if\rangle$) lifetime (Spiro, 1983; Clark and Stewart, 1979). The denominator in equation 2.2 is known as the resonance Raman term, since it is evident that as the energy of the laser (E_L) approaches the difference in energy between the ground and final state $(E^{iv} - E^{gn})$, the denominator will approach zero; however, due to the damping factor Γ the term does not vanish. Therefore, resonance Raman spectroscopy is simply accomplished by tuning the laser frequency to match the energy of the electronic transition of the chromophore of interest. A direct consequence of the process is the dependence of the Raman intensity on the transition electric dipole moment, or to a first approximation, on the extinction coefficient of the transition of interest. As previously mentioned in the section of absorption spectroscopy, heme proteins have strong π ----> $\pi*$ electronic bands in their absorption spectra, and hence they appear as one of the most suitable

sys
res
tic
the
asp
tiv
Fra
mec
wit
ope
obt
imp
pro
lar
Cal

tec
Ram
unc
con
et
Kei
and
(19
Fig
com

systems to be studied by resonance Raman spectroscopy. Since resonance Raman is specific for the heme chromophore vibrations (Spiro, 1983), other modes, such as those arising from the protein amino acids can be nearly eliminated. Other aspects of resonance Raman spectroscopy are: 1) the operative mechanisms responsible for mode enhancement such as Franck-Condon and Herzberg-Teller (vibronic coupling) mechanisms; the former is responsible for modes observed with Soret (B-state) excitation, while the latter is the operative mechanism in the RR spectra of heme proteins obtained with Q-band excitation (Spiro, 1983); 2) a second important aspect in the resonance Raman spectra of heme proteins is the polarization properties of the heme molecular vibrations (Rousseau et al., 1981; Ondrias, 1980; Callahan, 1983).

1) **Resonance Raman Difference Spectroscopy**

Resonance Raman difference spectroscopy (RDS) is a technique which allows for the simultaneous detection of Raman spectra from two different samples, reducing the uncertainty in peak position from 2-3 cm^{-1} obtained with conventional spectrometers to as low as 0.1 cm^{-1} (Shelnutt et al., 1981). The technique was originally reported by Keifer and coworkers (Keifer, 1973; Keifer et al., 1975), and modified latter by Rousseau (1981) and Shelnutt et al. (1981). A block diagram of our RDS setup is depicted in Figure 2.6, and in Figure 2.7 I outline the RDS hardware components. A custom made spinning cuvette (Presicion Cells

Optical Rail
Channel 1
1

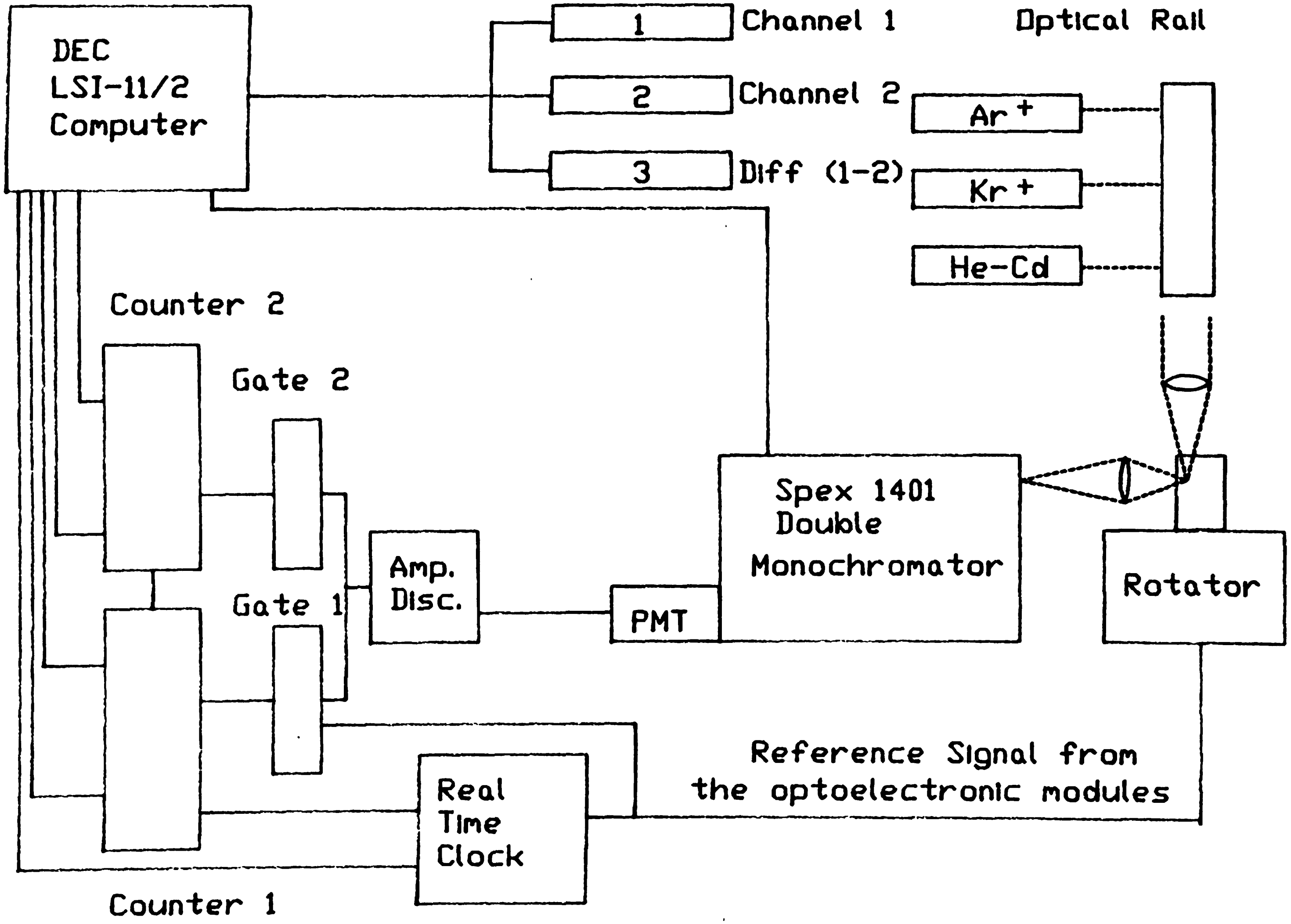
DEC
LSI-11/2
Computer
1
2
3
Channel 1
Channel 2
Diff (1-2)
Optical Rail
Ar +
Kr +
He-Cd
Counter 2
Gate 2
Gate 1
Amp.
Disc.
PMT
Spex 1401
Double
Monochromator
Rotator
Real
Time
Clock
Reference Signal from
the optoelectronic modules
Counter 1

Figure 2.6: Block diagram of the resonance Raman difference apparatus.

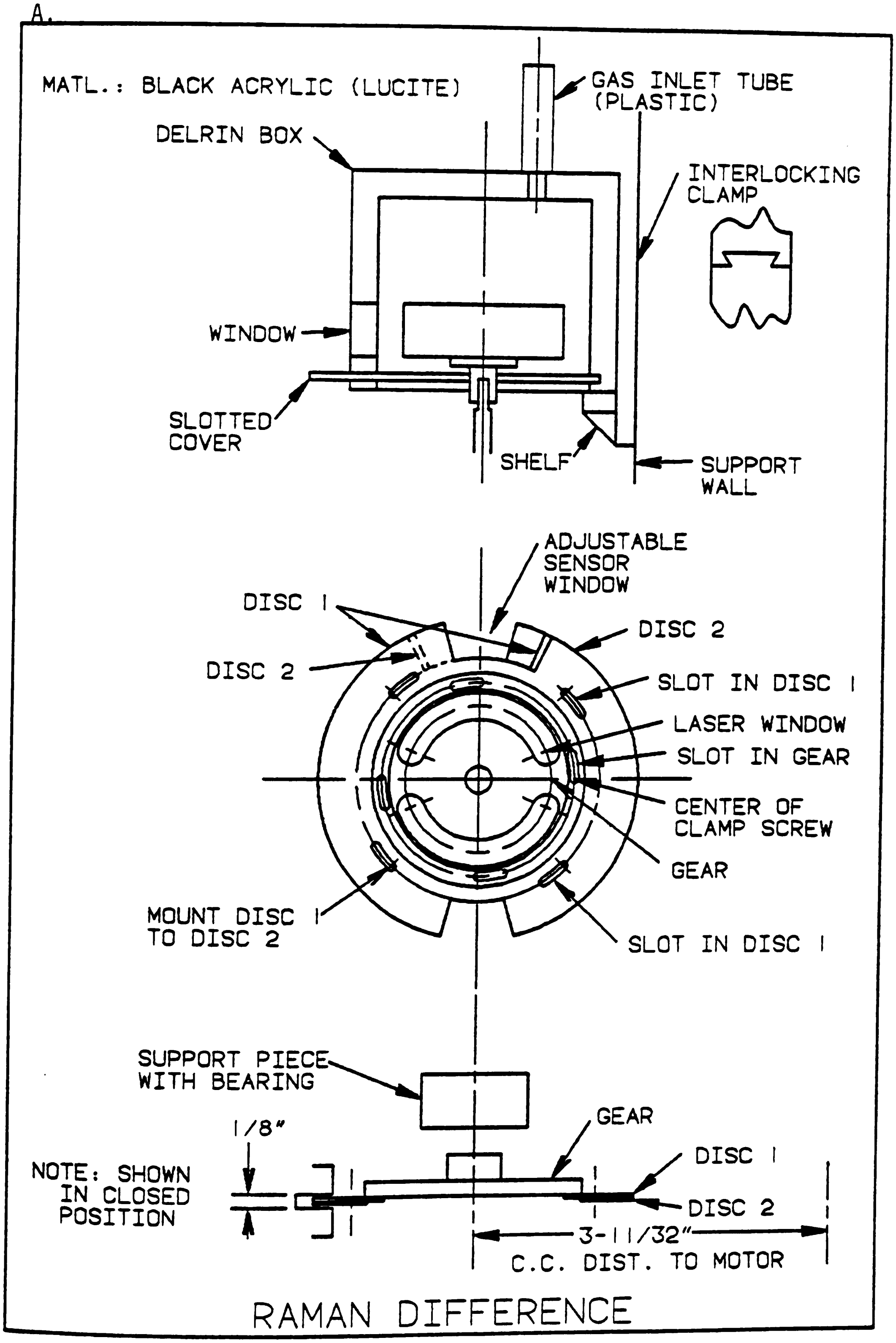
A.
MATL.: BLACK ACRYLIC (LUCITE)
GAS INLET TUBE (PLASTIC)
DELRIN BOX
INTERLOCKING CLAMP
WINDOW
SLOTTED COVER
SHELF
SUPPORT WALL
ADJUSTABLE SENSOR WINDOW
DISC 1
DISC 2
DISC 2
SLOT IN DISC 1
LASER WINDOW
SLOT IN GEAR
CENTER OF CLAMP SCREW
GEAR
MOUNT DISC 1 TO DISC 2
SLOT IN DISC 1
SUPPORT PIECE WITH BEARING
GEAR
1/8"
DISC 1
NOTE: SHOWN IN CLOSED POSITION
DISC 2
3-11/32"
C.C. DIST. TO MOTOR
RAMAN DIFFERENCE

Figure 2.7: Schematic of the Raman difference hardware (A) and split spinning cuvette (B).

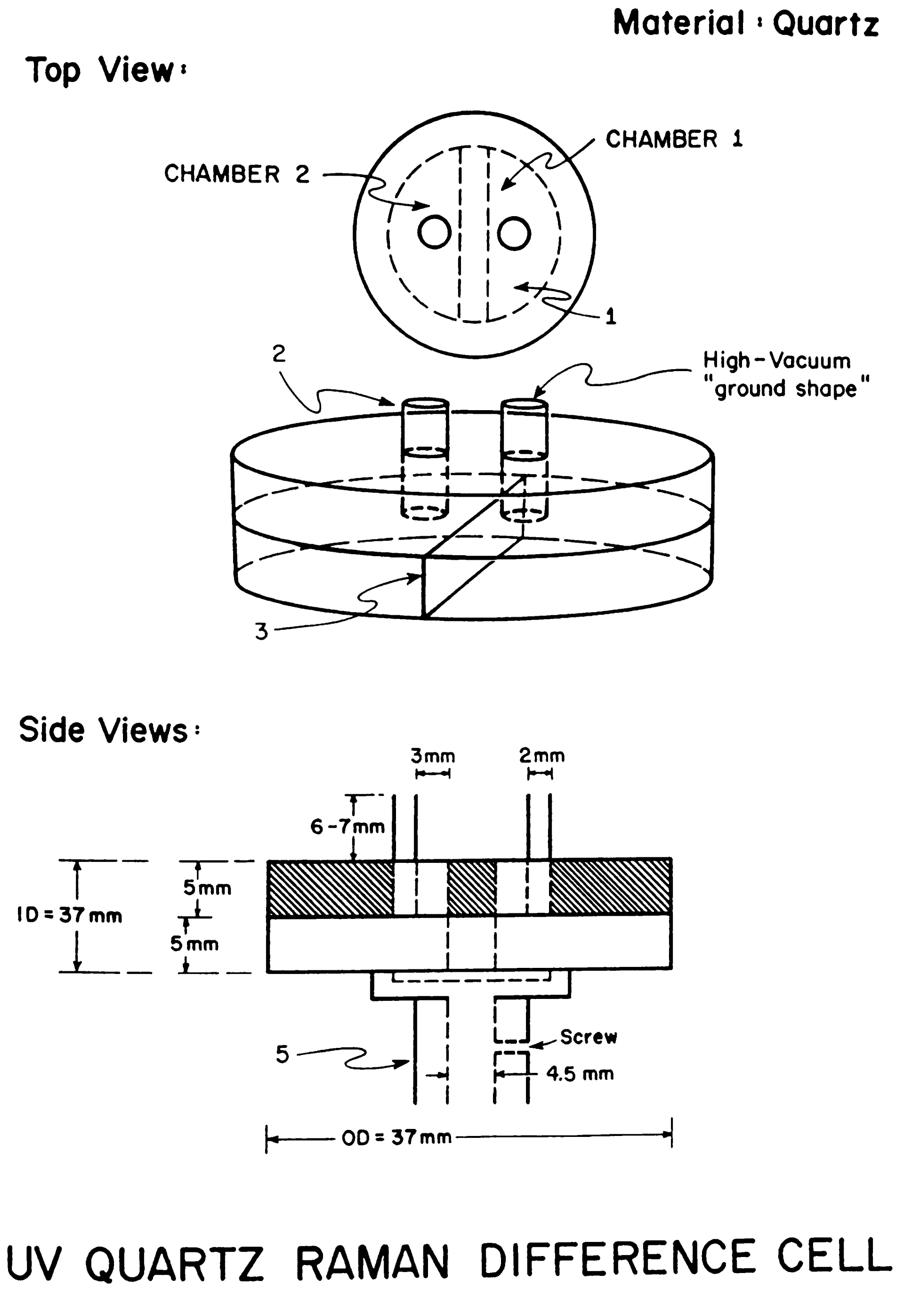
Material : Quartz
Top View:
CHAMBER 1
CHAMBER 2
1
2
High-Vacuum "ground shape"
3
Side Views:
3mm
2mm
6-7mm
5mm
5mm
ID = 37mm
Screw
5
4.5 mm
OD = 37mm
UV QUARTZ RAMAN DIFFERENCE CELL

Figure 2.7B (Continued):

Inc.
arat
sary
the
ment
elec
elec
puls
part
comp
The
whic
tube
posi
spin
set
the
sync
prov
resp
11/2
subt
obta
ted
from
magn
time

Inc.) which is divided down the center to provide two separate compartments is used. Figure 2.8 describes the necessary digital and timing logic used in the implementation of the RDS. As the cuvette spins (at ~32 RPS) the two compartments are alternatively illuminated by the laser beam and electronically detected as the cuvette rotates. Two optoelectronic modules on the motor mount are used to generate pulses which are 180^0 apart, and synchronized with the partitionin the cuvette. The pulses are shaped in two comparators which subsequently trigger a Flip-Flop (F-F). The complementary outputs from the F-F control two gates which are fed by the count pulses from the photomultiplier tube (PMT) and the shaped optoelectronic pulses. The position of the adjustable windows, which rotate with the spinning cuvette to provide the optoelectronic pulses, is set so that counts associated with samples in each half of the cuvette are separated and detected separately. A synchronizing pulse is taken from one of the shapers to provide a reference. The signals are accumulated in their respective counters and subsequently stored in the DEC LSI-11/2 computer. The two separate spectra can be plotted, subtracted, or ratioed (i.e., channel 1/ channel 2) to obtain accurate peak positions. In the RDS spectra reported here, the monochromator was advanced in steps ranging from 0.1 to 0.50 cm^{-1} allowing a better determination of the magnitude of the shift in the difference spectrum, the dwell time was varied from 0.25 to 0.5 sec^{-1}, and the spectral

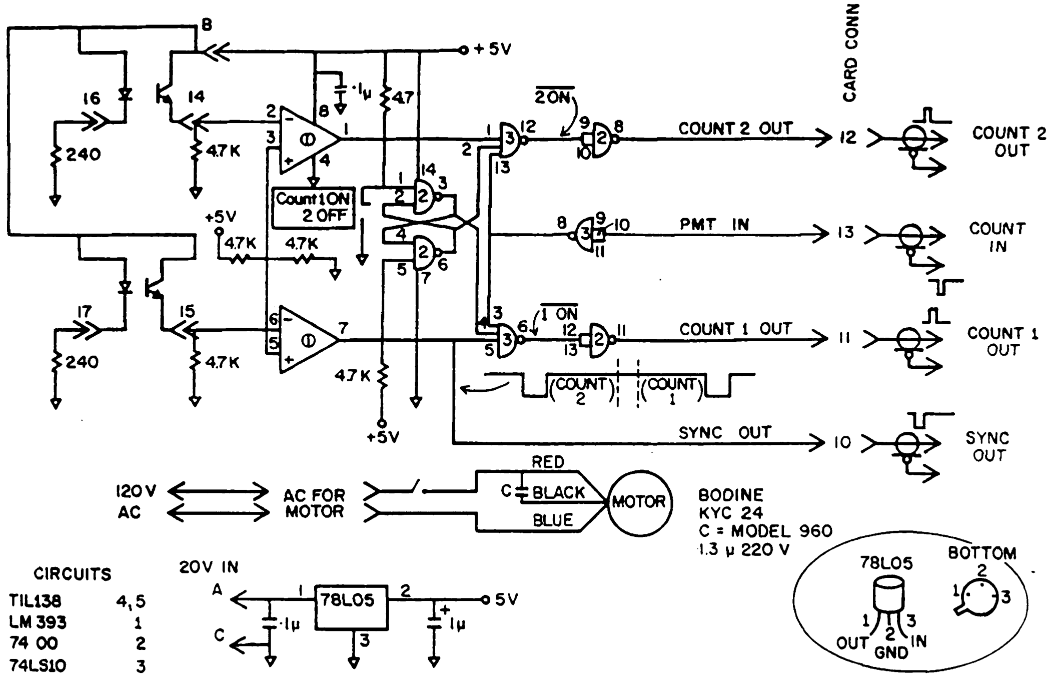
CARD CONN
+5V
8
16
14
240
4.7K
2
3
8
·1μ
47
1
4
Count 1 ON
2 OFF
+5V
4.7K
4.7K
17
15
240
4.7K
6
5
7
4.7K
+5V
2ON
COUNT 2 OUT
12
COUNT 2 OUT
PMT IN
13
COUNT IN
1 ON
COUNT 1 OUT
11
COUNT 1 OUT
(COUNT 2)
(COUNT 1)
SYNC OUT
10
SYNC OUT
RED
120V AC
AC FOR MOTOR
C
BLACK
BLUE
MOTOR
BODINE
KYC 24
C = MODEL 960
1.3 μ 220 V
78L05
BOTTOM
OUT
GND
IN
CIRCUITS
TIL138 4,5
LM 393 1
74 00 2
74LS10 3
20V IN
A
C
·1μ
78L05
·1μ
5V

RAMAN SPINNING SAMPLE LOGIC

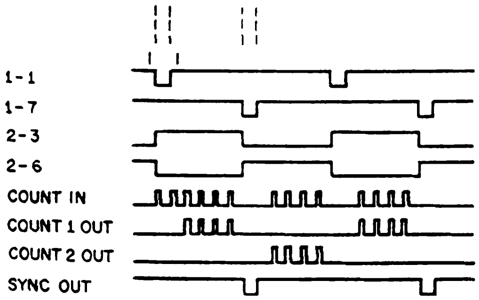
1-1
1-7
2-3
2-6
COUNT IN
COUNT 1 OUT
COUNT 2 OUT
SYNC OUT

RAMAN SPINNING SAMPLE TIMING

Figure 2.8: Schematic of the digital and timing logic for the resonance Raman difference Apparatus

width
on th
latte
width
tiona
param
RDS e

can b
resul
Sheln
of th
diffe
(1980
simpl
frequ
peak-
given

where
Raman
sity.
Loren
tivel
lines
to th

width was chosen at 3.0 cm^{-1} as determined by the broadening on the high frequency Raman lines. The setting of this latter parameter is of particular relevance since the half width at half height (Γ) of the Raman line is proportional to the spectrometer resolution and is one of the parameters used to calculate the frequency difference in the RDS experiment.

With the RDS technique, quantitative frequency shifts can be readily calculated from the derivative shape of the resulting difference spectrum (Rousseau, 1981; Keifer, 1980; Shelnutt et al., 1981). In this regard, detailed analysis of the determination of frequency differences by the Raman difference technique has been published by Laane and Keifer (1980), Rousseau (1981), and Shelnutt et al. (1981). For simplicity, we reproduce here the relationship between the frequency separation, $\Delta\nu$, of the Raman lines, and the peak-to-peak intensity, I_D^0 , in the difference spectrum, given as:

$$\frac{\Delta\nu}{\Gamma} = \frac{I_D^0}{I_D} \tag{2.3}$$

where Γ is defined as the halfwidth at half height of the Raman line under question, and I_D is the Raman line intensity. The derivation of the above expression assumes a Lorentzian line shape for the Raman lines as well as relatively small frequency differences between the two Raman lines of interest. If $\Delta\nu$ is small, higher terms contributing to the difference intensity can be neglected (Rousseau,

1981)
smalle
that i
the ab
tively
accura
peaks
detail
of err
freque
recent
we hav
no art
ence s
buffer
experi
signal
contro
to 0.5
0.4 cm
throug

A
study
in Fig
chrome
associ
differ

1981).. In addition, when the frequency difference is much smaller than the halfwidth at half height of the Raman line, that is, if $\Delta\nu / \Gamma <<< 1$, then it is more accurate to use the above intensity expression to calculate $\Delta\nu$. Alternatively, if $\Delta\nu / \Gamma$ is greater than unity then it is more accurate to use the frequency separation between the two peaks to obtain a measure of the frequency difference. A detailed analysis of mechanical factors and various sources of errors that could influence the determination of small frequency differences in the RDS experiments has been recently presented by Rousseau (1981). In the present study we have taken all the neccessary precautions to ensure that no artifactual differences are contributing to the difference spectrum. As a routine test, the RDS of solvents and buffers used here were scanned before and after each Raman experiment to monitor spectrometer resettability. When signal averaging was neccessary, special care was taken in controlling the spectrometer step size (usually between 0.1 to 0.50 cm^{-1}) and the start of each scan to be within 0.1 to 0.4 cm^{-1}. The laser output power was kept constant at 10 mW throughout the recording of the RDS.

As an example of the application of this technique to study the resonance Raman spectra of heme proteins we report in Figure 2.9 the resonance Raman spectra of reduced cytochrome $\underline{c}^{2+}$ in protonated and deuterated buffers and the associated Raman difference spectrum. A frequency difference shift of -2.27 cm^{-1} is clearly seen in the

Figure 2.9: Resonance Raman spectra of ferrocytochrome *c*$^{2+}$ in protonated and deuterated buffers (pH = pD = 7.4), and the associated Raman difference spectrum. Cytochrome *c*$^{2+}$ was 30 μM. Upon use of deuterated buffers tye 1362 cm^{-1} line was shifted down by 2.27 cm^{-1} as calculated from the RDS spectrum.

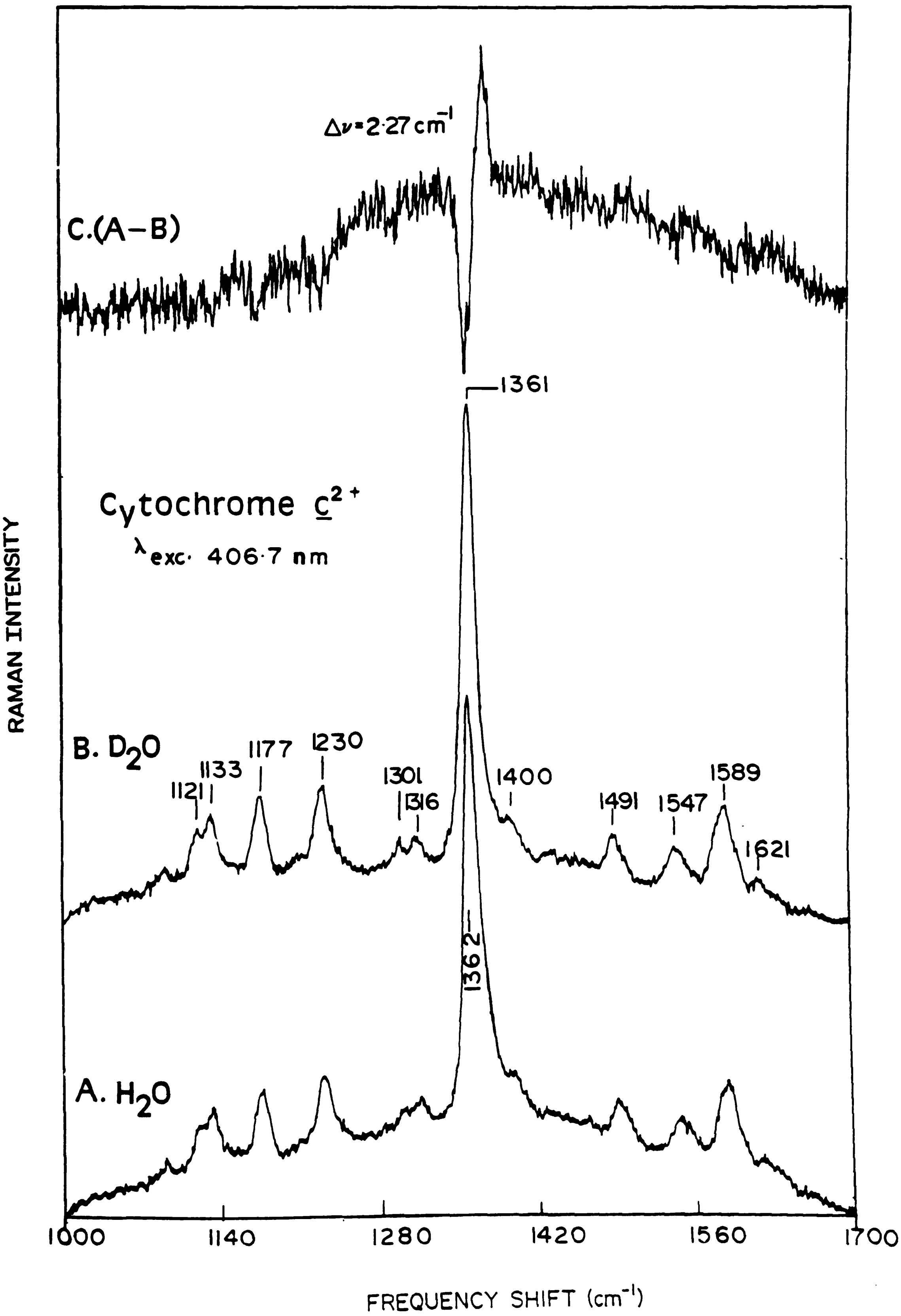
C.(A−B)
Δν=2·27 cm⁻¹
Cytochrome c²⁺
λexc· 406·7 nm
1361
B. D₂O
1121
1133
1177
1230
1301
1316
1400
1491
1547
1589
1621
1362
A. H₂O
RAMAN INTENSITY
1000
1140
1280
1420
1560
1700
FREQUENCY SHIFT (cm⁻¹)

diffe
reduc
Resor
ident
oxida
1975;
cytoc
ty of
pocke
is di
tion)

repor
equip
(PMT)
from
(406.
Coher
laser
out o
laser
chrom
nm we
pumpe
at th
exper
ments

difference spectrum in the 1362 cm^{-1} resonance Raman line of reduced cytochrome c^{2+} upon use of deuterated buffers. Resonance Raman spectra of hemeprotein model compounds have identified this band as a marker Raman line for heme oxidation-state and porphyrin core size (Kitagawa et al., 1975; Spiro, 1983). The detected sensitivity of this band in cytochrome c^{2+} to deuterium atoms indicates the accessibility of protein exchangeable sites on the vicinity of the heme pocket of cytochrome c. The significance of these results is discussed elsewhere (Centeno and Babcock, in preparation).

The Raman instrumentation used in the experiments reported here consists of a Spex 1401 double monochromator equipped with a cooled RCA 31034C photomultiplier tube (PMT). Laser excitation in the Soret region was obtained from a Spectra Physics Model 164-11 Kr^{+} ion laser head (406.7 nm and 413.1 nm) equipped with a high field magnet, a Coherent Innova 90 Kr^{+} laser, and a He-Cd (441.6 nm) Liconix laser. To separate the 406.7 nm and 431.1 nm lines coming out of the Kr^{+} laser, a prism, positioned in front of the laser cavity, was used. Resonance Raman spectra of cytochrome oxidase in resonance with the visible α-band at 605 nm were obtained using a dye laser with Rhodamine 6G dye pumped with a Spectra Physics Ar^{+} ion laser. Power incident at the sample was typically 10 mW (for Soret excitation experiments) and ~80-110 mW (for visible excitation experiments). Temperature at the sample was maintained at 4-6 °C, cont

ther

nect

tion

foll

spec

The

izat

(CH_2

CH_2C

tic

enzy

doub

to g

ture

exch

ENDO

copy

prov

ment

Bruk

ENDO

supp

controlled by a constant flow of liquid N_2 boil off. A thermocouple, positioned inside the sample holder and connected to a digital meter, was used. To measure depolarization ratios (i.e. $\rho = I_{\perp}/I_{\parallel}$), a polaroid disk was used, followed by a polarization scrambler which corrects for spectrometer response to different polarization directions. The polaroid disk was calibrated by obtaining known depolarization ratios of standard solvents in the low-frequency (CH_2Cl_2 and CCl_4) and in the high-frequency (C_6H_6 and CH_2Cl_2) ranges.

C. Electron Nuclear Double Resonance Spectroscopy (ENDOR)

In this thesis we have made use of electron paramagnetic resonance spectroscopy with the purpose of monitoring enzyme integrity and preparation quality. Electron nuclear double resonance spectroscopy, on the other hand, was used to gain information on the Cu_A^{2+}-ligand coordination structure and to investigate possible occurrence of protein H/D-exchangeable sites in the immediate vicinity of Cu_A^{2+}. ENDOR spectroscopy combines the sensitivity of EPR spectroscopy and the capability of nuclear magnetic resonance to provide structural information about the immediate environment of paramagnetic metal centers.

The EPR and ENDOR spectra were obtained by using a Bruker ER200D X-band spectrometer equipped with an ER152E ENDOR/TRIPLE accessory. Radio frequency (rf) power was supplied to an eighteen turn selenoid via a 100 W amplifier

(EN

syn

sta

(19

Oxf

ava

sub

mod

pow

in

thi

reg

100

opt

be

sub

tio

Per

pel

ave

CCl

bal

the

cons

con

(ENI 31002) driven at frequencies generated by a Wavetek synthesizer (model number 3000-446). The coil was of a free standing design similar to that described by Hurst et al. (1978), and slid into position on the quartz Dewar of an Oxford cryostat. The resonant cavity for ENDOR was that available commercially from Bruker. EPR spectra were subject to the following experimental conditions: field modulation approximately 1G at 12.5 kHz, and microwave powers typically 0.5 to 1.0 mW. ENDOR spectra were obtained in the region near the free proton precession frequency, this region corresponding to that defined as the "matrix" region by Hyde (1967). The applied radiofrequency power was 100 W, and this frequency was modulated at 15 kHz. The optimum microwave power/temperature combination was found to be 6-7 mW and 3.4-10 K, respectively.

D. Infrared (IR) Spectroscopy

Infrared (IR) spectra of heme $\underline{a}^{3+}Cl^-$ and the metal substituted porphyrin models, in KBr pellets and in solution, were obtained using a BOMEM FTIR (Model DA3.02) and Perkin Elmer spectrophotometers. For the solidified KBr pellets spectra the resolution was 2.0 cm^{-1} with an average of 150-250 scans. For the solution spectra we used CCl_4 as the solvent. The contributions of CCl_4 were fully balanced and subtracted from the porphyrin spectra yielding the spectrum of the porphyrin derivative. Nitrogen gas was constantly purged into the IR sample chamber to avoid H_2O contributions to the IR spectra.

I
M

Sum

pou

in

lab

and

abs

inf

sho

mod

sub

wit

fre

str

deu

rin

fre

whi

obs

eff

of

for

and

CHAPTER III

FORMYL ISOTOPIC SUBSTITUTION AND HYDROGEN BOND SENSITIVE MODES IN HEME A MODEL COMPOUNDS: MODELS FOR CYTOCHROME A

Summary:

To elucidate formyl (-CHO) modes in heme model compounds that mimic spectroscopic properties of cytochrome a in cytochrome c oxidase, we have synthesized isotopically labelled Cu^{2+} porphyrin (-CH^{18}O), Cu^{2+} porphyrin a (-CDO) and heme a (-CDO), and characterized them by using optical absorption and resonance Raman (RR) spectrocopies. The infrared (IR) spectrum of the ^{18}O-labelled Cu^{2+}porphyrin shows substantial frequency perturbations for IR formyl modes. Resonance Raman activity of E_u-type IR-allowed substituent modes is observed. Upon substitution of ^{16}O with ^{18}O at the carbonyl group, the $\nu_{C=O}$ stretching frequency decreases by 32 cm^{-1}, and the ring-formyl stretching (ν_{Cb-CHO}) upshifts by ~4 cm^{-1}. Similarly, deuterium substitution at the formyl proton of Cu^{2+} porphyrin a results in a 5 cm^{-1} downshift in the C=O stretching frequency and a 4 cm^{-1} upshift in the ν_{Cb-CHO} vibration, which is in agreement with analogous isotopic effects observed in the Raman spectra of benzaldehyde models. The effect of hydrogen bond formation between the carbonyl group of heme a and phenol H-donors on Raman frequency shifts of formyl vibrational modes was also investigated. The $\nu_{C=O}$ and $\Delta\nu_{\alpha}$(max) values appear to be related to the pka of the

H-d
ter
ana
spe
hem
int

I.

tra
is
con
of
ser
imp
oxi
sub
sig
enz
Tho
pro
eve
rep
whi
III
ato
on

H-donor, but are insensitive to H/D exchange at the OH terminal end of the phenol H-donor group. A comparison with analogous isotopic and H-bonding effects on the Raman spectra of benzaldehyde suggests that the H-bond in isolated heme a is a weak bond, which contrasts to the stronger interaction observed in cytochrome a.

I. Introduction:

Although the nature of the coupling between electron transfer and proton pumping activity in cytochrome c oxidase is a matter of some controversy (Wikstrom et al., 1982), considerable advances have been made towards the elucidation of plausible protein and/or chromophoric sites which could serve as structural/functional linkages between these two important aspects of energy transduction in cytochrome oxidase. For instance, the non-chromophore containing subunit III has been implicated on the basis of the significant diminution in proton pumping activity when the enzyme was depleted of this polypeptide (Penttila, 1983; Thompson et al., 1985). However, cytochrome oxidase from prokaryotic sources containing two (Solioz et al., 1982) and even one subunit (Sone et al., 1984) has been recently reported to exhibit appreciable proton pumping activity, which made the above interpretation of the role of subunit III in the oxidase H$^+$-pump somewhat uncertain. The Cu^{2+}_A atom has also been proposed to be involved in proton pumping on the basis of a detailed interpretation of its unusual EPR

spec
rece
liga

oxid
prot
al.,
stro
that
macr
prot
redo
prot
obse
freq
rela
apro
Babc
obse
iron
mode
loca
by a
a (C

shif
nyl

spectroscopic properties (Chan et al., 1979), as well as on recent results from chemical modification studies at the Cu_A ligand-coordination sphere (Blair et al., 1986).

The heme *a* chromophore of cytochrome *a* in cytochrome oxidase has been suggested as the site for the redox-linked proton pumping activity (Wikstrom et al., 1981; Wikstrom et al., 1982; Babcock and Callahan, 1983). Based upon specstroscopic evidence, Callahan and Babcock (1983) concluded that the formyl (-CHO) group at position 8 of the heme *a* macrocycle is involved in a hydrogen bond interaction with a protein H-donor residue (see Figure 3.1), communicating redox events at the heme *a* iron atom to the rest of the protein surroundings. This conclusion was reached from the observed red-shift in the α -maximum and the downshifted frequency of the $\nu_{C=O}$ of oxidized and reduced cytochrome *a* relative to the low-spin, six-coordinated heme *a* model in aprotic (non-hydrogen bonding) solvents (Callahan and Babcock, 1983). The strength of the H-bond interaction was observed to depend upon the redox state of the cytochrome *a* iron atom, and accordingly, a redox-driven proton pumping model was proposed in which the H-bonded proton is translocated along a chain of hydrogen bonded residues, triggered by a redox-dependent conformational change in the cytochrome *a* (C=O...H) structure.

Since the above assignments relied heavily on the red-shifted absorption maximum and on the behavior of the carbonyl group stretching frequency in cytochrome *a*, it appears

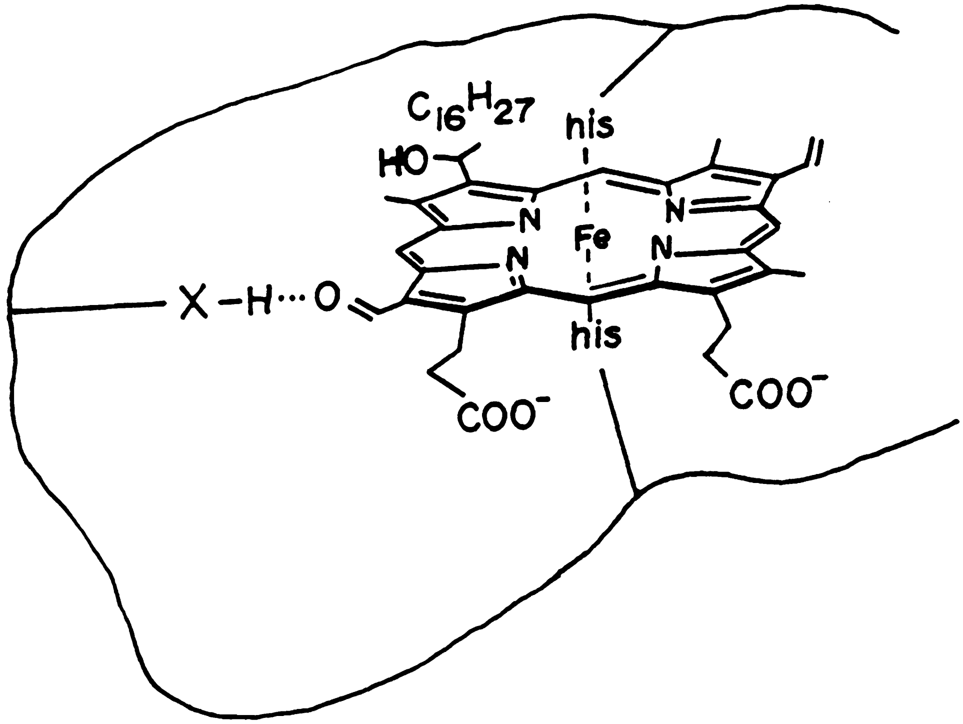
C16H27
HO
his
N
N
Fe
N
N
his
X–H···O
COO⁻
COO⁻

Figure 3.1: Proposed hydrogen bonded structure of cytochrome a in cytochrome c oxidase. The protein residue is designated as X-H (Babcock and Callahan, 1983).

of p

mode

vibr

fron

Insi

grou

subs

forn

(H-(

H-bo

pres

such

fiec

al.

aggr

tior

appe

(Var

here

its

-CH(

bonc

grou

isot

mode

esta

of particular interest to investigate other formyl related modes and hence to separate the formyl H-bond sensitive vibrations contributing to the RR spectrum of cytochrome a from other heme macrocycle and/or protein vibrations. Insights into the internal vibrational modes of the formyl group of heme a were reported by Choi et al. (1983). By substituting the formyl-carbon hydrogen with deuterium, formyl modes involving the ring-formyl stretch and the (H-CO) bend were indentified and observed to be sensitive to H-bonding (Choi et al., 1983). Other ring vibrations, presumably sensitive to the presence of the formyl group, such as ν_{11} (Cb-Cb) and ν_{38} (Cb-Cb), were also identified as H-bond sensitive modes. Nevertheless, the Choi et al. (1983) assignments are weakened by extensive heme a aggregation in their studies as well as by chemical saturation of the formyl group double bond, as evidenced by the appearance of the 565 nm band in their absorption spectrum (Vanderkoii and Stotz, 1965; Babcock, 1987).

To quantify these hydrogen bonding effects, we report here the resonance Raman (RR) and IR spectra of heme a and its 4-vinyl-8-formylporphyrin analog, in which the isolated -CHO group has been studied under the influence of hydrogen bonding effetcs and after isotopic labelling at the formyl group. The results obtained are compared with analogous isotopic and hydrogen bonding effects observed for formyl modes in simpler aldehyde-containing systems with the aim of establishing trends of formyl sensitivity to hydrogen

bor
moc
wit
str
phe
H-d
cha
H-d
the
of
spe
and
unc
or
vin
the
it

II.

MeI
in
H_2O
and
the

bonding. The patterns of frequency shifts in the heme a model compounds and in benzaldehyde are similar for modes with substantial formyl character, such as the formyl stretching frequency and the ring-CHO frequency. The use of phenol-OH and its deuterated derivative (phenol-OD_6) as H-donors to the formyl group does not result in additional changes that could be attributed to H/D exchange at the H-donor; however, placing an electron withdrawing group at the phenol ring (i.e., Cl^-), markedly increases the strength of the H-bond interaction. Comparison of the infrared spectra of heme a^{3+} Cl^-, Cu^{2+} porphyrin labelled with ^{18}O and protoporhyrin IX Cl^- in KBr pellets and in solution, uncovered most of the formyl modes that are not Raman active or that overlapped with porphyrin macrocycle vibrations. The vinyl stretching frequency was not possibly identified in the IR spectra of heme a and its Cu^{2+} porphyrin analog, but it was observed at 1626 cm^{-1} for protoporphyrin IX-chloride.

II. Results and Discussion:

A. Effects of hydrogen bonding on the absorption spectra of heme a complexes:

The absorption spectra of ferric and ferrous heme a $(N\text{-}MeIm)_2$ in aprotic (non-hydrogen bonding) solvents are shown in Figure 3.2A. The effect of hydrogen-bond formation, with H_2O and p-Cl-phenol as the H-donors, is shown in Figs 3.2B and 3.2C, respectively. Table 3.1 summarizes our results on the observed changes in the absorption spectra of heme a and

Figure 3.2: Absorption spectra of heme a $(N\text{-}MeIm)_2$ under various hydrogen bonding condition:

A) (---) heme $a^{3+}(N\text{-}MeIm)_2/CH_2Cl_2$
(——) heme $a^{2+}(N\text{-}MeIm)_2/CH_2Cl_2$
B) (——) heme $a^{3+}(N\text{-}MeIm)_2/H_2O$-detergent
(---) heme $a^{2+}(N\text{-}MeIm)_2/H_2O$-detergent
C) (——) heme $a^{3+}(N\text{-}MeIm)_2/CH_2Cl_2$
(---) heme $a^{3+}(N\text{-}MeIm)_2$ + p-Cl-phenol/CH_2Cl_2
(-——-)heme $a^{2+}(N\text{-}MeIm)_2$ + p-Cl-phenol/CH_2Cl_2.

The detergent used in all these samples was 0.07 M cetryltetrametryl ammonium bromide (CTAB).

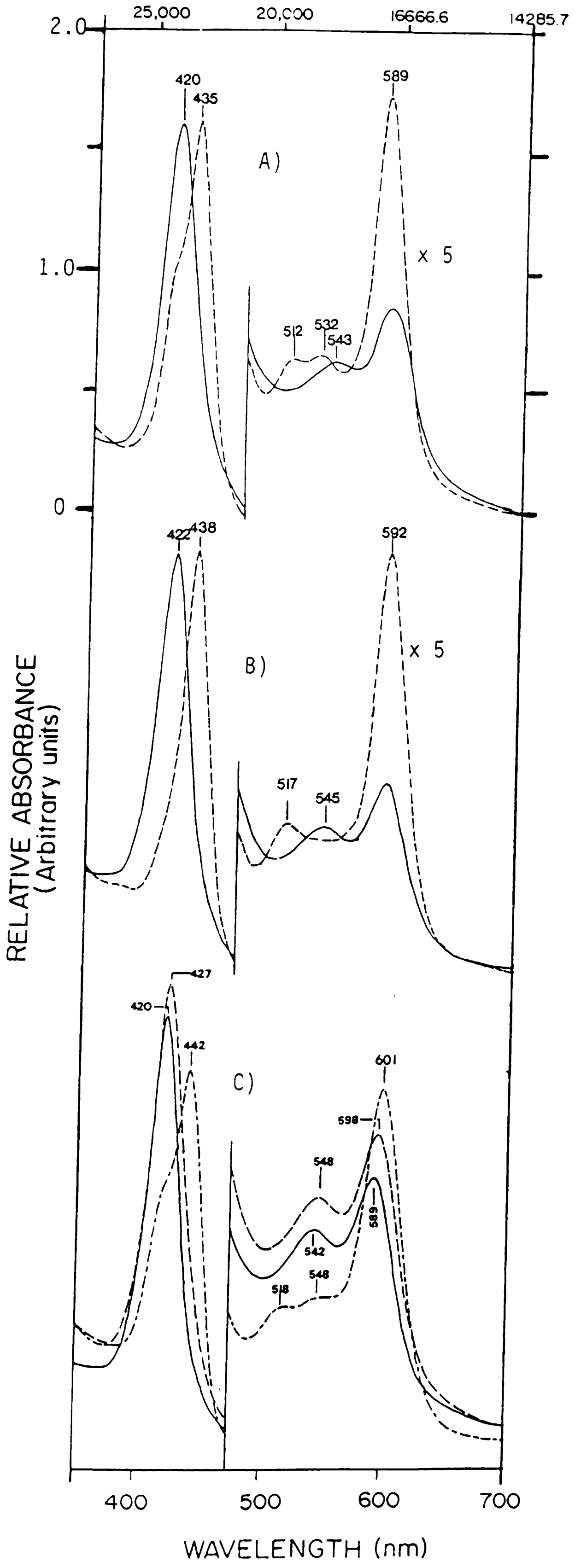
25,000
20,000
16666.6
14285.7
2.0
1.0
0
420
435
589
A)
x 5
512
532
543
422
438
592
B)
x 5
517
545
427
420
442
C)
601
598
548
542
589
518
548
RELATIVE ABSORBANCE
(Arbitrary units)
400
500
600
700
WAVELENGTH (nm)

Table

Specie

Heme a

CH_2Cl
H_2O

+ p-cr
+ Ph-C
+ Ph-C
+ p-F-
+ p-Cl

Heme a

CH_2Cl
H_2O

+ p-cr
+ Ph-C
+ Ph-C
+ p-Cl

Cu^{2+} P

CH_2Cl
DMSO-

+ p-cr
+ Ph-O
+ Ph-O
+ p-F-
+ p-Cl
+2,4-C

Cu^{2+} (

CH_2Cl

+ p-cr
+ Ph-O
+ Ph-O
+ p-F-
+ p-Cl
+2,4-C

Table 3.1. Spectroscopic Characteristics of Hydrogen Bonded Complexes of Heme *a*, Cu^{2+} *a*, and Cu^{2+} Porphyrin

Species:	λ^{α}_{max}	$\Delta\bar{\nu}_{\alpha}$ (cm^{-1})	λ^{β}_{max}	$\Delta\bar{\nu}_{\beta}$ (cm^{-1})	$\nu_{(C=O)}$	$\Delta\bar{\nu}_{(C=O)}$	pKa
Heme *a*$^{3+}$(N-MeIm)$_2$							
CH_2Cl_2	588	---	420	---	1673	----	---
H_2O	592	115	422	113	1655	18	---
+ p-cresol	594	172	423	133	1655	18	10.8
+ Ph-OH	595	201	424	225	1652	21	9.89
+ Ph-OD	595	201	424	225	1652	21	9.89
+ p-F-Ph	597	257	425	281	1652	21	9.80
+ p-Cl-Ph	599	313	427	390	1650	23	9.05
Heme *a*$^{2+}$(N-MeIm)$_2$							
CH_2Cl_2	589	---	435	---	1645	---	----
H_2O	592	86	438	158	1635	10	----
+ p-cresol	595	171	438	158	1633	12	10.8
+ Ph-OH	599	284	440	262	1630	15	9.89
+ Ph-OD	599	284	440	262	1630	15	9.89
+ p-Cl-Ph	601	339	442	365	1626	19	9.05
Cu^{2+} Porphyrin *a*							
CH_2Cl_2	595	---	414	---	1672	---	----
DMSO-d_6	596	---	414	---	1672	---	----
+ p-cresol	605	---	277	417	1647	25	10.8
+ Ph-OH	607	332	422	458	1643	29	9.89
+ Ph-OD	607	332	422	458	1643	29	9.89
+ p-F-Ph	608	359	423	514	1640	32	9.80
+ p-Cl-Ph	610	413	425	603	1638	34	9.05
+2,4-Cl-Ph	613	493	426	626	1638	34	7.05
Cu^{2+} (4-vinyl-8-formyl) Porphyrin							
CH_2Cl_2	598	---	415	---	1672	---	----
+ p-cresol	605	193	418	115	1647	25	10.8
+ Ph-OH	607	250	420	228	1641	31	9.89
+ Ph-OD	607	250	420	228	1641	31	9.89
+ p-F-Ph	608	275	421	285	1639	33	9.80
+ p-Cl-Ph	610	328	424	453	1637	35	9.05
+2,4-Cl-Ph	612	382	425	509	1635	37	7.05

Cu^{2+}
ly s
elec
form
used
acid
use
favo
of t
Hydr
of t
The
deri
to 4
and
to 5
redu
are
bond
new

tran
inte
(Gou
Q-ba
porp

Cu^{2+} porphyrin a with a series of phenol-OH and its variously substituted phenol derivatives. In order to study the electronic and vibrational properties of the porphyrin a formyl group as a function of the pKa of the H-donor, we used Cu^{2+} porphyrin a owing to the fact that it is stable to acidic donors and does not bind axial ligands easily. The use of acidic donors with heme a $(N\text{-}MeIm)_2$ derivatives favors the formation of high-spin heme a due to protonation of the imidazole ligand coordinated to the heme a iron. Hydrogen bonding to the carbonyl group results in a lowering of the transition energy for both the Soret and α-bands. The magnitude of these shifts is stronger for the phenol derivatives as noticed by the shifting of these transitions to 442 and 601 nm, respectively. In addition to the Soret and α-transitions, two visible bands in the region from 500 to 550 nm appear to be altered upon H-bond formation. For reduced (bis-imidazole) heme a^{2+} in CH_2Cl_2 two transitions are clearly observed at 532 and 512 nm which, upon hydrogen bond formation, are apparently diminished and replaced by a new absorption at 517 nm.

Changes detected in these heme a optical electronic transitions upon formyl hydrogen bond formation can be interpreted within Gouterman's four orbital model (Gouterman, 1959). This model predicts that the Soret and Q-bands, originates from electronic transitions from the porphyrin highest occupied molecular orbitals of a_{1u} and a_{2u}

sy
(
(a
pr
to
Th
tr
gr
pe
sy
de
wi
dr
co
ex
bo
H-
in
en
tr

(c
he
of
de
in
in

symmetry to the lowest unoccupied molecular orbitals of e_g (π^*) symmetry. The resulting nearly degenerate transitions ($a_{1u}e_g$ and $a_{2u}e_g$) interact via configuration interaction to produce the α-band and Soret bands. The β-band (Q_{0-1}) to the blue of the α-band arises from vibronic coupling. Therefore, perturbations in the position of these electronic transitions are expected to result in perturbations of the ground and/or excited state properties. In heme a, the H-C=O peripheral substituent is conjugated to the porphyrin π-system, and its contribution to the electronic transition depends upon the extent of interaction of its π-orbitals with the porphyrin π-system. Due to the electron withdrawal caused by hydrogen bonds, a significant increase in conjugation between the C=O and porphyrin π-orbitals is the expected behavior for this group when acting as a hydrogen bond acceptor or electron donator. As the strength of the H-bond increases, electron withdrawal by the C=O group increases significantly, causing a further decrease in energy, and hence red-shift, in the porphyrin electronic transitions.

In Figure 3.3, we have plotted the observed red shift (calculated in cm^{-1}) in the Soret and α-band maxima of heme a^{2+} $(N\text{-}MeIm)_2$ and Cu^{2+} porphyrin a models as a function of the pKa of the phenol and its variously ring substituted derivatives (see Table 3.1). As the acidity of the H-donor increases, the red-shift in the Soret and α-band absorption increases, in agreement with the expected behavior for a C=O

Figure 3.3: Plot of observed red-shift in the Soret (A) and α-band transition of Cu^{2+} porphyrin *a* as a function of the acidity (pKa of phenol H-donor derivative. Data obtained for heme *a* (N-MeIm)$_2$ and Cu^{2+} porphyrin are also included.

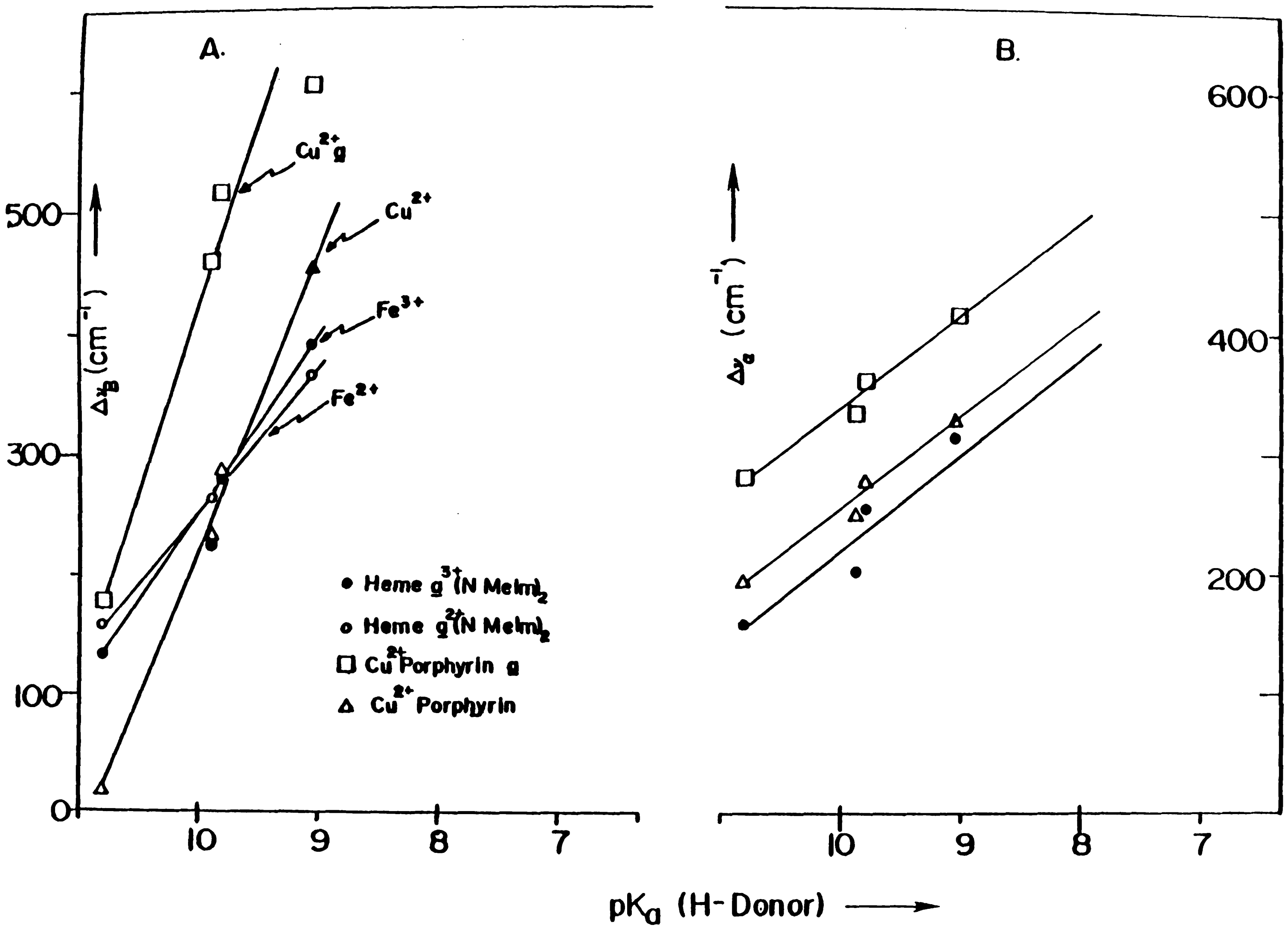
A.
Cu^{2+} g
Cu^{2+}
Fe^{3+}
Fe^{2+}
● Heme g^{3+}(N MeIm)$_2$
○ Heme g^{2+}(N MeIm)$_2$
□ Cu^{2+}Porphyrin g
△ Cu^{2+} Porphyrin
$\Delta\nu_B$ (cm^{-1})
0
100
300
500
10
9
8
7
B.
$\Delta\nu_a$ (cm^{-1})
200
400
600
10
9
8
7
pK$_a$ (H-Donor)

gr
of
re
Ba
abs
te
19
I

hy
up
H-
th
of
an

its
th
are
obs
mM)
bon
gro
al.
the

fre

group when acting as a hydrogen bond acceptor with a series of chemically related H-donors (Arnett et al., 1974). These results are of particular relevance, since Callahan and Babcock (1983) had observed red-shifted Soret and α-band absorptions in the cytochrome a spectrum, which was attributed to hydrogen bond interactions (Babcock and Callahan, 1983).

B. Effect of H-bonding and isotopic substitution on the Raman spectra of benzaldehyde.

In order to characterize vibrational effects of hydrogen-bonding, benzaldehyde model compounds were studied upon replacing its -CHO proton by a deuteron and upon use of H-donors to the carbonyl oxygen. Results from this part of the study should help us in understanding the contribution of formyl modes to the resonance Raman spectrum of heme a and hence to quantify H-bonding effects in cytochrome a.

Representative Raman spectra of benzaldehyde-CHO and its H-bonded derivatives, with phenol-OH and phenol-OD as the H-donors, and the associated Raman difference spectrum are depicted in Figure 3.4. The shoulder at 1707 cm^{-1} observed at higher concentration of the H-donor (i.e., 1.25 mM) indicates the formation of a 1:2 complex in which the H-bonding structure is due to interaction of the acceptor C=O group with two donor molecules as suggested by Ramaswamy et al. (1967). Table 3.2 summarize the formyl frequencies and their respective assignments (Zwarich et al., 1971).

H/D exchange at the phenol group does not result in frequency shifts in the benzaldehyde/phenol complex that

Figu
ativ
diff
was
were

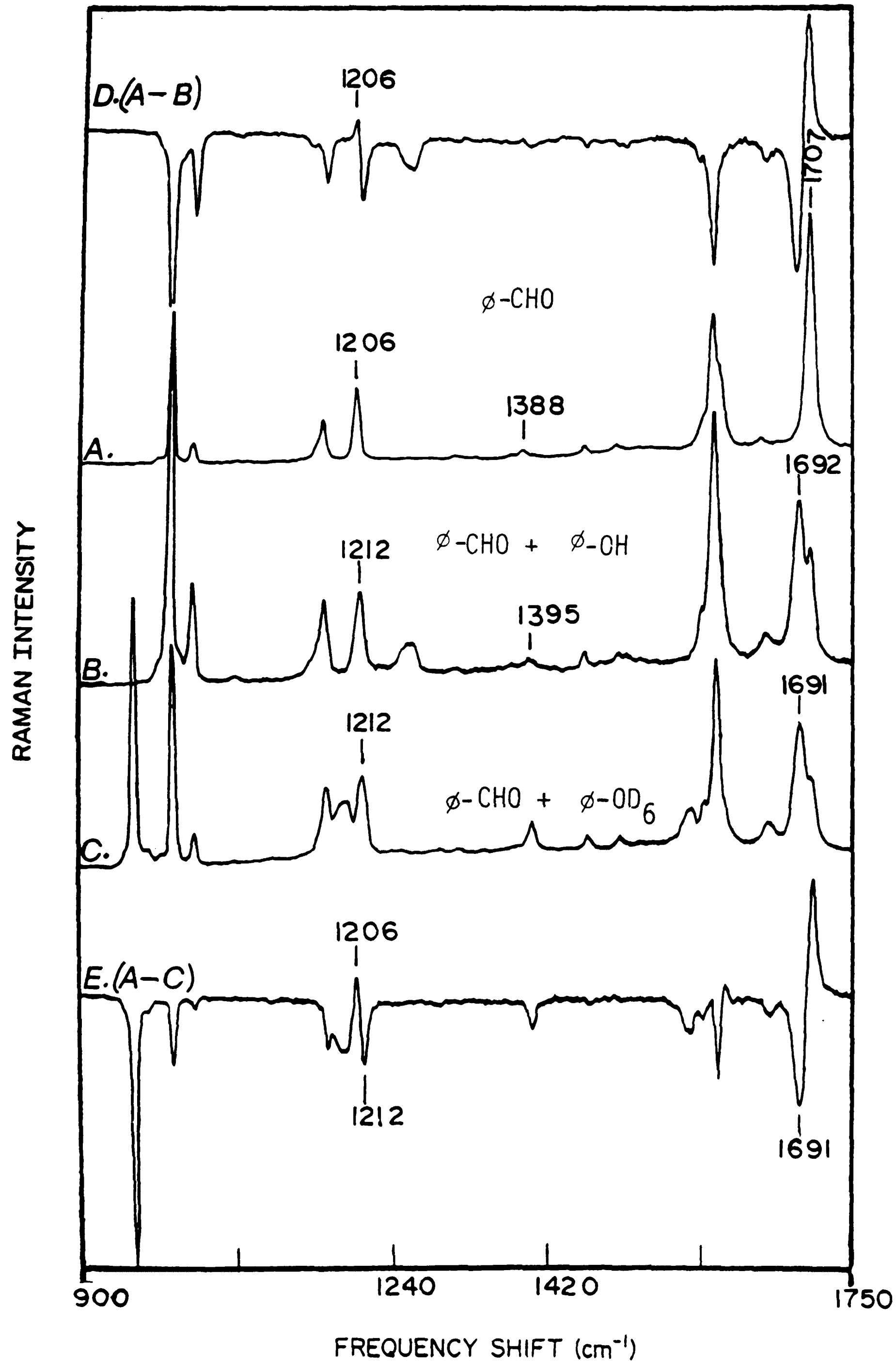

Figure 3.4: Raman spectra of benzaldehyde-CHO and its H-bonded derivatives with phenol-OH and phenol-OD as H-donors. The associated Raman difference spectrum is also illustrated. Benzaldehyde concentration was in the range from 2-2.5 M. Phenol-OH and phenol-OD concentrations were maintained at 1.25 mM. Laser wavelengths at 441.6 nm.

Table

Ass
νc=
$\Delta\bar{\nu}$(c=
δ(H-
δ(D-
ν (ø
ν (ø
δ
Ring
δ (ø

a. Assi
b. Fre
H-d
c. The
forr

Table 3.2. Summary of Raman Frequencies (cm^{-1}) for Hydrogen-Bond Modes in Benzaldehyde

Assignments:[a]	Benzaldehyde-CHO			Benzaldehyde-CDO		
	-CHO	C_6H_6O	C_6D_6O	-CDO	C_6H_6O	C_6D_6O
$\nu_{C=O}$	1707	-----	-----	1691	-----	-----
$\Delta\bar{\nu}(C=O...H/D)$	----	1692 (-15) (1689)[b]	1691 (-16)	----	1676 (-15)	1675 (-16)
$\delta(H-C=O)$	1388	1395 (+7)	1394 (+6)	----	----	----
$\delta(D-C=O)$	----	----	-----	1042	1048 (+6)	1048 (+6)
$\nu(\phi-CHO)$	1206	1212 (+6) (1215)[b]	1212 (+6)	----	----	----
$\nu(\phi-CDO)$	----	----	----	1215	1222 (+7)	1223 (+8)
$\delta(C=O)$	649	642 (-7) (637)[b]	642 (-7)	641	635 (-6)	635 (-6)
Ring folding	441	442[c] (442)[b,c]	442[c]	436	437[c]	437[c]
$\delta(\phi-CHO)$	225			214		

a. Assignments taken from Zwarich et al. (1971).

b. Frequency observed when p-Cl-phenol was used as the H-donor.

c. The Raman intensity of this mode decreases upon H-bond formation.

cc

H-

H-

di

be

H-

19

Dr

ph

ac

be

fr

Th

(

qu

(δ

th

Th

wh

Wh

te

cm

12

th

mo

could be attributed to isotopic exchange at the phenol H-donor, and thus to strengthening or weakening of the H-bond interaction by deuterium substitution. This lack of difference of H-bonding energies in the H vs D complexes has been previously observed in the IR spectra for a series of H-bonded complexes in crystals of the type O-H...O (Novak, 1974). Similar conclusions were reached by Boettcher and Drago (1974), who observed that isotopic substitution at the phenol-OH did not affect the H-bonding energies in phenol/acetone complexes.

Additional conclusions that can be extracted from the benzaldehyde model studies concern the observed trends in frequency shifts in formyl modes upon formation of a H-bond. These formyl modes are the formyl-proton bending mode (δ_{H-CO}) at 1388 cm^{-1}, the phenyl-formyl stretching frequency ($\nu_{\phi-CHO}$) at 1206 cm^{-1}, the carbonyl bending mode ($\delta_{C=O}$) at 649 cm^{-1}, the ring twisting mode at 441 cm^{-1}, and the in-plane ring-CHO deformation mode at 245 cm^{-1} ($\nu\phi$-CHO). The formyl H-bend shifts to lower frequencies (to 1042 cm^{-1}) when the -CHO is substituted by D (Zwarich et al., 1971). When the C=O is H-bonded, the bending coordinate is restricted and the frequency increases, as is indicated by its 6 cm^{-1} upshift. The phenyl-formyl stretching frequency at 1206 cm^{-1} shifts up to 1215 cm^{-1} upon deuterium exchange at the aldehyde proton. We observe a 6 cm^{-1} upshift in this mode upon H-bonding, which can be rationalized if

th
mo
su
in
at
ra
sp
ph
Ra
a

(
th
ha
an
ob
fo
th
ni
ly
he
ν_{cb}
be
19
mo

the ν_{Cb-CHO} is vibrationally coupled to the formyl H-bending mode at 1388 cm^{-1}. Therefore, upon H-bond (or isotopic substitution), this interaction is relieved, resulting in an increase in the stretching frequency. A ring-twisting mode at 441 cm^{-1} appears to be sensitive to formyl-proton deuteration as evidenced by its shift to 436 cm-1 in the Raman spectrum of C_6H_5-CDO. Upon formation of an H-bond with phenol-OH or phenol-OD, a significant diminution in the Raman intensity of this twisting mode was detected, without a noticeable frequency shift.

C. **Formyl modes in the resonance Raman and infrared spectra of heme a and its Cu^{2+} Porphyrin analog.**

The identification of the formyl hydrogen deformation ($\delta_{H-C=O}$) and ring-formyl stretching (ν_{Cb-CHO}) modes in the resonance Raman spectra of reduced heme $\underline{a}^{2+}$ $(N\text{-MeIm})_2$ have been recently reported (Choi et al., 1983). The analysis and assignments were based upon a comparison with observed D/H shifts in benzaldehyde models. The in-plane formyl hydrogen bending mode was identified at 1390 cm^{-1} on the basis of a small (~2 cm^{-1}) D/H induced upshift accompanied by the appearance of a new mode at 1077 cm^{-1}. Similarly, a 10 cm^{-1} upshift in the 1220 cm^{-1} line of aggregated-heme $\underline{a}^{2+}$ $(N\text{-MeIm})_2$ was also reported and assigned to the ν_{Cb-CHO} stretch in agreement with a similar mode observed in benzaldehyde spectra (Choi et al., 1983; Zwarich et al., 1971). Choi et al. (1983), however, assigned these formyl modes for aggregated heme $\underline{a}^{2+}(N\text{-MeIm})_2$ in the presence of

K(

c(

f(

Cu

su

th

ca

fc

cc

sc

Ta

up

th

44

fo

at

us

sp

in

$\underline{a}^3$

(F

sh

Fo

th

Fr

16

KCN/D_2O aqueous solution, and hence their assignments correspond to the frequencies of an H-bonded C=O group.

Our results on the H/D exchange experiments at the formyl group of ferric and ferrous heme a $(N\text{-}MeIm)_2$ and its Cu^{2+} porphyrin a model in non-hydrogen bonded solvents support the Choi et al. (1983) assignments; we have extended this analysis by characterizing the RR spectra of isotopically substituted Cu^{2+} $(-CH^{18}O)$ porphyrin. The effects of formyl deuteration on the RR spectra of low-spin six-coordinate heme a $(N\text{-}MeIm)_2$ and Cu^{2+} porphyrin a in aprotic solvents are depicted in Figures 3.5 and 3.6, respectively. Table 3.3 summarizes the formyl modes that were detected upon isotopic substitution. We have included in Figure 3.5 the RR spectra of reduced heme a $(N\text{-}MeIm)_2$ obtained with 441.6 nm excitation, with the aim of identifying trends in formyl group vibrations upon increasing the electron density at the C=O substituent by reducing the iron. We have also used Cu^{2+} porphyrin a owing to its ability to mimic the spectroscopic and vibrational properties of ferrric heme a in solution. The carbonyl stretching frequencies of heme a^{3+} (-CHO) (Figure 3.5 , trace A) and Cu^{2+} porphyrin a (Figure 3.6, trace A) are observed at 1672 cm^{-1}, which shifts down to 1667 cm^{-1} (-5 cm^{-1}) upon formyl H/D exchange. For the ferrous heme a case in CH_2Cl_2 (Figure 3.5, trace C), the 1644 cm^{-1} line, previously assigned by Van Steelandt-Frendrup et al. (1981) to the $\nu_{C=O}$ stretch, shifts down to 1637 cm^{-1} (-8 cm^{-1}) upon increasing the mass at the formyl

Figure 3.5: Resonance Raman (RR) spectra of ferric (traces A and B) and ferrous (traces C and D) non-hydrogen bonded heme a (N-MeIm)$_2$ in dry CH_2Cl_2, after treatment with KCN/H_2O (traces A and C) and KCN/D_2O (traces B and D). The formyl-deuterated heme a^{3+} (N-MeIm)$_2$ was extracted in CH_2Cl_2 after lowering the pD of the KCN/D_2O solution with a slightly acidic (pD 6.2) succinate solution. Heme a^{3+} (N-MeIm)$_2$was reduced using a methanolic solution of cryptand/dithionite complex. The RR spectra of ferric heme a correspond to an average of 16 scans, while the reduced spectra are 6 scans. The uncertainty in the Raman measurements is $\pm$ 1 cm^{-1} for the stronger and narrower peaks, as determined from the halfwidth at halfheight of the oxidation state marker band at 1375 cm^{-1}. Solvent and imidazole peaks are indicated by *. Excitation wavelenghts are 406.7 nm (traces A and B) and 441.6 nm (traces C and D).

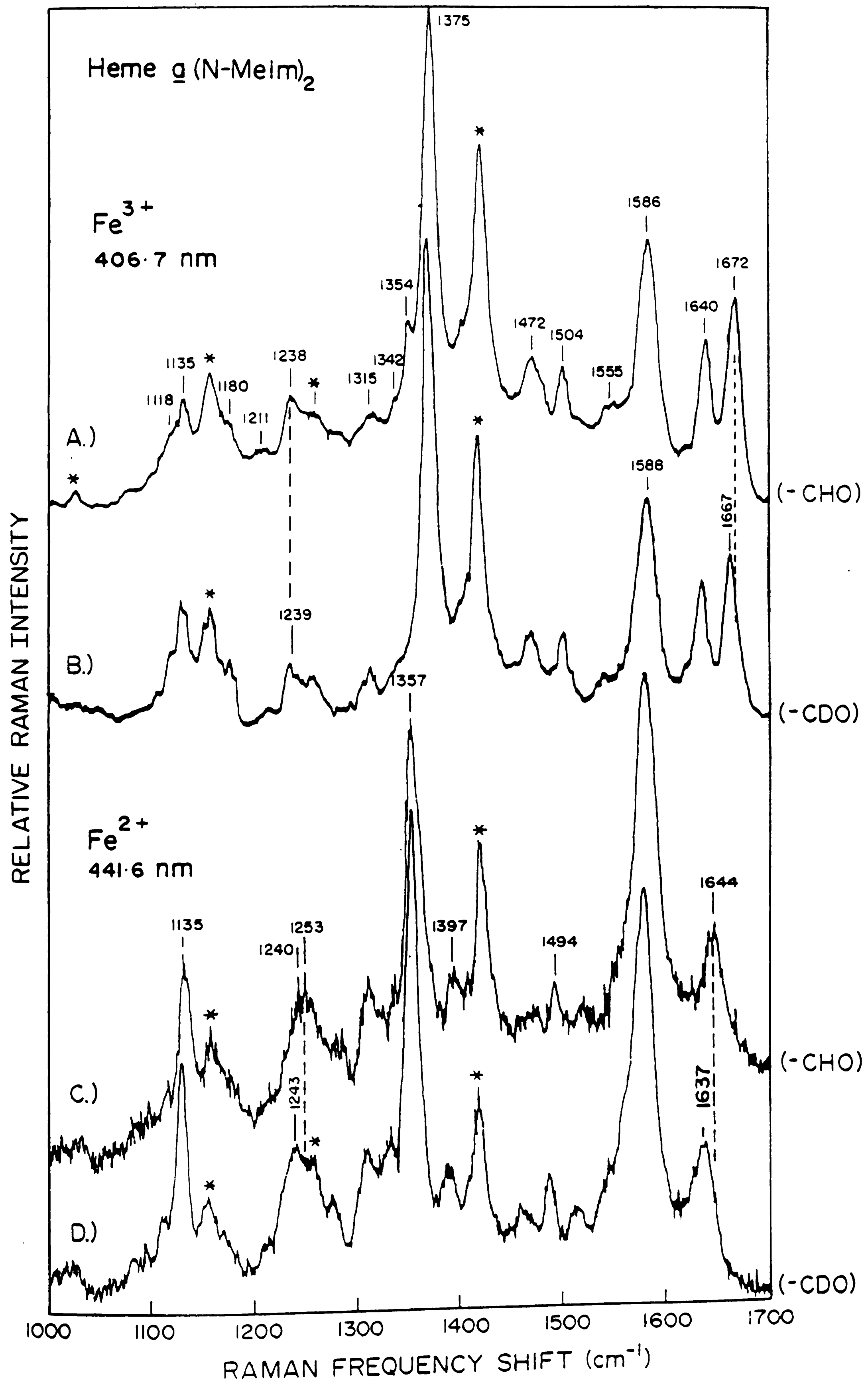
Heme a (N-MeIm)$_2$
Fe^{3+}
406·7 nm
Fe^{2+}
441·6 nm
A.)
B.)
C.)
D.)
(-CHO)
(-CDO)
(-CHO)
(-CDO)
1375
1586
1672
1640
1354
1472
1504
1555
1342
1315
1238
1135
1180
1118
1211
1588
1667
1239
1357
1644
1135
1253
1240
1397
1494
1243
1637
*
RELATIVE RAMAN INTENSITY
RAMAN FREQUENCY SHIFT (cm^{-1})
1000
1100
1200
1300
1400
1500
1600
1700

Figure 3.6: Resonance Raman spectra of Cu^{2+} porphyrin a with normal (-CHO) and deuterated (-CDO) formyl group substituent, in dry CH_2Cl_2. Excitation wavelength at 406.7 nm. Modes sensitive to formyl-proton deuteration are indicated by the dash line.

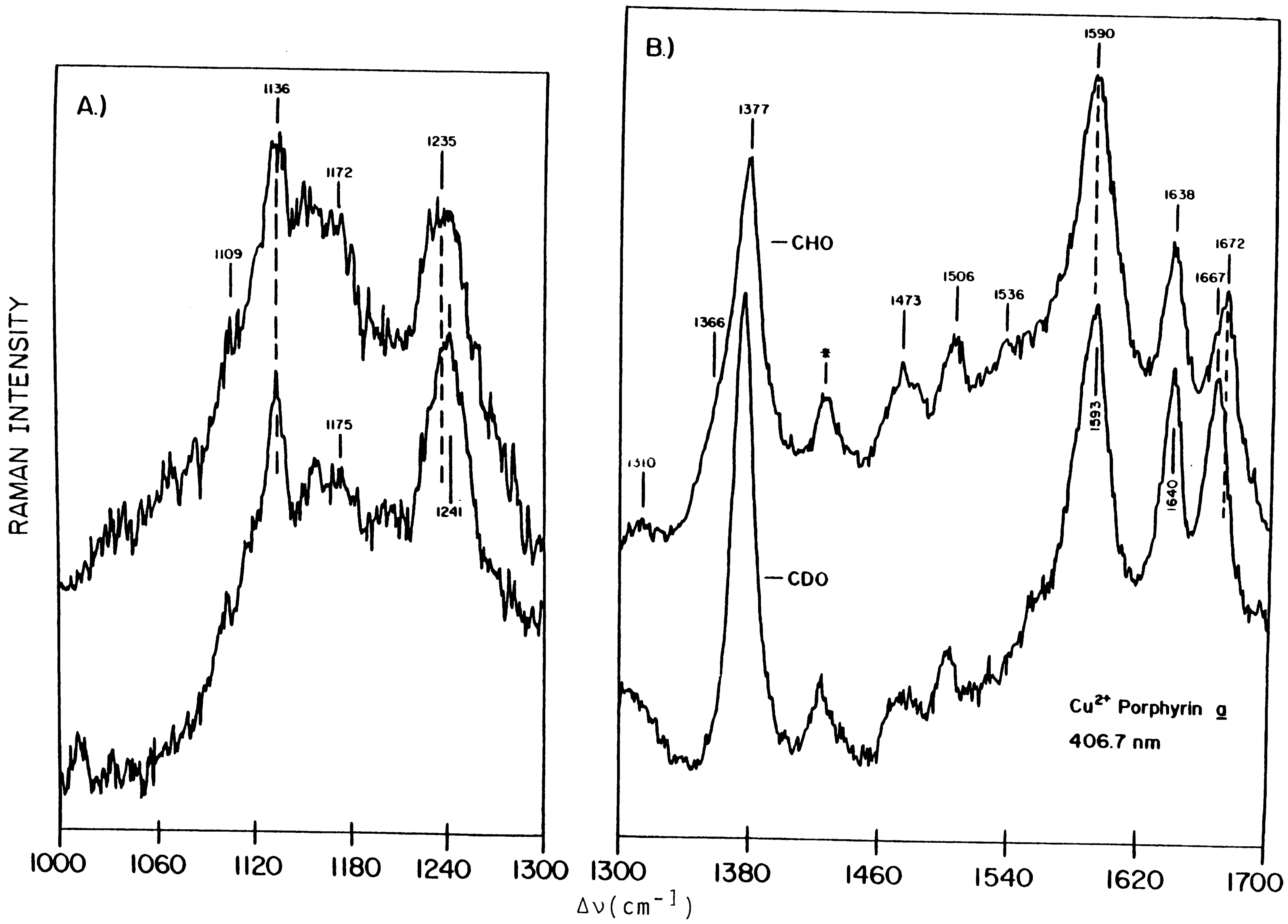
RAMAN INTENSITY
A.)
1109
1136
1172
1235
1175
1241
1000
1060
1120
1180
1240
1300
B.)
1310
1366
1377
—CHO
—CDO
*
1473
1506
1536
1590
1593
1638
1640
1667
1672
Cu²⁺ Porphyrin a
406.7 nm
1300
1380
1460
1540
1620
1700
Δν(cm⁻¹)

Table

Modes

$\nu_{C=O}$

ν_2 C_b-

$\delta_{H-C=O}$

ν_{13}
(ν_{C_b}-

Pyr.

ν_8 (δ

---

a. Fr
ob
b. Th
c. Th
13
d. De
e. Fr
f. Fr

Table 3.3. Formyl-Sensitive Modes in Heme a $(N\text{-}MeIm)_2$ (-CHO/-CDO) and Cu^{2+} Porphyrin a (-CHO/-CDO)

Modes:	Species: Pa^{3+}	+ Ph-OD	Pa^{2+}	+ Ph-OD	$Cu^{2+}a$	+ Ph-OD
$\nu_{C=O}$	1672	1652	1645	1630	1672	1643
	(1667)[a]	(1650)	(1637)	(1630)	(1667)	(1641)
ν_2 C_b-C_b	1586	1589	1585	1588	1590	1597
	(1588)	(1589)	(1587)	(1589)	(1593)	(1595)
$\delta_{H-C=O}$	(1399)[b]	1405	1395[c]	1397[c]		
ν_{13}	1238	1241	1240	1243	1235	1243
(ν_{Cb-CHO})	(1240)	(1241)	(1243)	(1245)	(1241)	(1243)
Pyr. fold					450	( )[d]
					453[e]	
					461[f]	
			345		345	
ν_8 (δ_{Cb-S})			335	348	339	350

[a] Frequencies (cm^{-1}) within parenthesis correspond to those observed upon formyl-proton deuteration.

[b] This mode was observed for heme $a^{3+}(N\text{-}MeIm)_2$ in CCl_4.

[c] This mode overlap with a porphyrin macrocycle mode at 1395 cm^{-1}.

[d] Decreases in Raman intensity upon H-bonding.

[e] Frequency observed for Cu^{2+} porphyrin.

[f] Frequency observed for Ni^{2+} porphyrin a.

subs

the

H/D

ted

grou

cm^{-1}

form

cont

ing

and

$(C_a$-

and

rang

freq

and

and

freq

at ~

MeIm

H/D

Cu^{2+}

for

porp

cm^{-1}

and

ferr

substituent. The $\nu_{C=O}$ frequency shifts that we detect in the heme a and Cu^{2+} porphyrin a (-6 cm^{-1}) derivatives upon H/D formyl exchange are in good agreement with those reported by Williems and Bocian (1984) for the deuterated formyl group of formyl-substituted metalloporphyrin in which a 10 cm^{-1} shift was reported.

Other vibrational modes that appear to be sensitive to formyl proton substitution, and that contain substantial contribution from porphyrin peripheral substituents according to the normal coordinate analysis of Abe et al. (1978) and Choi et al. (1982) are the following: ν_2 (C_b-C_b), ν_{13} (C_a-C_b), (ν_5 + ν_9) (C_b-S) in the high-frequency region, and ν_8 (δ_{Cb-S}) and ν_9 (δ_{Cb-S}) in the low-frequency range. In the RR spectrum of ferric heme a, the high-frequency vibrations ν_2 and ν_{13} are seen at 1586 cm^{-1} and 1238 cm^{-1} for heme a^{3+} (CHO), shifting up to 1588 cm^{-1} and 1241 cm^{-1} for heme a^{3+} (CDO), respectively. The frequency of the non-fundamental mode (ν_5 + ν_9) expected at ~1250 - 1255 cm^{-1} is largely overlapped by a strong N-MeIm band at 1259 cm^{-1} and hence its frequency upon formyl H/D exchange could not be ascertained. The RR spectrum of Cu^{2+} porphyrin a reproduced the frequency shifts observed for ν_2 and ν_{13} in heme a. In the spectrum of Cu^{2+} porphyrin a (CHO), these latter modes are observed at 1590 cm^{-1} and 1235 cm^{-1}, respectively, shifting up to 1593 cm^{-1} and 1241 cm^{-1} (see Figure 3.6). The formyl hydrogen bend of ferric heme a is difficult to assess, owing to the strong

con
use
dete
exch
form
the
with
al.,
heme
disp
spec
assi
1418
agre

8-fo
oxyg
ence
freq
Of i
freq
whic
simi
441
its
stat
spec

contribution of CH_2Cl_2 to a line at 1423 cm^{-1}; however, upon use of CCl_4 as the solvent, a weak line at 1399 cm^{-1} was detected which shifts up to 1403 cm^{-1} upon formyl H/D exchange (spectrum now shown). The RR enhancement of this formyl hydrogen bending mode is expected to be stronger in the spectrum of reduced heme a, but it strongly overlaps with the porphyrin ν_{29} B_{2g} frequency at 1395 cm^{-1} (Abe et al., 1978; Choi et al., 1983). The infrared (IR) spectra of heme a^{3+} Cl^- in KBr and in solution (Figures 3.8 and 3.9) display a band at 1410 cm^{-1}, which is not observed in the IR spectrum of protoporhyrin IX-Fe^{3+} Cl^-, and accordingly it is assigned to the δ_{HC-O} bend. Its upshifted frequency to 1418 cm-1 upon ^{18}O-substitution (see Figure 3.8) is in agreement with a similar upshifts in benzaldehyde models.

The high-frequency RR spectra of 2,6-dipentyl-4-vinyl-8-formyl Cu^{2+} porphyrin with unsubstituted $CH^{16}O$ and with oxygen-18 labelled $CH^{18}O$, and the associated Raman difference spectrum (RDS) are depicted in Figure 3.7. The low-frequency region from 150 to 600 cm^{-1} is also illustrated. Of interest in this low-frequency spectrum is the upshift frequency (+4 cm^{-1}) for a mode at 453 cm^{-1} to 457 cm^{-1}, which we attribute to the pyrrole ring-folding mode since a similar feature is observed in the RR of benzaldehyde at 441 cm^{-1}. The infrared spectra of ferric heme a^{3+} Cl- and its isotopically labelled Cu^{2+} porphyrin analog in the solid state are shown in Figure 3.8. The solution state IR spectra of heme $a^{3+}Cl^-$, Cu^{2+} ($-CH^{16}O$) porphyrin and the

Figure 3.7: Resonance Raman spectra of 4-vinyl-8-formyl Cu^{2+} porphyrin with normal ($-CH^{16}O$) and ^{18}O-labelled ($-CH^{18}O$) formyl group substituent in dry CH_2Cl_2. The Raman difference spectrum from 1000-1700 cm^{-1} is also illustrated. A frequency difference of +3.8 cm^{-1} in the ν_{13} RR mode at 1240 cm^{-1} is calculated from the RDS. A low frequency line at 453 cm^{-1} in the RR spectrum of Cu^{2+} ($-CH^{16}O$) porphyrin shifts up to 457 cm^{-1} upon ^{18}O substitution. Excitation wavelength at 406.7 nm.

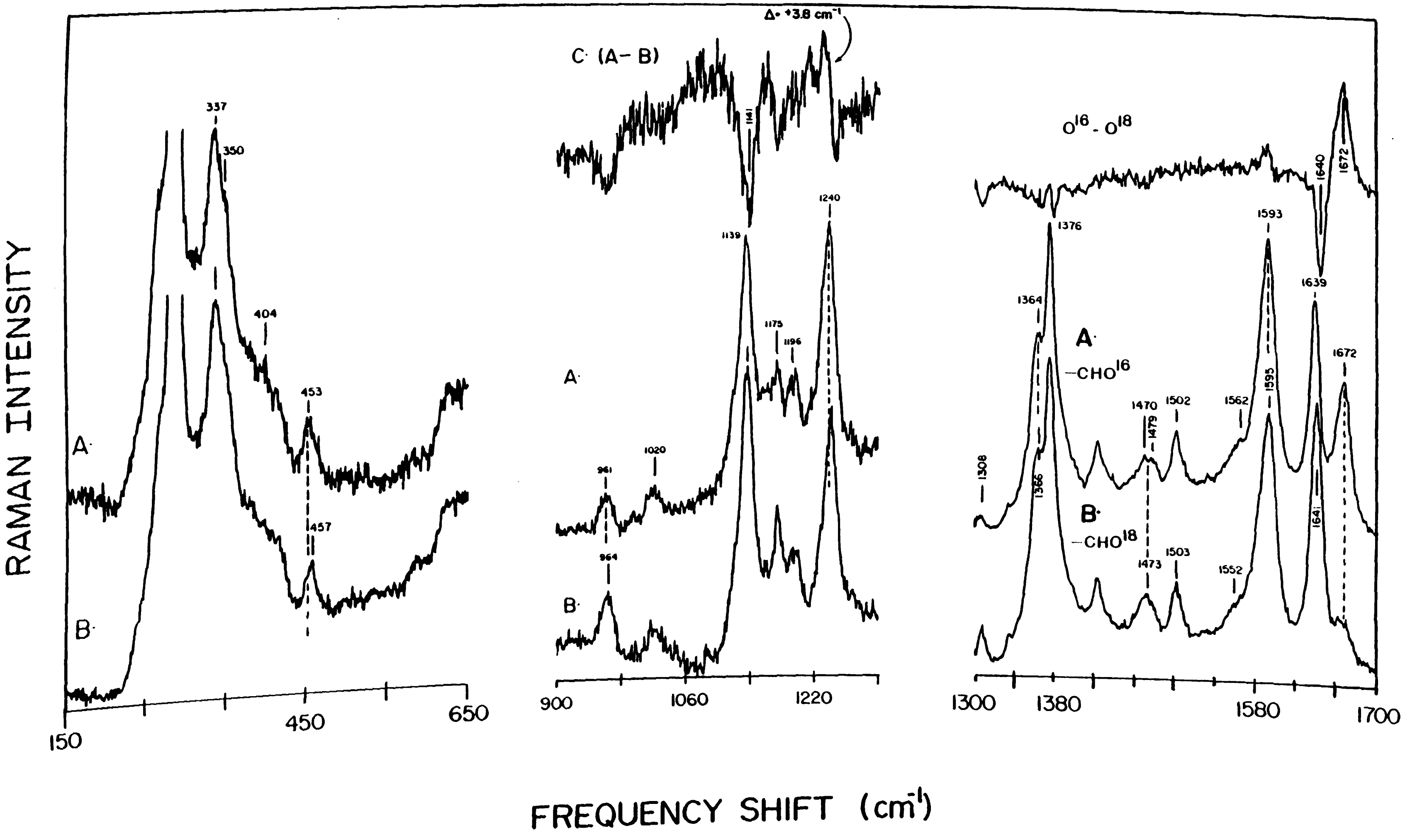
RAMAN INTENSITY
FREQUENCY SHIFT (cm⁻¹)
A·
B·
337
350
404
453
457
150
450
650
C· (A− B)
Δ· +3.8 cm⁻¹
1141
1139
1240
1175
1196
961
1020
964
900
1060
1220
O¹⁶ - O¹⁸
1640
1672
1376
1593
1364
1639
A· —CHO¹⁶
1470
1479
1502
1562
1595
1308
1366
B· —CHO¹⁸
1473
1503
1552
1641
1300
1380
1580
1700

Figure 3.8: Infrared (FTIR) spectra of heme $\underline{a}^{3+}Cl^-$ $(-CH^{16}O)$, $Cu^{2+}(-CH^{16}O)$ porphyrin, and Cu^{2+} $(-CH^{18}O)$ porphyrin derivatives in KBR pellets in the region from 1000 to 1800 cm^{-1}. Instrumental conditions: resolution 2 cm^{-1}; sensitivity 1 second; number of scans, 250 .

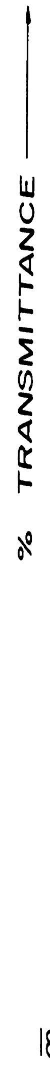

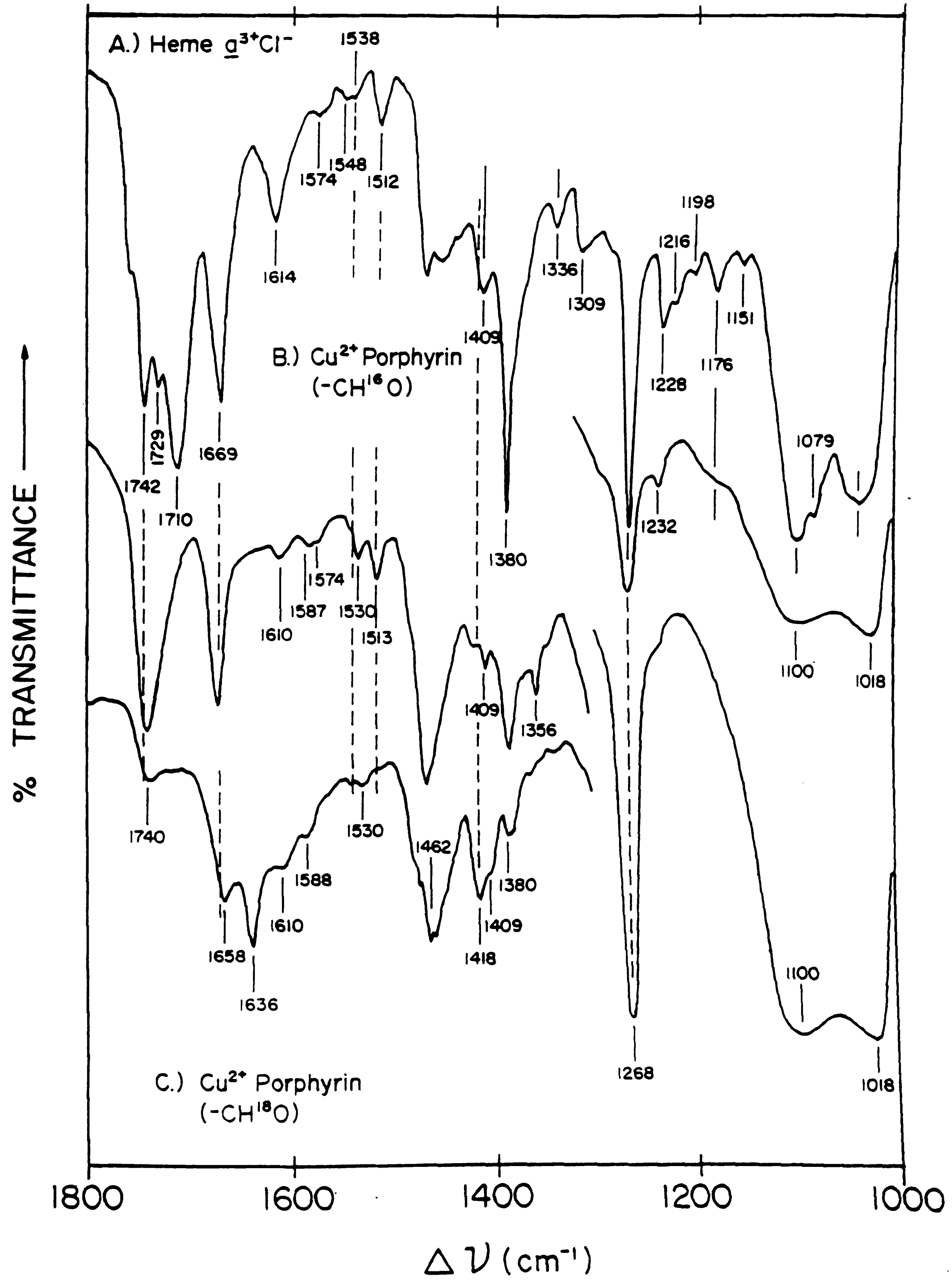
A.) Heme a3+Cl−
1538
1574
1548
1512
1614
1336
1309
1198
1216
1151
1228
1176
1409
B.) Cu2+ Porphyrin
(-CH16O)
1729
1742
1710
1669
1079
1380
1232
1610
1587
1574
1530
1513
1100
1018
1409
1356
1740
1530
1462
1588
1610
1380
1409
1658
1418
1636
1100
1268
1018
C.) Cu2+ Porphyrin
(-CH18O)
% TRANSMITTANCE
1800
1600
1400
1200
1000
Δν (cm−1)

dim

Fig

inf

In

for

sub

mod

of

al.

of-

sub

Wil

ana

wit

it

sub

sym

and

spe

tia

ν_{13}

ser

and

vib

sub

IR-dimethylester of protoporphyrin Fe^{3+} Cl^- are displayed in Figure 3.9. In Table 3.4 we summarize the observed RR and infrared frequencies sensitive to formyl ^{18}O-substitution. In addition, frequency shifts caused by hydrogen bond formation to the C=O group in Cu^{2+} ($CH^{16}O$) and Cu^{2+} ($CH^{18}O$) substituted porphyrins are also indicated in Table 3.4.

While the RR spectra of hemeproteins and porphyrin model compounds appear to be more sensitive to enhancement of in-plane porphyrin skeletal modes (Spiro, 1983; Choi et al., 1982), additional information on the activity of out-of-plane porphyrin modes and internal vibrations of the C_b-substituents should be apparent in the IR spectra. Recently, Willems and Bocian (1984 & 1985) carried out a comprehensive analysis of the IR and RR spectra of Ni^{2+} deuteroporphyrins with conjugated carbonyl substituents. From these studies, it was clear that unsymmetrical implantation of conjugated substituents at the porphyrin periphery lowers the effective symmetry to produce splitting of E_u modes in the IR spectra and selective activity for some of these modes in the RR spectra. They also concluded that Raman modes with substantial peripheral substituent character such as ν_2, ν_8, and ν_{13} were strongly substituent dependent. Differences observed by Willems and Bocian (1984) in the frequency of ν_8 and ν_{13} were attributed to kinematic effects in the vibrational Hamiltonian, which are induced by changes in substituent masses. The above authors were able to identify IR-allowed E_u modes that exhibited large dependence on

Figure 3.9: Infrared (FTIR) spectra of heme a^{3+}Cl^{-}, Cu^{2+} (-CH^{16}O) porphyrin, and the dimethylester (DME) derivative of protoporphyrin IX Fe^{3+}-Cl^{-} in carbon tetrachloride (CCl$_4$) solutions. Instrumental conditions: resolution 2 cm^{-1}, sensitivity 1 second, one scan. Solvent contributions were substracted.

TRANSMITTANCE

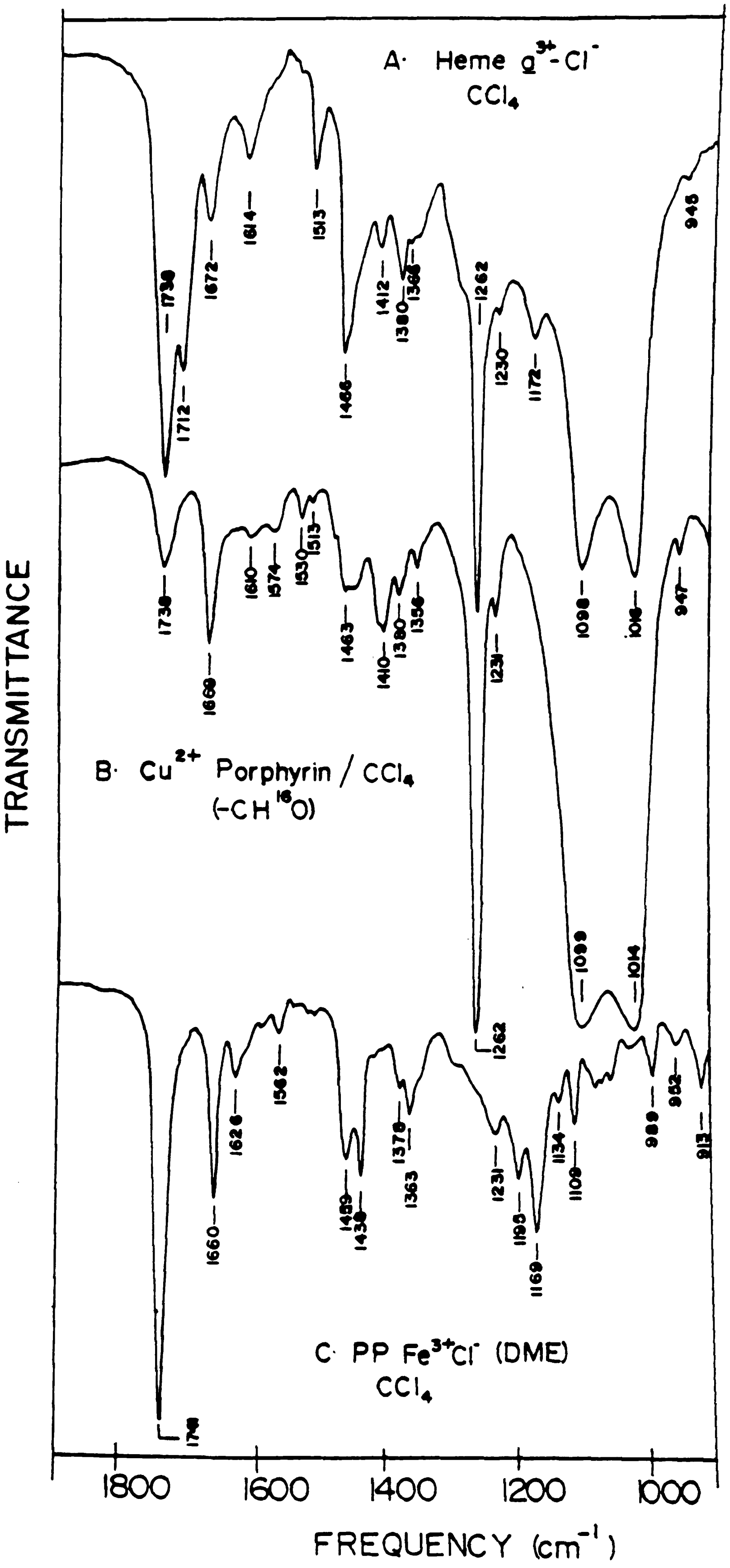
A· Heme a3+-Cl−
CCl4
1738
1712
1672
1614
1513
1466
1412
1380
1368
1262
1230
1172
946
1738
1668
1610
1574
1530
1513
1463
1410
1380
1356
1231
1098
1016
947
B· Cu2+ Porphyrin / CCl4
(-CH16O)
1099
1014
1262
1660
1626
1562
1459
1438
1378
1363
1231
1195
1169
1134
1108
989
952
913
C· PP Fe3+Cl− (DME)
CCl4
1741
TRANSMITTANCE
1800
1600
1400
1200
1000
FREQUENCY (cm−1)

Subs

Modes

$\nu_{C=O}$

ν_2 C_b-

ν_{38} C_b

$\delta_{H-C=O}$

ν_{41} C_a

ν_{42} C_b

$\nu(C_b$-

ν_{13}

Pyr.

fold

$\nu_{46}\delta C_b$-

---

a. Po

(1

b. Re

th

of

c. Ob

Table 3.4. Resonance Raman (RR) and Infrared (IR) Frequencies (cm^{-1}) Sensitive to $-CH^{16}O$ ---- $-CH^{18}O$ Substitution at the Formyl Group of Cu^{2+} (4-Vinyl-8-Formyl) Porphyrin.

Modes:[a]	Cu^{2+} ($-CH^{16}O$)		Cu^{2+} ($-CH^{18}O$)		$-CH^{16}O$ + Ph-OD
	RR	IR	RR	IR	RR
$\nu_{C=O}$	1672	1669			1643
ν_2 C_b-C_b	1593		1595		1598
ν_{38} C_b-C_b		1530 1513[b]		1530 (~1480)[b]	
$\delta_{H-C=O}$	1399[c]	1410		1418	1405[c]
ν_{41} C_a-N	1365	1356	1367	(~1370)	1365
ν_{42} C_b-S $\nu(C_b-CHO)$		1261 1232		1268 (~1260)	
ν_{13}	1238		1243		1248
	960		964		963
		754 734		744	
Pyr. fold	453		457		(453)
$\nu_8 \delta C_b$-S	350 337		350 337		348

---

a. Porphyrin mode assignments follow those by Abe et al. (1978).

b. Replacement of ^{16}O by ^{18}O result in the disappearance of the 1513 cm^{-1} IR line with the concomitant appearance of a new shoulder at ~1480 cm^{-1}.

c. Observed in CCl_4 solutions.

pe

ν_{38}

Th

ν_{42}

th

al

th

by

$\underline{a}^2$

le

en

fr

th

Th

Ni

th

se

te

st

fe

at

co

sp

en

sp

peripheral substituent symmetry lowering effects, such as ν_{38} (C_b-C_b; 1550-1560 cm^{-1}) and ν_{41} (Ca-N; 1360-1366 cm^{-1}). The increased splitting and hence, loss of degeneracy of ν_{42} (C_b-S; 1260-1268 cm^{-1}) and ν_{43} (C_b-S; 1165-1172 cm^{-1}) in the IR spectrum of Ni^{2+}(2,4-diformyldeuteroporphyrin) was also suggested.

The assignment of some of these IR-allowed E_u modes in the RR spectra of heme a derivatives was recently attempted by Choi et al. (1983). By comparing the RR spectra of heme a^{2+} $(N\text{-}MeIm)_2$ obtained with two different excitation wavelengths (514.5 and 592 nm), the above authors suggested the enhancement and splitting of ν_{37} (C_a-Cm) mode with RR frequencies at 1614 cm^{-1} and 1588 cm^{-1}, presumably through the X- and Y- electronic dipole transitions, respectively. The arguments advanced by Willems and Bocian (1984) for Ni^{2+} formyl substituted porphyrin, however, does not confirm these observations, since splitting of ν_{37} was not observed. Splitting of ν_{38} in heme a^{3+} Cl^- was also suggested by Spiro and coworkers from a comparison of the solid state IR spectra of ferric five coordinate heme a Cl^- and ferric protoporphyrin IX Cl^-; in their study a small feature at 1525 cm^{-1} in the IR spectrum of the latter compound was correlated with lines at 1544 cm^{-1} and 1512 cm^{-1} in the IR spectrum of heme a^{3+} Cl^-.

Because of the confusion in the frequencies and apparent vibrational splittings of ν_{37} and ν_{38} modes in the IR spectra of heme a, and owing to the expected contributions

of
id
so
po
th
Th
ti
Th
st
ev
ex
PP
st
is
ti
he
al
ed
be
up
IR
en
in

th
di

of the formyl group to these E_u modes, we took the task of identify them by using the IR spectra of heme a^{3+} Cl$^-$ in the solid and solution states. The Cu^{2+} (CH^{16}O)/(CH^{18}O) porphyrin derivatives have also been useful and we assess the sensitivity of these E_u modes to formyl H-bond effects. The IR spectra of heme a^{3+} Cl- reported here differ substantialy from those reported by Spiro and coworkers (1983). These spectral differences are as follows: both the solid state (Figure 3.8) and solution spectra (Figure 3.9) show no evidence for enhancement of the vinyl stretching frequency expected at 1626 cm^{-1} which is evident in the IR spectrum of PPIX(DME)-Fe^{3+} Cl$^-$ (see Figure 3.9, trace C); a relatively strong band at 1614 cm^{-1} is detected in our IR spectra, but is absent in the Choi et al. (1983) spectrum; a new absorption at 1410 cm^{-1} was reproducibly detected with all the heme a^{3+} Cl- and conjugated carbonyl Cu^{2+} models that was also absent in the Choi et al. (1983) spectrum. As mentioned above, we assign this latter mode to the formyl-hydrogen bend, and its upshifted frequency to 1418 cm^{-1} (+8 cm^{-1}) upon ^{16}O ----> ^{18}O substitution supports our assignment. The IR spectra reported here were reproduced with three different heme a^{3+} Cl$^-$ preparations and with two different FTIR instruments.

Isotopically substituted Cu^{2+} (CH^{18}O) porphyrin display the $\nu_{c=o}$ frequency at 1640 cm-1, as detected by the RDS difference spectrum (see Figure 3.7). This 32 cm-1 shift

in
dif
1.
mag
suc
(Ka
Pin
198
upc
(se
pla
^{18}
shi
4 c
the
RR
con
IR
por
str
sol
We
hem
wit
men
com
com

in $\nu_{C=O}$ is in good agreement with the 42 cm^{-1} frequency difference calculated from the reduced masses (μ_2/μ_1 = 1.025) of the C=O carbonyl group. Carbonyl shifts of this magnitude have been reported in the past for simple systems such as isotopically labelled diisopropylketones (Karabatsos, 1960), ^{18}O-labelled benzophenone (Halmann and Pinchas, 1958), and ^{18}O-labelled acetone (Kamoun and Mirone, 1980). Formyl modes previously observed to be perturbed upon -CHO deuteration in heme a and Cu^{2+} porphyrin a models (see Figures 3.5 and 3.6) are also seen to be altered upon placement of labelled-^{18}O. Upon substitution of ^{16}O ----> ^{18}O, the RR spectrum of Cu^{2+} porphyrin revealed a frequency shift in ν_2 at 1593 cm^{-1} shifting up to 1595 cm^{-1}, and a 4 cm^{-1} upshift in the ν_{13} mode at 1240 cm^{-1} as detected by the RDS difference spectrum. The sensitivity of this latter RR mode to formyl-proton and oxygen-substitution indicates considerable contribution from the ring-formyl stretch. The IR spectra of heme a^{3+} Cl^- and its normal Cu^{2+} ($CH^{16}O$) porphyrin model in KBr and solution states show a sharp strong band at 1260 cm^{-1}, which is not observed in the solution spectra of PPIX-Fe^{3+} Cl^- (see Figure 3.9, trace C). We assign this IR band to the ν_{42} $\nu(C_b-S)$ E_u mode of heme a^{3+} Cl^-. It appears to be split into two components with frequencies at 1260 cm^{-1} and 1230 cm^{-1}. Upon replacement of ^{16}O by ^{18}O at the formyl oxygen, the higher energy component shifts up to 1268 cm^{-1}, while the lower energy component appears to move under the stronger 1260 cm^{-1} line.

Th
of
ti
al
co
Fi
ag
Ni
bu
ne
fo
ca

po
(s
(C
th
si
ν_{41}
(F
id
co
an
at
li
cm
ho

The $^{16}O/^{18}O$ induced upshift of the higher energy component of ν_{42} (1260 --- 1268 cm^{-1}) is consistent with a substantial contribution from the ν_{Cb-CHO} stretch to this IR-allowed mode. The direction of its frequency shift is consistent with that observed in the benzaldehyde model (see Figure 3.4 and Table 3.2). Our results are in good agreement with the recent analysis of the formyl modes of Ni^{2+} (2,4-diformydeuteroporphyrin), in which strong contributions from the ring-formyl stretch to the IR-active component ν_{42} mode was concluded from deuteration of the formyl proton (Willems and Bocian, 1984). In this latter case, loss of degeneracy on the ν_{42} was also detected.

The oxidation state marker band region of Cu^{2+} porphyrin displays two bands at 1376 cm^{-1} and at 1364 cm^{-1} (see Figure 3.7). The former band is assigned to the ν_4 (C_a-N) vibration while the latter appears to correspond to the RR active component of the ν_{41} IR-allowed E_u mode, since the IR spectra of Cu^{2+} porphyrin clearly indicate that ν_{41} is split with frequencies at 1380 cm^{-1} and 1356 cm^{-1} (Figure 3.8). The second component of ν_{41} cannot be identified in the RR spectrum since it falls within a rather congested region. In the case of heme $\underline{a}^{3+}$ Cl^-, the solid and solution state IR spectra display at strong absorption at 1380 cm^{-1}, with a weak shoulder at 1366 cm^{-1}. The former line is assigned to the ν_{41} IR-allowed mode and the 1366 cm^{-1} might correspond to the second split component of ν_{41}; however, the RR spectrum of heme $\underline{a}$ does not show activity

fo
sp
pr
sp
ag
th
13
(s
ha
(-
th
ac
at
ap
wi

KB
ba
fo
cm
co
cm
15
tu
fr
cm
The

for either of these ν_{41} vibrations. Interestingly, the RR spectrum of Cu^{2+} porphyrin a (see Figure 3.6) does show a pronounced shoulder at ~1366 cm^{-1} which might well correspond to the second RR active component of the ν_{41}, in agreement with results from Cu^{2+} porphyrin. H/D exchange at the formyl group of Cu^{2+} porphyrin a appears to shift this 1366 cm^{-1} shoulder under the strong ν_4 band at 1377 cm^{-1} (see Figure 3.6) as noticed by the narrower bandwith at halfheight (i.e., $\Gamma = 8$ cm^{-1}) in the RR spectrum of Cu^{2+} (-CDO) porphyrin a. Similarly, upon $^{16}O/^{18}O$ substitution, the 1356 cm^{-1} IR absorption apparently vanishes, but this is accompanied by a significant increase in intensity of a line at ~1370 cm^{-1} in the RR spectrum of Cu^{2+} porphyrin. This apparent upshift in this ν_{41} component is also consistent with strong formyl character.

The IR spectra of heme a^{3+} Cl^- and Cu^{2+} porphyrin, in KBr pellets, in the region from 1500 to 1600 cm^{-1} display bands at 1574 cm^{-1} (weak), 1544 cm^{-1} (weak), and 1512 cm^{-1} for the former compound, while for the latter bands at ~1574 cm^{-1} (weak), 1530 cm^{-1} and 1513 cm^{-1} are observed. The corresponding solution spectra show a single band at 1513 cm^{-1} for heme a^{3+}-Cl^- and weaker absorptions at 1574 cm^{-1}, 1530 cm^{-1}, and 1513 cm^{-1} for Cu^{2+} porphyrin. Upon substitution of isotopically labeled-^{18}O, the 1513 cm^{-1} IR line from Cu^{2+} porphyrin vanishes, while the 1530 cm^{-1} and 1574 cm^{-1} bands retain most of their IR absorption intensity. The IR spectrum of PPIX-Fe^{3+} Cl^- in solution illustrates IR

ab
sh
in
ag
ri
$\underline{a}^{3}$
se
(h
Th
--
su
qu
he
ex
er
E_u
th
co

an
th
et
an
ob
of
Th
br

absorptions at 1588 cm^{-1} (weak), 1562 cm^{-1}, and a weak shoulder at 1508 cm^{-1}. We assign the strongest absorption in PPIX-Fe^{3+} Cl^{-} at 1562 cm^{-1} as due to ν_{38} (C_b-C_b), in agreement with similar assignments made for Ni-protoporphyrin (Willems and Bocian, 1984; Abe et al., 1978). For heme $\underline{a}^{3+}$ Cl^{-} and its Cu^{2+} ($CH^{16}O$) porphyrin derivative, this mode seems to split with frequencies at 1544 cm^{-1} and 1513 cm^{-1} (heme a) and at 1530 cm^{-1} and 1513 cm^{-1} (Cu^{2+} porphyrin). The disappearance of the 1513 cm^{-1} IR absorption upon $CH^{16}O$---> $CH^{18}O$ substitution is consistent with this mode having substantial contribution from the formyl group. The frequency differences between the 1544 cm^{-1} ν_{38} component of heme $\underline{a}^{3+}$ Cl- and 1530 cm^{-1} component of Cu^{2+} porphyrin is explained on the basis of the presence of different peripheral substituents. Our observation of splitting of the ν_{38} E_u mode in the IR spectrum of heme a is in agreement with that by Choi et al. (1983); however, we believe that the corresponding frequency in PPIX-Fe^{3+} Cl^{-} is at 1562 cm^{-1}.

The 1614 cm^{-1} and 1610 cm^{-1} IR lines of heme $\underline{a}^{3+}$ Cl^{-} and Cu^{2+} porphyrin, respectively, appears to correspond to the ν_{37} (Ca-Cm) vibrational mode frequency described by Abe et al. (1978). This mode is largely resistant to splitting, and under our experimental conditions, RR activity is not observed. It also appears to be insensitive to substitution of ^{18}O at the -CHO group oxygen, as is shown in Figure 3.8. The contribution to ν_{37} is predominantly C_a-C_m methine bridge (Abe et al., 1978), although Spiro and coworkers have

su
It
ap

fr
po
16
Fe
pr
de
vi
ma
me
tw
pl
di
of
vi
gr
its
ti
2,
Cu
the
To
st
nee

suggested that this assignment should be of C_b-C_b character. It is our opinion that the former assignment would be more appropriate in view of the isotopic evidence presented here.

We have not been able to identify the vinyl stretching frequency of heme a^{3+} Cl^- and its 4-vinyl-8-formyl-Cu^{2+} porphyrin model. This vinyl mode is expected around 1625-1628 cm^{-1}, by analogy with the 1626 cm^{-1} absorption of PPIX-Fe^{3+} Cl^- (see Figure 3.9). In the RR spectra of heme proteins enhancement of vinyl modes has been suggested to depend upon the extent of vibronic coupling between the vinyl π-orbitals with the excited state of the porphyrin macrocycle (Choi et al., 1982), and hence lack of enhancement might be an indication of a slight out-of-plane twisting of the vinyl group with respect to the porphyrin plane. Recently, Rousseau et al. (1983) attributed the discrepancies in frequencies observed for the vinyl groups of hemoglobin A and leghemoglobin as due to different vinyl-protein interactions resulting in different vinyl group conformation. In the isolated heme a chromophore and its Cu^{2+} porphyrin analog, it is likely that steric interactions between the heme a hydroxylfarnesil tail at position 2, or the pentyl (i.e., $-(CH_2)_4CH_3$) group at position 2 in Cu^{2+} porphyrin, and the vinyl group hydrogens will not allow the vinyl π-bond system to assume a coplanar configuration. To address this interesting observation, crystal structure studies of heme a^{3+} Cl^- and its 4-vinyl-8-formyl models, are needed.

the
deu
3.2
in
as
fer
H-b
spe
phe
spe
wit

pro
3.1
(15
tiv
phy
and
al.
add
rev
dec
to
spe

D. H-Bonding Effects in Heme a Models.

Raman spectra of H-bonded benzaldehyde indicate that the C=O stretching and deformation modes are insensitive to deuterium exchange at the H-donor (see Figure 3.4, and Table 3.2), and hence suggest a weak H-bond. This seems to hold in the RR spectra of heme a and its Cu^{2+} porphyrin models, as shown in Figures 3.10 to 3.12. In Figure 3.10, the RR of ferric heme $a^{3+}(N\text{-}MeIm)_2$ non-hydrogen bonded in CH_2Cl_2, and H-bonded to phenol-OH and phenol-OD, are compared. The RR spectra of ferrous heme $a^{2+}(N\text{-}MeIm)_2$ in the presence of phenol-OD as the H-donor are shown in Figure 3.11. The RR spectra of Cu^{2+} porphyrin under the influence of H-bonding with phenol-OH and phenol-OD are illustrated in Figure 3.12.

The low-frequency RR of ferrous heme a in aprotic, protonated, and deuterated solvents are shown in Figure 3.13. Our interest in measuring the low-frequency regions (150-650 cm-1) of the RR spectra of heme a and its derivatives arise because of the expected contribution from porphyrin peripheral substituents to ν_8 (δ_{Cb-S}, 330-350 cm^{-1}) and ν_9 (δ_{Cb-S}, 265-275 cm^{-1}) modes as suggested by Abe et al. (1978), and recently by Willems and Bocian (1984). In addition, our hydrogen-bonding studies with benzaldehyde reveal a low-frequency mode at 441 cm^{-1} for ø-CHO which decreases in intensity upon H-bonding formation, and shifts to lower frequencies upon formyl-proton deuteration. The RR spectrum of Cu^{2+} porphyrin displays a band at 453 cm^{-1} (see

Figure 3.10: Resonance Raman (RR) spectra of ferric non-hydrogen bonded heme a^{3+}(N-MeIm)$_2$ (in CH_2Cl_2) (trace A) and ferric heme a^{3+}(N-MeIm)$_2$ (in CCl_4) hydrogen bonded to phenol-OH (trace B) and phenol-OD$_6$ (trace C). The bottom trace (D) is the Raman difference spectrum between samples B and C recorded with the Raman difference apparatus. Exitation wavelength at 406.7nm. Average of ten scans.

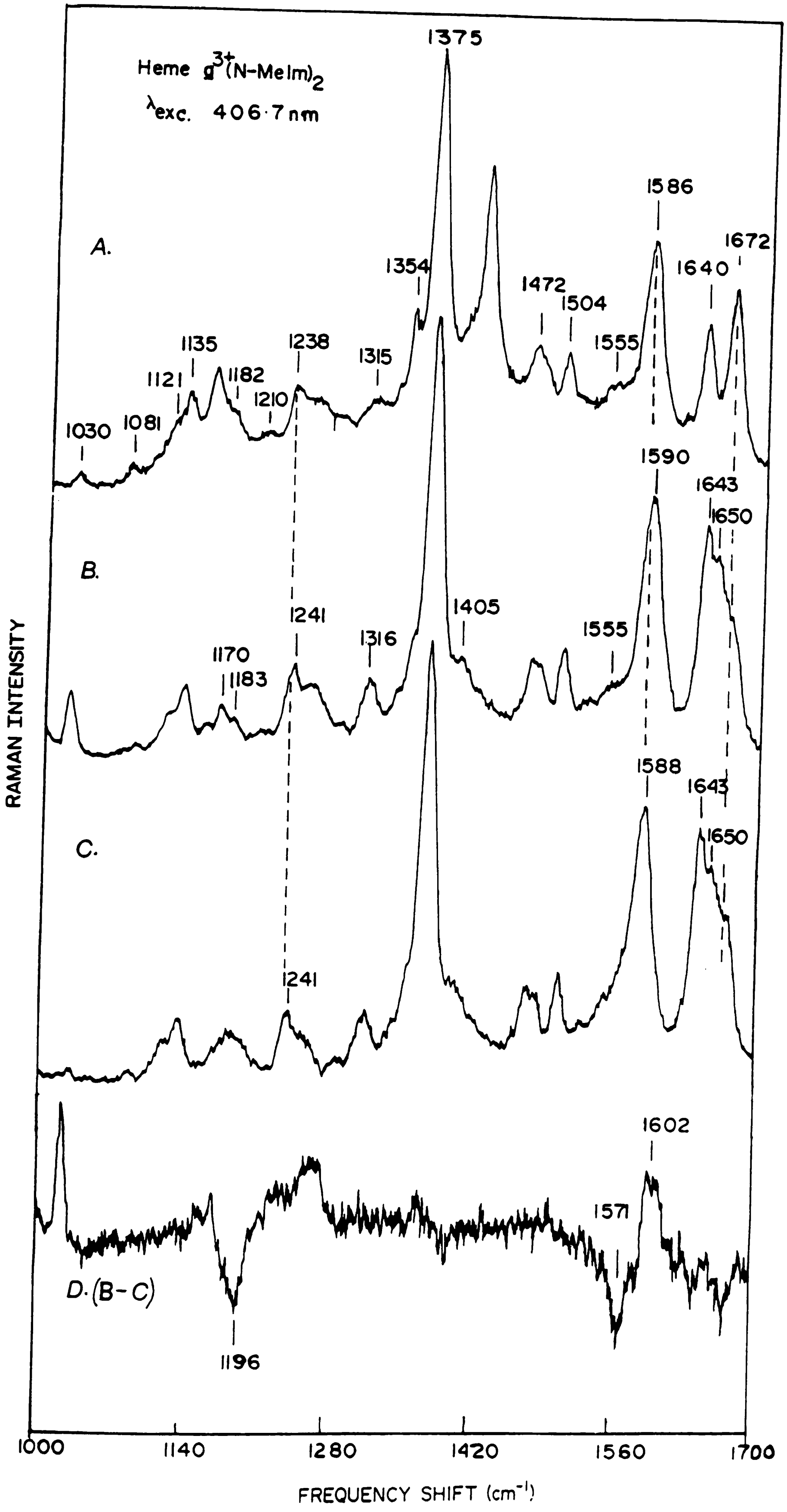
Heme g^{3+}(N-MeIm)$_2$
$\lambda_{exc.}$ 406·7 nm
A.
1375
1586
1672
1640
1354
1472
1504
1555
1135
1238
1315
1121
1182
1210
1030
1081
B.
1590
1643
1650
1405
1241
1555
1316
1170
1183
C.
1588
1643
1650
1241
D.(B−C)
1602
1571
1196
RAMAN INTENSITY
1000
1140
1280
1420
1560
1700
FREQUENCY SHIFT (cm^{-1})

RAMAN INTENSITY

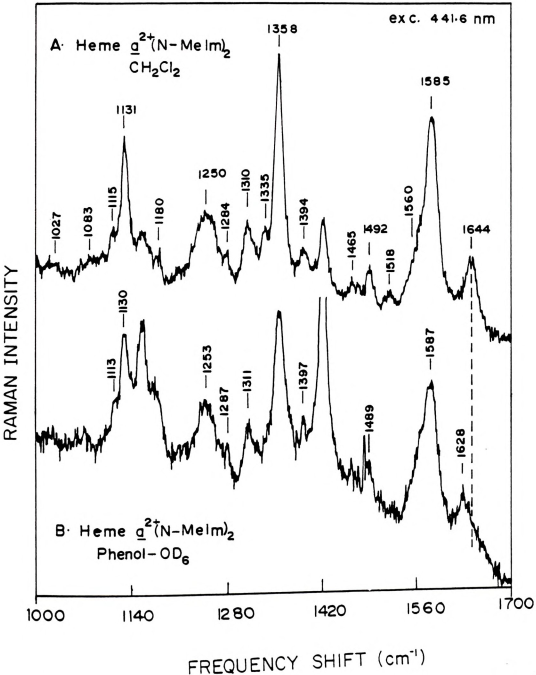

Figure 3.11: Resonance Raman spectra of ferrous heme $\underline{a}^{2+}$ (N-MeIm)$_2$ H-bonded to phenol-OD$_6$ in dry CH_2Cl_2.

Figure 3.12: Resonance Raman (RR) spectra of Cu^{2+} ($-CH^{16}O$) porphyrin in CH_2Cl_2 (trace A) and under hydrogen bonding to phenol-OH (trace B) and phenol-OD_6 (trace C). The bottom trace illustrates the Raman difference spectrum between samples B and C. Excitation wavelength is 406.7 nm.

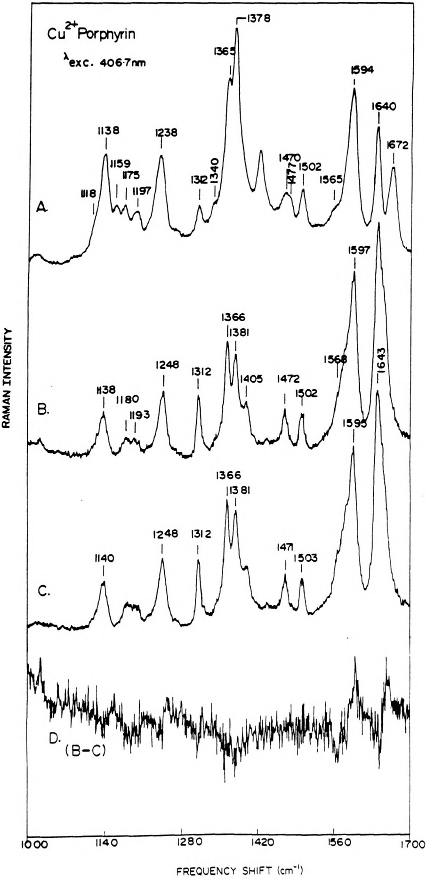
Cu^{2+} Porphyrin
$\lambda_{exc.}$ 406.7nm
A.
1118
1138
1159
1175
1197
1238
1312
1340
1365
1378
1470
1477
1502
1565
1594
1640
1672
B.
1138
1180
1193
1248
1312
1366
1381
1405
1472
1502
1568
1597
1643
C.
1140
1248
1312
1366
1381
1471
1503
1595
D.
(B−C)
RAMAN INTENSITY
1000
1140
1280
1420
1560
1700
FREQUENCY SHIFT (cm^{-1})

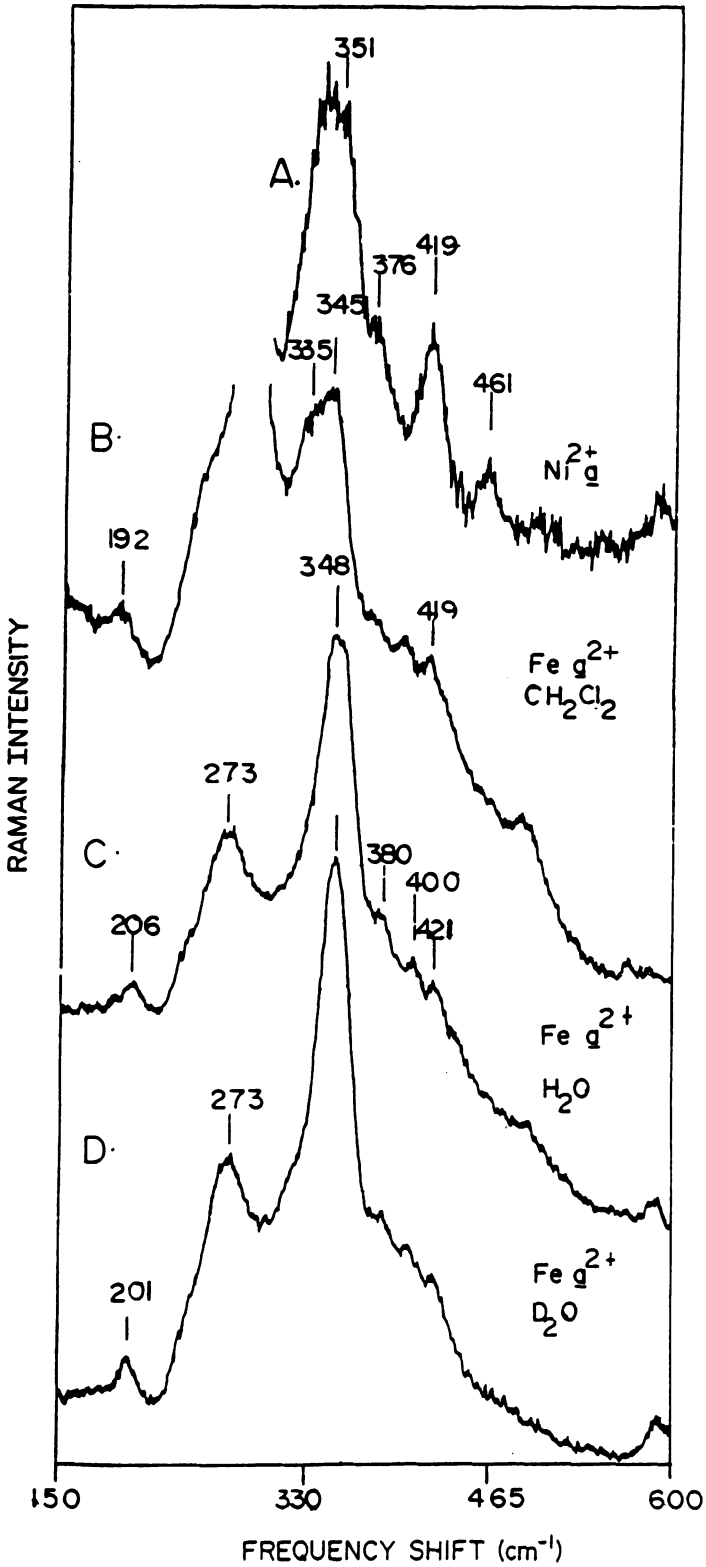

Figure 3.13: Low frequency resonance Raman spectra of heme $\underline{a}^{2+}$(N-MeIm)$_2$ in CH_2Cl_2 and under hydrogen bonding conditions (traces C and D). The RR spectrum of Ni^{2+} porphyrin $\underline{a}$ is also illustrated. Excitation wavelength is at 406.7 nm.

Figu
a H-
form
Ni^{2+}
obse
assi
form
vent
appe
Figu
sing
3.13
shif
with
Vibr
prev

dete
upon
(ν
resp
cm^{-1}
10 c
upsh
obse
subs
buti

Figure 3.7) which decreases in intensity in the presence of a H-donor. Intensity changes in this line upon H-bond formation was also observed in the RR spectra of Cu^{2+} and Ni^{2+} porphyrin a (spectra not shown). Based upon these observations and the assignments made for benzaldehyde, we assign this mode to a pyrrole folding mode with substantial formyl character. For heme $a^{2+}(N\text{-}MeIm)_2$ in aprotic solvents, two low-frequency modes at 335 cm^{-1} and 345 cm^{-1} appear to be sensitive to H-bonding effects (traces B and C, Figure 3.13) since upon use of hydrogen bonding solvents a single band is observed at ~348 cm^{-1} (traces C and D, Figure 3.13). This behavior is consistent with the 335 cm^{-1} line shifting up to ~348 cm^{-1} and becoming vibrationally coupled with the 345 cm^{-1} line (assigned as 2 ν_{35}) upon H-bonding. Vibrational coupling between ν_8 and 2 ν_{35} modes has been previously suggested (Abe et al., 1978).

In the high-frequency region, the formyl-related modes detected by isotopic substitution undergo frequency shifts upon H-bonding to the carbonyl oxygen. Modes at 1586 cm^{-1} (ν_2) and 1238 cm^{-1} are upshifted by 4 cm^{-1} and 3 cm^{-1}, respectively; and the formyl-hydrogen bend shifts up to 1405 cm^{-1}. In the RR spectrum of Cu^{2+} porphyrin (Figure 3.12), a 10 cm^{-1} upshift is detected in the frequency of ν_{13}. This upshifted frequency agrees with the direction of shift observed for the IR-allowed ν_{42} Eu mode upon $^{16}O \text{---}> {}^{18}O$ substitution (Figure 3.8), and accordingly a marked contribution from the $\nu_{C_b\text{-}CHO}$ stretching motion to the ν_{13}

Rama

The

bond

form

mode

diff

spec

tion

this

to H

aque

phen

is t

equa

and

This

hydr

H fo

terc

doub

elon

Raman active mode is consistent with the Raman and IR-data. The sensitivity of ν_2 (Cb-Cb) to isotopic and hydrogen bonding effects at the formyl group of heme a and its formyl-containing derivatives stems from its pyrrole-ring mode composition. Choi et al. (1983) interpreted frequency differences in ν_2 between heme a and protoporphyrin as specifically due to the heme a formyl-vinyl trans disposition. The data presented here appears to be consistent with this interpretation.

Of interest in the evaluation of formyl modes sensitive to H-bonding is the $\nu_{C=O}$ stretching. For ferric heme a in aqueous detergent, $\nu_{C=O}$ shifts down by 17 cm^{-1}, with phenol-OH/-OD the downshift is 21 cm^{-1} and when p-Cl-phenol is the donor the shift is 25 cm^{-1} (see Table 3.1). The equal shifts in the $\nu_{C=O}$ frequency upon use of phenol-OH and phenol-OD indicate a weak H-bond (Singh and Wood, 1969). This interpretation predicts no isotopic perturbation to the hydrogen bond distance ($R_{O...O}$) as a result of changing the H for D and indicate that the motion of the proton and deuteron is approximately harmonic. For this type of H-bond, a double minimum potential surface (with high barrier) with an elongated R(O...O), has been proposed (Emsley, 1984).

IV.

for

4-v

all

cal

the

of

data

subs

and

and

Heme

unde

subs

-CHC

sinc

obse

inte

acid

in

pres

the

oxid

resi

at t

IV. Conclusions:

The evidence presented here in the identification of formyl modes in the RR and IR spectra of heme a and its 4-vinyl-8-formyl Cu^{2+} derivatives indicates that several IR-allowed E_u-modes appear to be split, owing to the asymmetrical disposition of the vinyl-formyl groups, and that some of these vibrations become Raman active as a direct consequence of the strong asymmetry of the porphyrin macrocycle. Our data from the isotopic studies of the formyl modes indicate substantial coupling between the C=O stretching frequency and the ν_{Cb-CHO} ring-formyl stretching. We have used RR and infrared spectroscopies to investigate this proposal. Heme a and Cu^{2+} porphyrin a formyl modes have been studied under the influence of H-bonding formation and isotopic substitution at the H-donor. Our results indicate that the -CHO...H/D H-bond interaction is a weak H-bond interaction since no isotopic effect in the formyl vibrations was observed. On the contrary, the strength of the H-bond interaction increases for a series of phenol donors with acidic pKa values. This was evidenced by the increase in $\nu_{C=O}$ and red-shifted α -band. These observations are presented as factors that might influence the strength of the cytochrome a...protein interaction in cytochrome oxidase, since changes in the pKa of the formyl surrounding residue are expected to bring about conformational changes at the H-bonded site. For heme a, Cu^{2+} porphyrin a, and

Cu^{2+}

acti

effe

This

upsh

benz

ring-

Cu^{2+} porphyrin, the ν_{13} Raman mode displays considerable activity towards formyl isotopic and hydrogen-bonding effects as evidenced by its 10 cm^{-1} upshifted frequency. This upshifted frequency is consistent with a similar upshift observed in the $\nu_{Cb-CHO...H/D}$ motion of benzaldehyde, and suggests a similar contribution of this ring-formyl stretch to the heme *a* ν_{13} RR active mode.

Vi

I.

cyt
mum
its
a c
oxi
H-b
iro
mec
H-b

bon
of
to
res
cha
com
thr
dis
int
und

CHAPTER IV

Visible Excitation Resonance Raman Spectra of Cytochrome a in Cytochrome Oxidase.

I. Introduction:

The unusual spectroscopic properties of cytochrome a in cytochrome oxidase, its red-shifted α -band absorption maximum and altered carbonyl stretching frequencies relative to its isolated heme a models, have been interpreted as due to a cytochrome a hydrogen bonded formyl group in the *in situ* oxidase (Babcock and Callahan, 1983). The strength of this H-bond interaction was observed to be dependent upon heme iron redox state and accordingly a redox-linked proton pump mechanism was proposed which relies on a change in the H-bond geometry.

Due to the mechanistic implications of this hydrogen bonding interaction in the functional and structural aspects of cytochrome a in cytochrome oxidase, it is of importance to identify other cyt a formyl sensitive vibrations in the resonance Raman spectrum of cytochrome a^{2+}. In the previous chapter we developed a systematic approach with heme a model compounds, with the aim of uncovering formyl sensitive modes throughout the Raman spectrum of heme a that can be used to disentangle other hydrogen bonding sensitive modes in the intact chromophore. We have studied the isolated heme a under the influence of formyl isotopic substitution with the

goal
nal
resu
imid
purp
vibr
memb
the
inte
Rama

cyto
Rama
tran
exci
thos
a^{2+}
in t
been
1983
agre
oxid
cyt
to t
heme
to s
pH-d

goal of identifying and separating formyl modes from internal porphyrin macrocycle vibrations. We have also discussed results obtained after placing the isolated heme a (bis-imidazole) model under hydrogen bonding conditions with the purpose of establishing trends of formyl hydrogen bond vibrations and the strength of this interaction in the membrane bound chromophore. In this chapter, we will use the results developed with these heme a model compounds to interpret the cytochrome a^{2+} visible excitation resonance Raman (RR) spectrum, studied under H/D exchange conditions.

To isolate the vibrations of cytochrome a from those of cytochrome a_3, we have used visible excitation resonance Raman spectroscopy, in resonance with the $Q_{(0-0)}$ $\pi \rightarrow \pi^*$ transition of reduced cyt a^{2+} at 605 nm. With this laser excitation, the vibrations of cyt a^{2+} are isolated from those of cyt $a_3{}^{2+}$, owing to the dominant contribution of cyt a^{2+} to the 605 nm α-band (Vanneste, 1967). Previous work in the visible excitation range of cytochrome oxidase has been reported (Bocian et al., 1979; Callahan and Babcock, 1983). The results from these two separate investigations agree with the prediction that the visible spectra of oxidized, reduced and mixed-valence oxidase is dominated by cyt a modes and that these appear to be largely insensitive to the ligation and spin-state transformations at the cyt a_3 heme. Babcock and Callahan (1983) used these observations to study the sensitivity of the cyt a vibrations to alkaline pH-denaturation effects. Their results revealed significant

pert
rais
for
cyto

vati
of c
heme
solv
depe
mode
beha
vibr
valu
in t
caus
a ar
resu
sens

II.

A.

by a
1976
expe
15 μ

perturbations of the cyt a visible spectrum as the pH was raised form 7.4 to 10.5, which was interpreted as evidence for the occurrence of a cyt a hydrogen bonded structure in cytochrome oxidase.

Our present investigation extend these original observations. We have studied the RR visible excitation spectra of cyt a^{2+} under the influence of small perturbations at the heme a hydrogen bond induced by the presence of deuterated solvents. We have also studied the depolarization ratio dependence of cyt a vibrational modes and found that a few modes exhibit characteristic anomolous polarization behavior, while the great majority of the visible excitation vibrations appear as polarized modes, approaching a $\rho = 0.33$ value. This is interpreted as due to significant lowering in the molecular symmetry of the heme a porphyrin macrocyle caused by the unusual peripheral substituent pattern of heme a and strong cyt a ... protein interactions, that appear to result in the additional enhancement of Eu substituent sensitive modes and low ρ values.

II. Materials and Methods:

A. Materials:

Cytochrome oxidase from beef heart muscle was isolated by a modified Hartzell-Beinert procedure (Babcock et al., 1976). The oxidase concentration for visible excitation experiments was maintained at 150 μM (heme a basis), and 15 μM for the optical absorption. The buffer-detergent

sys
lau
cor
(Gl
pro
pro
buf
(NH
gat
and
cha
M E
was

ven
ted
cyc
add
the
pro
tho
sig
Cha

system consisted of 50 mM HEPES (pH (or pD)=7.4) and 0.5% lauryl maltoside. The pD of the deuterated buffer was corrected to pD=pH + 0.4 prior to the Raman experiment (Glasoe and Long, 1960). Deuterium exchange in the resting protein was carried out by the following experimental protocol: cytochrome oxidase was reprecipitated in D_2O-buffer by increasing the concentration of saturated $(NH_4)_2SO_4$ (pD 7.4), the pellets were obtained by centrifugation at 19K for ~30 minutes, resuspended in D_2O/maltoside, and dialyzed for six hours at 4° C against two volume changes of a medium consisting of 50 mM HEPES (pD 7.4), 0.01 M EDTA, 0.5% lauryl maltoside in D_2O. This entire procedure was repeated twice.

To prepare the mixed-valence oxidase in deuterated solvents, the resting non-inhibited protein was either incubated in D_2O-buffer for approximately 2-3 days and/or redox-cycled (reduced and reoxidized in D2O-buffer), prior to the addition of 10 mM cyanide. We have previously observed that the addition of cyanide to the resting freshly prepared protein in D_2O/buffer does not yield appreciable changes in those cyt a modes with substantial formyl character. The significance of these observations will be discussed on Chapter VI.

B.

dif
Cha
pro
Rho
ion
105
par
and
abs
exc
164
Cob
a I
zat

II.
A.

100
and
Fig
spe

B. Instrumentation:

The Raman spectrometer, detection system and Raman difference apparatus employed in this study are described in Chapter II. Excitation in the visible absorption band was provided by a Spectra Physics Model 375 dye laser with Rhodamine 6G dye pumped by a Spectra Physics Model 165 Ar^+ ion laser. Power incident at the sample was typically 80-105 mW. The formation and integrity of the reduced and partially reduced oxidase derivatives were monitored before and after the visible excitation experiment by using optical absorption and Soret excitation RR spectra. The Soret excitation lines were provided by a Spectra Physics Model 164-11 Kr^+ ion laser equipped with a high-field magnet, a Coherent Kr^+ ion laser Innova 90K, and the 441.6 nm line of a Lyconix He-Cd laser. The method used to measure depolarization ratios is outlined in Chapter II.

II. Results:

A. Visible Excitation Resonance Raman Spectra of Cytochrome a^{2+} iN H_2O/D_2O Buffers:

The 605 nm excitation resonance Raman spectra from 1000-1700 cm^{-1} of reduced cytochrome oxidase in protonated and deuterated buffers are depicted in Figures 4.1 and 4.2. Figures 4.3 and 4.4 show the corresponding low-frequency RR spectra (150-1000 cm^{-1}). The difference spectrum (i.e.,

Figure 4.1: Visible excitation (605 nm) resonance Raman spectra of reduced cytochrome _c_ oxidase in: A) H_2O and B) D_2O buffers in the region from 1000 to 1300 cm^{-1}. The Raman difference spectrum (H_2O - D_2O) is shown in trace C. Oxidase concentration is 165 μM (heme _a_ basis). Frequency shifts on resonance Raman lines at 1228 cm^{-1} and 1173 cm^{-1} of +5 cm^{-1} and +7 cm^{-1}, respectively, were calculated from the Raman difference spectrum. Modes at 1045 cm^{-1} and 1218 cm^{-1} are attributed to D_2O.

RAMAN INTENSITY

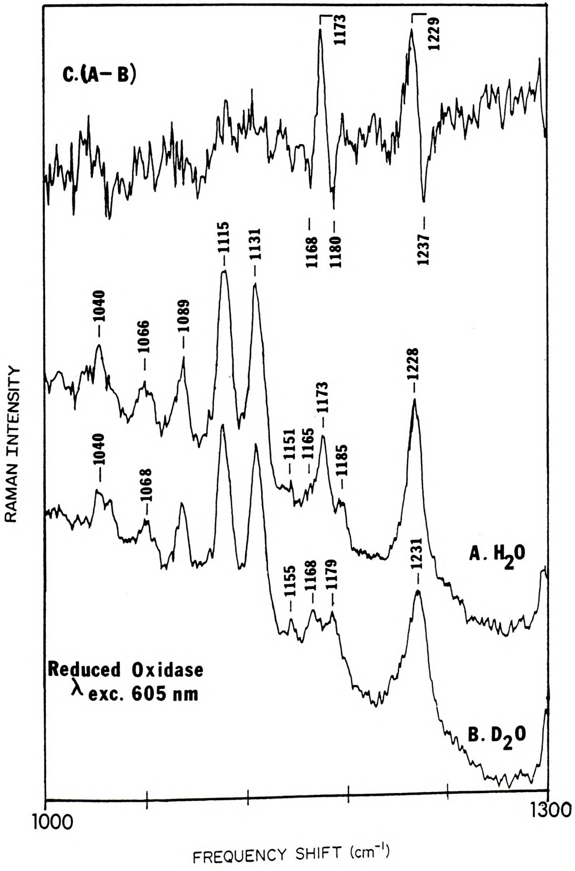
C.(A− B)
1173
1229
1168
1180
1237
1115
1131
1040
1066
1089
1228
1151
1165
1173
1185
1040
1068
A. H_2O
1155
1168
1179
1231
Reduced Oxidase
λ exc. 605 nm
B. D_2O
RAMAN INTENSITY
1000
1300
FREQUENCY SHIFT (cm^{-1})

Figure 4.2: Visible excitation (605 nm) resonance Raman spectra of reduced cytochrome c oxidase in: A) H_2O and B) D_2O buffers in the range from 1300 to 1700 cm^{-1}. The Raman difference spectrum (H_2O - D_2O) is shown in trace C. Oxidase concentration is 165 μM (heme a basis). Frequency shifts in modes at 1310 cm^{-1}, 1329 cm^{-1}, and 1615 cm^{-1} are detected. Increased intensity in the 1545 cm^{-1} vibration is also evident.

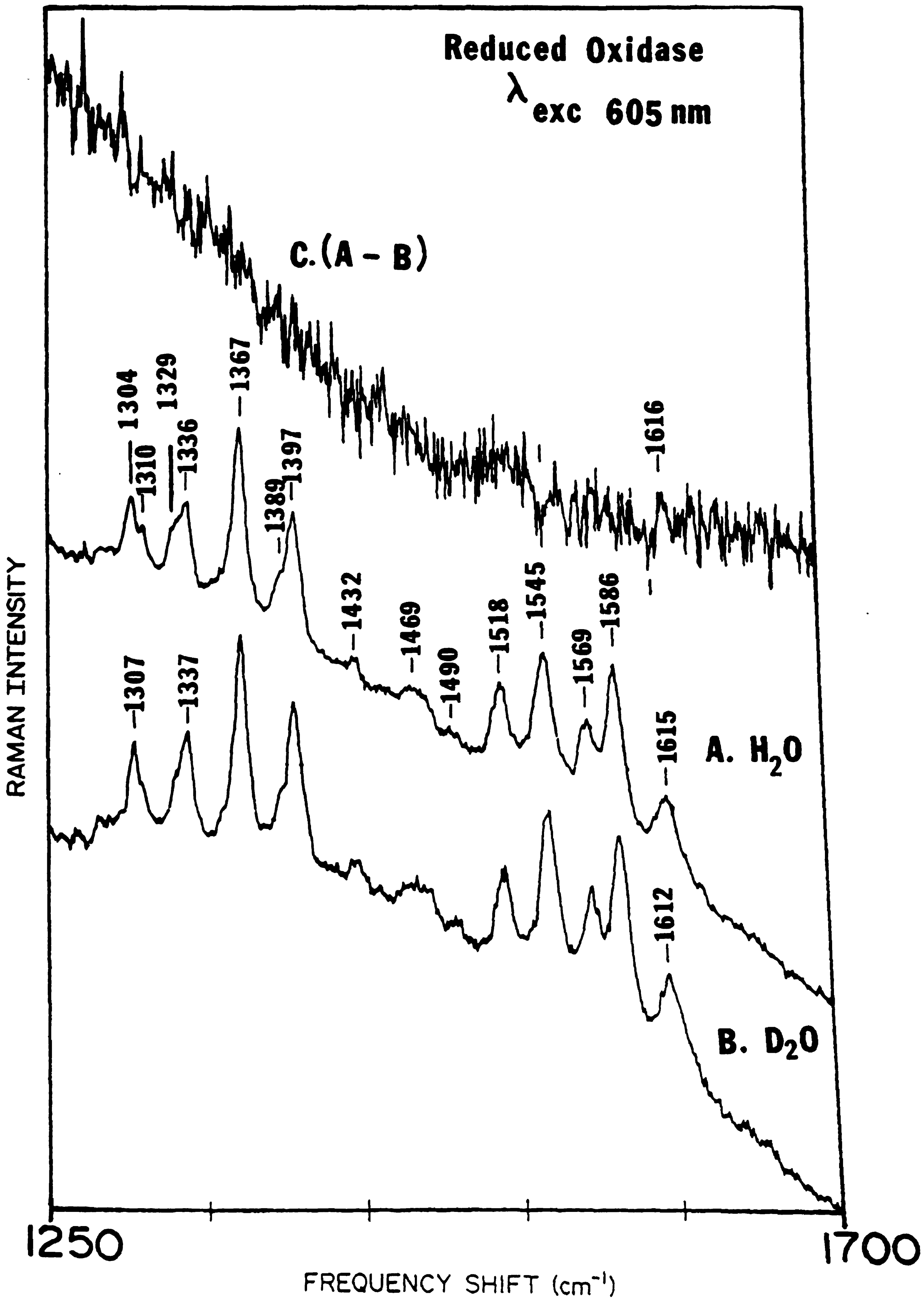
Reduced Oxidase
λexc 605 nm
C.(A - B)
1304
1310
1329
1336
1367
1389
1397
1432
1469
1490
1518
1545
1569
1586
1616
A. H_2O
1307
1337
1615
1612
B. D_2O
RAMAN INTENSITY
1250
1700
FREQUENCY SHIFT (cm^{-1})

H_2O

or

the

sum

deu

mot

fre

beh

whi

cm-

are

con

The

ρ val

Str

spe

B.

cha

fre

122

exc

fre

106

res

H_2O-D_2O) is shown at the top of each figure. No smoothing or background (baseline) subtraction was performed in any of the RR spectra shown in this chapter. Tables 4.1 and 4.2 summarize the frequency changes detected upon protein deuteration and the corresponding suggested normal modes of motion; mode depolarization ratios are also included. High frequency vibrations exhibiting anomalous polarized (ap) behavior are seen at 1585 cm^{-1}, 1336 cm^{-1}, and 1305 cm^{-1}, while depolarized (dp) vibrations are at 1131 cm^{-1}, 1173 cm^{-1}, 1167 cm^{-1}, and 1569 cm^{-1}. The remaining vibrations are polarized (~ 16 modes) with ρ values approaching 0.33, consistent with the lower symmetry of the heme a chromophore The anomalously polarized A_{2g} modes, particularly ν_{19}, show values between 0.75 and 1.0 rather than infinite (Spiro and Strekas, 1974), a phenomenon also observed with heme a spectra (Babcock et al., 1979; Woodruff et al., 1982).

B. Effects of deuterium substitution for cyt a^{2+} modes above 1000 cm^{-1}.

Deuterium induced frequency shifts and/or intensity changes in cyt a^{2+} vibrational modes are observed for high-frequency visible excitation lines at 1068 cm^{-1}, 1173 cm^{-1}, 1228 cm^{-1}, 1310 cm^{-1}, 1329 cm^{-1}, and 1546 cm^{-1}. With the exception of the latter mode, which does not change in frequency position, the other listed vibrations shift to 1065 cm^{-1}, 1180 cm^{-1}, 1233 cm^{-1}, 1312 cm^{-1}, and ~1333 cm^{-1}, respectively. The resonance Raman spectra of the mixed-

Tabl

Tent

Mode
ν_5
$2\nu_{33}$
ν_{44}
ν_{22}
ν_{43}
ν_{30}
ν_{14}
ν_{13}
ν_{21}

ble 4.1.

entative Assignments for the Observed High-Frequency Modes in the Resonance Raman Spectrum of Cyt $\underline{a}^{2+}$.[a]

de:	Symmetry:	Assignments:[b]	$(I_\perp/I_\parallel)$	$\underline{a}^{2+}\underline{a}_3^{2+}$		
			ρ	H_2O	D_2O	cm^{-1}
	A_{1g}	$\nu(C_b-S;38)$[c]	0.25	1040	1040	0
$_{33}$	A_{1g}	$\delta(C_\alpha-C_b-C_b;28)$ $\nu(C_b-C_b;15)$	0.41	1066	1068	+2
			0.32	1089	1089	0
$_4$	E_u	$\nu(C_b-S;29)$ $\nu(C\ -C_b;26)$	0.25	1115	1113	-2
$_2$	A_{2g}	$\nu(C_b-S;28)$	0.53	1131	1133	+2
			?	1151	1155	+4
				1165(sh)		
$_3$	E_u	$\nu(C_b-C_\alpha=C_\beta)$	0.65	1173	1180	+7
$_0$	B_{2g}	$\nu(C_b-S;50)$	0.63	----	1168	
$_4$		$\nu(C_b-S;30)$	?	1185 (sh)	1184 (sh)	
$_3$	B_{1g}	$\nu(C_m-H;67)$ $\nu(Cb-CHO)$	0.40	1228	1233	+5
$_1$	A_{2g}	$\delta(C_m-H;53)$ $\nu(C_b-C_b;18)$	0.97	1304	1307	+3
		$\delta CH=$	dp	1310	1312	+2
		$\delta_s=CH_2$	dp	1329	1333	+4
			0.96	1336	1337	+1

ν_{41}

ν_{20} d

ν_{29}

ν_{28}

ν_{11} (

ν_{38}

ν_{37}

ν_{19}

ν_{10}

ν(C

----

a) R
and
thos
equa
wave
inte

b) N
sugg
and

c) T
et a
pare
comp

d) T
This
ρ=0.
anom

	E_u	$\nu(C_a\text{-}N;50)$	0.34	1367	1367	0
1	A_{2g}?	$\nu(C_b\text{-}S;24)$	0.40	1389	1391	+2
	B_{2g}	$\nu(C_\alpha\text{-}C_b;47)$ $\nu(C_b\text{-}C_b;26)$	0.56	1397	1398	+1
			0.36	1432	1431	-1
	B_{2g}	$\nu(Ca\text{-}Cm;52)$	0.32	1469	1467	-2
			?	1490 (sh)	1490 (sh)	
(e)	B_{1g}	$\nu(C_b\text{-}C_b;57)$ $\nu(C_b\text{-}S;16)$	0.45	1518	1520	+2
	Eu	$\nu(C_b\text{-}C_b;53)$ $\nu(C_b\text{-}S;16)$	0.25	1545	1545	0
	A_{2g}	$\nu(Ca\text{-}Cm;36)$	0.70	1569	1569	0
	Eu	$\nu(Ca\text{-}Cm;67)$	0.65	1586	1586	0
	B_{1g}	$\nu(C_b\text{-}C_b)$ (f)	0.46	1615	1612	-3
C=O)						

Results obtained with Q-state excitation at 590, 595, 602
605 nm wavelengths. The data reported in this Table are
se observed with 605nm excitation. These results were
ally reproduced with the different excitation
elengths; however, many of the modes display an
ensity-wavelength dependence.

Normal mode numbering and assignment followed those
gested by Abe et al.(1978); Choi et al.(1982); Willems
Bocian (1984 and 1985) and Lee et al.(1986).

The calculated potential energy distribution (PED) (Abe
l. 1978) for each of tabulated modes is shown within
enthesis at the right-hand side of the normal mode
position assignment.

The assignment of ν_{20} at 1389 cm^{-1} is still uncertain.
is due in part to the fact that the proposed mode shows
40 instead of $\rho > 0.75$ as would be the expected for an
alously polarized mode (A_{2g}).

Cont

e) T
is i
the
symm
as
grou
porp
with

f) T
freq

s
d

inued Table 4.1:

he assignment of ν_{11} at 1518 cm^{-1} with visible excitation n agreement with Choi's (1983) under Soret excitation, lower frequency of this mode as compared with more etric porphyrins (i.e.,NiOEP ν_{11}=1576 cm^{-1}) was explained ue to the asymmetric disposition of the vinyl-formyl ps in heme a, which results is an alteration of the hyrin π system and hence lowering of the ν_{11} frequency respect to the more symmetric (D_{4h}) porphyrin.

his mode might overlapp with the carbonyl stretching uency expected at 1612 cm^{-1} .

h: shoulder
p: depolarized
p: polarized
?: too weak to be measured.

valence protein in H_2O/D_2O buffers resulted essentially in identical features as those observed for fully reduced protein, and therefore are not reproduced here. The highest frequency polarized band at 1615 cm^{-1} seems to shift down to 1610 cm^{-1} as judged by close examination of the RDS, which displays a negative trough at 1610 cm^{-1} and a weak (positive) peak at 1616 cm^{-1}. The frequency position of this 1615 cm^{-1} mode is of considerable interest since it falls in the region where the following cyt $\underline{a}^{2+}$ modes are expected: $\nu_{C=O}$ at 1616-1612 cm^{-1} (Babcock and Callahan, 1983); $\nu_{C=C}$ at 1622-1625 cm^{-1}; ν_{10} (Ca-Cm) at 1620 cm^{-1} (Callahan and Babcock, 1981; Choi et al., 1983) and ν_{37} (Ca-Cm) at ~1607-1610 cm^{-1} (Choi et al., 1983; Babcock, 1987). Our current data cannot provide an unambiguous assessment of the origin of this high frequency vibration; nonetheless, it is noticed that in our series of experiments with the mixed-valence oxidase, a 4 cm^{-1} downshifted frequency was also observed upon H/D solvent exchange, which mplies a possible formyl contribution to this mode.

The 1546 cm^{-1} line appears to increase in intensity for euterium exchanged protein. This mode has been assigned to s, an Eu mode with substantial contribution from porphyrin eripheral substituents (Abe et al., 1978; Babcock, 1987). sible excitation spectra of low-spin heme $\underline{a}$(bis-imidazole) mplexes also displayed a similar band at 1544 cm^{-1} abcock et al., 1979; Kitagawa et al., 1977). A comparison our data with those obtained by Callahan and Babcock

983) on the alkaline pH treatment of reduced cytochrome idase appears to indicate that cyt a^{2+} modes observed to altered upon raising the pH are also sensitive to uterium solvent atoms, and hence to H-bonding effects at e cyt a H-bonded structure.

Additional cyt a^{2+} hydrogen bonding sensitive modes are pected to appear in the mid-frequency range of the visible citation RR spectrum, from 1200-1260 cm^{-1}, as evidenced by e heme a model compound data discussed in Chapter III. In rticular, the ring-formyl stretch in heme a(bis-imidazole) Cu^{2+} porphyrin a has been assigned at ~1235-1238 cm^{-1}, ifting up to 1243 cm^{-1} upon H-bond formation (see Figure 11, Chapter III). In the RR spectrum reported here, we served a band at 1228 cm^{-1} for the reduced protein in H_2O, ich shifts up to 1233 cm^{-1} upon use of deuterated buffers. e RDS illustrates these changes by displaying peaks at 26 cm^{-1} (+) and 1238 cm^{-1} (-). A shoulder at 1218 cm^{-1} is nsistently observed upon use of D_2O-buffer solutions; wever, this line may be properly assigned to a D_2O ntribution since control experiments from the D_2O-buffers ow a strong and broad D_2O peak at 1207 cm^{-1} as well as a ak at 1043 cm^{-1}.

The remaining high frequency cyt a^{2+} deuterium nsitive modes are observed modes at 1068 cm^{-1}, 1173 cm^{-1}, 0 cm^{-1}, and 1329 cm^{-1}. In cytochrome oxidase, the larized mode at 1068 cm^{-1} is only active with Q-state citation, and its suggested assignment (i.e., 2 ν_{33}

$_{2g}$ $\nu_{C_\alpha - C_b - C_b}$) implies contribution from the porphyrin eripheral substituents. Its RR enhancement has been uggested to originate from porphyrin low-symmetry nvironments (Willems and Bocian, 1984). The shifted requency of the 1173 cm^{-1} band in the deuterated protein ppears to be accompanied by the enhancement of a new mode t 1168 cm^{-1}, presumably ν_{30} B_{2g} ν(Cb-S) (Choi et al., 982; Lee et al., 1987). Comparison of these results with vailable RR assignments of heme model compounds with vinyl nd formyl groups as the peripheral substituents (Tsubaki et l., 1980; Choi et al., 1982a,b), suggest the enhancement of inyl modes in this region.

. Low-Frequency Cyt a^{2+} Vibrations Below 1000 cm^{-1}

The low frequency visible excitation RR spectra of cyt $^{2+}$ are shown in Figures 4.3 and 4.4. In Table 4.2 we ımmarize these vibrational modes along with their suggested ssignments and measured depolarization ratios. No anomlously polarized Raman lines were observed in these low equency spectra, but depolarized behavior for lines at 298 $^{-1}$, 747 cm^{-1}, 789 cm^{-1}, and 981 cm^{-1} were detected. Upon e of deuterated buffers, frequency changes are as follows: 5 cm^{-1} shifts down to 242 cm^{-1}, 265 cm^{-1} to 262 cm^{-1}, 298 $^{-1}$ to 295 cm^{-1}, 344 to 342 cm^{-1}, 439 to 432 cm^{-1}, 659 to 6 cm^{-1}, 789 cm^{-1} to 785 cm^{-1}, 955 to 951 cm^{-1}, and 981 to 6 cm^{-1}. Intensity differences are also noted for modes at

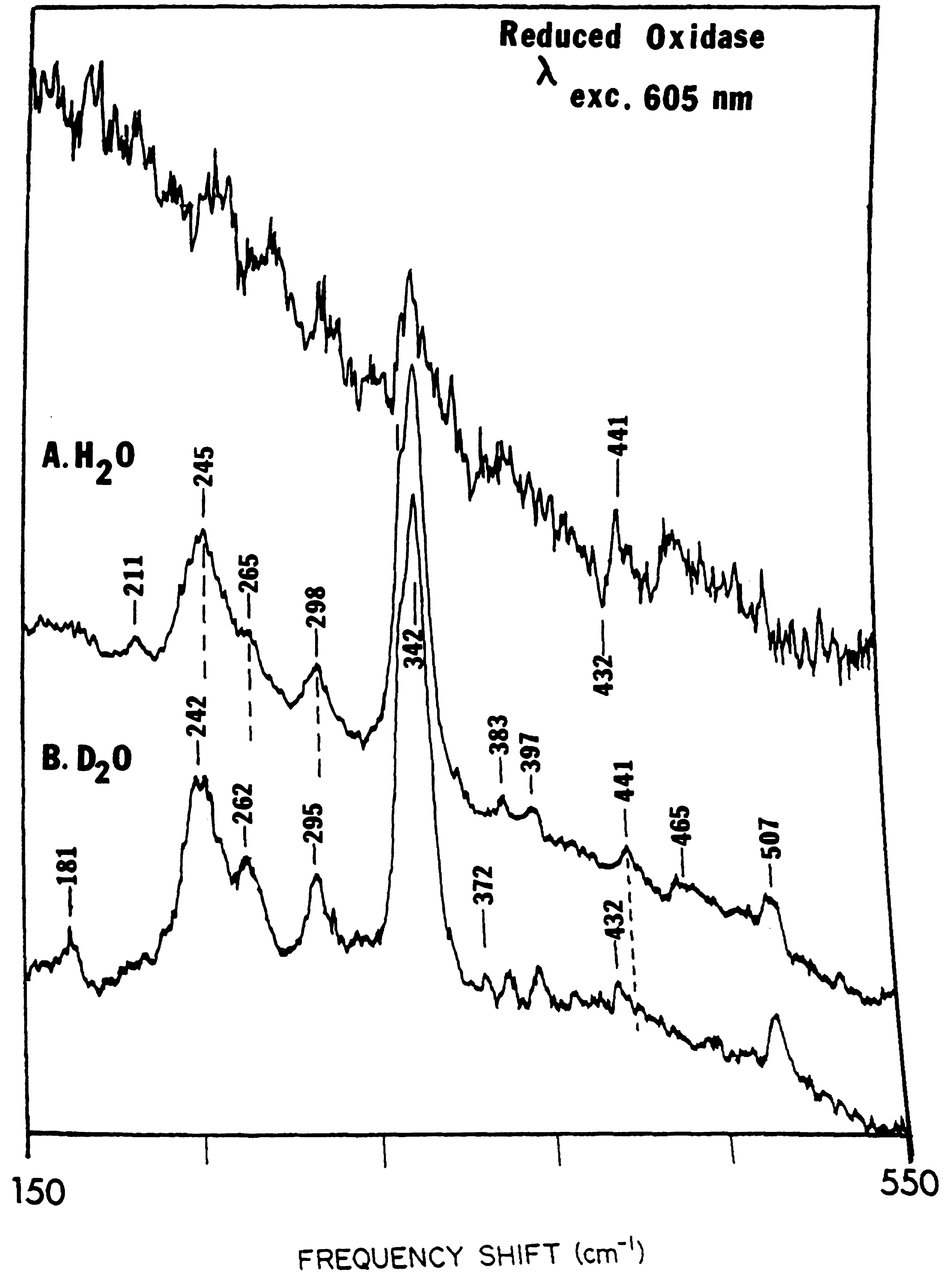

igure 4.3: Low frequency visible excitation (605 nm) resonance Raman ectra of fully reduced cytochrome oxidase in A) H_2O and B) D_2O buffers the range from 150 cm^{-1} to 550 cm^{-1} . The top trace correspond to e Raman difference spectrum.

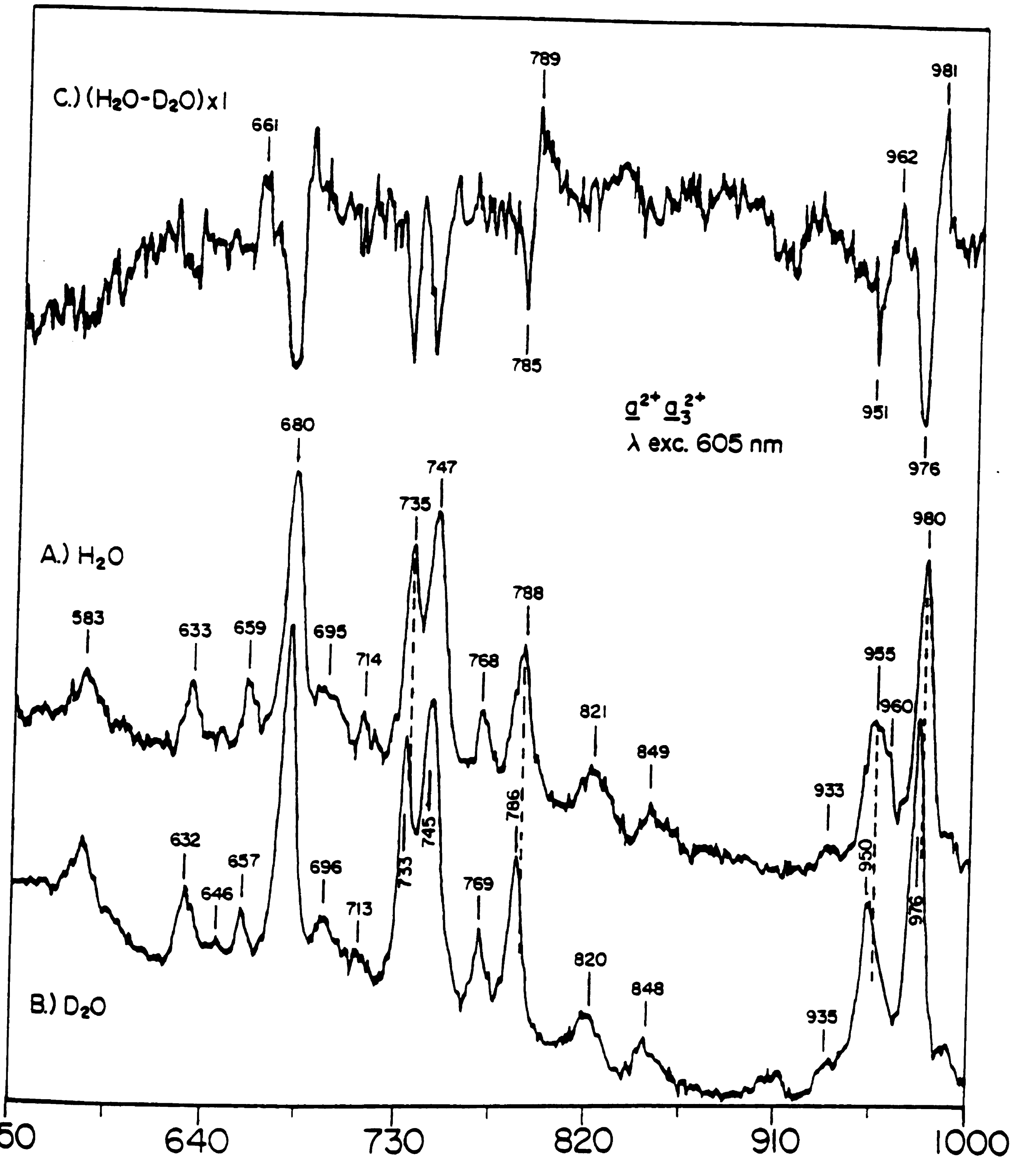

igure 4.4: Low frequency visible excitation (605 nm) RR spectra reduced cytochrome oxidase obtained with the Raman difference trumentation.

le 4.2.

ntative Assignments for the Observed Low-Frequency Modes the Visible Excitation Resonance Raman Spectrum of Cyt $\underline{a}^{2+(a)}$

e	Symmetry	Assignments^{b,c}	$(I_\perp/I_\parallel)$	$\underline{a}^{2+}\underline{a}_3^{2+}$		
			ρ	H_2O	D_2O	cm^{-1}
					185	
				211		
	A_{1g}	δ(Cb-S;23)	0.40	245	242	-3
	Eu	δ(Cb-S;43)	0.37	265	262	-3
	B1g	δ(Cb-S;84)	0.65	298	295	-3
	A1g	δ(Cb-S;57)	p	341	343	+2
5		δ(Cb-S)	too weak	383	383	0
				397	397	0
		Pyr. fold	p	441	432	-9
					477	
				465		
		Pyr. fold	0.52	507	503	-4
	Eu	δ(Cb-S;29)	0.45	583	583	0
			0.25	633	632	-1
				647	646	-1
		δ(C=O)		659	656	-3
	A1g	(Cb-C$_\alpha$-N;20)	p	681	680	-1
			?	695	695	0

ntinued Table 4.2:

$_4$	A2g	δ(Cb-S;29)	?	713 (w)	711 (w)	-2
$_7$	Eu	δ(Cb-S;27)	0.35	735	735	0
$_6$	B1g	$\delta(C_\alpha$-N-C_α;14) ν(Cb-S;14)	0.65	747	745	-2
				768	769	+1
$_2$	B2g	δ(Cb-S;50)	0.73	789	785	-4
				821	820	-1
				849	848	+3
$_5$	Eu	ν(Cb-S;20)	0.33	955	951	-4
				960	---	
$_2+\nu_{35}$)		ν(Cb-S)	0.65	981	975	-6

The data reproduced in this table were obtained with 605 nm excitation.

Mode numbering and assignment were similar to those suggested by Abe et al. (1978), Choi et al. (1982); Willems and Bocian (1984 & 1985) and Lee et al. (1986).

The estimated potential energy distribution (PED) (Abe et al., 1978) for each of the tabulated modes is also included.

w : weak
sh : shoulder
S : substituent
p : polarized
dp : depolarized

343 cm^{-1}, 680 cm^{-1}, the doublet at 735-744 cm^{-1}, and 976 cm^{-1}.

The depolarized Raman line at 298 cm^{-1} is only active under Q-state excitation and its 3 cm^{-1} downshift upon H/D protein exchange is consistent with its proposed substituent character (see Table 4.2). Interestingly, 488 nm excitation of $Fe^{3+}(OEP)(N\text{-}MeIm)_2$ reveals a line at 290 cm^{-1}, which was assigned to the symmetric stretching mode ($\nu_{(N-Fe-N)s}$) involving the iron and the two imidazole ligands (Kitagawa et al., 1976). Although it is likely that in cyt a^{2+} this band gains Raman activity owing to the lower heme a symmetry, it is interesting to speculate whether it can be related to the cyt a iron-ligand stretching mode. This type of in-plane ν_{N-Fe-N} stretch, however, is expected to exhibit polarized behavior owing to its totally symmetric character (A_{1g} species), and hence its enhancement with visible excitation wavelengths might be forbidden on the basis of symmetry. The Raman line at 439 cm^{-1} is weak under visible excitation, but strong with Soret excitation. Its 8 cm^{-1} downshift to 431 cm^{-1} is observed with both Q - and Soret band excitation (see Centeno, Chapter and Argade et al., 1985), and accordingly a cyt a contribution is suggested. The appearance of this line in the Soret excitation RR spectra of mixed-valence oxidase in D_2O and its downshifted frequency were recently interpreted by Argade et al. (1986) as due to the occurrence of internal formyl labile protons in cyt a. An alternate explanation and assignment has been proposed in Chapter III and corroborated in Chapter V as due to a heme a pyrrole folding mode containing the formyl group as the peripheral substituent. This was suggested on the basis of isotopic and H-bonding studies at the heme a formyl site. The resonance enhancement of this mode in the *in situ* chromophore appears to be a result of the vibrational asymmetry of the cyt a macrocycle induced by the strong electron withdrawing capabilities of its H-bonded C=O group (see Chapter V).

Another important cyt a formyl-related mode is the in-plane bending C=O motion ($\delta_{C=O}$) expected to show resonance enhancement in the region from 662 cm^{-1} to 630 cm^{-1}, as revealed by the model compounds data discussed in Chapter III. The 605 nm spectrum of cyt a exhibit Raman bands at 659 cm^{-1}, 647 cm^{-1}, and 633 cm^{-1}. H/D exchange appears to result in a downshift of the 659 cm^{-1} line to 656 cm^{-1} as detected by the derivative shape of the RDS with a positive peak at 662 cm^{-1} and a negative trough at 654 cm^{-1}. A similar Raman difference spectrum was also observed when B-state excitation was used (see Chapter V, Figure 5.11).

The remainder of the cyt a^{2+} H-bonding formyl group related frequencies observed to shift as a result of the deuterium perturbation are: 788 cm^{-1} to 785 cm^{-1}, 955 cm-1 to 951 cm^{-1}, and 980 cm^{-1} to 976 cm^{-1} (see Figure 4.4). All these vibrational modes are observed to be depolarized (dp), and their Soret excitation enhancement is rather weak (see Figure 5.11 Chapter V). Their calculated potential energy distribution (Abe et al., 1978) reveals up to 50% Cb-S substituent character (i.e., 789 cm^{-1}), and therefore frequency shifts might be expected.

IV. Discussion:

A. High Frequency Vibrational Assignments of Cyt a^{2+}:

The resonance Raman spectra of fully reduced cytochrome oxidase obtained with Soret-band excitation in the region above 1600 cm-1 are a convolution of cyt a^{2+} and cyt a$_3$$^{2+}$ vibrational modes (Babcock, 1987). Cyt a^{2+} modes are expected at 1612 cm^{-1} ($\nu_{C=O}$), at 1625 cm^{-1} ($\nu_{C=C}$), and at 1623 cm^{-1} (ν_{10} B_{1g}) (Callahan and Babcock, 1983; Babcock, 1987), while cyt a$_3$$^{2+}$ modes are expected at 1665 cm^{-1} $\nu_{C=O}$), 1625 cm^{-1} ($\nu_{C=C}$), and at 1609 cm^{-1} (ν_{10} B_{1g}). However, since cyt a^{2+} is the dominant absorber on the α-band region of reduced cytochrome oxidase (Vanneste, 1967), visible excitation on the 605 nm band is predicted to provide detailed information on just cyt a^{2+} vibrational modes. In fact, two independent studies of cytochrome oxidase with laser excitation on the 600 nm region have provided evidence that the visible excitation resonance Raman spectra of reduced cytochrome oxidase are independent of the oxidation, coordination, and spin-state of the cyt a$_3$ heme chromophore (Bocian et al., 1979; Callahan and Babcock, 1983). The pH-dependent spectral shifts of cyt a^{2+} studied by Callahan and Babcock (1983) suggested that upon disruption of the cyt a...protein H-bonding interaction by more alkaline pH's, lines at 1569 cm^{-1}, 1329 cm^{-1} and 1114 cm^{-1} were significantly altered. The 1569 cm^{-1} and 1329 cm^{-1} were observed to decrease in Raman intensity, whereas the 1114 cm^{-1} was observed to decrease in intensity and shift down to 1109 cm^{-1} at pH 10.5. Their visible excitation spectrum also illustrated (see Figure 7 in Callahan and Babcock, 1983) a downshift for a Raman mode at 1173 cm^{-1} (to 1168 cm^{-1}) when the pH of the reduced enzyme was raised from pH 7.4 to pH 10.5. As shown in Figure 4.2, our present data on the H/D dynamics at the cyt $\underline{a}^{2+}$ site corroborates these findings, since we observed that upon use of deuterated buffer, modes at 1173 cm^{-1}, 1228 cm^{-1}, and 1329 cm^{-1} shifts to 1178 cm^{-1}, 1233 cm^{-1}, and 1333 cm^{-1}, respectively. Therefore, the fact that both H/D-exchange and alkaline pH-denaturation affects the same cyt $\underline{a}^{2+}$ vibrational modes supports the cyt $\underline{a}^{2+}$ hydrogen bonded structure at the formyl group (Babcock and Callahan, 1983).

Although modes at 1615 cm^{-1} and 1546 cm^{-1} in the 605 nm RR spectrum of the reduced protein do not seem to respond to protein denaturation effects, our study indicates that these modes might be related to the occurrence of exchangeable protons at the cyt $\underline{a}$ site. The 1615 cm^{-1} line appears to shift down to 1610 cm^{-1} (-5 cm-1) and the 1546 cm^{-1} increases in intensity upon protein H/D exchange. Deuterium induced frequency shifts in the carbonyl stretching frequency of resting and reduced oxidase of -4 and -5 cm-1, respectively, have been recently observed upon Soret excitation of oxidized and reduced (Copeland and Spiro, 1986; Centeno and Babcock, unpublished observations). Interestingly, visible excitation (592 nm) of ferrous heme *a* (bis-imidazole) in aprotic solvents resulted in the enhancement of high frequency modes at 1640 cm^{-1} and 1612 cm^{-1} (Babcock et al., 1979). The former mode was assigned to the carbonyl group stretch (Babcock, 1987), while the latter mode was assigned to the ν_{10} frequency (Choi et al., 1983).

The 1329 cm^{-1}, 1310 cm^{-1}, and 1173 cm^{-1} are assigned to cyt *a* vinyl modes in agreement with the appearance of analogous modes in the RR spectra of protoporphyrin (Choi et al., 1982a; Choi et al., 1982b), and vinyl, formyl-substituted model compounds (Tsubaki et al., 1980). The vinyl scissors mode ($\delta_{s=CH_2}$) is expected to be enhanced with Q-band excitation, while the in-plane $\delta_{CH=}$ bending mode is Soret active. We assign the former vinyl mode to the 1329 cm^{-1} depolarized band, which shifts up (under the 1336 cm^{-1}) upon protein deuteration. The spectral behavior of the 1173 cm^{-1} line is quite unusual, since it is observed that upon deuteration it splits into two new components with, frequencies at 1180 cm^{-1} and 1167 cm^{-1}. However, on the basis of model compounds and the analogous effects observed in vinyl deuterated Ni (PP) RR spectra, we assign the 1173 cm^{-1} band which shifts to 1180 cm^{-1} as due to the ring-vinyl stretching frequency, and the 1168 cm^{-1} peak as the ν_{30} ($^{\nu}$Cb-S) B_{2g} mode. Enhancement of these vinyl modes in the RR spectra of cyt $\underline{a}^{2+}$ (observed upon protein deuteration and/or pH-denaturation) might be indicative of considerable reduction of the heme $\underline{a}$ symmetry caused by the formation of the formyl hydrogen bonding structure throughout the ring y-axis, which contains the formyl and vinyl groups as the peripheral substituents. Alternatively, the fact that we have observed deuterium induced changes in vinyl and formyl sensitive modes implies that the enhancement of vinyl modes in the cyt $\underline{a}^{2+}$ spectrum arises from structural perturbations at the vinyl peripheral substituent. This observation will be discussed in Chapter VI.

The spectral changes observed in the 1228 -->1233 cm^{-1} bands of cyt $\underline{a}^{2+}$ have also been recently investigated by Soret excitation on reduced and mixed-valence cytochrome oxidase (Argade et al., 1986; Centeno and Babcock, in preparation; see also Figure , Chapter VI). With B-state excitation, we noted upshifts for modes at 1228 cm^{-1} and 1247 cm^{-1} to 1233 cm^{-1} and 1250 cm^{-1}, respectively. With Soret excitation, the 1247 cm^{-1} mode is assigned to a (ν_5 + ν_9) combination mode which might not be strongly enhanced with Q-band state excitation owing to its totally symmetric character (i.e., A_{1g}). The 1228 cm^{-1} line, on the other hand, is assigned to ν_{13} B_{1g} (Abe et al., 1978), and accordingly, its strong activity with Q-band excitation is expected (Spiro and Strekas, 1972; Shelnutt, 1978). The derivative shape of the Raman difference spectrum shown in Figure 4.1 (C) is in fair agreement with a recently published RDS spectra obtained with 441.6 nm excitation (Argade et al., 1986) that shows a positive peak at 1236 cm^{-1} and negative troughs at 1223 cm^{-1} and 1249 cm^{-1}. Our cyt *a*$^{2+}$ frequencies reported here might differ from those of Argade et al. (1986) owing to the selective enhancement of cyt *a*$^{2+}$ vibrations with visible excitation as discussed above.

B. Low Frequency Vibrations of Cyt a^{2+}

Low frequency resonance Raman vibrations of heme proteins are particularly sensitive to heme structural changes and enviromental interactions, porphyrin macrocycle deformation modes (Choi et al., 1983), metal-ligand stretches (Spiro, 1983), and peripheral substituent deformation motions (Choi et al., 1983). In addition, RR enhancement of IR-allowed Eu-type modes, which attain resonance Raman activity due to the low-symmetry molecular environment of the porphyrin ring, has also been observed (Willems and Bocian, 1985). This symmetry reduction in heme model compounds and heme proteins has been attributed to the asymmetric disposition of peripheral substituents as well as to protein-chromophore interactions (Choi et al., 1983; Valance and Strekas, 1982; Callahan et al., to be submitted).

The effects of symmetry lowering on the RR vibrational modes of metalloporphyrins have been well documented (see Woodruff et al., 1985; Choi and Spiro, 1983; and Ozuki et al., 1979). For metalloporphyrins exhibiting D_{4h} symmetry, the expected active vibrations are those contained in the cross product of Eu x Eu = A1g + A2g + B1g + B2g symmetry; see Table 4.3 (Spiro and Strekas, 1974). Reduction of the heme molecular symmetry to either D_{2h} or C_{2h} point group symmetry is expected to transform the above symmetry representations according to Table 4.3 (Wilson et al., 1955). Therefore, the appearance of totally symmetric RR bands ($\rho \lesseqq 1/3$) can be predicted with any of the point group symmetry transformations described in Table 4.3.

The fact that the low frequency visible excitation spectrum of cyt $\underline{a}^{2+}$ (Figures 4.3 and 4.4) displays strongly polarized modes at 343 cm^{-1}, 681 cm^{-1}, 960 cm^{-1}, as well, as the unique doublet with frequencies at 735 cm^{-1} and 747 cm^{-1}, is certainly an indication of the lower heme $\underline{a}$ ring symmetry in cyt $\underline{a}$. In addition, the strong electron withdrawing capabilities of the H-bonded carbonyl group in cyt $\underline{a}^{2+}$ is also expected to affect the symmetry of the heme ring, allowing the above spectral effects to be observed.

The low frequency cyt $\underline{a}^{2+}$ modes sensitive to protein deuteration effects lie at 245 cm^{-1}, 265 cm^{-1}, 298 cm^{-1}, 439 cm^{-1}, 659 cm^{-1}, 789 cm^{-1}, 955 cm^{-1}, and 980 cm^{-1}. Their estimated potential energy distribution (PED), as revealed by the normal coordinate analysis of Abe et al. (1978),

Table 4.3:

Correlation Table for Species with D_{4h}, D_{2h}, and C_{2h} Point Group Symmetry[a]

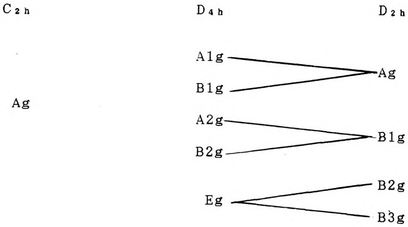
C2h
D4h
D2h
A1g
B1g
Ag
A2g
B2g
B1g
Eg
B2g
B3g
Ag

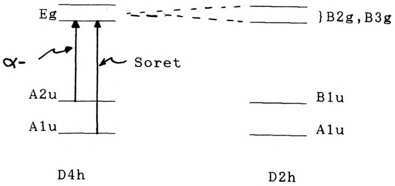
Eg
}B2g,B3g
α-
Soret
A2u
A1u
B1u
A1u
D4h
D2h

Eu x Eu = A1g + A2g +B1g +B2g

---

a) From Wilson et al. (1955).

suggest a large contribution from the heme peripheral substituents, such as the vibrations at 298 cm^{-1} and 789 cm^{-1} modes, which exhibit an estimated 84% and 50% Cb-S character, respectively. Structural information on the cyt a peripheral formyl group can therefore be inferred by monitoring vibrational changes in the above listed hydrogen bonding sensitive modes.

V. Conclusions:

In this Chapter we have studied the resonance Raman spectra of reduced cytochrome oxidase obtained with visible excitation wavelengths that are in resonance with the cyt a^{2+} Q(0-0) $\pi \text{ ----> } \pi*$ transition at 605 nm. Under these resonance conditions the spectra obtained are attributed to the cyt a^{2+} heme moiety. The identification of cyt a hydrogen bonding sensitive modes has been established by studying the *in situ* cyt a chromophore under the influence of deuterated buffers. Frequency shifts on many of these cyt a (formyl) H-bonding sensitive vibrations agree with previous visible excitation studies on the pH-dependent spectral shifts of reduced cytochrome oxidase, and confirm the H-bonded structure of cyt a. The enhancement and frequency perturbations on many of the cyt a low frequency modes implies considerably lower vibrational symmetry, which in part arises from the strong electron withdrawal capabilities of its H-bonded C=O group. Finally, this study is presented as an alternative approach to be used in the interpretation of the structure and enviromental conditions of cyt a in cytochrome oxidase from different prokaryotic and eukaryotic systems.

CHAPTER V

Hydrogen Bond Sensitive Vibrations of Cytochrome *a* in Cytochrome Oxidase

I. Introduction:

Formyl (-CHO) hydrogen bonding sensitive vibrations of cytochrome *a* (cyt *a*) in cytochrome oxidase have been identified in reduced and mixed-valence oxidase derivatives by controlled denaturation of the enzyme under acidic conditions. The effect of lowering the pH of reduced cytochrome oxidase is to transform the cytochrome a_3 (cyt a_3) heme to a six-coordinate low spin state and to disrupt the hydrogen bond structure to the cyt *a* formyl peripheral substituent, resulting in diminished resonance Raman intensity for some cyt *a* low frequency modes. A comparison of these cyt *a* hydrogen bonding vibrations with those studied for heme *a* $(N\text{-}MeIm)_2$ and/or benzaldehyde in Chapter III, under H-bonding conditions, results in a nearly complete assessment of the cyt *a* aldehyde vibrations. As with the visible excitation spectra (Chapter IV), we have also detected significant intensity enhancement of substituent sensitive IR-allowed Eu modes in the Soret excitation spectra of H-bonded cyt *a*. This is interpreted as a heme *a* symmetry lowering effect in cyt *a* induced by the strong electron withdrawing capabilities of its -HC=O group at position 8, and its hydrogen bonding interaction with the protein polypeptide backbone. Our results provide further information about the molecular and protein environment of cyt *a* and support the hydrogen bonded structure proposed for this chromophore in cytochrome oxidase (Babcock and Callahan, 1983).

II. Materials and Methods:

The isolation of cytochrome oxidase and its inhibitor complexes is described in Chapters II and IV, respectively. The buffer-detergent system and the procedures to obtain the desired pH level are given in Chapter II. The Raman instrumentation and optical absorption spectrophotometer used are described in Chapter II. Some of the resonance Raman spectra reported here were recorded with Raman difference instrumentation (see Chapter II for details).

III. Results:

A. Low pH Effects on the RR Spectra of Reduced Cytochrome Oxidase

The optical absorption spectra of reduced cytochrome oxidase at different pH levels are shown in Figure 5.1. The resonance Raman spectra of these pH-treated oxidase samples in the high- and low-frequency regions are depicted in Figures 5.2 and 5.3, respectively. As the pH was lowered from 7.4 to 4.5, the following optical absorption changes were distinguished: 1) in the Soret region, the absorption maximum was blue shifted from 443 nm to 434 nm, i.e., to higher energy than the Soret maximum of heme $\underline{a}^{2+}$(N-MeIm)$_2$ in protic solvents (see Figure 3.1 Chapter III); 2) in the visible absorption region, we observed a blue shift of the

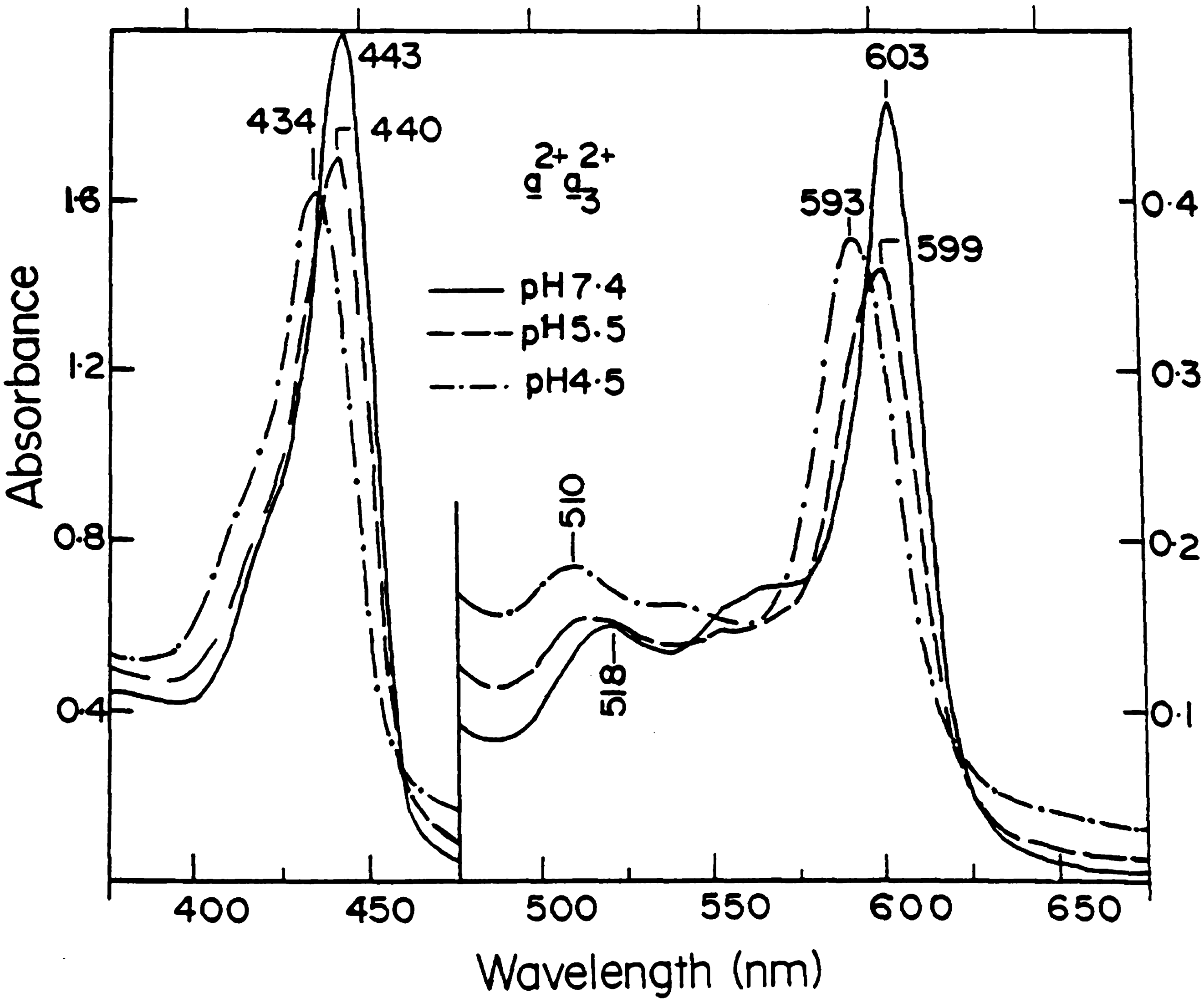

Figure 5.1: Optical absorption spectra of reduced cytochrome _c_ oxidase at neutral and acidic pH. Enzyme concentration was approximately 25 μM (heme _a_ basis) for all samples.

maximum from 603 nm to 593 nm, as well as a shift of the 518 nm band to 510 nm. These absorption changes produce a species that resemble low-spin, six-coordinate bis-imidazole ferrous heme a (absorption maxima at 438 nm (Soret), 518 nm, and 594 nm (α-band)).

The high-frequency resonance Raman spectra of these pH treated oxidase samples, obtained under 441.6 nm and 406.7 nm excitation are depicted in Figure 5.2 along with the RDS spectrum for 441.6 nm excitation. Vibrations that decrease in intensity upon lowering the pH of the reduced oxidase solution are: bands at 1665 cm^{-1} (cyt a_3^{2+} $\nu_{C=O}$), 1612 cm^{-1} (cyt a^{2+} $\nu_{C=O}$), 1569 cm^{-1} (ν_{38}, cyt a^{2+} or ν_2, cyt a_3^{2+}), 1468 cm^{-1} (ν_{28}, cyt a_3^{2+} Ca-Cm), 1289 cm^{-1}, 1228 cm^{-1} (ν_{13}), and 1115 cm^{-1}. As the intensities of the 1665 cm^{-1} and 1612 cm^{-1} lines diminish, the corresponding Raman intensity of the 1638 cm^{-1} and 1586 cm^{-1} lines, increases. Frequency shifts are also noted for modes at: 1396 cm^{-1}---> 1393 cm^{-1}, 1330---> 1334 cm^{-1}, 1246---> 1243 cm^{-1}, and 1228---> 1226 cm^{-1}. These changes are readily evident from inspection of the RDS spectrum (RDS = pH 7.4 - pH 5.3) shown in the bottom trace of Figure 5.2. No frequency changes were evident in ν_4 at 1354 cm^{-1} as revealed by the RDS (trace 5.2D), suggesting that the acid induced changes in either cyt a and/or cyt a_3, may be confined to structural alterations at the heme periphery and in the spin state. The difference spectrum in the carbonyl region of cyt a and cyt a_3 display positive peaks at 1612 cm^{-1} and 1665 cm^{-1} and

Figure 5.2: High frequency resonance Raman spectra of reduced cytochrome oxidase at the indicated acidic pH level, and under the indicated excitation wavelengths. The Raman difference instrumentation was used to record the pH 7.4 - 5.35 spectrum under 441.6 nm excitation. Enzyme concentration was approximately 50 μM (heme a basis). Instrumental conditions: resolution , 5 cm^{-1}; time constant, 1 second; scan rate, 50 cm^{-1}/minute.

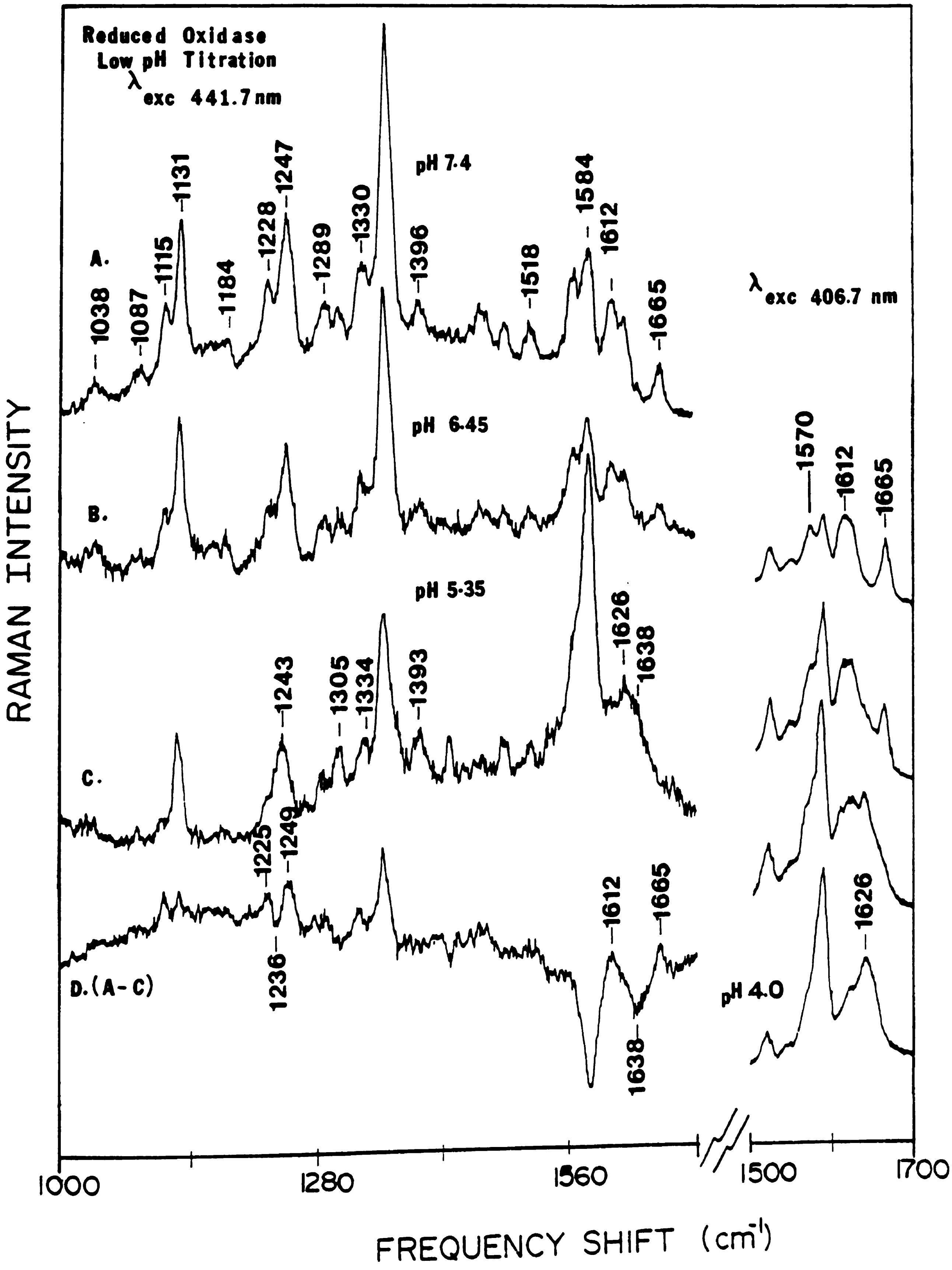
Reduced Oxidase
Low pH Titration
λ_{exc} 441.7 nm
λ_{exc} 406.7 nm
A.
pH 7.4
1038
1087
1115
1131
1184
1228
1247
1289
1330
1396
1518
1584
1612
1665
B.
pH 6.45
1570
1612
1665
C.
pH 5.35
1243
1305
1334
1393
1626
1638
D.(A-C)
1225
1249
1236
1612
1665
1638
1626
pH 4.0
RAMAN INTENSITY
1000
1280
1560
1500
1700
FREQUENCY SHIFT (cm^{-1})

a negative trough at 1638 cm^{-1}, indicative of a hydrophobic environment for both heme a formyl groups at pH 5.3 (Van Steelandt-Frendrup et al., 1981; Babcock and Callahan, 1983). In the mid-frequency region, the RDS has positive peaks at 1226 cm^{-1} and 1249 cm^{-1} with a negative trough at 1236 cm^{-1}. The assignment of heme substituent normal modes of motion contributing to this mid-frequency region is of importance since it is in this region where the ring-formyl stretching mode of benzaldehyde and heme $a^{2+}(N\text{-}MeIm)_2$ models have been assigned (1206 cm^{-1} and 1230 cm^{-1} respectively; Zwarich et al., 1971; Choi et al., 1983). Our isotopic substitution and H-bonding studies on heme a models indicated that upon formyl H-bond formation this mode will shift up by ~6-8 cm^{-1} (see Figure 3.10 Chapter III). Therefore, removal of this H-bonding interaction should drop the frequency of this mode, provided that no significant coupling with other formyl modes occurs (see Discussion). This is indeed shown by the RDS (trace 2D) in Figure 5.2, which displays a negative trough at ~1236 cm^{-1} and a positive peak at 1225 cm^{-1}.

Figure 5.3 shows the low-frequency RR spectra of reduced oxidase under the same pH conditions. Low-frequency modes at 215, 268, 367, 395, 438, 633, 714, and 850 cm^{-1} are seen to decrease in intensity, while modes at 342 cm^{-1}, 750 cm^{-1}, and 683 cm^{-1} shift down to 337 cm^{-1}, 746 cm-1, and 679 cm-1, respectively. The former two modes are correlated with spin-state transitions at the cyt a_3 iron as the a_3

Figure 5.3: Low frequency resonance Raman spectra of reduced cytochrome oxidase at the indicated pH levels. The bottom trace was obtained with the Raman difference instrumentation and 441.6 nm excitation. Experimental conditions as in Figure 5.2.

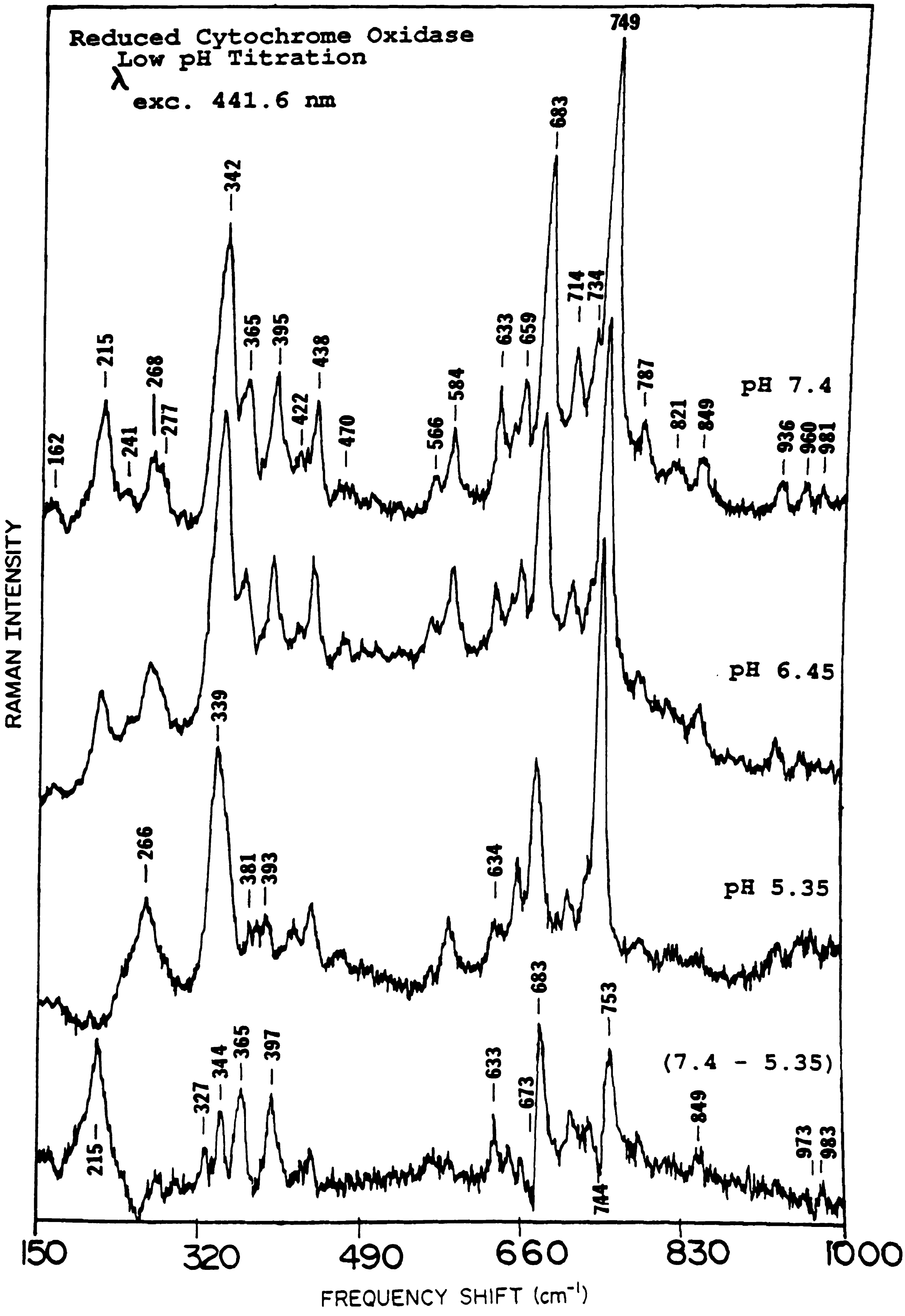
Reduced Cytochrome Oxidase
Low pH Titration
λ exc. 441.6 nm
749
683
342
714
734
365
395
633
659
215
268
438
787
422
584
277
821
849
241
470
566
936
960
981
162
pH 7.4
pH 6.45
339
266
381
393
634
pH 5.35
683
753
344
365
397
633
(7.4 - 5.35)
327
673
849
973
983
215
744
RAMAN INTENSITY
150
320
490
660
830
1000
FREQUENCY SHIFT (cm⁻¹)

changes from high-spin five-coordinate with lines at 215 cm^{-1}, ~277 cm^{-1} (RDS), 327 cm^{-1} (RDS), 365 cm^{-1}, 404 cm^{-1} (RDS), 683 cm^{-1}, and 757 cm^{-1} (RDS) to low-spin six-coordinate with lines at ~243 cm^{-1}, 344 cm-1, and 678 cm-1, and 746 cm-1. The low-frequency resonance Raman difference spectra of reduced and mixed-valence cytochrome oxidase (Figure 5.3 trace D, and Figure 5.4 trace C) reveal all these cyt $\underline{a}_3$ changes as the pH is lowered to 4.5. Further indication of spin transformations at the cyt $\underline{a}_3$ are given by the shift of its $\nu_{C=O}$ stretch from 1665 to 1638 cm^{-1}, and decreased intensity for modes at 1469 cm^{-1} and 1569 cm^{-1} (Babcock and Salmeen, 1979). Low-frequency cyt $\underline{a}^{2+}$ vibrations sensitive to acid pH denaturation are apparent in the RDS (Figure 5.3) at 344 cm^{-1}, 397 cm^{-1}, 438 cm^{-1}, 633 cm^{-1}, 715 cm^{-1}, 850 cm^{-1}, and 981 cm^{-1}.

A disruption of the hydrogen bonded formyl group structure of cytochrome $\underline{a}$ should manifest itself as an increase in frequency of $\nu_{C=O}$ and an absorption blue-shift (Babcock & Callahan, 1983). These spectral shifts are indeed observed; the cytochrome $\underline{a}$ formyl stretching frequency at 1610 cm^{-1} (Callahan & Babcock, 1983) shifts to 1640 cm^{-1} at pH 4.5 and the Soret and α-band absorption maxima blue-shift by approximately 10 nm under the same conditions. Since the α-band absorption blue-shift and the $\nu_{C=O}$ frequency upshift are linearly related (Babcock & Callahan, 1983), this is consistent with the presence of weakly hydrogen bonding environment for both heme a species at acidic pH. A structural schematic describing the coordination change of cyt a_3^{2+} and the formyl environment shift of cyt a^{2+}, based upon the carbonyl frequency shifts of each chromophore, is given in Figure 5.8A.

B. Low-pH Induced Effects in the RR Spectra of Cyanide Inhibited Cytochrome Oxidase

The results described in Figures 5.1 through 5.3 clearly indicate that structural perturbations at both cytochromes a and a_3, induced by acidic pHs, are actually taking place in fully reduced cytochrome oxidase. To assign the cyt a aldehyde vibrations with confidence, it is desirable to deconvolute its RR spectrum from that of cyt a_3. In Chapter IV we demonstrated that such spectral separation is indeed possible by employing laser excitation in the visible region of reduced cytochrome oxidase in resonance with the -band of cyt a^{2+} at 605 nm. Since the contribution of cyt a^{2+} to the α-band of reduced oxidase is estimated to be ~90% (Vanneste, 1967), nearly complete spectral separation of cyt a^{2+} vibrations is observed. On the other hand, when Soret excitation is employed, as in the present investigation, an alternate method to separate the contributions of cyt a and cyt a_3 requires the use of respiratory inhibitors, such as CO, CN-, HCOO-, etc., that bind to the heme a_3 iron, thereby removing its absorption maximum from resonance with the 441.6 nm laser excitation (Salmeen et al., 1978). almeen et al. (1978) and more recently Ching et al. (1986)

made use of this ligand-binding deconvolution method to investigate the vibrational properties of the mixed-valence, cyanide bound protein. In the present study, we have used the mixed-valence cyanide inhibited enzyme (i.e., $\underline{a}^{2+}$ $\underline{a}_3^{3+}$-CN$^-$) to isolate the pH induced spectral changes of cyt $\underline{a}^{2+}$ ($B_{max.}$= 443 nm) from those of cyt $\underline{a}_3^{3+}$-CN$^-$ ($B_{max.}$= 427nm). With 406.7 nm excitation, approximately equal enhancement of vibrational mode for cyt $\underline{a}_3^{3+}$·CN and cyt $\underline{a}^{2+}$ will occur (Babcock et al., 1981). In contrast, the 441.6 nm excitation RR spectrum of $\underline{a}^{2+}$ $\underline{a}_3^{3+}$-CN$^-$ is expected to enhance essentially cyt $\underline{a}^{2+}$ modes. Accordingly, a resonance Raman difference spectrum of ($\underline{a}^{2+}$ $\underline{a}_3^{2+}$ - $\underline{a}^{2+}$ $\underline{a}_3^{3+}$-CN$^-$ = $\underline{a}_3^{2+}$) would yield the cyt $\underline{a}_3^{2+}$ spectrum (Salmeen et al., 1978; Ching et al., 1986) and uncover the acid pH-induced changes at this chromophore. This is illustrated by the Raman difference spectrum displayed in Figure 5.4, where fully reduced and mixed-valence oxidase samples, at pH 6.35 $\pm$ 0.01, are simultaneouly compared. At this pH the acid-induced changes at cyt $\underline{a}_3$ are not fully developed; nonetheless, this Figure serve as useful indicators of those mode expected to be perturbed by acidic pHs at the $\underline{a}_3$ heme site. Cyt $\underline{a}_3^{2+}$ vibrations are seen at 1665 cm^{-1}, 1569 cm^{-1}, and 1225 cm^{-1} (Figure not shown) (Babcock et al., 1981) and at 215 cm^{-1}, ~278 cm^{-1}, 330 cm^{-1}, 365 cm^{-1}, 404 cm^{-1}, 682 cm^{-1}, and 752 cm^{-1} (Figure 5.4). Similar cyt $\underline{a}_3^{2+}$ frequencies were observed in Figures 5.2 and 5.3 to be sensitive to acid pH denaturation effects.

Figure 5.4: Low frequency resonance Raman spectra of fully reduced (A) and partially reduced cyanide inhibited cytochrome oxidase (B) obtained with 441.6 nm excitation at the indicated pH levels. The difference spectrum (bottom trace) corresponds to the deconvoluted cytochrome $\underline{a}_3^{2+}$ spectrum at pH 6.35. Oxidase concentration was 45 μM (heme $\underline{a}$ basis). Cyanide concentration was 10 mM. The spectra are the average of 6 scans.

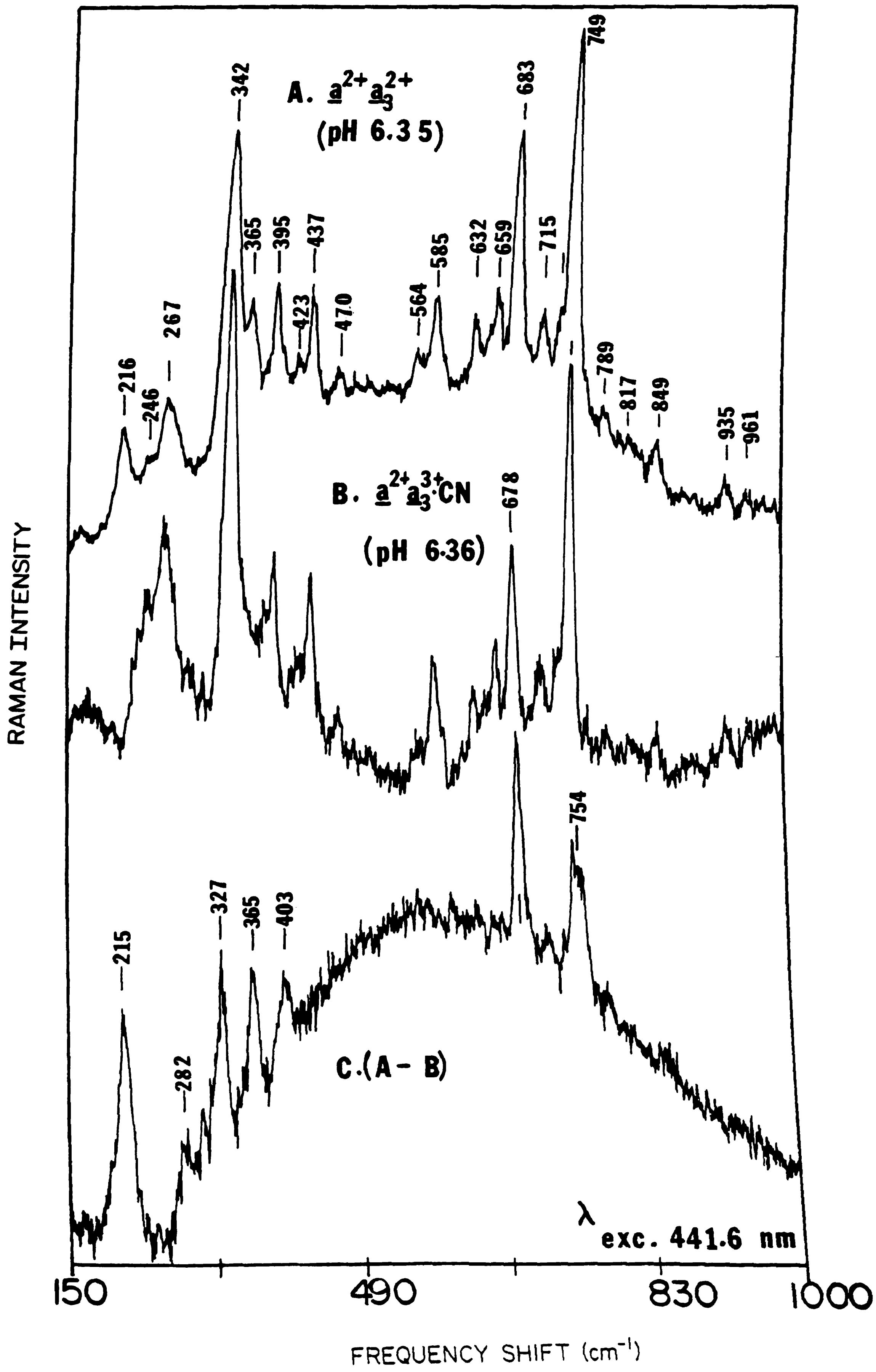
A. $\underline{a}^{2+}\underline{a}_3^{2+}$
(pH 6.3 5)
B. $\underline{a}^{2+}\underline{a}_3^{3+}$·CN
(pH 6·36)
C.(A – B)
216
246
267
342
365
395
423
437
470
564
585
632
659
683
715
749
789
817
849
935
961
678
215
282
327
365
403
754
λ exc. 441.6 nm
RAMAN INTENSITY
150
490
830
1000
FREQUENCY SHIFT (cm⁻¹)

The optical absorption spectra of mixed-valence oxidase, at essentially the same pH levels as those studied with fully reduced protein, are depicted in Figure 5.5. As with the fully reduced oxidase, the Soret and α-band maxima of cyt $\underline{a}^{2+}$ in mixed-valence protein are shifted towards shorter wavelengths, from 442 to 434 nm and 603 to 594 nm, respectively, when the pH is lowered from 7.4 to 4.5. In addition, the cyt $\underline{a}^{2+}$ near-visible line at 518 nm shifts to 510 nm as previously observed (see Figure 5.1). In the case of the cyt $\underline{a}_3{}^{3+}$-CN$^-$, its low-spin absorption transitions remain largely unaltered at 427 nm (sh), 592 nm (sh) and 552 nm.

The resonance Raman spectra of mixed-valence cytochrome oxidase at various pH levels are displayed in Figures 5.6 and 5.7. With 406.7 nm excitation (Figure 5.7A), we see enhancement of cyt $\underline{a}_3{}^{3+}$-CN$^-$ modes at 1672 cm^{-1} ($\nu_{C=O}$), 1640 cm^{-1} (ν_{10} Ca-Ca), 1620 cm^{-1} ($\nu_{C=C}$), and 1586 cm^{-1} (ν_2 Cb-Cb). Likewise, cyt $\underline{a}^{2+}$ modes at this wavelength are seen at ~1612 cm^{-1} ($\nu_{C=O}$), 1618 cm^{-1} ($\nu_{C=C}$), 1586 cm^{-1} (ν_2 Cb-Cb) and 1569 cm^{-1} (ν_{38} Cb-Cb). The 441.6 nm excitation spectra of these acid treated mixed-valence oxidase samples in the high and low-frequency ranges are shown in Figures 5.7 B and 5.6 , respectively. As mentioned previously, these spectra are dominated by vibrations from the cyt $\underline{a}^{2+}$ heme moiety. The pH induced changes of cyt $\underline{a}^{2+}$ vibrational modes in mixed-valence cytochrome oxidase are identical to those observed with fully reduced oxidase

Figure 5.5: Optical absorption spectra of partially reduced, cyanide-inhibited cytochrome oxidase at several pH levels. Enzyme concentration was approximately 50 μM (heme a basis), cyanide concentration was 20 mM.

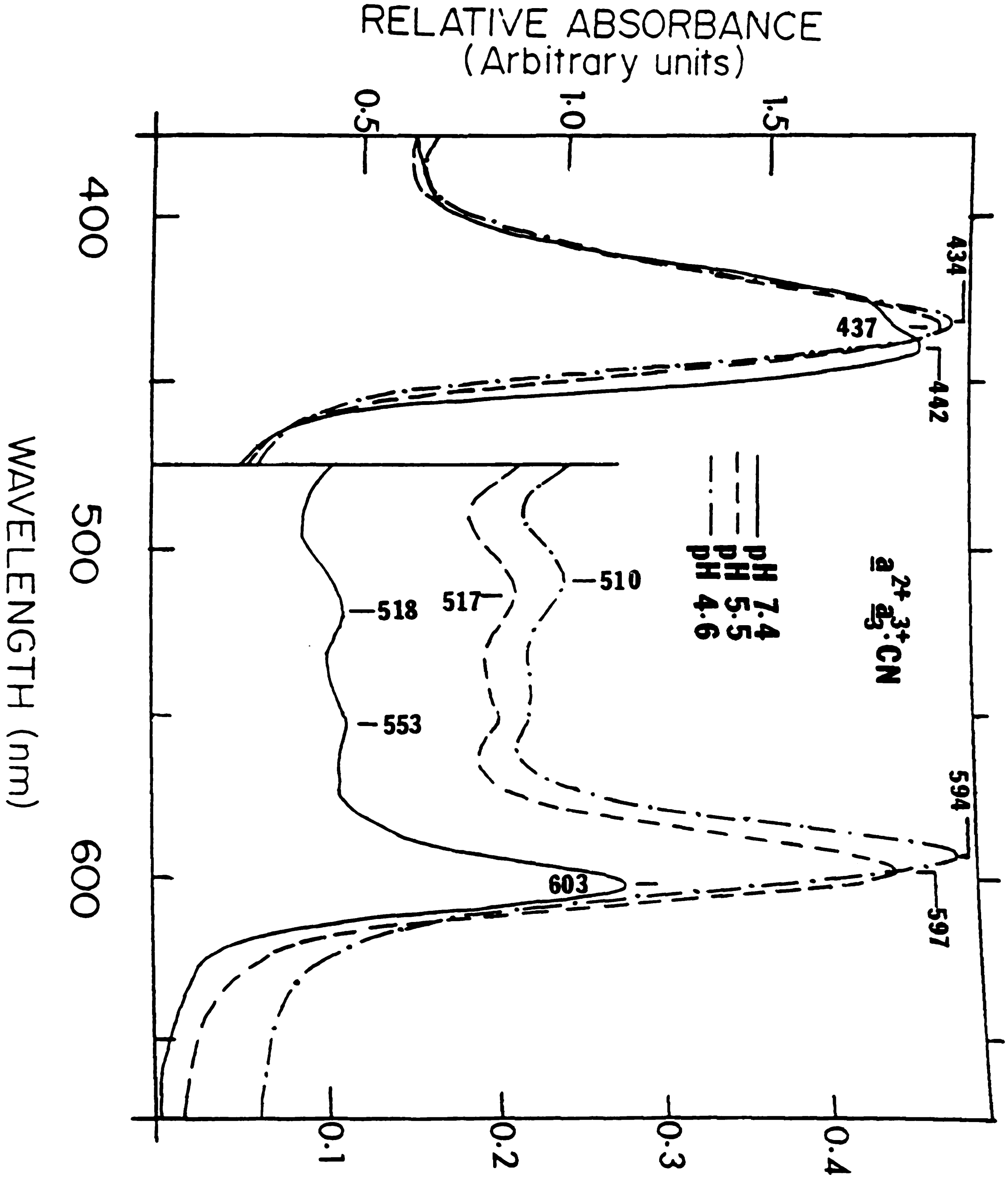
RELATIVE ABSORBANCE
(Arbitrary units)
0.5
1.0
1.5
400
500
600
WAVELENGTH (nm)
0.1
0.2
0.3
0.4
434
437
442
a2+ a3 3+·CN
pH 7.4
pH 5.5
pH 4.6
510
517
518
553
594
597
603

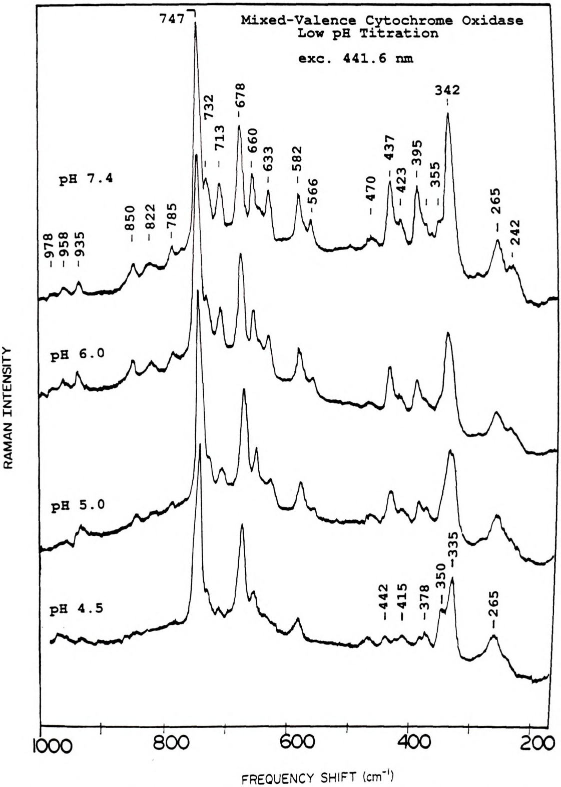

Figure 5.6: Low frequency resonance Raman spectra of mixed-valence cytochrome oxidase at the indicated acidic pH levels.

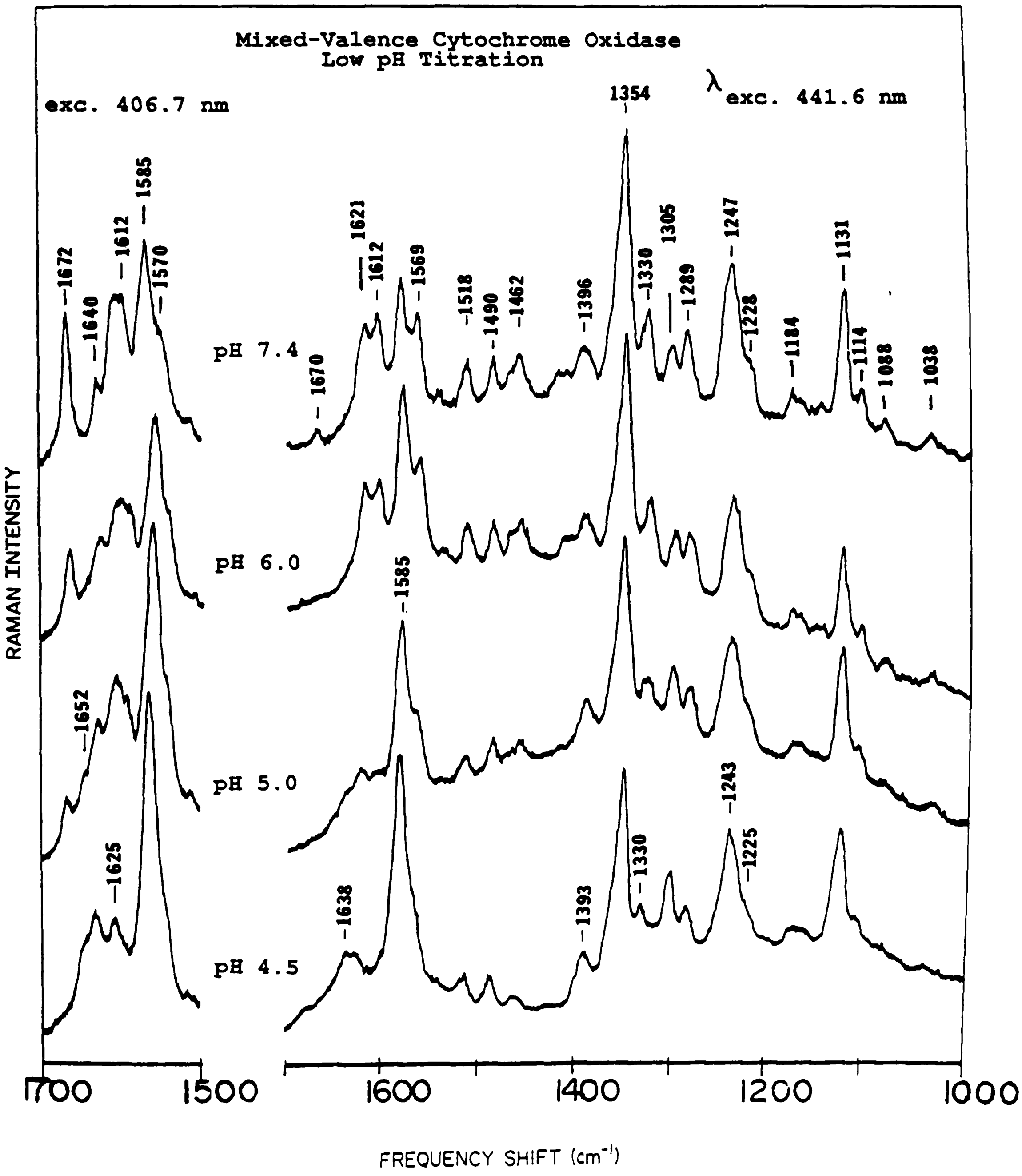

Figure 5.7: High frequency resonance Raman spectra of mixed-valence cytochrome oxidase at the indicated pH levels.

samples (see Table 5.3). Therefore, the acid induced shifts in the cyt $\underline{a}^{2+}$ carbonyl frequency (1612 cm^{-1}-->1640 cm^{-1}) observed in both sets of data support the occurrence of the hydrogen bonded structure in cyt $\underline{a}$. The direction of $\nu_{C=O}$ shift in cyt $\underline{a}^{2+}$ upon H-bond formation is the same as those observed for heme $\underline{a}$ $(N\text{-}MeIm)_2$, Cu^{2+} porphyrin $\underline{a}$, and benzaldehyde (see Table 5.1 and Figures 3.1 and 3.8 in Chapter III). The remainder of the cyt $\underline{a}^{2+}$ hydrogen bond sensitive vibrations can be assigned based upon our previous (-CHO) H-bonding assignments in benzaldehyde and heme $\underline{a}$ models. In these model compounds we observed upshifts for the in-plane formyl-proton (δ_{H-CO}) vibration at 1388 (to 1395 cm^{-1}) and in the ν_{Cb-CHO} stretching mode at 1206 (to 1212 cm^{-1}) upon H-bond formation (see Table 5.2). The downshifts in modes at 1228 cm^{-1} (to 1225 cm^{-1}) and 1396 cm^{-1} (to 1393 cm^{-1}) upon removal of the cyt $\underline{a}$ formyl H-bonding perturbation are consistent with our model compound data. Similarly, in the low frequency region, benzaldehyde and Cu^{2+} porphyrin display modes at 441 cm^{-1} and 453 cm^{-1}, respectively (see Chapter III). In Figure 5.7 intensity changes are noticeable for cyt $\underline{a}$ low-frequency modes at 633 cm^{-1}, 438 cm^{-1}, and 397 cm^{-1}, which is observed upon disruption of the formyl H-bonding structure. These modes are assigned to out-of-plane vibrations (Abe et al., 1978; Choi et al., 1983) with contributions from the ring-peripheral substituents. Therefore, it appears reasonable to assume that one immediate structural effect of the cyt $\underline{a}$ formyl hydrogen bonded

Table 5.1:

High Frequency Vibrational Assignments of Cytochromes a and a_3

	RED CYT OX pH 7.4		PRED CN- pH 7.4	
ASSIGNMENT	$a^{2+(b)}$	$a_3^{2+(a)}$	a^{2+}	a_3^{3+}-CN^-
ν(C=O)		1665		1672
$\Delta\nu$(C=O...H)	1612		1612	
ν_{10}, B1g	1620	1610	1620	1640
ν_2, A1g	1586	1575	1586	1589
ν_{38}(1), Eu	1569		1569	
ν_3, A1g	1491	1467	1493	1507
ν_4, A1g	1356	1356	1356	1373

---

a. While the cyt a_3^{2+} frequencies are enhanced with both 406.7 nm and 441.6 nm excitations, those of cyt a_3^{3+}-CN^- are observed with 406.7 nm (see text).

b. High frequencies vibrations of cyt a^{2+} are enhanced with both 406 .7 nm and 441.6 nm.

Table 5.2:

High Frequency Aldehyde Group Vibration Assignments and Shifts Observed for Benzaldehyde in the Presence of Hydrogen Donors and Cytochrome $\underline{a}^{2+}$ at Neutral and Acid pH.

				Cyt $\underline{a}^{2+}$		
Assign[a]	Ph-CHO (cm-1)	C_6H_6O (cm-1)	CF_3COOH (cm-1)	pH4.5 (cm-1)	pH7.4 (cm-1)	Assign.
ν(C=O)	1707	1692 (-15)	1681 (-26)	1638	1612 (-26)	ν(C=O)
ν_{8b}, ring	1588	1585 (-3)	1585 (-3)			
δH-CO	1388	1395 (+7)	1403 (+15)	1394	1396 (+2)	δH-CO
(wk)	1312	1315 (+3)	1318 (+6)			
νPh-CHO	1206	1212 (+6)	1214 (+8)	1225	1230 (+5)	ν Cb-CHO
				1178	1185 (+7)	ν C_b-C_α -C_β
δC=O	649	642 (-7)	?			
Ring Fold	441	441		438	438	Pyr. Fold
δ(Ph-CHO)	225	?				

---

[a] Zwarich et al., 1971

formation is to cause a lowering in the effective molecular symmetry of the heme macrocyle (Woodruff, 1982), providing new routes by which IR-allowed Eu-type out-of-plane modes could become resonance enhanced. A description of these modes in the RR spectra of cyt $\underline{a}^{2+}$ is given in Table 5.3.

IV. Discussion:

Our previous assignments of the hydrogen bonded formyl structure of cyt $\underline{a}$ have been based on the absorption red-shift of this heme center relative to low-spin heme $\underline{a}$ model compounds, and on its downshifted formyl stretching frequency. Because of this frequency downshift, the formyl group frequency overlaps with several porphyrin ring vibrations which makes small frequency shifts or perturbations difficult to observe. The band assignments given in the Tables are made with reference to the previous studies of Abe et al. (1978), Choi et al. (1983), and Willems and Bocian (1984). The pattern of vibrational shifts and their assignments confirm the hydrogen bonded structure of cyt $\underline{a}$ and allow small perturbations at the cyt $\underline{a}$ formyl group to be identified.

To identify the cyt $\underline{a}$ hydrogen bond sensitive vibrations unambiguously,it is necessary to follow the vibrations and frequency shifts caused by changes in acidity for both cyt $\underline{a}$ and $\underline{a}_3$ or to enhance selectively the vibrations of cyt $\underline{a}$. We have used both of these tactics by following the acid

Table 5.3:

pH Sensitive Vibrations (cm^{-1}) at Cytochrome $\underline{a}^{2+}$ Observed With 441.6 nm excitation.

cyt $\underline{a}^{2+}$ (pred $\bar{\mathrm{C}}$N-)	cyt $\underline{a}^{2+}$ (red cyt ox)			
pH 7.4 4.5	pH 7.4 4.5	heme $\underline{a}^{2+}$ $(NmeIm)_2$ (aq)	Mode	Assign
263-->265	272-->262			
342-->334	342-->335	335	$\nu_8(A_{1g})$	δCbS
355-->350 I	345-->348 I	350	$2\nu_{35}$	
395-->392	394-->392 D			γCbS
420-->415 D	420-->415 D			pyr fold
438-->440 D	438-->440 D			pyr fold
564--> D	564--> D		$\nu_{49}(Eu)$	CaCbCb
583-->586	583-->586	585	$\nu_{48}(Eu)$	δCbS
632-->638 D	633-->636 D			δCO
710-->715 D	712-->715 D		$\nu_{47}(Eu)$	δCbS
785--> D	788--> D		$\nu_{32}(B_{2g})$	δCbS
822--> D	820--> D		$\nu_6(A_{1g})$	CaCmCa
849--> D	850--> D			γCmH
1113-> D	1115-> D	1113 W	$\nu_{22}(A_{2g})$	CbS
1185->1178	1184->1178		$\nu_{30}(B_{2g})$	νCb-S
1228->1225		1220 (sh)		νPh-CHO
1290->1288	1293->1289	1287	$\nu_{42}(Eu)$	
1330->1334	1330->1334	---		δS=CH_2
1396->1394	1397->1393	1390	$\nu_{20} + \nu_{29}(A_{2g})$	δH-CO
1569-> D	1569-> D	1555->1558	ν_{38},Eu	
1612->1638	1612->1638	1645->1630		ν(C=O)

Continued Table 5.3:

1622-> D	1622-> D	---	ν(C=C)

a) Mode assignments from Abe et al. (1978) and Choi et al., (1983).

I -- Intensity increase
D -- Intensity decrease
W -- Weak

This page
have
been omitted.

pH dependence of the RR spectrum of the fully reduced enzyme and of the partially reduced cyanide inhibited complex. The optical absorption and the RR spectra of reduced cytochrome oxidase established that cyt $\underline{a}_3{}^{2+}$ undergoes a high- to low-spin conversion as the pH is lowered from 7.4 to 5.0. At more acidic pH levels, both heme chromophores display spectra typical of low-spin ferrous heme $\underline{a}$ in a nonaqueous environment. This indicates that the native cyt $\underline{a}$ hydrogen bonded formyl group interaction has been disrupted (see schematic, Figure 5.8A). In this low pH titration of the $\underline{a}^{2+}$ $\underline{a}_3{}^{3+}$-CN$^-$ complex, cyt $\underline{a}_3$ remains in the low-spin ferric form throughout, but its carbonyl frequency downshifts from a position indicative of of a non-hydrogen-bonding environment at 1672 cm^{-1} to a frequency which suggests a hydrogen-bonding environment (1655 cm^{-1}). While the spectrum of cyt $\underline{a}_3{}^{3+}$-CN$^-$ remains essentially unchanged at acidic pH, cyt $\underline{a}^{2+}$ displays the absorption blue-shift and $\nu_{C=O}$ frequency upshift indicative of its formyl environment shifting from a hydrogen bonded to a weakly or nonhydrogen bonded configuration (Figure 5.8B). Similar spectral shifts for cyt $\underline{a}$ were also observed in an alkaline pH titration of cytochrome oxidase (Callahan and Babcock, 1983). The fact that both acidic and alkaline pH are able to disrupt the hydrogen bonded form of cyt $\underline{a}$ implies that neither denaturation system titrates a specific amino acid, but rather results in a gradual unfolding of the polypeptide backbone, as discussed previously (Callahan and Babcock, 1983).

Figure 5.9: Schematic of proposed structural changes of reduced (A) and partially reduced plus cyanide (B) heme _a_ chromophores of cytochrome oxidase at acid pH levels. See text for further discussion.

A. Structural Schematic

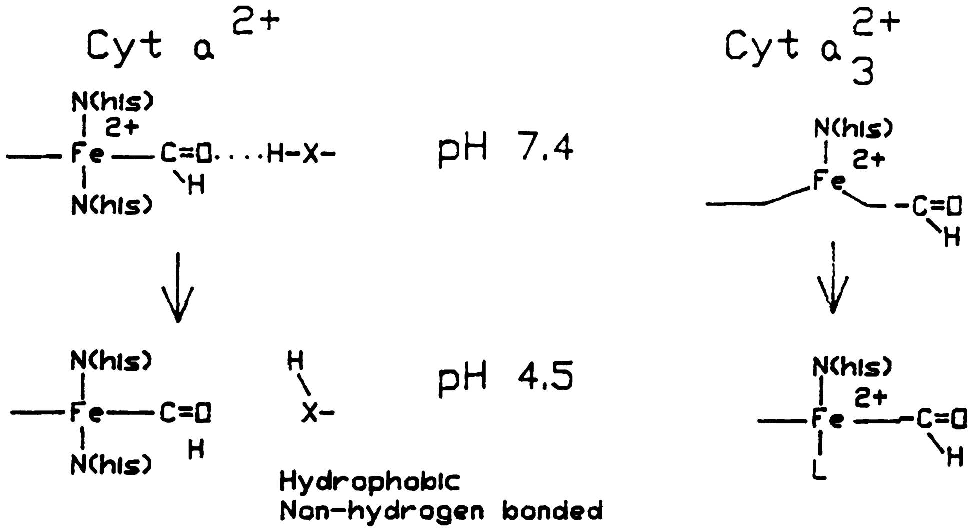
Cyt a 2+
Cyt a_3^{2+}
N(his)
2+
Fe
C=O····H-X-
H
N(his)
pH 7.4
N(his)
2+
Fe
C=O
H
pH 4.5
N(his)
Fe
C=O
H
N(his)
H
X-
N(his)
2+
Fe
C=O
H
L

Hydrophobic
Non-hydrogen bonded

B. Mixed-Valence

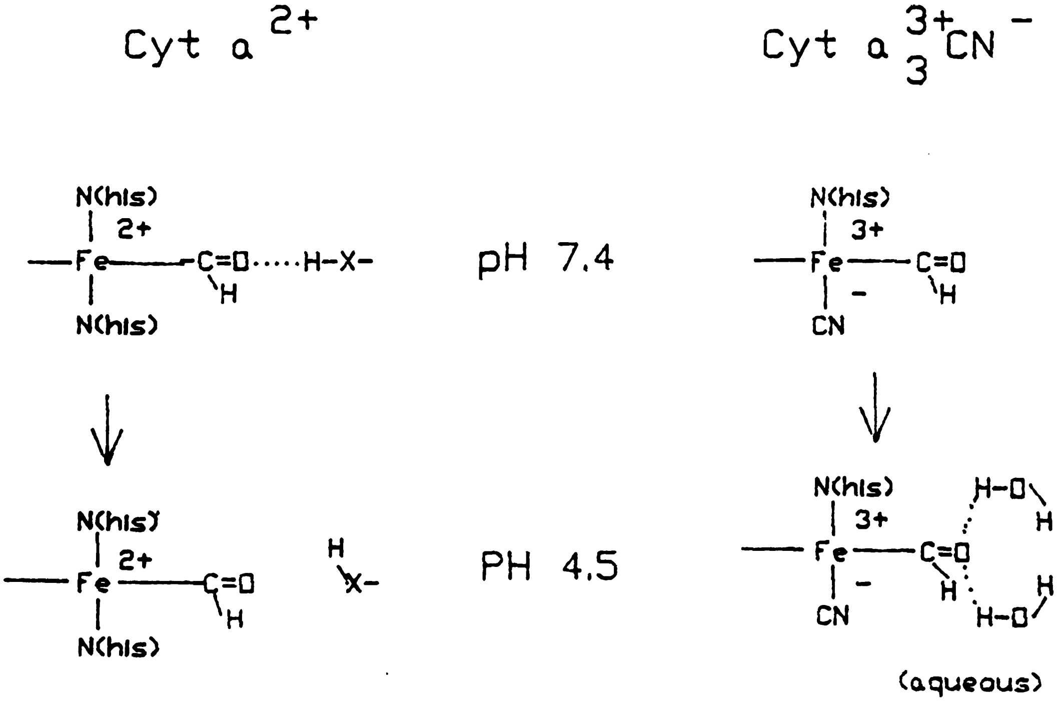
Cyt a 2+
Cyt $a_3^{3+}CN^-$
N(his)
2+
Fe
C=O·····H-X-
H
N(his)
pH 7.4
N(his)
3+
Fe
C=O
H
-
CN
N(his)
2+
Fe
C=O
H
N(his)
H
X-
PH 4.5
N(his)
3+
Fe
C=O
H
-
CN
H-O
H
H
H-O

(aqueous)

hydrophobic
Non-hydrogen bonded

A. Assignments of Hydrogen Bonding Sensitive Vibrations of Cyt $\underline{a}^{2+}$ in the High Frequency Region:

For both reduced and mixed-valence cytochrome oxidase, the major cyt $\underline{a}$ band shifts are: decreases at 1612, 1570, 1545, 1396-->1393, 1330-->1334, and 1118 cm^{-1} (Table 5.3). There has been some disagreement over the assignment of the 1612 cm^{-1} vibration to $\nu_{C=O}$ of cyt $\underline{a}$. Other workers have assigned this band to ν_{10}, a B_{1g} core-size marker band (Ogura et al., 1984; Choi et al., 1983). The ν_{10}, B_{1g} mode of high-spin cyt $\underline{a}_3{}^{2+}$ should also occur in this approximate frequency region, and it is assigned as a weaker, overlapping band at 1612 cm^{-1} based on correlations with appropriate heme $\underline{a}^{2+}$ model compounds (Van Steelandt-Frentrup et al., 1981) and core-size marker correlations (Choi et al., 1983).

The fact that the cyt $\underline{a}^{2+}$ formyl stretching frequency is shifted down to 1612 cm^{-1}, at lower frequency than ν_{10} and $\nu_{C=C}$ (see below) without coupling to these vibrations can be explained as follows. The 1612 cm^{-1} $\nu_{C=O}$ band is a polarized mode and therefore is defined as a totally symmetric vibration (Callahan and Babcock, 1981; Choi et al., 1983; Willems and Bocian, 1984). Because of the different symmetry of ν_{10} (B_{1g}; Abe et al., 1978) at 1623 cm^{-1}, no vibrational coupling of $\nu_{C=O}$ with this mode is expected. For the vinyl stretching frequency, the physical disposition of the vinyl and the carbonyl groups across the heme $\underline{a}$ ring diminishes the likelihood of vibrational coupling.

The remainder of the H-bond sensitive formyl group frequency vibrations are seen to shift in cyt a^{2+} as follows: 1396--> 1393 cm^{-1}, 1228-->1225 cm^{-1}, 1247-->1243 cm^{-1}, 1185-->1179 cm^{-1}, 981-->975 cm^{-1}, and 395-->392 cm^{-1} (Table 5.3). The 1396 cm-1 band is assigned as the in-plane (δ_{H-CO}) bending vibration (Choi et al., 1983). There are two overlapping bands at this position, ν_{20}, A_{2g}, and ν_{29}, B_{2g}, seen with visible excitation at 1389 cm^{-1} and 1397 cm^{-1}, respectively (Callahan and Babcock, 1983; Choi et al., 1983; see Figure 4.2 Chapter IV), which have ~25% (Cb-S) stretching character. With either assignment, a frequency shift is predicted. Our visible excitation studies (see Chapter IV) reveal a +2 cm^{-1} upshift on the 1389 cm^{-1} peak. In addition, our heme a model compound studies reveal a mode at 1399 cm^{-1} (see Chapter III, Figure 3.10) which shifts up to 1405 cm^{-1} upon formyl hydrogen bond formation. Accordingly, the sensitivity of this mode in reduced and CN^{-} inhibited protein to pH-denaturation is consistent with the models and with the *in situ* enzyme visible excitation studies. The 1228 cm^{-1} band (ν_{Cb-CHO}) has been previously discussed (Choi & Spiro, 1983; Willems and Bocian, 1984). Visible excitation on intact cytochrome oxidase reveals a +5 cm^{-1} upshift in this band upon deuterium incorporation (see Figure 4.2 Chapter IV). Similarly, hydrogen bonding studies in Cu^{2+} porphyrin a resulted in +6 cm^{-1} shift for this Raman band upon H-bond formation. Our observation of a downshifted frequency in this line upon pH denaturation (and disruption of the hydrogen bond to the $\underline{a}^{2+}$ formyl) of reduced and cyanide inhibited protein is consistent with these previous data. The cyt $\underline{a}^{2+}$ band shift observed at 1185 cm-1 and described as ν_{30}, B_{2g} (Willems and Bocian, 1984) has a potential energy distribution which contains ~50% (Cb-S) stretching character.

The pH sensitive vibration of cyt $\underline{a}^{2+}$ having vinyl character are identified as: decrease in $\nu_{C=C}$ intensity at 1622 cm^{-1} and a shift in $\delta_{s=CH_2}$ at 1330 cm^{-1}. The Soret excitation spectra seem to indicate a shift of the 1330 cm^{-1} band to 1334 cm^{-1}. However, visible excitation spectra clearly show two bands at 1334 and 1329 cm^{-1}, with the 1329 cm^{-1} band decreasing in intensity as the cyt $\underline{a}$ formyl hydrogen bond is disrupted (acidic pH data not shown, alkaline pH - Callahan and Babcock, 1983), and upshifts to 1333 cm^{-1} in the presence of deuterated buffers (see Figure 4.2 Chapter IV). The nature of the 1334 cm^{-1} band is not clear at this time, but we assign the 1329 cm^{-1} vibration to the vinyl internal mode $\delta_{s=CH_2}$ (Choi et al., 1982), and it is seen to decrease in intensity in parallel with $\nu_{C=C}$ at 1622 cm^{-1} as the formyl hydrogen bond is removed. Neither of these vinyl internal modes are observed for heme $\underline{a}^{2+}$ $(N\text{-}MeIm)_2$ (Table 5.3). They have been reported previously for ferrous heme $\underline{a}$ model compounds (Choi and Spiro, 1983), but were present owing to overreduction with $Na_2S_2O_4$ (Babcock, 1986). The selective enhancement of the vinyl modes in cyt $\underline{a}^{2+}$ may be caused by the strong hydrogen bonding perturbation along the y-axis of the heme a ring, which contains both the formyl and vinyl peripheral substituents. Choi et al. (1983) have suggested that the enhancement of the vinyl modes in protoheme RR spectra is caused by significant coupling to porphyrin modes. Lacking such vinyl-skeletal mode coupling in heme a, the hydrogen bond perturbation of cyt a allows the vinyl mode to couple into the heme a RR spectra. Alternatively, the presence of the vinyl bands in the RR spectrum of cyt a^{2+} may indicate that there is a structural perturbation at the vinyl peripheral substituent in the enzyme as well as at the formyl group.

B. Low Frequency Vibrational Assignments

The remainder of the vibrational shifts fall into three categories: 1) strictly D_{4h} allowed modes, A_{1g} symmetry vibrations that have substantial Cb-S character, such as ν_8, A_{1g} which shifts from 343-334 cm^{-1}; 2) D_{4h} modes which are strictly forbidden with Soret excitation but which become allowed under low symmetry conditions such as ν_{20} A_{2g} and ν_{29} B_{2g} which shift from 1396-1393 cm^{-1} and ν_{22} A_{2g} at 1115 cm^{-1} and ν_{32}, B_{2g} at 785 cm-1, both of which decrease in intensity as the pH is lowered; and 3) low symmetry allowed modes such as out-of-plane vibrations ν_{45} at 981 cm^{-1} which shifts down to 976 cm^{-1}, γ_{CmH} at 850 cm^{-1} and γ_{Cb-S} at 395 cm^{-1}, and Eu modes, ν_{38}, ν_{42}, ν_{47}, ν_{48} (Table 5.3), all of

which have considerable Cb-S stretching or bending character.

In this work, ν_8 of cyt a^{2+} is identified at 342 cm^{-1}. This band shifts to 334 cm^{-1} at pH 4.5 and a band increases in intensity at ~348 cm-^{1}. This pair of vibrations is assigned to ν_8 and 2 ν_{35}, respectively. These vibrations both have considerable (Cb-S) in-plane bending character and are believed to couple via Fermi resonance (Abe et al., 1979). The extent of their coupling apparently depends upon the nature of the iron axial ligands (Choi and Spiro, 1983) and formyl interactions (Copeland and Spiro, 1986).

The effects of symmetry reduction on metalloporphyrin spectra have been discussed by Woodruff et al. (1985), Ozuki et al. (1979), and Choi and Spiro (1983). On reducing the heme molecular symmetry from D_{4h} to C_{2h}, the predicted effects are those observed here; that is, A_{1g}, A_{2g}, B_{1g}, B_{2g} modes transform as A_g (Wilson et al., 1955) and would be expected to be observed with both Soret and visible excitation because A-term RR scattering is dominant, depolarization ratios approach 1/3, and the IR allowed Eu modes may split and acquire Raman intensity by symmetry reduction (Bocian et al., 1986). Protein-induced symmetry lowering in cyt c^{2+} has been used to explain the presence of Eu modes in its low frequency RR spectrum (Valence and Strekas, 1982). The symmetry lowering effect of the hydrogen bonded formyl group of cyt a allows all of the above effects to be observed. The cyt a^{2+} RR spectrum does not display the extreme symmetry lowering effects of a metallochlorin (Andersson et al., 1986), but rather, lies intermediate between the spectra observed for M^{2+} octaethylchlorin and protoheme.

D2O incorporation studies have been carried on beef heart cytochrome oxidase (Argade et al., 1986; Copeland & Spiro, 1986; Centeno et al., unpublished results) to probe the exchangeability of the cyt a hydrogen bonded proton. Small frequency shifts were observed for $\nu_{C=O...H}$ in D_2O vs. H_2O buffers, as would be expected if deuterium were substituted for hydrogen in the cyt a formyl hydrogen bonded structure. Because of the several overlapping bands near 1612 cm^{-1}, it is difficult to clearly assess the effect of D_2O on cyt a. However, with reference to the vibrations reported here and in Chapter IV, it can be seen that several of the hydrogen bond sensitive vibrations are affected, i.e., 1611, 1330, 1230, 1183, 436 and 340 cm^{-1} (Argade et al., 1986) and 1610, 1330, 1230, 350 and 343 cm^{-1} bands (Copeland & Spiro, 1986), thus supporting the above authors' conclusions that deuterium is substituted for hydrogen in the native structure of cyt a. A further examination of the vibrations reported here may be useful in determining the role of cyt a in energy transduction. This will be the subject of Chapter VI.

V. Concluding Remarks:

In the present study we have attempted to probe the cyt $\underline{a}^{2+}$ aldehyde vibrations by controlling an acidic pH denaturation of the reduced and mixed-valence oxidase derivatives. Lowering the pH of the reduced oxidase solution brought about a dual chomophoric effect as spin state changes in cyt $\underline{a}_3$ and disruption of the hydrogen bonded structure of cyt $\underline{a}$ were observed. The cyt $\underline{a}$ formyl hydrogen bonding assignments made here are suggested as a useful tool to gain insights into the structure and environmental conformation of cyt $\underline{a}^{2+}$ in cytochrome oxidase from other eukaryotic and prokaryotic species. In the following chapter we will use these formyl assignments, together with those suggested in Chapter IV, to study the proposed role of the cyt $\underline{a}^{2+}$ formyl hydrogen bonding structure in the oxidase proton pump action.

CHAPTER VI

EVIDENCE FOR CYTOCHROME A INVOLVEMENT ON THE CYTOCHROME *C* OXIDASE PROTON PUMP MECHANISM: A RESONANCE RAMAN AND ENDOR STUDY.

I. Introduction:

Since the original report by Wikstrom (1977) of the proton pumping action of membrane-bound cytochrome oxidase, experimental evidence on the redox-linked proton pumping activity has accumulated that supports the view of the H^+-pump as an integral part of this terminal enzyme. Two mechanistic models for proton pumping activity in cytochrome oxidase have been proposed. The first model involves conformational changes at the periphery of the cytochrome *a* heme induced by H-bonding interactions with a protein residue (Babcock and Callahan, 1983); the second model proposes redox-linked ligand exchange reactions at Cu_A^{2+} as the basis for the proton translocation. In the work reported here, we present spectroscopic results for cytochrome *a* and Cu_A^{2+} that were obtained in order to probe the feasibility and mechanistic implications of these two proposals. The cytochrome *a* site has been studied by resonance Raman (RR) spectroscopy, while the Cu_A^{2+} site was studied by electron nuclear double resonance (ENDOR) spectroscopy.

The cytochrome *a* heme model proposed by Babcock and Callahan (1983), involves the formyl group in a H-bonding interaction with an acid-base ionizable protein donor as the basis for the redox-linked proton pump mechanism. From changes in the cytochrome a carbonyl stretching frequency, Babcock and Callahan (1983) suggested that the strength of this H-bonding interaction was dependent upon the redox state of the cytochrome a heme-iron. The carbonyl stretching frequency of ferric cytochrome a was observed at 1650 cm^{-1} shifting down to ~1612 cm^{-1} upon iron ion reduction. The proposed mechanism predicted the occurrence of exchangeable protons at the protein H-donor site and an enhanced H/D-exchange rate upon catalytic cycles of reduction and re-oxidation. Resonance Raman spectroscopy provides a suitable tool by which these two proposals may be examined owing to the sensitivity of resonance Raman frequencies to heme structure and immediate chromophore-protein environment. Indeed, recently reported Soret-excitation Raman spectra of reduced (Copeland and Spiro, 1986) and mixed-valence cytochrome oxidase (Argade et al., 1986), as well as a visible-excitation resonance Raman study (Centeno et al., in preparation), have provided further evidence for labile protons at the cyt a protein vicinity.

In this Chapter we report the resonance Raman results of experiments on the H/D-exchange rate at the cytochrome a H-bonded site as studied during enzyme turnover. The results presented here show that, for a freshly prepared sample of reduced protein in D_2O, the H/D-exchange at the protein H-donor is complete after ~10 hours. For "activated" (reduced and reoxidized) oxidase, the rate of deuterium incorporation is dramatically accelerated. Comparison of the resonance Raman spectra of cytochrome oxidase under different reductant concentrations and varying D_2O-incubation times allows us to distinguish between fast- and slow- changes in the vibrational spectra of reduced and mixed-valence oxidase. Slow-changes are identified as specific H-bonding effects and are detected for modes with substantial carbonyl contribution. On the other hand, fast-changes involving H/D exchange or non-specific protein effects are detected by resonance enhancement of vinyl modes and a low-frequency pyrrole folding mode.

In the Cu_A based proton-pump model, Chan and coworkers proposed that redox-linked ligand-displacement at the Cu_A ligand-coordination serves as the driving force for the translocation of protons to the cytosol side of the membrane. This model also predicts the occurrence of exchangeable protons in the immediate protein vicinity of the Cu_A ligand-coordination site. To test this proposal, we have used electron nuclear double resonance (ENDOR) spectroscopy on the Cu_A EPR signal of resting and redox-cycled cytochrome oxidase in deuterated solvents. ENDOR spectroscopy is capable of detecting weakly interacting protons in the vicinity of paramagnetic centers (e.g., O'Malley and Babcock, 1986) and has been recently used to study H/D-exchange kinetics in the ubiquinone component of the bacterial photosynthetic system (Okamura and Feher, 1986). This technique has also been used to establish the identity of the ligands around the Cu_A^{2+} metal center (Stevens et al., 1982). Results from these studies have demonstrated that ENDOR spectroscopy is a sensitive technique to study differences in protein ligation at the metal centers. Our ENDOR spectra of native and redox cycled oxidases in protonated and deuterated buffers reveal the existence of exchangeable protons near Cu_A.

II. Results:

A. Resonance Raman Spectra of Resting Cytochrome Oxidase:

The optical absorption spectra of resting cytochrome oxidase in protonated and deuterated buffers, in the Soret region, are shown in Figure 6.1. For oxidized oxidase incubated in H_2O, the Soret maximum was observed at 422.6 nm, while in D_2O the Soret maximum was shifted to 420 nm. This transition in the Soret absorption maximum required 10-12 hours, at ice bath temperatures, for completion. Shifts in the Soret absorption maximum towards shorter wavelengths are consistent with increased population of high-spin heme iron, presumably at the heme of cytochrome $\underline{a}_3$ (Vanneste, 1967).

The resonance Raman spectra of resting cytochrome oxidase and the associated difference spectrum are shown in Figure 6.2. The cytochrome $\underline{a}^{3+}$ carbonyl stretching frequency, observed at 1650 cm^{-1} in the sample in H_2O (Babcock and Callahan, 1983), is shifted down to 1647 cm^{-1} in D_2O, as illustrated by the derivative shape of the Raman difference spectrum (RDS) with a negative peak at 1645 cm^{-1} and a positive peak at 1652 cm^{-1}. This observation confirms work by

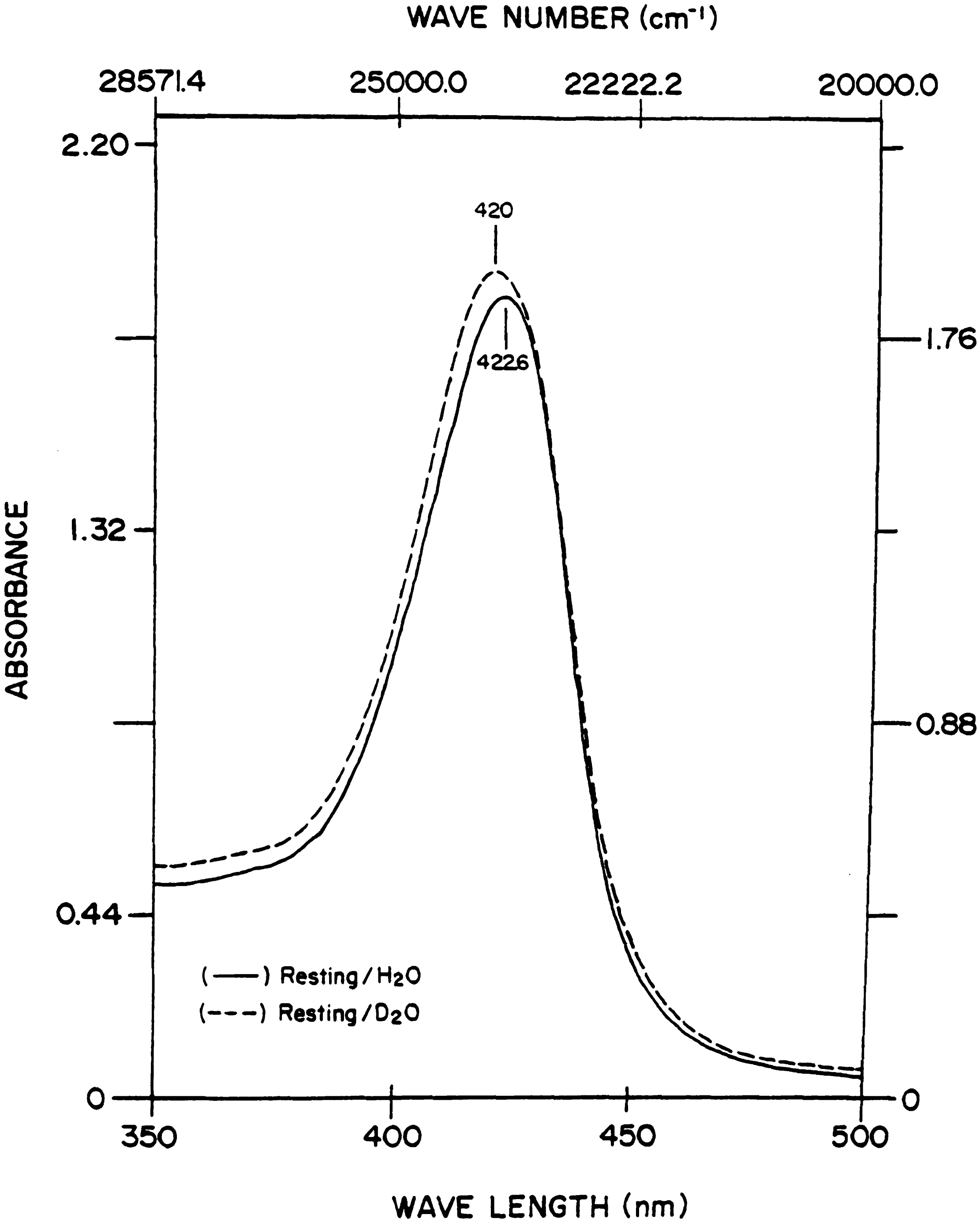

Figure 6.1: Optical absorption spectra of resting cytochrome oxidase in H_2O and D_2O buffers. Oxidase samples were incubated for 12 hours in the resting state. Oxidase concentration was 60 μM.

Figure 6.2: Resonance Raman (RR) spectra and the associated Raman difference spectrum (RDS) of resting cytochrome oxidase in protonated and deuterated buffers from 1000 to 1400 cm^{-1} (A) and from 1300 to 1700 cm^{-1} (B). Cytochrome oxidase used on these experiments was incubated in the resting form for 12 hours. Enzyme concentration was approximately 80 μM (heme *a* basis). Laser excitation frequency at 406.7 nm.

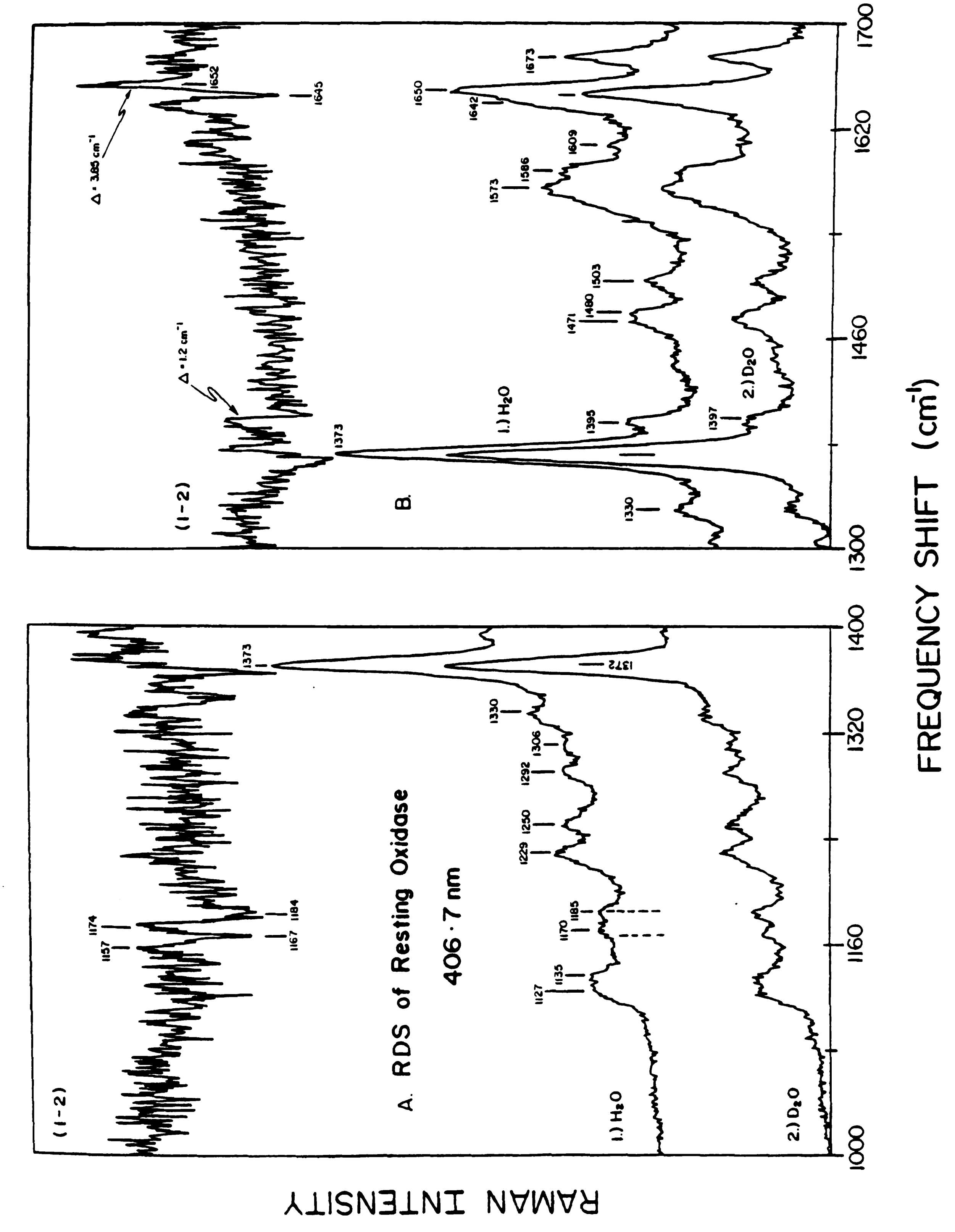
A. RDS of Resting Oxidase
406·7 nm
(1-2)
1.) H₂O
2.) D₂O
1127
1135
1157
1167
1170
1174
1184
1185
1229
1250
1292
1306
1330
1373
1372
1000
1160
1320
1400
B.
(1-2)
Δ = 1.2 cm⁻¹
Δ = 3.85 cm⁻¹
1.) H₂O
2.) D₂O
1330
1373
1395
1397
1471
1480
1503
1573
1586
1609
1642
1645
1650
1652
1673
1300
1460
1620
1700
FREQUENCY SHIFT (cm⁻¹)
RAMAN INTENSITY

Copeland and Spiro (1987) who used conventional resonance Raman instrumentation to detect the shift in the $\nu_{C=O}$ band of cytochrome a^{3+} upon H/D exchange. In the present work, we used Raman difference techniques to obtain these shifts more quantitatively. The expression used to obtain the relationship between the frequency separation of the lines, $\Delta\nu$, and the peak-to-peak intensity ($I_D{}^o$) of the difference spectrum is given by Rousseau (1981): $\Delta\nu = 0.38\Gamma(I_D{}^o/I_D)$ where Γ is the bandwidth at half-maximum, and I_D is the peak intensity. Using the above expression, we obtain a shift in the carbonyl stretching frequency of -3.85 cm^{-1}. This downshift in $\nu_{C=O}$ of cytochrome a^{3+} was interpreted by Copeland and Spiro (1986) as indicative of stronger H-bonding in D_2O, and hence a lower C=O stretching frequency.

A resonance Raman (RR) line at 1398 cm^{-1} assigned to cytochrome a^{3+} (Callahan and Babcock, 1981) loses intensity and shifts up by +1.2 cm^{-1} upon use of deuterated buffers. Resonance Raman studies of heme a model compounds (Choi et al., 1983) indicate that the in-plane bend of the formyl group (δ_{H-CO}) occurs at ~1390 cm^{-1} and overlaps strongly with a porphyrin mode (ν_{29} B_{2g} C_b-C_b) expected at 1395 cm^{-1}. Raman spectra of benzaldehyde compounds display this formyl H-bending motion at 1388 cm^{-1} (Zwarich et al., 1971) which, upon H-bonding, shifts up to 1395 cm^{-1} (Δ =8 cm^{-1}) (Centeno et al., in preparation; see Figure 3.3, Chapter III). Similarly, our previous RR study on the formyl modes of bis-imidazole heme a and its Cu^{2+} porphyrin a models indicates that a mode at 1399 cm^{-1} shifts up to 1403 cm^{-1} upon H-bond formation. Conversely, the small but reproducible shift in the corresponding frequency of the isolated protein upon H/D exchange, can be indicative of an unusual hindered formyl motion in the cytochrome a heme chromophore. This might be due to stronger protein interactions and/or to weaker coupling of the H-bending mode and other formyl-related motions.

As shown in Figure 6.2, H/D exchange effects in resting cytochrome oxidase are also detected in the 1170-1184 cm^{-1} region. The RDS, in Figure 6.2 indicates that lines at 1157 cm^{-1} and 1174 cm^{-1} shift into two new vibrations at 1166 cm^{-1} and 1184 cm^{-1} upon H/D exchange. In contrasts to the vibrational changes in the carbonyl stretching region which are observed to take ~10 hours for full completion, the above shifts were quickly established in D_2O. Significant contribution from π-conjugated porphyrin peripheral substituents to Raman modes in this region have been documented and indeed normal coordinate analysis indicates substantial ring-substituent stretching character in the region from 1167-1172 cm^{-1} (Abe et al., 1978; Lee et al., 1986). Resonance Raman studies on vinyl-containing protoporphyrin model compounds (Choi et al., 1982; Choi et al., 1983) have identified the ring-vinyl stretching frequency at 1172 cm^{-1}. Our observations of a 10 cm^{-1} upshift on this line upon protein deuteration is consistent with its vinyl assignment.

B. Resonance Raman Spectra of Redox-Cycled Oxidase:

Raman spectra above 1000 cm^{-1} of redox-cycled oxidase obtained with 406.7 nm excitation are depicted in Figure 6.3. Traces 6.3A and 6.3B correspond to the redox-cycled oxidase in protonated and deuterated buffers, respectively. Several vibrational changes are detected between these two samples. At first glance, the broad feature centered at 1619 cm^{-1} in trace 6.3A splits into two clear bands at 1608 cm^{-1} and 1625 cm^{-1} for the redox-cycled oxidase in D_2O. In addition, in the mid-frequency region, bands at 1186 cm^{-1}, ~1228 cm^{-1}, 1246 cm^{-1}, 1306 cm^{-1}, and 1330 cm^{-1} to shift in frequency and/or change in relative intensity upon reduction and reoxidation in D_2O. A weak peak at ~1043 cm^{-1} and a shoulder centered at ~1218 cm^{-1} consistently appear upon use of deuterated buffers. Since D_2O itself displays a weak peak at 1043 cm^{-1} and a strong and broad peak at ~1207 cm^{-1}, we infer that the 1218 - 1220 cm^{-1} mode in the spectra of Figure 6.3 most likely arises from a D_2O contribution and not from cytochrome $\underline{a}$ as recently suggested (Argade et al., 1986). Oxidase samples used to record traces 6.3C and 6.3D were inhibited in the resting ($\underline{a}^{3+}\underline{a}_3{}^{3+}$) form immediately after suspension of the oxidase in D_2O-buffer by addition of 6 mM CN- (pD 8.0). After formation of the $\underline{a}^{3+}\underline{a}_3{}^{3+}CN$ derivative (as monitored by the optical absorption spectrum), the reducting system, ascorbate/TMPD, was added and Raman spectra were obtained (trace 6.3C). The resulting

Figure 6.3: Resonance Raman (RR) spectra of mixed valence cytochrome oxidase under various turnover conditions as monitored with 406.7 nm excitation. Oxidase samples A, B, and C were freshly prepared. Oxidase used on trace B was freshly prepared and immediately reduced with 10 mM ascorbate/20 μM TMPD in the presence of excess dioxygen, and allowed to redox-equilibrate for 45 minutes, then 6-10 mM cyanide was added to form the $\underline{a}^{2+}\underline{a}_3{}^{3+}$- CN^- derivative. Oxidase used on trace C was freshly prepared and immediately inhibited in the resting form by the addition of 6-10 mM cyanide; then after 15-25 minutes of incubation, reductant asc/TMPD was added to produce the mixed-valence derivative resulting in spectrum C. Trace D was the observed Raman spectrum of sample C after an incubation period of 24 hours. Trace E show the Raman spectrum of the D_2O buffer. T.O.= turnover.

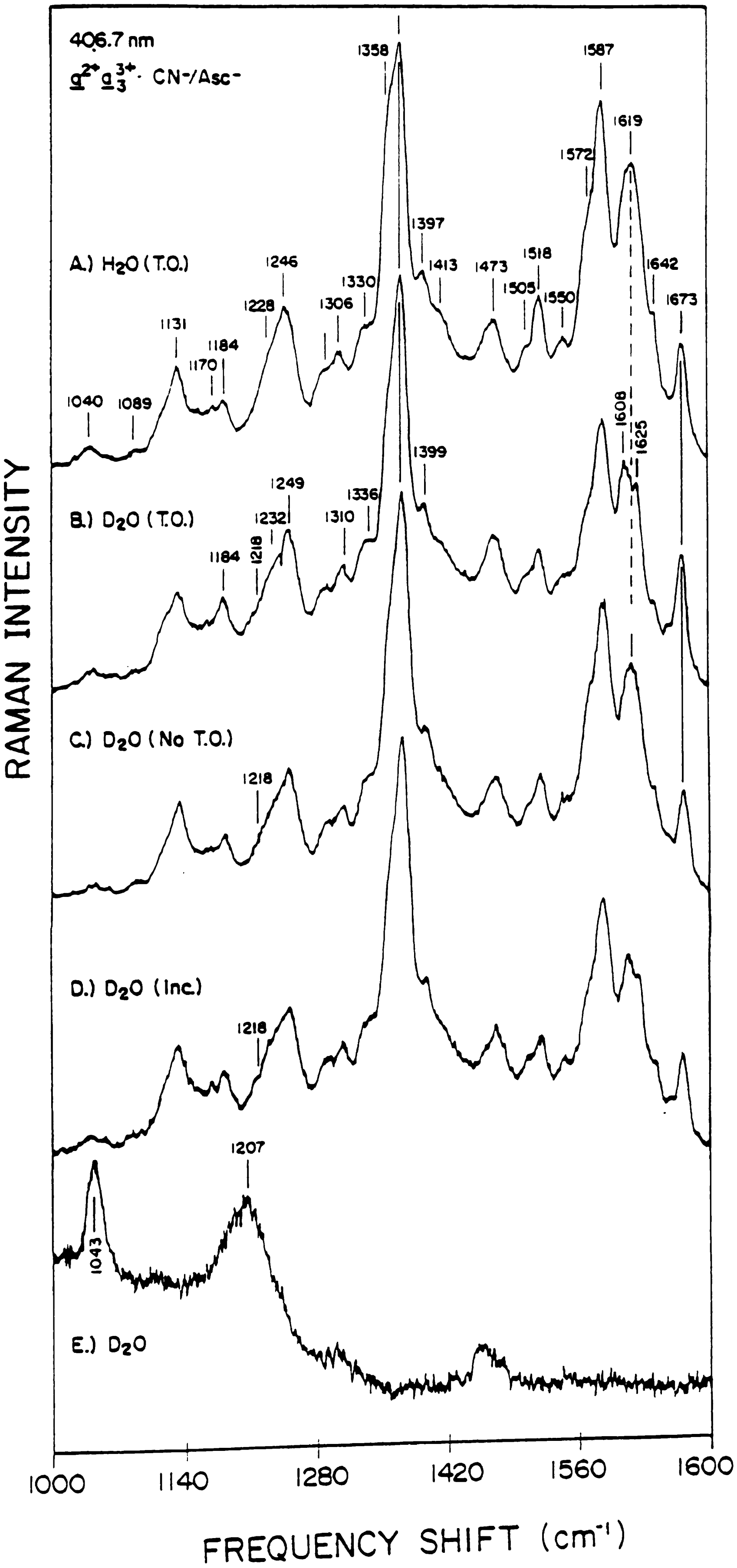
406.7 nm
a²⁺a₃³⁺· CN⁻/Asc⁻
A.) H₂O (T.O.)
B.) D₂O (T.O.)
C.) D₂O (No T.O.)
D.) D₂O (Inc.)
E.) D₂O
1358
1587
1619
1572
1397
1413
1473
1518
1505
1550
1642
1673
1246
1330
1228
1306
1131
1184
1170
1040
1089
1608
1625
1399
1249
1336
1232
1310
1218
1184
1218
1218
1207
1043
RAMAN INTENSITY
1000
1140
1280
1420
1560
1600
FREQUENCY SHIFT (cm⁻¹)

Raman spectrum displays a broad feature centered at 1619 cm^{-1}, and non-shifted modes at 1228 cm^{-1} and 1246 cm^{-1}. Nevertheless, shifts in modes at 1184 cm^{-1}, 1305 cm^{-1}, and 1330 cm^{-1} and the D_2O shoulder at ~1218-1220 cm^{-1}, were detected. Comparison of traces 6.3A and 6.3C suggest that the addition of cyanide to the resting (non-redox cycled) oxidase appears to lock the cytochrome a site into an initially non-exchangeable conformation as noted by the similarities between these two spectra. The resonance Raman spectrum of sample 6.3C taken 24-hours after incubation is shown on trace 6.3D. The spectral similarities between this latter spectrum and that of trace 6.3B (redox-cycled oxidase) are obvious; that is, splitting of the 1619 cm^{-1} line into two new lines at 1608 cm^{-1} and 1625 cm^{-1}, as well as the apparent upshift in modes at ~1228 cm^{-1} and 1246 cm^{-1}. The resonance Raman spectra of fully reduced cytochrome oxidase in the carbonyl stretching region, is shown in Figure 6.4. As with the mixed-valence protein, we observed a clear splitting of the 1619 cm^{-1} line to 1608 cm^{-1} and 1625 cm^{-1} after 12 hours of incubation of the ascorbate/TMPD reduced oxidase. Dithionite-reduced protein failed to reproduce the frequency shift in the cytochrome a^{2+} $\nu_{C=O}$ line over the same period of incubation (spectra not shown, but see Figure 6.5). These apparent reductant dependence differences in $\nu_{C=O}$ were further studied .

Figure 6.5 shows a plot of the observed frequency shift in $\nu_{C=O}$ as a function of incubation time for the reduced

Figure 6.4: Resonance Raman (RR) spectra of fully reduced cytochrome oxidase observed in the carbonyl stretching region of cytochrome *a*$^{2+}$. Trace A is the corresponding RR spectrum in protonated buffers. Trace B show the RR spectrum of a freshly prepared sample in deuterated buffers; traces C and D are the corresponding spectra after 6 and 12 hours of incubation, respectively. Instrumental conditions: laser excitation at 406.7 nm with a nominal output power of 15 mW (at the sample); resolution 5 cm^{-1}; scan rate 20 cm^{-1}/minute; time constant 0.5 sec. Oxidase sample conditions: concentration 80 μM(heme *a* basis); reductant ascorbate/TMPD; Soret maximum observed at 443 nm; temperature at the sample was maintained at 4 ^{o}C.

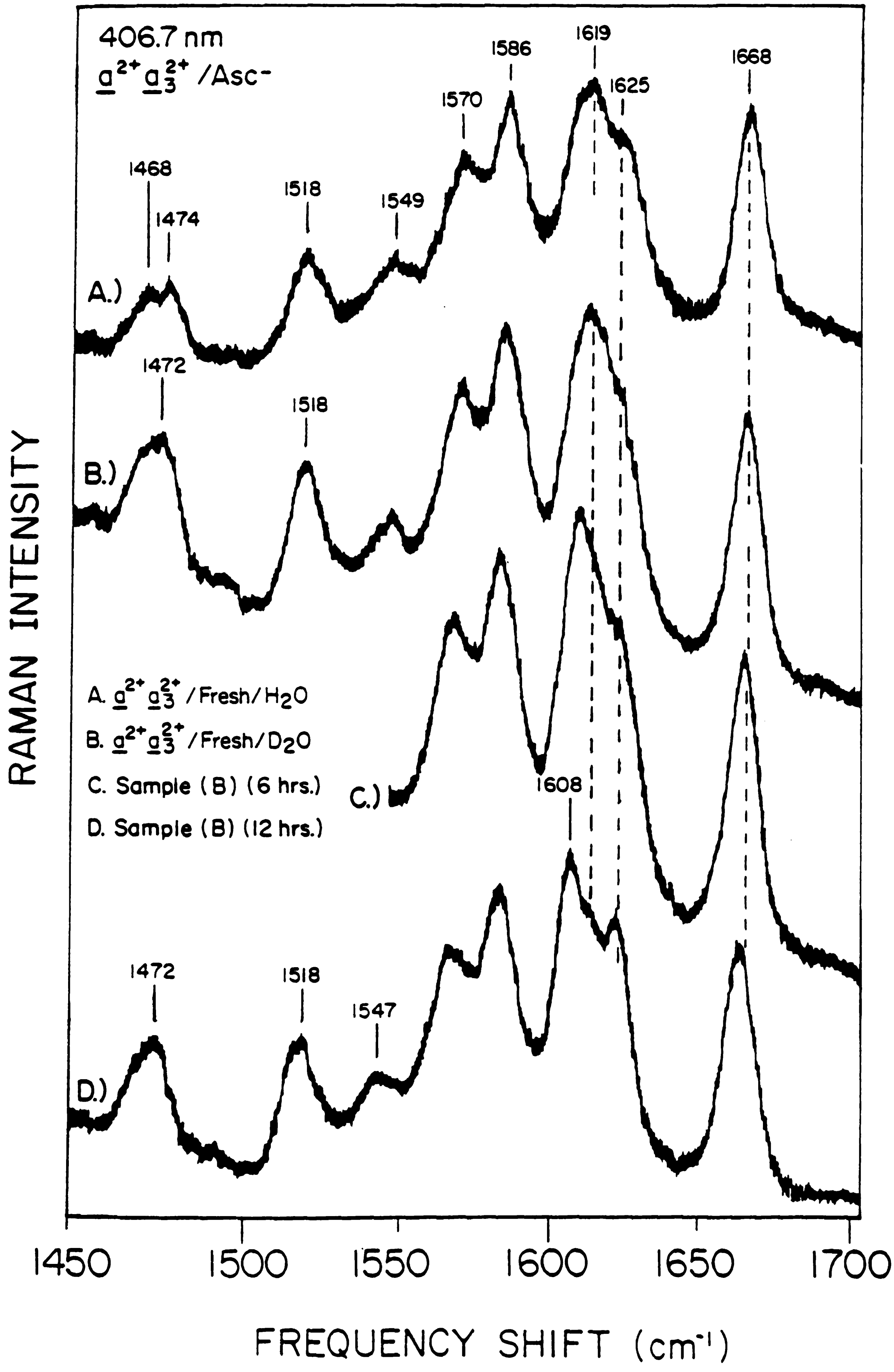
406.7 nm
$\underline{a}^{2+}\underline{a}_3^{2+}$ /Asc⁻
1468
1474
1518
1549
1570
1586
1619
1625
1668
A.)
1472
1518
B.)
C.)
1608
1472
1518
1547
D.)
A. $\underline{a}^{2+}\underline{a}_3^{2+}$ /Fresh/H_2O
B. $\underline{a}^{2+}\underline{a}_3^{2+}$ /Fresh/D_2O
C. Sample (B) (6 hrs.)
D. Sample (B) (12 hrs.)
RAMAN INTENSITY
1450
1500
1550
1600
1650
1700
FREQUENCY SHIFT (cm^{-1})

oxidase in D_2O. In these experiments, two individual freshly prepared samples (non-inhibited) of resting oxidase dissolved in D_2O buffer were placed in separated compartments of the divided spinning cell. Reductant, ascorbate (10 mM)/TMPD (20 μM), was added to one compartment, while a few grams of solid $Na_2S_2O_4$ were placed in the other compartment to produce the fully reduced oxidase derivatives. Both samples were capped and their Raman spectra in the cytochrome a carbonyl stretching region were simultaneously recorded at different times of incubation. As shown in Figure 6.5, the dithionite reduced protein does not display any considerable shifts in the cytochrome a carbonyl mode even after one day of incubation. However, the ascorbate/TMPD reduced protein demonstrates a shift of the broad band at ~1619 cm^{-1} to 1608 cm^{-1} at the end of six hours of incubation.

The downshifted frequency of the cytochrome a carbonyl stretching mode has been followed as a function of the number of electrons donated from ascorbate to cytochrome a, with the aim of revealing the number of enzymatic turnovers needed to trigger full incorporation of deuterium atoms at the C=O...H protein site. Our results are illustrated in Figure 6.6. Individual oxidase samples were freshly prepared for each Raman measurement. The number of enzyme catalytic cycles were estimated from the ascorbate concentration and the oxidase concentration by assuming complete consumption of the former. The spectrometer resettability was checked after each individual measurement by recording the Raman

Figure 6.5: Plot of frequency of the cytochrome $\underline{a}^{2+}$ carbonyl stretching frequency as a function of incubation time in D_2O. Oxidase samples were reduced with asc/TMPD (○) and solid sodium dithionite (⊡) in the Raman difference cell. The spectra were recorded simultaneously with the RDS apparatus in the region from 1500 to 1700 cm^{-1} at the indicated times of incubation. T.O.=turnover

Frequency Shift ($\underline{a}^{2+}c=o$) vs. Incubation Time

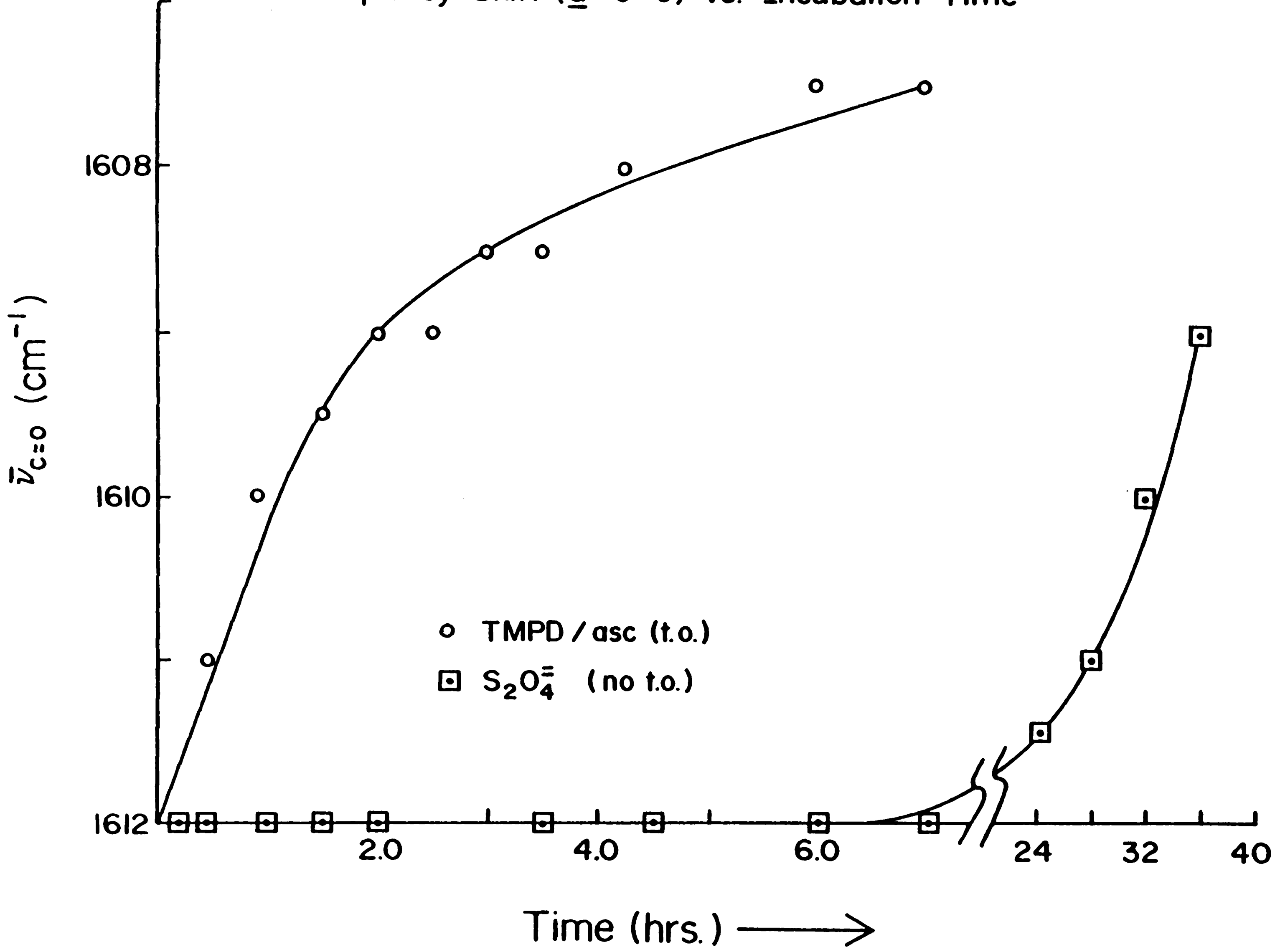

Figure 6.6: Resonance Raman (RR) spectra of redox-cycled oxidase as a function of enzyme turnover catalytic cycles induced by increasing the concentration of ascorbate in the solution. An individual oxidase sample was freshly prepared for each separate measurement. The oxidase concentration was maintained at 80 μ M (heme a basis), while the ascorbate concentration was monotonical increased to 0.6 mM, 1.2 mM, 1.8 mM, 3.0 mM, 4.2 mM, and 4.8 mM, respectively. The number of turnovers (T.O.) was calculated as the ratio of concentration of ascorbate used per oxidase. Laser excitation wavelength is at 406.7 nm.

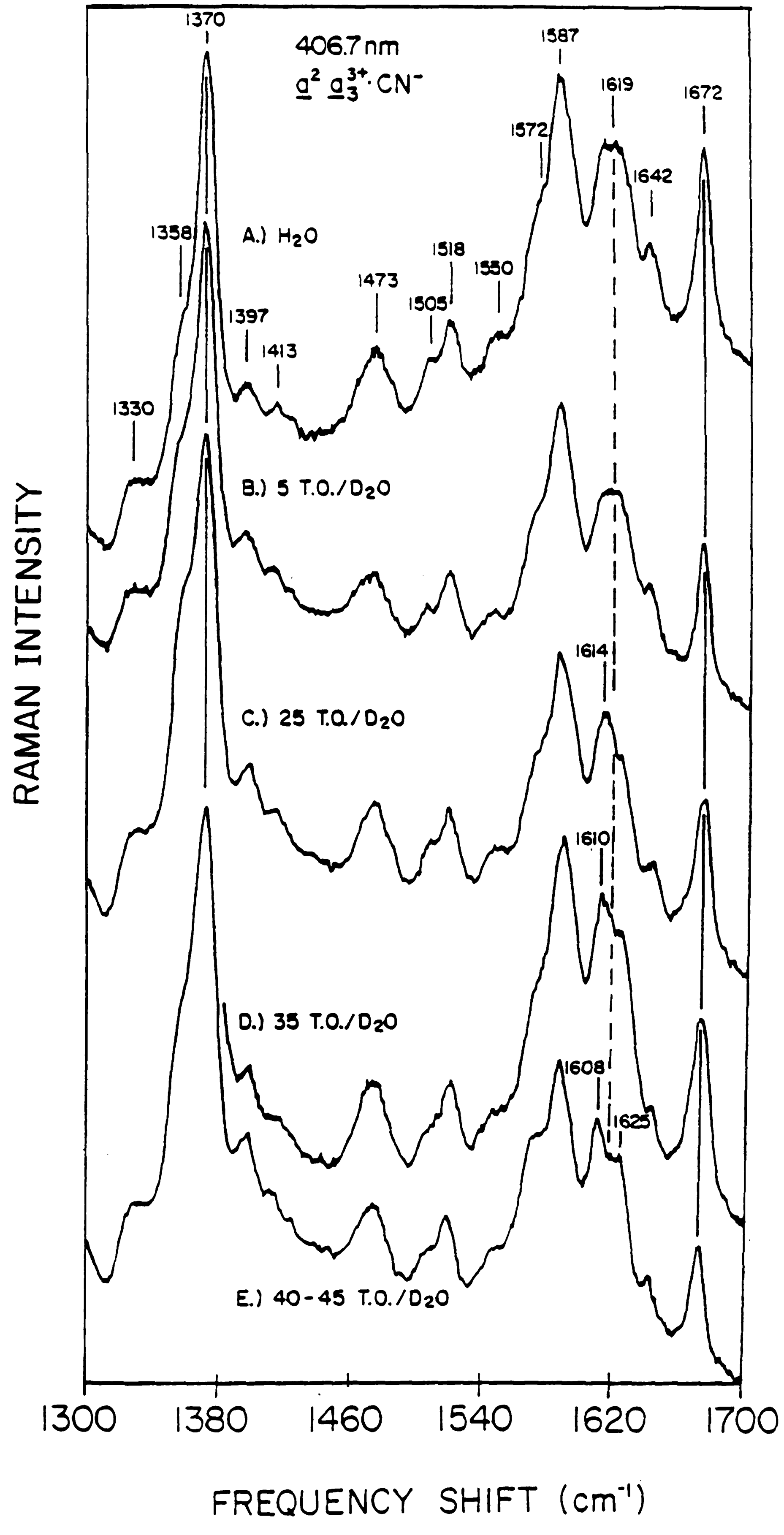
406.7 nm
$\underline{a}^2\,\underline{a}_3^{3+}\cdot CN^-$
A.) H_2O
B.) 5 T.O./D_2O
C.) 25 T.O./D_2O
D.) 35 T.O./D_2O
E.) 40-45 T.O./D_2O
1370
1358
1330
1397
1413
1473
1505
1518
1550
1572
1587
1619
1642
1672
1614
1610
1608
1625
RAMAN INTENSITY
1300
1380
1460
1540
1620
1700
FREQUENCY SHIFT (cm⁻¹)

spectra of protonated and fully exchanged oxidase derivatives. The resonance Raman spectrum of the control protein sample in H_2O is shown in trace 6.6A. After the end of the first five catalytic cycles (in D_2O) (trace 6.6B), the carbonyl stretching frequency appears as a "buried" vibration under the broad feature at 1619 cm^{-1}, indicating lack of deuterium incorporation. For the oxidase following 25 (trace 6.6C) and 35 turnovers (trace 6.6D), $\nu_{C=O}$ is seen at 1614 cm^{-1} and 1610 cm^{-1}, respectively. Full development of spectral changes in the cytochrome $\underline{a}^{2+}$ carbonyl frequency were achieved after 35-40 cycles of reduction and reoxidation, as monitored by the shift of this band to 1608 cm^{-1}. In addition to the differences observed in the cytochrome a carbonyl stretch, modes at 1228 cm^{-1} and 1248 cm^{-1} appears to shift slowly as it was noticed by the relative intensity of the Raman difference spectrum of reduced and mixed valence oxidase obtained at different times of sample incubation.

Representative RR difference spectra of redox-cycled cytochrome oxidase with 441.6 nm and 406.7 nm excitations in the high-frequency region are shown in Figure 6.7A and 7B, respectively. The RDS spectrum shown in these Figures has been normalized to the intensity of the ν_4 oxidation state marker bands at 1370 cm^{-1} (Figure 6.7B) and 1355 cm^{-1} (Figure 6.7A). We have noticed that the use of different multiplication factors (in the range of 0.98 to 0.65) resulted in a difference spectra with altered relative

Figure 6.7: Resonance Raman spectra and the associated Raman difference spectra of redox-cycled mixed-valence cytochrome oxidase obtained with 441.6 nm (7A) and 406.7 nm (7B) excitation frequencies. Freshly prepared cytochrome oxidase (60 μM) in H_2O and D_2O was reduced with 4.8 mM ascorbate/ 20 μM TMPD in the presence of excess substrate, and allowed to redox-equilibrate for 45 minutes, then 10 mM CN^- was added to form the mixed-valence ($\underline{a}^{2+}\underline{a}_3{}^{3+}$-$CN^-$) derivative. The spectra are the sum of 10 scans. Other experimental conditions as describe in Figure 6.2.

Figure 6.7A:

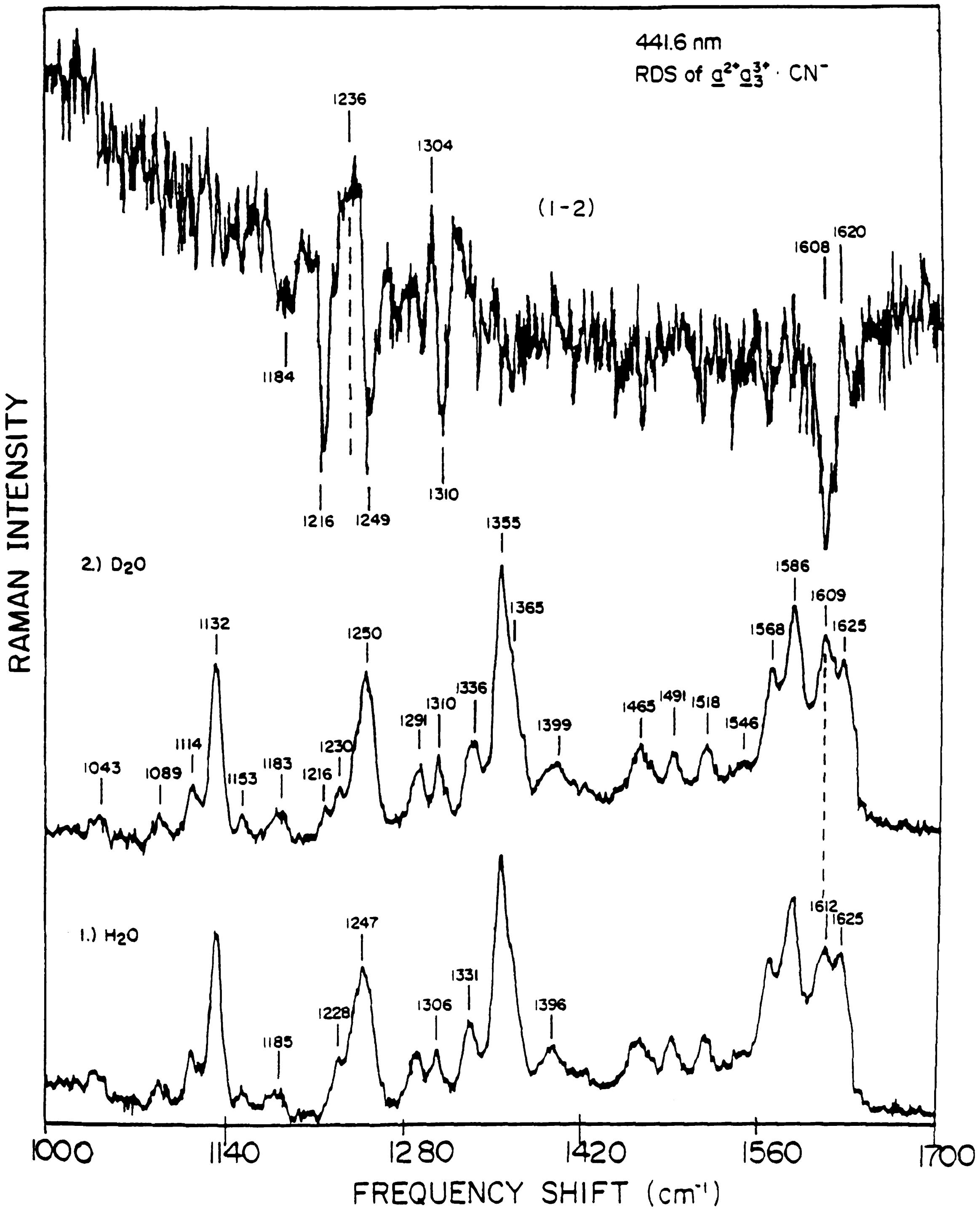
441.6 nm
RDS of a2+a33+ · CN−
(1-2)
1236
1304
1184
1216
1249
1310
1608
1620
2.) D2O
1043
1089
1114
1132
1153
1183
1216
1230
1250
1291
1310
1336
1355
1365
1399
1465
1491
1518
1546
1568
1586
1609
1625
1.) H2O
1185
1228
1247
1306
1331
1396
1612
1625
RAMAN INTENSITY
1000
1140
1280
1420
1560
1700
FREQUENCY SHIFT (cm−1)

Figure 6.7B:

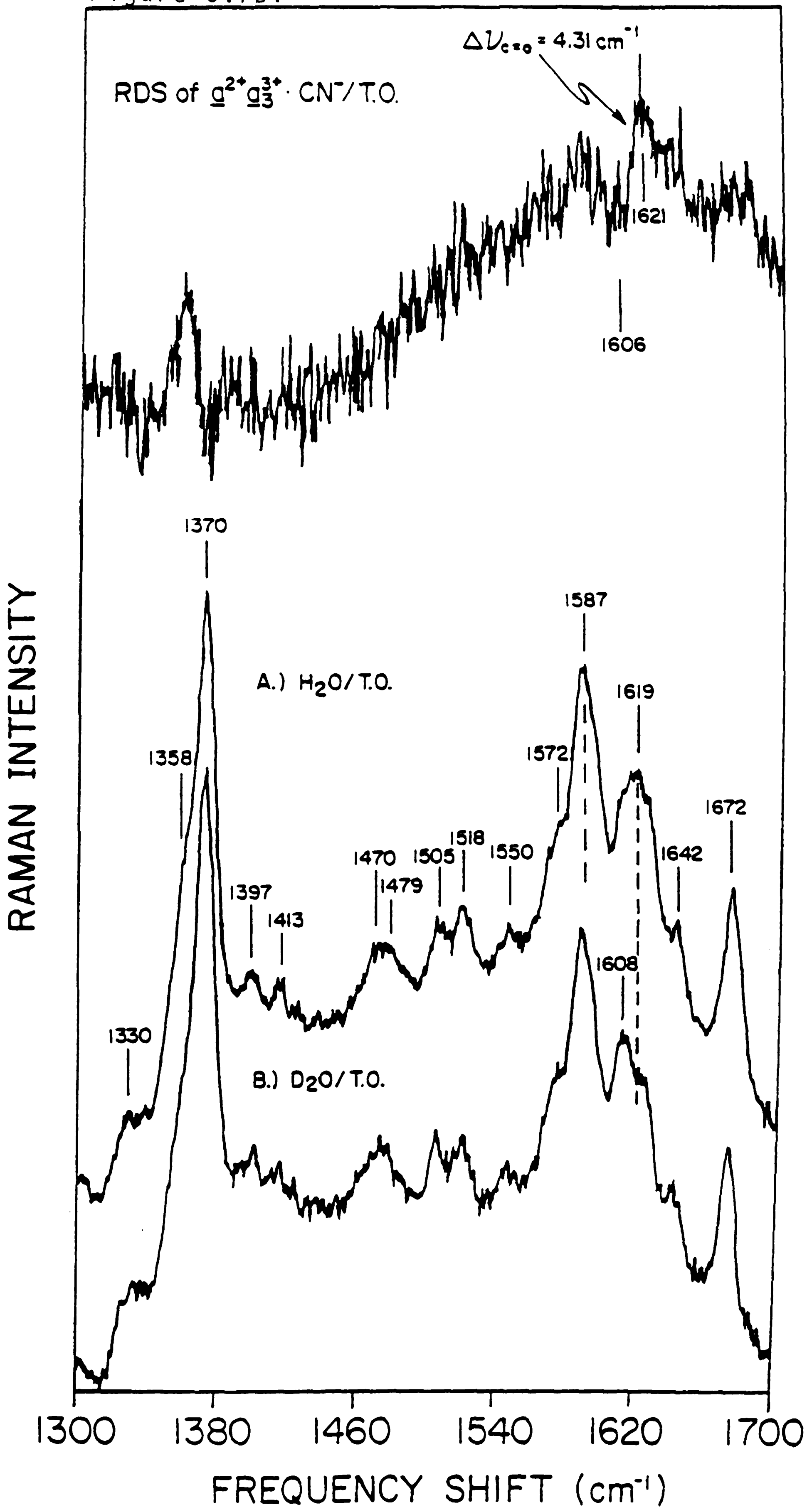
$\Delta\nu_{C=O}$ = 4.31 cm^{-1}
RDS of $\underline{a}^{2+}\underline{a}_3^{3+}$ · CN$^-$/T.O.
1621
1606
1370
1587
A.) H_2O/T.O.
1619
1358
1572
1672
1518
1470
1505
1550
1642
1397
1479
1413
1608
1330
B.) D_2O/T.O.
RAMAN INTENSITY
1300
1380
1460
1540
1620
1700
FREQUENCY SHIFT (cm^{-1})

intensities but frequency positions that were not affected. The most prominent changes are detected in the broad feature at 1619 cm^{-1} with 406.7 nm, and at 1612 cm^{-1} with 441.6 nm, both shifting down to 1608 cm^{-1} upon H/D-protein exchange. With 441.6 nm excitation, the intensity of the 1608 cm^{-1} increases considerably in intensity, an observation previously noted by Argade et al. (1986). The RDS at this wavelength demonstrate a strong negative peak at 1608 cm^{-1} and a positive peak at 1621 cm^{-1}, from where we calculated a shift of -3.31 cm^{-1} corresponding to the 1612 cm^{-1} line. With 406.7 nm excitation, the calculated frequency shift from the RDS, is -4.30 cm^{-1}, which represents an increase of 0.45 cm^{-1} as compared to the resting oxidase. Therefore, the H-bond interaction appears to be stronger in the reduced protein in the presence of deuterated buffers.

The low-frequency resonance Raman spectra of reduced and redox-activated protein (with ascorbate as the reductant) are shown in Figures 6.8A and 8B. Of particular interest are bands at 439 cm^{-1}, 661 cm^{-1}, and 981 cm^{-1} on the RR spectrum of the protonated protein. These modes are shifted to 432 cm^{-1}, 656 cm^{-1}, and 975 cm^{-1}, respectively. The downshifted frequency of the 439 cm^{-1} line was previously observed by Argade et al. (1986) and recently in the RR of intact mitochondria in deuterated buffers (Centeno and Babcock, unpublished observations).

In Figure 6.8B, the mid-range (600-1000 cm^{-1}) spectra have been expanded with an improved signal-to-noise ratio

Figure 6.8: Low frequency resonance Raman spectra of reduced (8B-1)and redox-cycled (8A and 8B-2) cytochrome oxidase in protonated and deuterated buffers. The respective Raman difference spectra are also indicated. Sample conditions as described in Figure 6.7. Laser excitation wavelength at 441.6 nm; resolution 5 cm^{-1}. Figure 8B-1 and 8B-2 show the mid-range (600-1000 cm^{-1}) resonance Raman spectra of reduced and redox-cycled cytochrome oxidase, respectively.

Figure 6.8A:

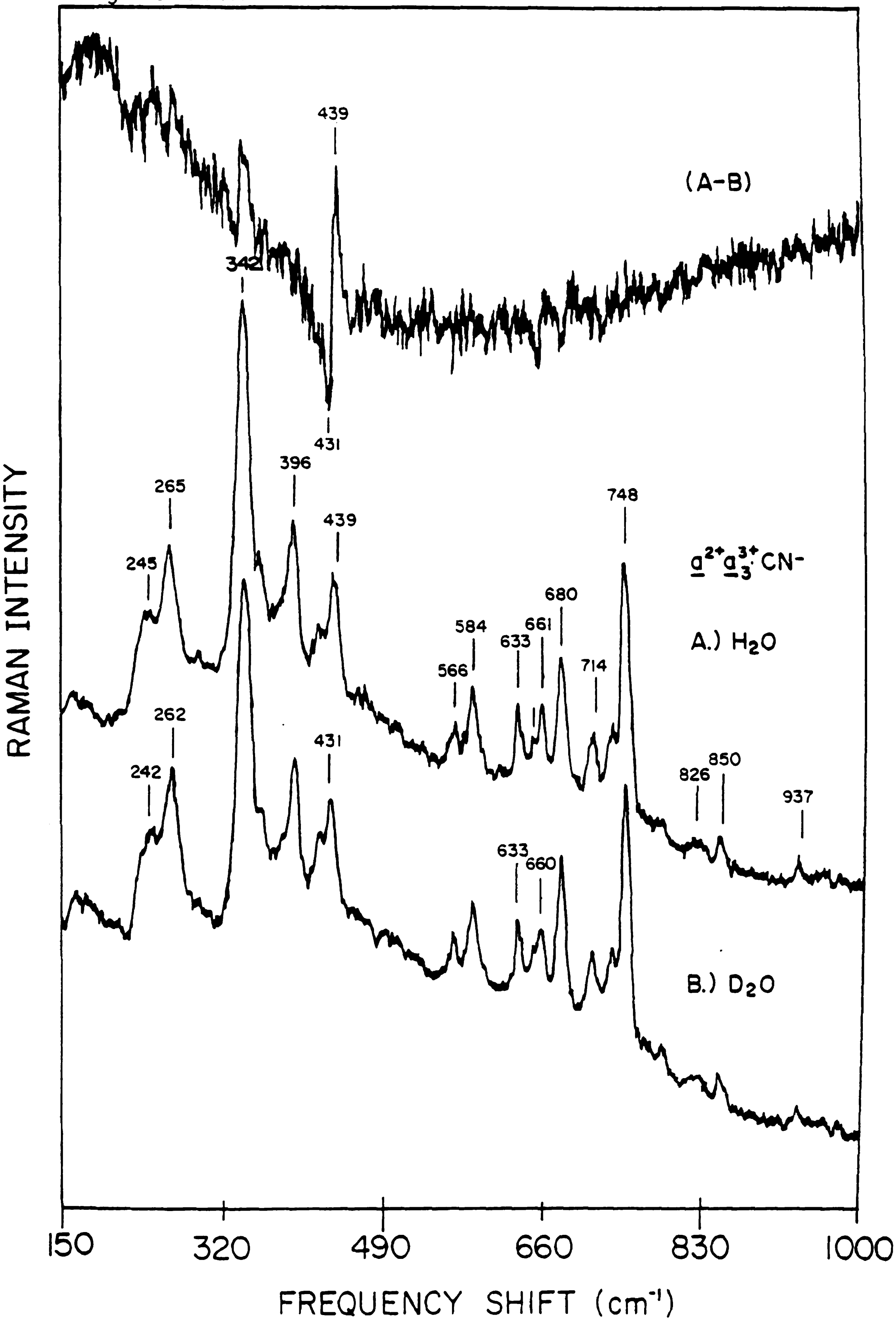
(A-B)
439
342
431
265
245
396
439
748
$a^{2+}a_3^{3+}$·CN-
680
A.) H2O
584
661
633
566
714
262
242
431
826
850
937
633
660
B.) D2O
RAMAN INTENSITY
150
320
490
660
830
1000
FREQUENCY SHIFT (cm-1)

Figure 6.8B:

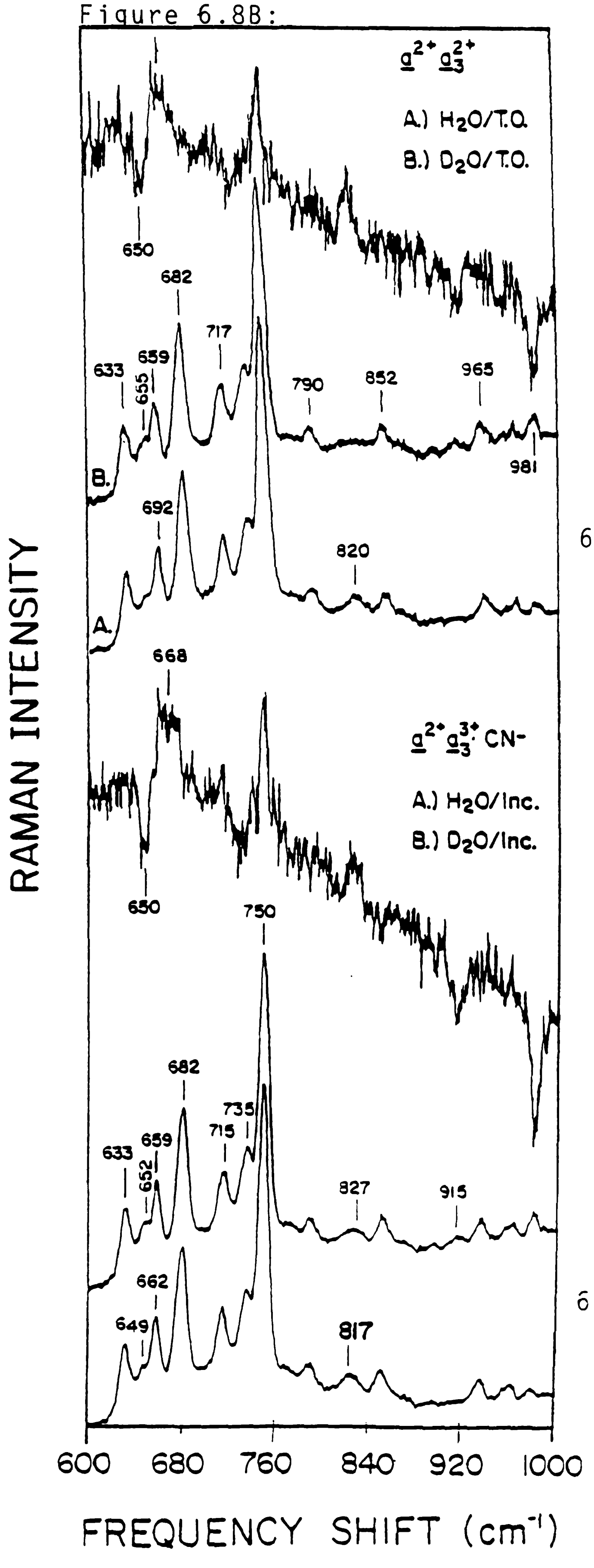

6.8B-1

6.8B-2

(16 scans total). The spectra shown in this Figure illustrate the downshifted frequency detected in the 661 cm^{-1} to 656 cm^{-1}.

C. EPR and ENDOR Studies of Resting and Redox-Cycled Oxidase

EPR and ENDOR spectroscopy are two magnetic resonance techniques widely applied to study paramagnetic centers in biological systems containing transition metal ions or organic radicals. While EPR spectroscopy measures the energy needed to change the spin orientation of the unpaired electron relative to the direction of the applied magnetic field, ENDOR spectroscopy uses radio frequency (rf) excitation to monitor the intensity of the EPR signal. Therefore, the ENDOR technique combines the capabilities of a nuclear magnetic resonance (NMR) experiment with the greater sensitivity of EPR. Owing to its inherently higher resolution relative to EPR, ENDOR can provide information about metal-protein interactions. In this work, EPR spectroscopy has been used to monitor enzyme quality and integrity. ENDOR spectroscopy was used to study the ligand coordination around the Cu$_A^{2+}$ center of cytochrome oxidase by investigating the accessibility of protein exchangeable sites at the vicinity of this metal center. Our work has been conducted with the aim of testing the redox-linked proton pumping model proposed by Chan and coworkers (1979 &

1986), who have suggested the Cu_A^{2+} ligand-coordination site.

D. EPR Spectra of Resting and Redox-Activated Oxidase

The EPR spectra of fully oxidized and redox-activated oxidase in protonated and deuterated buffers, respectively, are shown in Figure 6.9. EPR signals with g-values at $g_z=3.03$, $g_y=2.21$, and $g_x=1.45$ are attributed to the low-spin cytochrome $\underline{a}^{3+}$ (S=1/2) component (Hartzell and Beinert, 1976; Aasa et al., 1976). The EPR signal from Cu_A^{2+} (S=1/2) metal center is seen as an intense signal with g=2.02 and g =2.17. The EPR spectrum of resting oxidase and redox-cycled protein in protonated and deuterated buffers are essentially identical.

The ENDOR spectra of resting and redox-cycled protein in protonated and deuterated buffers obtained in the region of the cytochrome a EPR signal (g=3.0) are shown in Figure 6.10. The spectra are centered at the free proton Larmour frequency of 9.57, 9.58, and 9.69 MHz, respectively. The proton hyperfine couplings of these heme a proton ENDOR lines are 1.16, 0.92, 0.76, 0.72, and 0.16 MHz from 1 to 4, respectively. The proton ENDOR lines in Figure 6.10 are narrow in width, especially the two larger couplings, suggesting well-defined proton sites around the cytochrome a Fe nuclei.

To study the ENDOR spectra of Cu_A^{2+}, two regions of the EPR spectrum corresponding to g (g =2.03) and g (g =2.17) were selected. Setting the magnetic field at different

Figure 6.9: Electron paramagnetic resonance (EPR) spectra of cytochrome oxidase. Oxidase samples are: A) native in H_2O; B) redox-cycled in D_2O. Experimental conditions: temperature 4.2 K, frequency 9.46686 GHz; modulation field 3600 Gauss (centerfield).

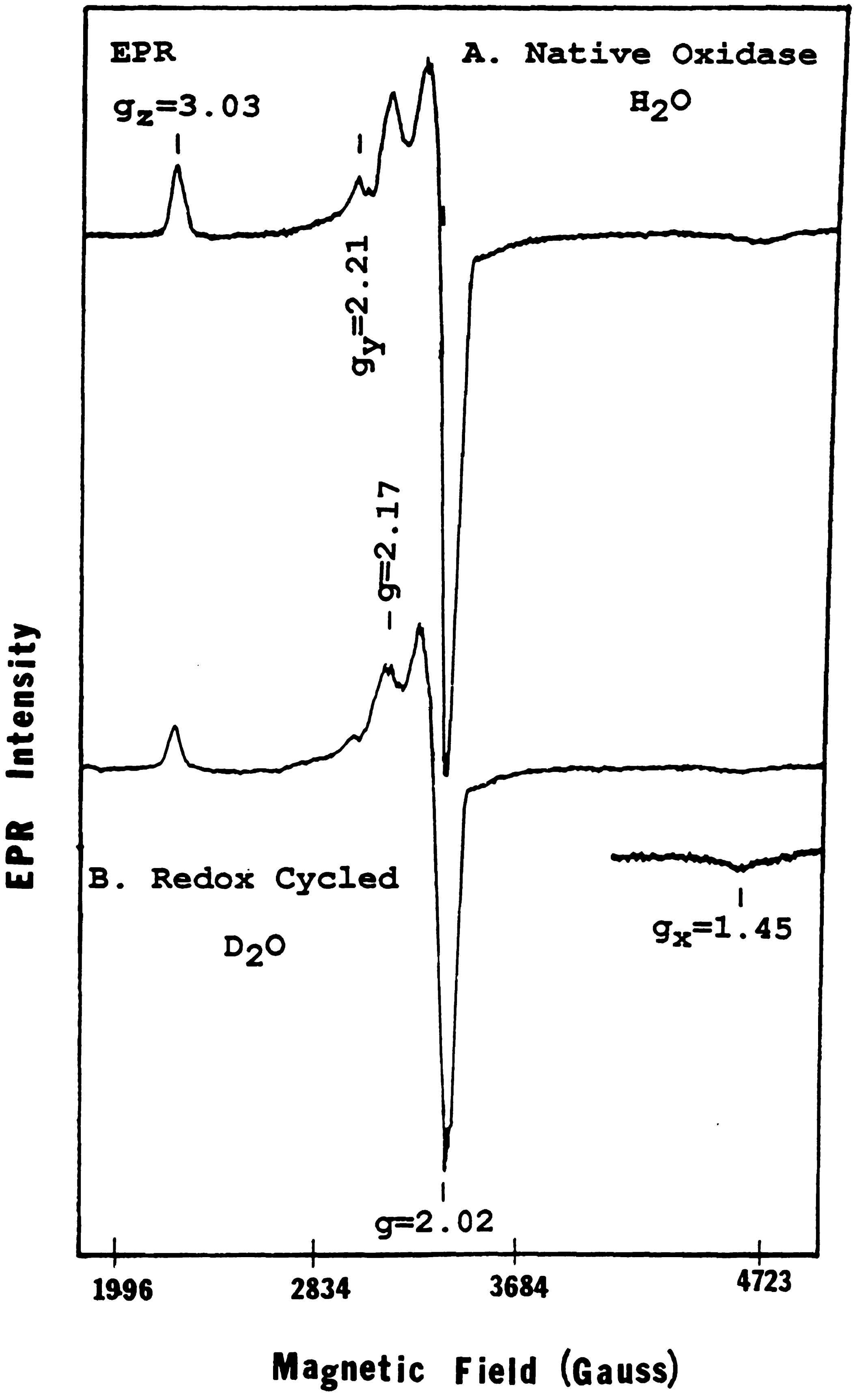
EPR
A. Native Oxidase
H₂O
g_z=3.03
g_y=2.21
g=2.17
B. Redox Cycled
D₂O
g_x=1.45
g=2.02
EPR Intensity
1996
2834
3684
4723
Magnetic Field (Gauss)

Figure 6.10: ENDOR spectra of cytochrome $\underline{a}^{3+}$ at the electronic g value of g = 3.03. ENDOR conditions are: temperature 4.2 K, frequency 7-12 MHz, field modulation 2248, 2251, and 2275 G, respectively. The spectra are centered at teh free proton frequency ν_H = 9.58 MHz. The oxidase samples are: A) resting oxidase in H_2O; B) resting oxidase in D_2O; C) and redox-cycled oxidase in D_2O.

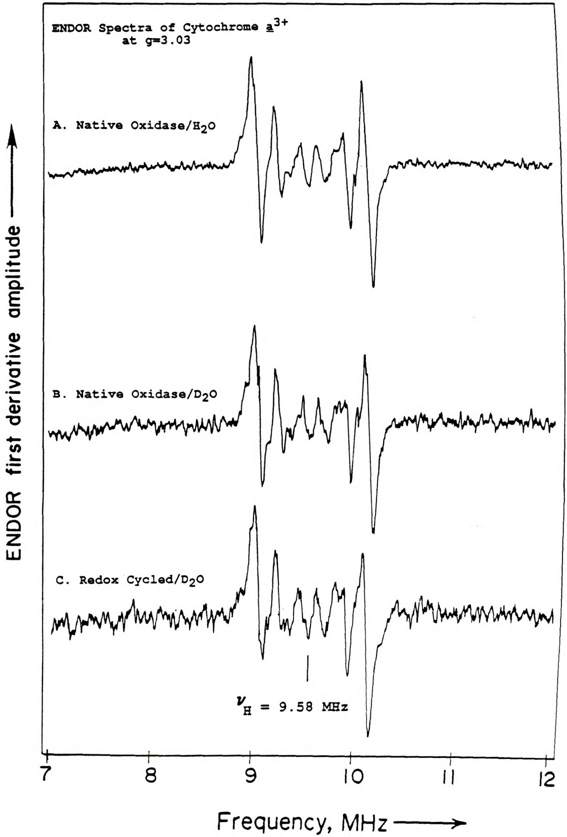
ENDOR Spectra of Cytochrome a^{3+} at g=3.03
A. Native Oxidase/H_2O
B. Native Oxidase/D_2O
C. Redox Cycled/D_2O
ν_H = 9.58 MHz
ENDOR first derivative amplitude
7
8
9
10
11
12
Frequency, MHz

g-values allows for selection in the orientation (Eachus and Ohms, 1985; O'Malley and Babcock, 1986). The ENDOR spectra of resting and redox-cycled oxidase in protonated and deuterated buffers in the $g_{\perp}$=2.02 region of the Cu_A EPR signal shows 4 pairs of peaks (lines a through d in Figure 6.11) centered at the free proton frequency (ν_H of 14.15 MHz), with proton hyperfine couplings of 1.70, 1.30, 0.80, and 0.40. Upon use of deuterated buffers, the lineshape, relative intensities, and peak positions remain unaltered. These lines are relatively narrow, again suggesting that the protons giving rise to these ENDOR transitions are from protons in well-defined sites relative to Cu_A^{2+} and unable to undergo H/D exchange.

The corresponding ENDOR spectra recorded at g =2.1717 of the Cu_A EPR signal are shown in Figure 6.12. Seven pairs of lines are clearly observed with hyperfine couplings of 3.24, 2.54, 1.84, 1.44, 1.14, 0.70, and 0.54 from a to g, respectively. In contrast to the similarities noted for the spectra depicted in Figure 6.11, a similar interpretation of the observed g lines appear to be complicated by changes in relative intensities. Thus peaks with the smallest coupling are observed to decrease in relative intensity (i.e., line g); lines d and e have become narrower, while line g broadens. This observation might be an indication of underlying lines arising from other proton sites. The large couplings, those of lines a and b in Figure 6.12, appears

Figure 6.11: Matrix ENDOR spectra of Cu_A^{2+} in cytochrome oxidase at the electronic g value of g =2.02 (perpendicular region). ENDOR experimental conditions are: temperature 2.2 K, frequency 9.4395 GHz, amplitude 10.7-15.7 MHz, magnetic field 3104.1 G. The oxidase samples are: A) resting oxidase in H_2O ; B) resting oxidase in D_2O; C) and redox-cycled oxidase in D_2O.

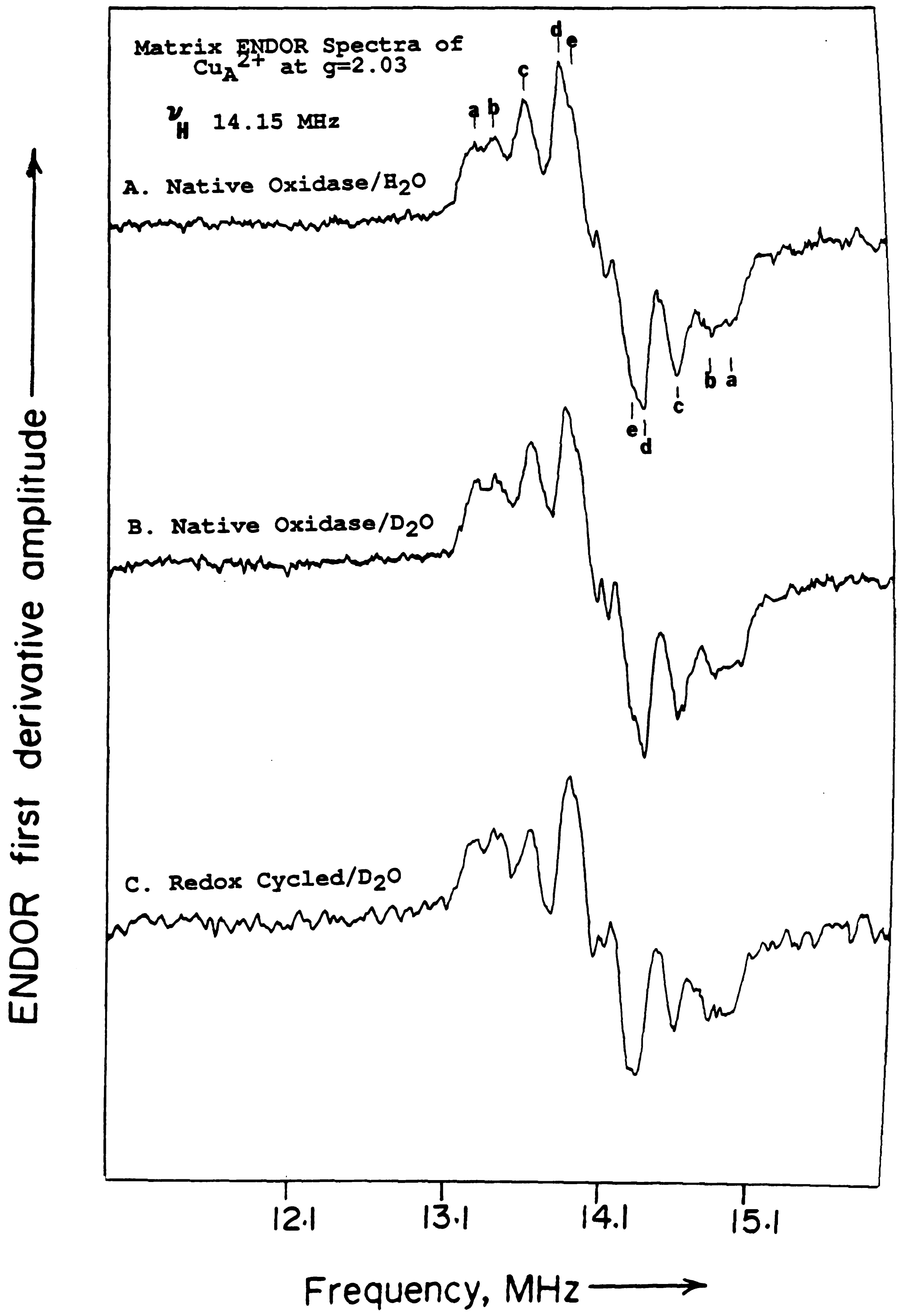
Matrix ENDOR Spectra of
Cu_A^{2+} at g=2.03
ν_H 14.15 MHz
a
b
c
d
e
A. Native Oxidase/H_2O
e
d
c
b
a
B. Native Oxidase/D_2O
C. Redox Cycled/D_2O
ENDOR first derivative amplitude
12.1
13.1
14.1
15.1
Frequency, MHz

Figure 6.12: Matrix ENDOR spectra of Cu_A^{2+} in cytochrome oxidase at the electronic g value of g = 2.1717 (parallel region). Same oxidase samples and experimental conditions as in Figure 6.11.

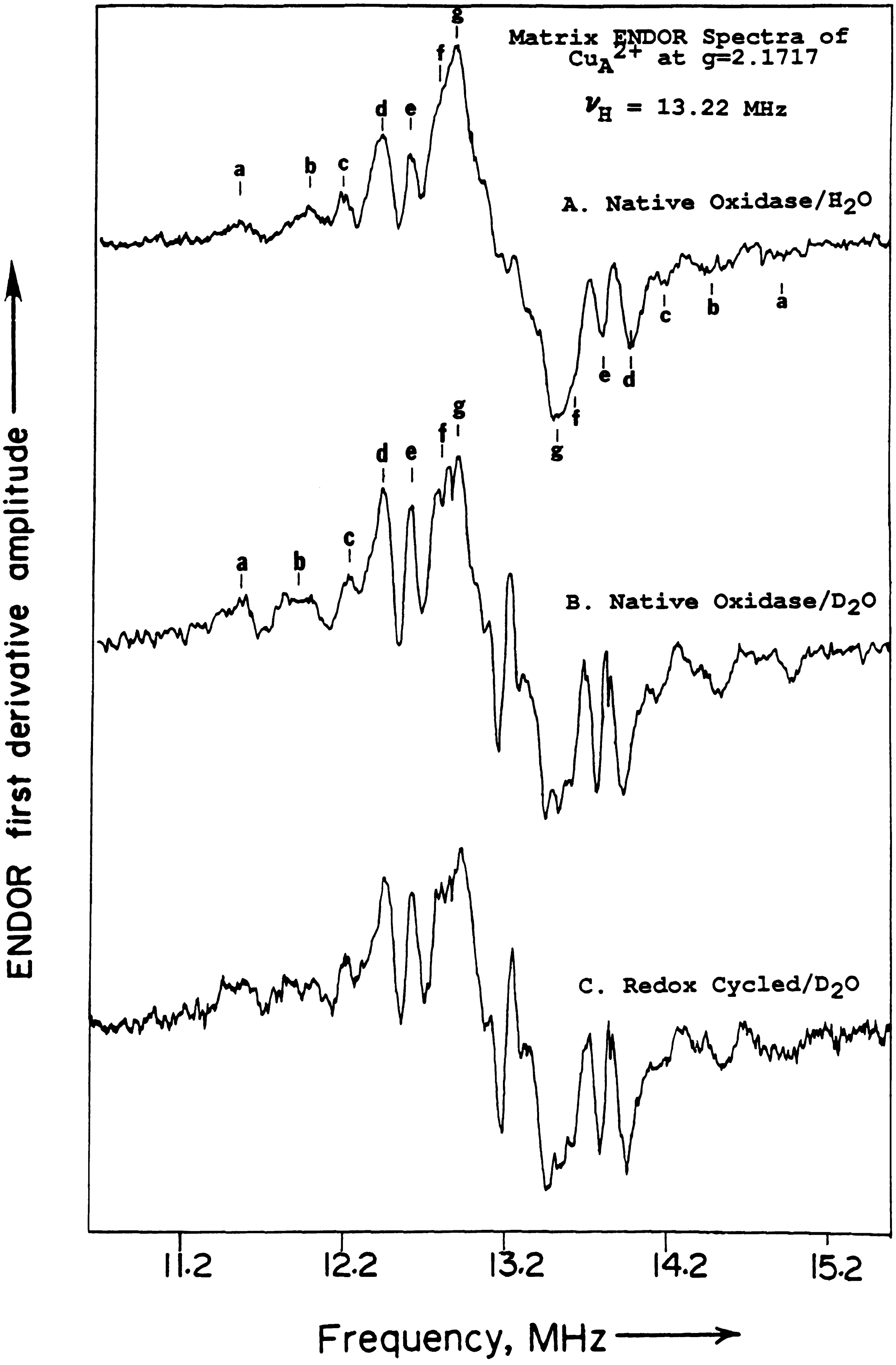
Matrix ENDOR Spectra of Cu_A^{2+} at g=2.1717
ν_H = 13.22 MHz
A. Native Oxidase/H_2O
B. Native Oxidase/D_2O
C. Redox Cycled/D_2O
a
b
c
d
e
f
g
ENDOR first derivative amplitude
11.2
12.2
13.2
14.2
15.2
Frequency, MHz

very broad in all the spectra shown in this Figure, suggesting loosely define proton sites nearby the Cu_A atom. However, upon H/D-exchange, these two lines occur at the same positions and does not display any significant decrease in relative intensity.

III. Discussion:

A. Enhancement of Cytochrome a Formyl H-Bonding Sensitive Modes:Slow H/D Exchange Process.

Our results in the resonance Raman difference spectra of resting (fully oxidized) cytochrome oxidase agree with those of Copeland and Spiro (1986), and support the proposed H-bond structure of cytochrome a in cytochrome oxidase (Callahan and Babcock, 1983). The deuterium shift obtained in the cytochrome a carbonyl frequency bands at 1650 cm^{-1} ($\Delta\nu_{C=O}$ =-3.85 cm^{-1}) and at the 1619 cm^{-1} RR envelope ($\Delta\nu_{C=O}$ =-4.31 cm^{-1}), suggest that the cytochrome a formyl-protein H-bond is fairly strong. This contrasts with recent H-bonding studies on heme a model compounds in which a lack of an isotope effect ($\Delta < 1$ cm^{-1}) on the isolated $\nu_{C=O}$ stretching frequency was reported (Centeno and Babcock, in preparation; see Chapter III). The occurrence of protein exchangeable sites, as studied by the deuterium isotope effect, have been also documented in other structurally related H-bonded heme proteins, such as carbonyl-horseradish c peroxidase (Smith et. al., 1983) oxymyoglobin and oxy-cobalthemoglobin (Kitagawa et al., 1982). In the latter case, a -2.5 cm^{-1} in the $\nu_{C=O}$ stretching frequency upon protein deuteration was detected, while in the latter case a 2-5 cm^{-1} upshift in the Co-O_2 stretching frequency was obtained by RDS techniques.

The sensitivity of the cytochrome a carbonyl group stretching frequency to redox changes at the heme a iron in the presence deuterated buffers was recently studied (Copeland and Spiro 1986; Argade et al., 1986). Both groups interpreted their results as evidence against the involvement of the cytochrome a formyl hydrogen bonding structure in the oxidase proton pumping activity, since no frequency shift in the $\nu_{C=O}$ line of ferrous cytochrome a was detected, after presumably turning the enzyme over in the presence of deuterated solvents with solid $Na_2S_2O_4$ as the electron donor. However, the above results should be interpreted with caution since it is known that the presence of $S_2O_4^{=}$ in solution will quickly react with all the oxygen available (Lambeth and Palmer, 1973). Hence, the oxidizing for cytochrome oxidase, O_2, will be depleted and turnover of the enzyme in the presence of dithionite will be sharply curtailed. In the work presented here, we have followed changes in the cytochrome a C=O stretching frequency for oxidase samples which have been reduced with TMPD and ascorbate (a known poor oxygen scavenger) as the electron sources. Our results indicate a significant decrease in the cytochrome a^{2+} C=O stretching when the ascorbate/TMPD couple was used as the reductant. A simple interpretation of these results indicates a need for substrate molecules during the reduction of cytochrome a and cytochrome a_3 to trigger conformational changes at the cyt a (-CHO...H-protein) site.

Important insights in the structure and solvent accessibility of the cytochrome a heme site have emerged from these experiments. A comparison of the oxidase/D_2O spectra allows us to distinguish between fast H/D-exchange sensitive modes detected at 1186 cm^{-1}, 1306 cm^{-1}, 1330 cm^{-1}, and 1625 cm^{-1}; and slow (hydrogen bond related) H/D exchange modes at 1619 cm^{-1}, 1608 cm^{-1}, 1398 cm^{-1},~1228 cm^{-1}, 1246 cm^{-1}, and 661 cm^{-1}. The data in Tables 6.1 and 6.2, on the classification of slow- and fast- exchange modes, indicate that the frequency position at which the latter modes occur are consistent with a substantial contribution to their normal mode of motion from the peripheral vinyl groups at position 4 (see Chapter IV), while the former set of frequencies appears to be associated with the cytochrome a formyl H-bonding modes (Callahan and Babcock, 1983; Choi et al., 1983; Babcock and Callahan, 1983; Centeno et al., in preparation). The occurrence of "relatively" faster and slower hydrogen-exchange classes in structural proteins has been well documented by Englander and coworkers (1972 and 1984) and recently by Segawa and Kume (1986) in their studies with myoglobin and lysozyme proteins, respectively. These studies indicated that, for structurally related H-bonded amides, H-exchange occurrs relatively slowly, while side-chain hydrogens exchanged rapidly. H-bonding in these

TABLE 6.1: Tentative Raman Frequency Assignments for Cytochrome a Formyl Modes in Cytochrome c Oxidase

ASSIGNMENTS:	OXIDASE DERIVATIVES					
	Resting		Mixed-Valence		Reduced	
	H_2O	D_2O	H_2O	D_2O	H_2O	D_2O
νC=O	1650	1646.2	(~1619)[a]	1608	(~1619)[a]	1608
			(1612)[b]	1608	(1612)[b]	1608
ν_2 νCb-Cb	--	--	1586	1583	1586	1583
δH-CO	1398	1399.2	1395	1398	1396	1398
ν_{13} C_α-Cb	--	--	1247	1249	1247	1250
	--	--	1228	1231.3	1229	1232
νCb-CHO	?	?	1236[c]	1249[c]	1236[c]	1249
	--	--	1131	1132	1131	1132
δC=O	652	647	660[d]	656	660	655
ν_8 δCb-S	--	--	342	341	342	341
$_9$ Cb-S	--	--	265	262	270	267

a) The carbonyl stretching frequency is expected at ~1612 cm^{-1} (Callahan and Babcock, 1983); however, it is "buried" within the strong envelope centered at ~1619 cm^{-1}; upon deuteration the $\nu_{c=o}$ is downshifted and detected at 1608 cm^{-1}.

b) Frequency observed with 441.6 nm excitation. Upon deuteration, this line increases in intensity and shifts down to 1609 cm-1 (1608 cm-1 as detected by the RDS) in the presence of ascorbate as reductant.

c) Frequencies observed in the Raman difference spectra. The group assignment is consistent with results from heme a model compounds.

d) A 5 cm^{-1} frequency shift in the δ(C=O) in-plane wag motion was calculated from the RDS.

TABLE 6.2: Summary of Raman Frequency Assignments for Cytochrome a Vinyl Modes in Cytochrome c Oxidase

ASSIGNMENTS:	OXIDASE DERIVATIVES:(a)					
	Resting		Mixed-Valence		Reduced	
	H_2O	D_2O	H_2O	D_2O	H_2O	D_2O
ν C=C	?	?	1625	1625	1625	1625
δ(=CH2)	1330	1335	1331	1336	1331	1336
δ(CH=)	1306?	1310?	1305	1310	1305	1310
$\nu Cb-C_{\alpha}-C_{\beta}$	1174	1184	1173	1183	1173	1183
$\nu_{30}\,\nu$(Cb-S)	1157	1167				
(δCH=) or ν_{45} Eu	982(w)	979(w)	981	978	981	978
			820[b]		820	
				914[c]		915
Pyr. fold.	--	--	438	430	439	431

a) All the vinyl modes listed in this Table were observed to exchange quickly.

b) This line is seen to decrease in intensity in the spectrum of the deuterated protein.

c) The enhancement of the 914 cm-1 resonance Raman mode is observed only in the spectrum of the deuterated protein.

structural proteins was found to be the major factor in modifying these hydrogen exchange rates. Interestingly, the observation of slow- and relatively fast- exchangeable protein-hydrogens on intact membraneous cytochrome oxidase was previously reported by Capaldi (1973) in an IR study of intact mitochondria. While 41% of the peptide hydrogens were quickly exchanged, 40% were found to be slowly exchanged, taking up to 72 hours for the exchange to level off (Capaldi, 1973). Capaldi accounted for his observations suggesting that protons involved in the slow-exchange process were those stabilized by H-bonds.

In addition to the frequency differences detected in the 1619 cm^{-1} envelope and 1612 cm^{-1} lines in Figures 6.6 and 6.7, other spectral differences in the RDS of the redox-cycled protein are also noted in the mid-frequency region for modes at 1184 cm^{-1}, ~1228-1236 cm^{-1}, 1246 cm^{-1}, 1306 cm^{-1}, and 1330 cm^{-1}. The difference pattern observed in the RDS of Figure 6.7A with negative peaks at 1216 cm^{-1} and 1249 cm^{-1} and a positive peak at 1236 cm^{-1}, was previously reported by Argade et al. (1986) where negative peaks at 1223 cm^{-1} and 1249 cm^{-1} and a positive at 1236 cm^{-1} were observed. To explain the apparent splitting in the 1236 cm^{-1} line to 1223 cm^{-1} and 1249 cm^{-1}, Rousseau and coworkers (1986) invoked a Fermi resonance mechanism which was suggested to occur due to a downshift of a weak mode located above the 1236 cm^{-1} line upon protein deuteration. As is shown on Figure 6.7A, we have detected frequency upshifts for Raman modes at 1228 cm^{-1} and 1246 cm^{-1} to 1230 cm^{-1} and 1250 cm^{-1}, respectively. We also observed the emerging of a new vibration at 1216 cm^{-1} which we assign here as due to a D_2O vibration. To disentangle the origin of these frequency perturbations and the direction of shifting in the spectrum of cytochrome *a*$^{2+}$, we have conducted the following experiments: 1) hydrogen bonding experiments with benzaldehyde compounds bearing (-CHO) and (-CDO) groups; 2) hydrogen bonding studies on heme *a* $(N\text{-}MeIm)_2$ model compounds, as well as formyl-isotopic substitution on model compounds (Centeno et al., in preparation); 3) selective pH-modification studies on resting, reduced, and mixed-valence protein (Callahan et al., 1987). Isotopic studies on benzaldehyde compounds have assigned the ring-formyl stretching frequency ($\nu_{Cb\text{-}CHO}$) at 1206 cm^{-1} and at 1215 cm^{-1} for ϕ-CHO and ϕ-CDO, respectively. This mode is observed to *upshift* to 1212 cm^{-1} and 1223 cm^{-1}, respectively, upon use of H-donors to the benzaldehyde C=O group. Our investigation on the spectroscopy of formyl-isotopically substituted heme *a* $(N\text{-}MeIm)_2$ and Cu^{2+} porphyrin *a*, suggested substantial contribution from a formyl-related mode, presumably $\nu_{Cb\text{-}CHO}$, to a Raman peak centered at 1238 cm^{-1} shifting up to ~1248 cm^{-1} upon H-bonding formation. We find no evidence of new vibrations at 1218-1223 cm^{-1} or Fermi resonance mode coupling in these hydrogen bonded heme *a* model compounds in the Raman region from 1200-1300 cm^{-1}. In addition to the work with the model compounds, we have recently observed that upon disruption of

the cytochrome *a* H-bonding interaction, the 1246 cm^{-1} and 1228 cm^{-1} lines were downshifted to 1243 cm^{-1} and 1226 cm^{-1}, respectively (Callahan et al., 1987). The RDS of the pH modified oxidase (RDS = pH7.4 - pH5.35; Figure 5.2 Chapter V), displays positive peaks at 1249 cm^{-1} and 1226 cm^{-1} and a negative peak at 1236 cm^{-1}, indicating the sensitivity of the 1236 cm^{-1} and 1246 cm^{-1} lines to H-bonding effects at the cytochrome *a* formyl group. Based upon these observations with the heme *a* model compounds and the enzyme data presented here, we suggest that the ν_{Cb-CHO} of cytochrome *a* lies below the strong mode at 1246 cm^{-1}, presumably at ~1236 cm^{-1} which is the frequency observed for the isolated heme *a* models. Upon protein deuteration this stretching motion shifts up under the 1249 cm^{-1} (~+8-10 cm^{-1} upshift as detected with the isolated model compound).

B. Low-Frequency Region:

Protein induced alterations in the low-frequency modes of cytochrome *a*$^{2+}$ were detected for modes at 439 cm^{-1}, 661 cm^{-1}, 820 cm^{-1}, and 981 cm^{-1}. The downshift in the 439 cm^{-1} line to 432 cm^{-1} induced by deuterated solvent was originally reported by Argade et al. (1986), and interpreted as due to internal formyl-proton deuteration in cytochrome *a*$^{2+}$, presumably catalyzed by an unusual protein environment. Downshifted frequency for this 439 cm^{-1} mode has also been observed in the Soret excitation RR spectra of intact mitochondria in deuterated buffers, as well as in isolated oxidase studied with excitation in the visible bands

(Centeno and Babcock, unpublished results). This mode appears to be insensitive to enzymatic cycles of reduction and reoxidation (see Figure 6.8A), and does not seem to require prolonged sample incubation in D_2O. Its Raman intensity was observed to be largely diminished upon pH-modification of reduced and mixed-valence oxidase (Callahan et al., 1987; see also Figure 5.3, Chapter V). Its RR enhancement with visible excitation support its origin as due to a cytochrome a vibrational mode. Interestingly, Raman studies of benzaldehyde and metal substituted heme a model compounds reveal a low-frequency mode at 441 cm^{-1} (see Table 3.1, Chapter III) which decreases markedly in intensity upon H-bond formation to the isolated C=O group in heme a, but shifts towards lower frequencies upon formyl-proton deuteration in benzaldehyde. This mode was assigned in the model compounds as due to a pyrrole folding mode containing a substantial contribution from the peripheral formyl group.

A low-frequency mode at 661 cm^{-1} is observed to shift down to 656 cm^{-1} upon use of deuterated buffers as detected by the RDS (see Figure 6.8B). Raman spectra of benzaldehyde and heme model compounds display a mode at 649 cm^{-1} and 638 cm^{-1}, respectively, assigned to the $\delta_{C=O}$ in plane motion. H-bonding formation in these model compounds shifts the $\delta_{C=O}$ to 641 cm^{-1} and 635 cm^{-1} (Centeno et al., in preparation), respectively. Accordingly, the sensitivity of this mode in the isolated enzyme to H/D exchange supports its formyl character.

C. ENDOR Results:

The ENDOR results reported appears to confirm the occurrence of exchangeable sites nearby the Cu_A^{2+} site, however, our data can not confirm the proposed involvement of this metal center in the redox-linked proton pumping activity of cytochrome oxidase (Chan et al., 1979; Blair et al., 1986). The g ENDOR spectra of resting and redox-cycled oxidase in protonated and deuterated buffers showed identical features. This suggests that these proton ENDOR signals might arise from protons at the nitrogen ligands of Cu_A^{2+} (Stevens et al., 1982). On the other hand, the ENDOR spectra obtained on the g region, show a complicated peak intensity pattern that could result from unresolved proton sites with slightly different hyperfine couplings. If the decrease in relative intensity of the small coupling lines in the g proton ENDOR spectra is due to accessibility of H/D exchange sites near the Cu_A atom, then we will expect that upon repeated cycles of reduction and reoxidation, the site will be fully deprotonated (Blair et al., 1986), and hence its ENDOR signal should either vanish or reappear. Nevertheless, the ENDOR spectra of the resting and turnover enzyme in D_2O are completely identical. Alternatively, it has been pointed out that the presence of D_2O will generally broaden the proton ENDOR lines, presumably due to its influence on proton relaxation time properties (Eachaus and Olms, 1985;

Baker et al., 1986), which in turn will result in intensity differences.

IV. Conclusions:

The original proposal of Callahan and Babcock (1983) of the involvement of the cytochrome a formyl group on a H-bonding interaction with a nearby protein residue was based upon the red-shift on the cytochrome a α-band and the downshifted $\nu_{C=O}$ frequency relative to its low-spin heme a model compounds. It was later recognized by the same workers that the strength of the cytochrome a (-HC=O...H-donor) interaction increases when cytochrome a was in the reduced state (Babcock and Callahan, 1983). These observations triggered the formulation of a redox-linked proton pump model (Babcock and Callahan, 1983) that predicts the occurrence of exchangeable protein protons and the enhanced incorporation of deuterium atoms at the H-bonding site as a function of enzyme catalytic redox-cycles.

In the present study, resonance Raman evidence has been presented supporting the mechanistic role of the cytochrome a formyl group in the oxidase proton pump mechanism. We based our conclusions on the frequency shifts in the cytochrome a carbonyl sensitive modes in resting, mixed-valence and reduced oxidase derivatives, upon H/D exchange, and on the sensitivity of these modes to redox cycles, especially modes at ~1619 cm^{-1}, 1396 cm^{-1}, 1228-1246 cm^{-1}, and 661 cm^{-1} in the protonated enzyme.

The vibrational differences between the cytochrome _a_ formyl and vinyl modes presented here allow us to distinguish the accessibility of fast and slow-protein labile sites near the periphery of the cytochrome _a_ heme chromophore. This observation might be a direct indication of non-structurally related protein exchangeable sites, as well as H-bonded, and hence structurally related, labile sites at the cytochrome _a_ protein vicinity.

Our present ENDOR data on resting and redox-cycled cytochrome oxidase have been interpreted as the occurrence of H/D exchangeable sites in the immediate protein environment around Cu_A^{2+} metal center. However, the likelihood of this Cu_A^{2+}center being the oxidase proton pumping site, remains unproven. It appear that other factors, such as temperature and proton relaxation rates in D_2O (Eachaus and Olms, 1985) might be significantly in influencing the dynamics of proton relaxation times as to obscure possible isotopic effects. Nevertheless, this work provide evidence that tightly bound protons (or matrix protons) are largely unlikely to exchanged with deuterium atoms from the solvent.

CHAPTER VII

Summary and Future Work

I. **Summary:**

The research described in this thesis deals with the application of resonance Raman spectroscopy to study structural and environmental aspects of cytochrome a in cytochrome oxidase. The H-bond structure at the formyl group of cyt a has been established by using heme a model compounds and by monitoring vibrational perturbations in the spectrum of cyt a^{2+} introduced by removal of this interaction and/or *in vivo* deuterium incorporation. The relationship between the cyt a hydrogen bonded structure and the oxidase redox-linked proton pumping activity was investigated by using oxidase samples in which the redox state of the cyt a heme iron and the peripheral formyl group vibrations were simultaneously studied. The implications of the Cu_A^{2+} center in the oxidase proton pumping activity was investigated by using ENDOR spectroscopy.

In an attempt to uncover formyl (-CHO) modes contributing to the resonance Raman spectrum of cyt a, we recorded (Chapter III) the RR spectra of (bis-imidazole) heme a and Cu^{2+} porphyrin a model compounds after formyl isotopic substitution and H-bonding conditions. The results reveal strong similarities between the models and the intact chromophore,in terms of the identification of formyl vibrational modes, but differ in that the H-bond in the isolated chromophore is a weak interaction, while in cyt a the H-bond is observed as a rather strong one.

The visible excitation spectra (605 nm excitation) of reduced cytochrome oxidase reported in Chapter IV produced essentially cyt a^{2+} vibrational modes. The influence of dissolving oxidase in buffered D_2O on cyt a^{2+} formyl-related modes and the enhancement of symmetry-forbidden E_u-type vibrations was interpreted as due to the strongly electron-withdrawing character of the H-bonded C=O group. When these data are compared with previous results from the alkaline pH denaturation studies (Callahan and Babcock, 1983) a good correlation is found between those cyt a modes sensitive to H/D exchange and pH denaturation effects, thus supporting the H-bond structure of cyt a.

Acidic denaturation of reduced and mixed-valence cytochrome oxidase produced structural changes in both chromophores (Chapter V). The action of low pH on the cyt a_3 site transforms this site from a high to a low-spin and exposes its peripheral carbonyl group to the aqueous environment. In cyt a, on the other hand, acidic pH resulted in the removal of its H-bond structure and hence, in the spectral separation of those RR modes that arise from this interaction.

The structural relationship between the cyt a formyl H-bonded structure and the oxidase redox-linked proton pump activity was studied under conditions in which the heme a iron redox-state and formyl vibrational changes were both monitored in the presence of buffered D_2O. The occurrence of relatively "fast" and "slow" H/D-exchange sensitive modes in the RR spectra of cyt a were investigated and explained on the basis of conformational changes at both the formyl and vinyl substituents of cyt a.

Spectroscopic studies of the Cu_A^{2+} site of cytochrome oxidase were described in Chapter VI. ENDOR spectroscopy indicates the accessibility of protein exchangeable sites near the Cu_A ligand coordination sphere; however, the identity and involvement of these protein exchangeable sites near Cu_A^{2+} in the oxidase proton pump remains unproven.

II. **Future Work**

A. Spectroscopy of Cytochrome Oxidase and Heme a Models

The work presented here on the spectroscopy of the heme a$(N\text{-}MeIm)_2$ model compounds has provided evidence for the identification of formyl (-CHO) vibrations that are sensitive to H-bonding effects in the intact cyt a chromophore. In addition, structural differences in heme a formyl and vinyl contributions to the vibrational spectrum were also noticeable (see Chapter III). To understand fully the individual influences of the formyl and vinyl groups on the vibrational properties of heme a, infrared studies in the C-H stretch and low frequency regions should be pursued further. Since IR spectroscopy is able to monitor all molecular bonds in the heme a macrocycle, including conjugated and saturated substituents, a comparative study of the C-H stretch region (about 2800 cm^{-1} to 3000 cm^{-1}) of heme a and protoporphyrin IX should be useful in establishing the conformation of the $-CH=CH_2$ group. Similar studies have already been reported in other metalloporphyrins. For instance, in chlorophylls a and b the intensities and frequency shifts of the C-H vibrational stretches were used to monitor the state of aggregation of these materials (Chapados and Leblanc, 1983; Chapados, 1985).

The extent to which the H-bond structure of cyt a increases the ring molecular asymmetry should be investigated further. Resonance Raman excitation profiles and detailed measurement of dispersion in the depolarization ratio ($\rho = I_{\perp}/I_{\parallel}$) of various Raman lines are suggested as two suitable experimental tools to gain insights in heme-protein interaction effects. Since the resonance Raman intensity depends on the extent of vibronic coupling, an analysis of the excitation profile (i.e., the Raman intensity as a function of the wavelength of the exciting line) of intact cytochrome oxidase and isolated heme a models should provide information on the properties of heme a in the ground and excited electronic states, and hence on the individual influences of the formyl and vinyl groups.

We should continue our efforts toward the understanding of factors that govern the coupling between electron transfer and proton translocation in cytochrome oxidase. In this thesis evidence has been presented that supports the cyt a

H-bonded structure (Chapters IV and V), and its mechanistic implications in the redox-linked proton pump activity were considered (Chapter VI). On the other hand, subunit III has been recently suggested as being an integral part (Pentilla, 1983; Sarti et al., 1985; Prochaska and Reynolds, 1986) or to serve as a regulatory control (Thompson et al., 1985) to the redox-linked proton pump activity. It has been shown that removal of this polypeptide causes a slight decrease in the electron transfer activity of the oxidase complex, but partially or completely abolishes the ability of the oxidase to catalyze redox-linked proton pumping. A resonance Raman study of cytochrome oxidase depleted of subunit III is therefore suggested as an alternative to obtain information on the H^+-pumping activity of cytochrome oxidase. Based upon our results and the proposed role of subunit III (Pentila, 1983; Thompson et al., 1985) it is predicted that in subunit III depleted oxidase, the H-bond interaction in cyt a will be a weaker interaction.

Finally, structural comparisons between cytochrome oxidase from other eukaryotic and procaryotic species can now be used to extend the cyt a^{2+} hydrogen bond assignments made in this work. For instance, our recent comparison of the resonance Raman spectra of isolated maize oxidase and mammalian protein, shown in Figure 7.1, indicates that the heme a environment of maize oxidase is altered, suggesting that this structural perturbation is associated with the

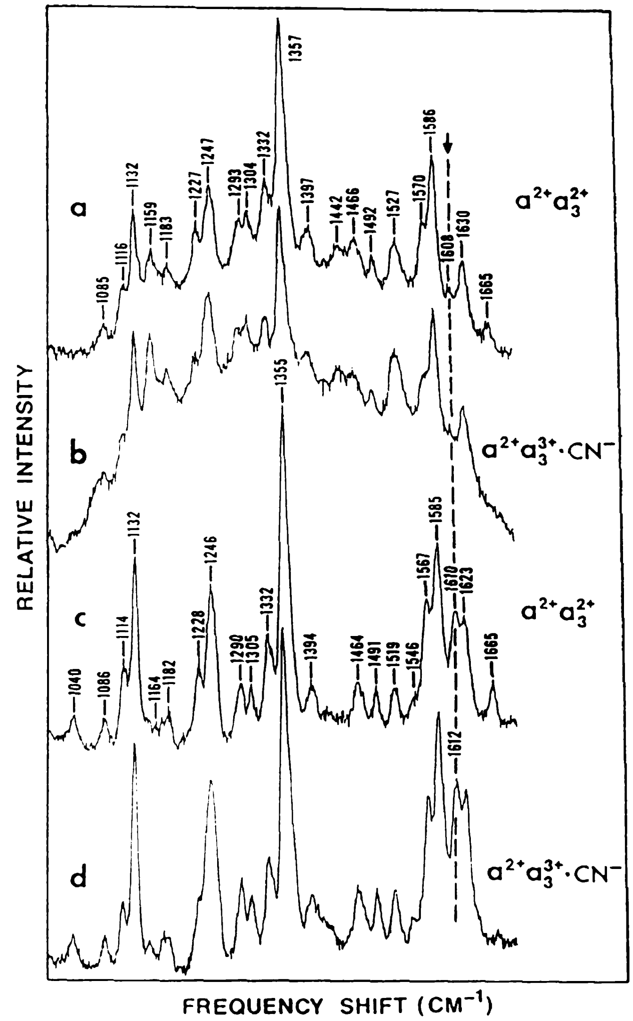

Figure 7.1: Comparison of the resonance Raman spectra of cytochrome oxidase isolated from maize (corn seedlings) and bovine beef heart mitochondria. Traces (a) and (b) correspond to the RR spectrum of reduced and cyanide inhibited maize oxidase, respectively. Traces (c) and (d) correspond to the RR spectrum of reduced and mixed-valence mammalian oxidase. Excitation wavelength is at 441.6 nm. Oxidase concentration: maize 9-14 μM; bovine 30-35 μM.

formyl group of the heme a porphyrin macrocycle (Dutch et al., 1986). This is evident by the absence of resonance enhancement of the C=O stretching frequency at 1612 cm^{-1}. Since the formyl group has been proposed to play a role in the proton pumping activity of cytochrome oxidase (Babcock and Callahan, 1983), further studies on the maize oxidase should be of considerable interest.

B. Hydrogen Bonding

To measure the magnitude of the H-bond interaction in heme a model compounds and in cyt a we have used a modified Badger-Bauer (1937) relation involving the observed wavenumber shift on C=O stretching frequency upon H-bond formation. This approximation normally neglects three important aspects of H-bond interactions: first, it ignores the directionality of the oxygen lone pair electrons; it assumes that the kinematic coupling between the C=O normal coordinate and other donor vibrations is negligible; and finally, it ignores the force constant of the O...H bond, allowing one to treat the H-bond as a diatomic molecule. An assessment of this latter approximation should become available by investigating the resonance Raman spectra of cytochrome a and its heme a model compounds in the region from 80-400 cm^{-1}, where vibrations coresponding to the stretching frequency of the O...H-O bond are expected to appear (Ginn & Wood, 1965; Spinner, 1983).

Insights into the dynamics of kinematic coupling between the C=O and other H-bond stretching vibrations can be studied by using modern calculations such as ab-initio SCF-MO as applied to hydrogen systems (Ditchfield et al., 1971; Chean & Krimm, 1986). For small systems these calculations have proven to be useful in determining the effective force resulting from interaction between the C=O and H-bonded stretching vibrations.

References Cited:

Aasa, R.; Albracht, S.P.J.; Falk, K.E.; Lanne, B.; & Vanngard, T. (1976) Biochim. Biophys. Acta 422, 260-272.

Abe, M.; Kitagawa, T.; & Kyoguku, Y. (1978) J. Chem. Phys. 69, 4526-4534.

Abe, M.; Kitagawa, T.; and Kyuguku, Y. (1978) J. Chem. Phys. 69, 880-890.

Adman, E.T.; Skenkump, R.E.; Sieker, L.E.; & Jensen, L.H. (1978) J. Mol. Biol. 123, 35.

Anderson, L.A.; Loehr, T.M.; Change, C.K.; & Mauk, G.M. (1985) J. Am. Chem. Soc. 107 ,182-191.

Antonini, E.; Brunori, M.; Colosimo, A.; Greenwood, C.; & Wilson, M.T. (1977) Proc. Natl. Acad. Sci. USA 74, 3128-3132.

Argade, P.V.; Ching, Y.C.; Sassaroli, M.; & Rousseau, D.L. (1986) J. Biol. Chem. 261(3), 5969-5973.

Arnett, E.M.; Mitchell, E.J.; & Murty, T.S.S.R. (1974) J. Am. Chem. Soc. 96, 3875-3891.

Azzi, A. (1980) Biochim. Biophys. Acta 594, 231-252.

Babcock, G.T. (1987) in "Biological Applications of Raman Scattering" (Spiro, T.G., ed.) in press.

Babcock, G.T.; Callahan, P.M.; McMahon, J.J.; Ondrias, M.R.; & Salmeen, I. (1982) in Electron Transport and Oxygen Utilization, Elsevier (North Holland Inc.) Chien Ho (ed).

Babcock, G.T.; Callahan, P.M.; Ondrias, M.R.; & Salmeen, I. (1981) Biochemistry 20, 959-966.

Babcock, G.T. & Callahan, P.M. (1983) Biochemistry 22, 2314-2319.

Babcock, G.T.; Jean, J.M.; Johnston, L.M.; Palmer, G.; & Woodruff, W.H. (1984) J. Am. Chem. Soc. 106, 8305-8306.

Babcock, G.T.; Jean, J.M.; Johnston, L.M.; Woodruff, W.F.; & Palmer, G. (1985) J. Inorg. Biochem. 23, 2337-2346.

Babcock, G.T.; & Salmeen, I. (1979) Biochemistry 18, 2493-2498.

Babcock, G.T.; Ondrias, M.R.; Gobeli, D.A.; VanSteelandt, J.; & Leroi, G.E. (1979) FEBS Lett 108 (1), 147-151.

Babcock, G.T.; VanSteelandt, J.; Palmer,G.; Vickery, L.E.; & Salmeen, I. (1979) in *Cytochrome Oxidase* (King, T.E.,et. al., eds.) Elsevier/North-Holland Biomedical Press, pp. 105-115.

Babcock, G.T.; Vickery, L.E.; & Palmer, G. (1976) J. Biol. Chem. 251, 7907-7919.

Babcock, G.T.; Vickery, L.E.; & Palmer, G. (1978) J. Biol. Chem. 253, 2400-2411.

Babcock, G.T.; Widger, W.R.; Cramer, W.A.; Oertling, W.A.; & Metz, J.G. (1985) Biochemistry 24, 3638-3645.

Baker, G.J.; Knowles, P.F.; Pandeya, K.B.; & Rayner, J.B. (1986) Biochem. J. 237, 609-612.

Baker, G.M.; Masato, N.; & Palmer, G. (1987) J. Biol. Chem. 262, 595-604.

Beinert, H.; Griffiths, D.E.; Wharton, D.C.; & Sands, R.H. (1962) J. Biol. Chem. 237, 2337-2346.

Beinert, H.; Hansen, R.E.; & Hartzell, C.R. (1976) Biochim. Biophys. Acta 423, 339.

Beinert, H.; Shaw, R.W.; Hanse, R.E.; & Hartzell, C.R. (1980) Biochim. Biophys. Acta 591, 458.

Bickar, C.; Bonaventura, J.; & Bonaventura, C. (1982) Biochemistry 21, 2661-2666.

Bickar, D.; Lehninger, A.; Brunori, M.; Bonaventura, J.; & Bonaventura, C. (1985) J. Inorg. Biochem. 23, 365-372.

Blair, B.F.; Gelles, J.; & Chan, S.I. (1986) Biophys. J. 50, 713-733.

Bocian, D.F.; Lemley, A.T.; Peterson, N.O.; Brudvig, G.W.; & Chan S.I. (1979) Biochemistry 18, 34396-4402.

Bocian, D.F.; Masthay, M.A.; & Birge, R.R. (1986) Chem. Phys. Letts. 125(5,6), 467-472.

Boelens, R.; Rademaker, H.; Weber, R.; & Van Gelder, D.F. (1984) Biochim. Biophys. Acta 765, 196-209.

Boettcher, J.W. & Drago, R.S. (1974) J. Chem. Phys. 78, 429.

Boobyer, G.J. & Orville-Thomas, W.J. (1966) Spectrochim. Acta 22, 147.

Bovil, A.J.; McConnell, A.A.; Nimmo, J.A.; & Smith, W.E. (1986) J. Phys. Chem. 90, 569-575.

Brudvig, G.W.; Blair, D.F.; & Chan, S.I. (1984) J. Biol. Chem. 259, 11,001-11,009.

Brudvig, G.W.; Stevens, T.H.; Morse, R.H.; & Chan, S.I. (1981) Biochemistry 20, 3912-3921.

Brunori, M.; Bickar, D.; Bonaventura, J.; & Bonaventura, C. (1985) J. Biol. Chem. 260(12), 7165-7167.

Brunori, M.; Colosimo, A.; Wilson, M.T.; & Sarti, P. (1983) FEBS Lett. 152, 75-78.

Brunori, M.; Sarti, P.; Antonini, G.; & Malatesta, F. (1986) Bioelectrochem. and Bioenerg. 16, 159-165.

Brunori, M. & Wilson, T. (1982) Trends Biochem. Sci. 7, 295.

Buse, G.; Meinecke, L.; & Bruch, B. (1985) J. Inorg. Biochem. 23, 149-153.

Callahan, P.M. (1983) Dissertation, Michigan State University, East Lansing, Michigan, 48824.

Callahan, P.M. & Babcock, G.T. (1983) Biochemistry 22, 452-461.

Callahan, P.M. & Babcock, G.T. (1981) Biochemistry 20, 952-958.

Callahan, P.M.; Centeno, J.A.; Ingle, R.; & Babcock, G.T. (1987) Biochemistry (to be submitted).

Capaldi, R.A.; (1982) Biochim. Biophys. Acta 694, 291-306.

Capaldi, R.A. (1973) Biochim. Biophys. Acta 303, 237-241.

Casey, R.A.; Chappell, J.B.; & Azzi, A. (1979) Biochem. J. 182, 149-156.

Centeno, J.A.; Callahan, P.M.; and Babcock, G.T. (1987) in preparation.

Centeno, J.A.; Bender, C.; & Babcock, G.T. (1987) in preparation.

Chan, S.I.; Bocian, D.F.; Brudvig, G.W.; Morse, R.H.; Stevens, T.H. (1979) Cytochrome Oxidase. (King, T.E.; Orii, Y.; Chance, B.; & Okuniki, K. eds.) pp. 177-188 Elsevier, Amsterdam.

Chance, B.; Saronic, C.; & Leigh, J.S., Jr. (1975) Proc. Natl. Acad. Sci. U.S.A. 72, 1635-1640.

Chance, B.; Saronic, C.; & Leigh, J.S., Jr. (1975) J. Biol. Chem. 250, 9226-9237.

Chance, B.; Kumar, C.; Powers, L.; & Chin, Y.C. (1983) Biophys. J. 44, 353-363.

Chancellor, T.; Quill, M.; Bergbreiter, E.; & Newcomb, M. (1978) J. Org. Chem. 43, 1245-1246.

Chapados, C. & Leblanc, R.M. (1983) Biophysical Chem. 17, 211-244.

Chapados, C. (1985) Biophysical Chem. 21, 227-242.

Cheam, T.C. & Krimm, S. (1986) J. Mol. Struct. 146, 175-189.

Ching, Y.C.; Argade, P.V.; & Rousseau, D.L. (1985) Biochemistry 24, 4938-4946.

Choi, S.; Lee, J.J.; Wei, Y.H.; & Spiro, T.G. (1983) J. Amer. Chem. Soc. 105, 3692-3707.

Choi, S. & Spiro, T.G. (1982) J. Am. Chem. Soc. 105, 3683-3692.

Choi, S.; Spiro, T.G.; Langry, K.C.; & Smith, K.M. (1982-a) J. Am. Chem. Soc. 104, 4337-4344.

Choi, S.; Spiro, T.G.; Langry, K.C.; Smith, K.M.; Budd, D.L.; & La Mar, G.N. (1982-b) J. Am. Chem. Soc. 104, 4345-4551.

Choi, S.; Spiro, T.G.; Langry, K.C.; & Smith, K.M.; (1982) J. Am. Chem. Soc. 104, 4337-4344.

Clark, R.J. & Stewart, B. (1979) in "Structure and Bonding" 36.

Cline, J.; Reinhammer, B.; Jensen, P.; Venters, R.; & Hoffman, B.M. (1983) J. Biol. Chem. 258, 5124-5128.

Clore, G.M.; Andreasson, L.E.; Karlsson, B.; Aasa, R.; & Malmstrom, B.G. (1980) Biochem. J. 185, 139-154.

ibid (1980) Biochem. J. 185, 155-167.

Clore, G.M. & Chance, E.M. (1979) Biochem. J. 177, 613-621.

Clore, G.M. & Chance, E.M. (1978) Biochem. J. 173, 811-820.

Colman, D.M.; Freeman, H.C.; Cuss, J.M.; Murata, M; Norri, V.A.; Ramshaw, A.M.; & Venkatapa, P. (1978) Nature, 272-319.

Copeland, R.A.; Naqui, A.; Chance, B.; & Spiro, T.G. (1985) FEBS Lett. 182, 375-379.

Copeland, R.A. & Spiro, G.T. (1986) FEBS Letts. 197(1,2) 239-243.

Denis, M. (1981) Biochim. Biophys. Acta 634, 30-40.

Denis, M. & Clore, M. (1981) Plant Physiol. 68, 229-235.

Denis, M.; Gayda, J.P.; Bertrand, P.; & Richaud, P. (1984) Physiol. Veg 22(5), 589-595.

Denis, M. & Richaud, P. (1982) Biochem. J. 206, 379-385.

Denis, M. (1986) Biochimie. 68, 459-470.

De Vrij, W.; Azzi, A.; & Konings, W.N. (1983) Eur. J. Biochem. 131, 97-103.

Dockter, M.E.; Steineman, A.; &Schatz, G. (1978) J. Biol. Chem. 253, 311-317.

Dutch, R.; Ingle, R.; Centeno, J.A.; Peiffer, P. ; Babcock, G.T.; and Ferguson-Miller, S. (1986) in *Plant Mitochondria* (Ed. Beechy, B. and Moose, A.) Plenum Publishing Co., New York.

Eachus, R.S. & Olm, M. (1985) Science 230, 268-274.

Einarsdottir, O. & Caughey, W.S. (1984) Biochim. Biophys. Res. Commum. 124 , 836-842.

Einarsdottir, O. & Caughey, W.S. (1985) Fed. Proc. 44, 1780 (Abst.)

Emsley, J. (1984) in *Structure and Bonding*, pp. 147-191, Springer-Verlag Berlin, Heidelberg.

Englander, S.W.; Downer, N.W.; & Teitelbaulm, H. (1972) Ann. Revs. Biochem. 41, 903-924.

Felton, R.H.; & Yu, N.T. (1978) in *Porphyrins*, 3, 347-393.

Findsen, E.; Centeno, J.A.; Babcock, G.T.; & Ondrias, M.R. (1987) J. Amer. Chem. Soc., in press.

Frey, T.G.; Kuhn, L.A.; Leigh, J.S., Jr.; Costedo, M.J.; & Chan, S.P. (1985) J. Inorg. Biochem. 23, 155-162.

Fuhrop, J-H. & Smith, K.M. (1975) in "Laboratory Methods in Porphyrin and Metalloporphyrin Research" Elsevier Scientific Publishing Company.

Fuller, S.D.; Capaldi, R.A.; & Henderson, R. (1979) J. Mol. Biol. 134, 305-327.

Fuller, S.D.; Capaldi, R.A.; & Henderson, R. (1982) Biochemistry 21, 2525-2529.

Fukumori, Y.; Nakayawa,, K.; & Yamanaka, T. (1985) J. Biochem. 98, 493-499.

Gelles, J.; Blair, D.F.; & Chan, S.I. (1986) submitted.

Georgevich, G.; Darley-Usmar, V.M.; Malatesta, F.; & Capaldi, R.A. (1983) Biochemistry 22, 1311-1322.

Gibson, Q.H. & Greenwood, C. (1963) Biochem. J. 86, 546-554.

Ginn, S.C. & Wood, J.L. Proc. Chem. Soc. 884 (1965).

Glasoe, P.D. & Long, F.A. (1960) J. Phys. Chem. 64, 188-190.

Gorren, A.C.F.; Dekker, H.; & Wever, R. (1985) Biochim. Biophys. Acta 809, 90-96.

Gouterman, M. (1959) J. Chem. Phys. 30, 1139-1161.

Gouterman, M. (1961) J. Mol. Spectrosc. 6, 138.

Greenwood, C. & Gibson, Q.H. (1967) J. Biol. Chem. 242, 1782-1787.

Greenwood, C.; Hill, B.; Barber, D.; Englinton, D.G.; & Thomson, A.J. (1983) Biochem. J. 215, 303-316.

Halaka, F. (1981) Dissertation, Michigan State University.

Halmann, M. & Pinchas, S. (1958) J. Chem. Soc. 1703.

Hartzell, C.R. & Beinert, H. (1976) Biochim. Biophys. Acta 368, 318-338.

Honami, K. & Oshima, T. (1984) Biochemistry 23, 454-460.

Hurts, G., Kraft, K. Schultz, R.; & Kreilick, R. (1982) J. Mag. Res. 49, 159.

Jones, G.D. & Wilson, M.T. (1984) J. Inorg. Biochem. 21, 159-168.

Kamoun, M. & Mirone, A. (1980) Chem. Phys. Letts. 75(2) 287-289.

Karabatsos, G.J. (1960) J. Org. Chem. 25(3), 315-318.

Karlson, B.; Aasa, R.; Vanngard, T.; Malmstrom, B.G. (1981) FEBS Lett 131, 186-188.

Keifer, W. (1973) Appli. Spectrosc. 27, 253.

Keifer, W.; Schmid, W.J.; & Topp, J.a. (1975) Appl. Spectrosc. 434-436.

Keifer, W. (1977) *Adv. Infrared and Raman Spectrosc.* 3, 142.

Keilin, D. & Hartree, E.F. (1939) Proc. Roy. Soc. London Ser. B 127, 167-191.

Kent, T.A.; Munk, E.; Dunham, W.R.; Filter, W.F.; Findling, K.L.; Yoshiba, T.; & Fee, J.A. (1982) J. Biol. Chem. 257, 12,489-12,492.

Kincaid, J.; Stein, P.; & Spiro, T.G. (1979) Proc. Natl. Acad. Sci. USA 76, 549-552.

Kitagawa, T.; Ogoshi, H.; Watanabe, E.; Yoshiba, Z-I (1975) J. Phys. Chem. 72(24), 2629-2635.

Kitagawa, T.; Abe, M.; Kyoguku, Y.; Ogashi, H.; Watanabe, E.; & Yoshibe, Z. (1976) J. Phys. Chem. (11) 80, 1181-1186.

Kitagawa, T.; Kyoguku, Y.; & Orii, Y. (1977) Arch. Biochem. Biophys. 181, 228-235.

Kitagawa, T.; Ondrias, M.R.; Rousseau, D.L.; Ikeda-Saito, M.; & Yonetani, T. (1982) Nature 298, 869-871.

Krishnan, R.S. & Shankar, R.K. (1981) J. Raman Spectrosc. 10, 1-7.

Kumar, C.; Naqui, A.; & Chance, B. (1984) J. Biol. Chem. 259(4), 2073-2076 .

Kumar, C.; Naqui, A.; & Chance, B. (1984) J. Biol. Chem. 259(9), 11,668-11,671.

Lambeth, D.O. & Palmer, G. (1973) J. Biol. Chem. 248(17), 6095-6103.

Lanne, J. & Keifer, W. (1980) J. Chem. Phys. 72, 5305

Lemberg, M.R. (1969) Physiolo. Rev. 49, 48.

Lorosh, J.; Haase, W.; & Huong, D.V. (1986) J. Inorg. Biochem. 27, 53-63.

Lorusso, M.; Capuano, F.; Boffoli, D.; Stefanelli, R.; & Papa, S. (1979) Biochem. J. 182, 133-147.

Ludvig, B. & Schatz, G. (1980) Proc. Natl. Acad. Sci. USA 76, 196-200.

Malmstrom, B.G. (1985) Biochim. Biophys. Acta 811, 1-12.

Malmstrom, B.G. (1986) Chem. Scripta

Martin, C.T.; Scholes, C.P.; & Chan, S.I. (1985) J. Biol. Chem. 260(5), 2857-2861.

McGovern-Moroney, P.; Scholes, T.A.; & Hinkle, P.C. (1984) Biochemistry 23, 4991-4997.

Mincey, T. & Traylor, T.G. (1978) Bioinorg. Chem. 9, 409-420.

Mitchell, P. (1979) Eur. J. Biochem. 95, 1-20.

Mitchell, P. & Moyle, J. (1983) FEBS Lett 151, 167-178.

Musci, G.; Desideri, A.; Murpurgo, L.; & Tosi, L. (1985) J. Inorg. Biochem. 23, 93-102.

Nalecz, K.A.; Bolli, R.; & Azzi, A. (1985) Biochim. Biophys. Res. Commun. 114, 822-828.

Naqui, A.; Chance, B.; & Cadenas, E. (1986) Ann. Rev. Biochem. 55, 137-166.

Nicholls, P. (1978) Biochem. J. 175, 1147-1150.

Nicholls, P. & Chanady, G.A. (1981) Biochim. Biophys. Acta 634, 256-265.

Novak, A. (1974) in Structure and Bonding vol. 18. 177-216.

O'Malley, P. & Babcock, G.T. (1986) J. Am. Chem. Soc. 108, 3995-4001.

Ogura, T.; Sone, N.; Tagawa, K.; & Kitagawa, T. (1984) Biochemistry 23, 2826-2831.

Ramaswamy, K.; Pichai, R.; & Chanadesikan, S.G. (1967) J. Mol. Spectrosc. 23, 416-424.

Reichardt, J.K.V. and Gibson, Q.H. (1983) J. Biol. Chem. 258, 1504-1507.

Reinhard, B.; Nalecz, K.A.; and Azzi, A. (1985) Arch. Biochem. Biophys. 240 (1), 102-116.

Richaud, P. and Denis, M. (1984) Arch. Biochem. Biophys. 232, 8-16.

Rousseau, D.L.; Friedman, J.M.; and Willams, P.E. (1979) in "Topics in Current Physics" (A. Weber, editor) Spring-Verlag Berlin, Heidelberg, 11. 203-252.

Rousseau, D.L. (1981) J. Raman Spectrosc. 10, 94-99.

Rousseau, D.L.; Ondrias, M.R.; LaMar, G.N.; Kong, S.B.; & Smith, K. M. (1983) J. Biol. Chem. 258(3), 1740-1746.

Sarti, P.; Jones, M.G.; Antonini, G.; Malatesta, F.; Colosimo, A.; & Wilson, M.T. (1985) Proc. Natl. Acad. Sci. U.S.A. 82, 4876-4880.

Scheiner, S. & Hillenbrand, E.A. (1985) Proc. Natl. Acad. Sci. 82, 2741-2745.

Scholes, C.P.; Janakiraman, R.; Taylor, H.; and King, T.E. (1984) Biophys. J. 45, 1027-1030.

Segawa and Kumer (1986)

Seiter, C.H.A. and Angelos, S.G. (1980) Proc. Natl. Acad. Sci. USA 77, 1806-1808.

Shaw, R.W.; Hansen, R.E.; Beinert, H. (1978) J. Biol. Chem. 253, 6637-6640.

Shelnutt, J.A.; Rousseau, D.L.; Dethmers, J.K.; and Margoliash, E. (1981) Biochemistry 20, 6485-6497.

Sievers, G.; Osterlund, K. & Ellfolk, N. (1979) Biochem. Biophys. Acta 581. 1-14.

Sigel, E. and Carafoli, E. (1978) Eur. J. Biochem. 89, 119.

Singh, T.R. & Wodd, J.L. (1969) J. Chem. Phys. 50(8), 3572-3576.

Smith, M.L.; Ohlsson, P-I.; and Paul, G.K. (1983) FEBS Letts. 162(2), 303-305.

Ohnishi, T.; Lo Brutto, R.; Salerno, J.C.; Bruckner, R.C.;& Frey, T.G. (1982) J. Biol. Chem. 257, 14,821-14,825.

Okunuki, K.; Hagihora, B.; Sekuzu, I.; & Horio, J. (1958) Proceedings of the International Symposium on Enzyme Chemistry, Tokyo and Kyoto, p. 264, Maruzen, Tokyo.

Ondrias, M.R. (1980) Ph.D. Dissertation Michigan State University, East Lansing, MI. 48824

Orii, Y. (1984) J. Biol. Chem. 259, 7187-7190.

Orii, Y. & King, T.E. (1976) J. Biol. Chem. 251, 7487-7493.

Ozaki, T.; Katagawa, T.; & Ogoshi, H. (1979) Inorg. Chem. 18, 1772-1776.

Palmer, G.; Babcock, G.T.; & Vickery, L.E. (1976) Proc. Natl. Acad. Sci. USA 73, 2206.

Papa, S.; Lorusso, M.; Capitanio, N.; & De Nitto, E. (1983) FEBS Lett 157, 7-14.

Penttila, T. (1983) Eur. J. Biochem. 133, 355.

Powers, L.; Blumberg, W.E.; Chance, B.; Barlow, C.H.; Leigh, T.S., Jr.; Smith, J.; Yonetani, T.; Vik, S.; & Peisach, J. (1979) Biochim. Biophys. Acta 546, 520-538.

Powers, L. & Chance, B. (1985) J. Inorg. Biochem. 23, 207-217.

Powers, L.; Chance, B.; Ching, Y.; & Angiolillo, P. (1981) Biophys. J. 34, 465-498.

Prochaska, L.J.; Bisson, R.; Capaldi, R.A.; Steffens, G.C.M.; and Buse, G. (1981) Biochim. Biophys. Acta 637, 361-373.

Prochaska, L.J. & Reynolds, K.A. (1986) Biochemistry 25, 781-787.

Proteau, G.; Wrigglesworth, J.M.; and Nicholls, P. (1983) Biochem. J. 210, 199-205.

Puttner, I.; Carafoli, E.; and Malatesta, F. (1985) J. Biol. Chem. 260, 3719-3723.

Raman, C.V. (1928) Nature London 121, 501.

Soliocz, M.; Carafoli, E.; and Ludwig, B. (1982) J. Biol. Chem. 257, 1579-1582.

Sone, N. and Hinckle, P. (1982) J. Biol. Chem. 257, 12,600-12,604.

Sone, N.; Naqui, A.; Kumar, C.; and Chance, B. (1984) Biochem. J. 223, 809-813.

Sone, N. and Kosako, T. (1986) The EMBO Journal 5(7), 1515-1519.

Sone, N. and Yanagita, Y. (1982) Biochim. Biophys. Acta 682, 216-226.

Spinner, E. (1983) J. Am. Chem. Soc. 105 (4), 756-761.

Spiro, T.G. & Strekas, T.C. (1972) Proc. Natl. Acad. Sci. USA 69(9) 2622-2626.

Spiro, T.G. & Burke, J.M. (1976) J. Am. Chem. Soc. 98, 5482-5489.

Spiro, T.G. (1983) in "Iron Porphyrins" (Lever, A.B.D. and Gray, H.B., eds.) Addison-Wesley Publishing Company, part II pp. 91-157.

Stevens, T.H.; Martin, C.T.; Wang, H.; Brudvig, W.; Scholes, C.P.; and Chan, S.I. (1982) J. Biol. Chem. 257 (20), 12,106-12,113.

Suarez, M.D.; Revzin, A.; Narlock, R.; Kempner, E.S.; Thompson, D.A.; Ferguson-Miller, S. (1984) J. Biol. Chem. 259, 13,791-13,799.

Takemori, S. & King, T.E. (1965) J. Biol. Chem. 240, 504-513.

Thelen, M.; O'Shea, A.S.; and Azzi, A. (1985) Biochem. J. 227, 163-167.

Thompson, D.A. and Ferguson-Miller, S. (1983) Biochemistry 22, 3178.

Thompson, D.A.; Gregory, L.; and Ferguson-Miller, S. (1985) J. Inorg. Biochem. 23, 357-364.

Thomson, A.J.; Greenwood, C.; Gadsby, P.M.A.; Peterson, J.; Englinton, D.G.; Hill, B.C.; and Nicholls, P. (1985) J. Inorg. Biochem. 23, 180-197.

Thomson, A.J.; Greenwood, C.; Peterson, J.; and Barrett, C.P. (1986) J. Inorg. Biochem. 28, 195-205.

Tsubaki, M.; Nagai, K.; & Kitagawa, T. (1980) Biochemistry 19, 379-385.

Tweedle, M.F.; Wilson, L.J.; Garcia-Iniquez, L.; Babcock, G.T.; and Palmer, G. (1978) J. Biol. Chem. 253, 8065-8071.

Tzagoloff, A.; Marino, G.; and Sebald, W. (1979) Ann. Rev. Biochem. 48, 419-441.

Valance, W.G. & Strekas, T.C. (1982) J. Phys. Chem. 86, 1804-1808.

Vanderkoii, G. and Stotz, L. (1965) J. Biol. Chem. 240, 3418-3424.

Van Gelder, B.F. (1966) Biochim. Biophys. Acta 118, 36.

Van Gelder, B.F. and Beinert, H. (1969) Biochim. Biophys. Acta 189, 1.

Vanneste, W.H. (1967) Biochemistry 5, 838-848.

VanSteelandt-Frendrup, J.; Salmeen, I.; and Babcock, G.T. (1981) J. Am. Chem. Soc. 103, 5981-5982.

Vinogradov, S.N. and Linnel, R.H. (1971) in "Hydrogen Bonding," Van Nostrand Reinhold Company, New York, Chapter 6, pp. 147-175.

Ward, B.; Callahan, P.M.; Young, R.; Babcock, G.T.; and Chang, C.K. (1983) J.Amer. Chem. Soc. 105 634-636.

Wharton, D.C. and Tzagoloff, A. (1964) J. Biol. Chem. 239, 2036.

Wikstrom, M.K.F. (1977) Nature 266, 271-273.

Wikstrom, M.K.F. (1984) Nature 308, 558-560.

Wikstrom, M.K.F. and Krab, K. (1979) Biochim. Biophys. Acta 549, 177-222.

Wikstrom, M.K.F.; Krab, K.; and Saraste, M. (1982) in "Cytochrome c Oxidase: A Synthesis," Academic Press, London.

Wikstrom, M.K.F. and Saari, H.T. (1977) Biochim. Biophys. Acta 462, 347.

Willems, D. & Bocian, D.L. (1984) J. Am. Chem. Soc. 106, 880-890.

Willems, D. & Bocian, D.L. (1985) J. Phys. Chem. 74, 5662.

Willems, D. & Bocian, D.L. (1985) J. Phys. Chem. 89, 234.

Wilson, E.B.; Decius, J.C., Jr.; & Cross, R.C. (1955) in "Molecular Vibration" McGraw Hill, New York, N.Y. p.336.

Wilson, M.T.; Peterson, J.; Antonini, E.; Brunori, M.; Colosimo, A.; and Wymann, J. (1981) Proc. Natl. Acad. Sci. USA 78, 7115.

Winter, D.B.; Bruyninckx, W.J.; Foulke, F.G.; Grinich, N.P.; and Mason, H.S. (1980) J. Biol. Chem. 255, 11,408-11,414.

Woodruff, W.H.; Kessler, R.J.; Ferris, N.S.; Dallinger, R.F.; Carter, K.; Antalis, T.M.; & Palmer, G. (1982) Adv. Chem. Ser. 201, 625.

Woodruff, W.H.; Norton, K.A.; Swanson, B.L.; and Fry, H.A. (1984) Proc. Natl. Acad. Sci. USA 81, 1263-1267.

Yamanaka, T.; Fujii, K.; and Kamita, Y. (1979) J. Biochem. 86, 821-824.

Yonetani, T. (1960) J. Biol. Chem. 235, 845-852.

Young, L.J. and Palmer, G. (1986) J. Biol. Chem. 261(28), 13,031-13,033.

Yoshiba, T. and Fee, J.A. (1984) J. Biol. Chem. 259, 1031-1046.

Yoshida, T.; Lorence, R.M.; Choc, M.G.; Tarr, G.E.; Findling, K.L.; and Fee, J.A. (1984) J. Biol. Chem. 259, 112-123.

Zwarich, R.; Smolarek, J.; and Goodman, L. (1971) J. Mol. Spec. 38, 336-337.

MICHIGAN STATE UNIVERSITY LIBRARIES
3 1293 03061 6860